ABSTRACT

ALNSOUR, NAJWA IBRAHIM HAMED ALLAH. Bi-Directional Exchange of Ammonia from Soils in Row Crop Agro-ecosystems (Under the direction of Dr. Wayne Robarge).

The overall goal of this work is to better understand the chemical and physical processes that control retention or release of ammonia (NH_3) from soil and to link these processes to emission and deposition fluxes of NH_3. Adequate knowledge is required to improve our understanding of the factors that govern the interaction of bicarbonate (HCO_3^-) and NH_3 emission from aqueous solutions and to identify the pool of ammonium (NH_4^+) in soils that actively influences the bi-directional exchange of NH_3. Detailed information on how elevated CO_2 and the subsequent change in its partial pressure above the air/liquid interface impacts NH_3 emissions/deposition is still far from being well understood, especially in biological systems that may be relatively well buffered as compared to simple aqueous solutions of pure salts. To address these knowledge gaps, release of NH_3 from phosphate buffered solutions (0.1M) of ammonium sulfate (AS) with or without the addition of HCO_3^- was measured using a glass reaction chamber in combination with annular denuder technology. The mass of NH_3 collected per unit time in a well-buffered phosphate solution (0.1M) increased linearly with total ammoniacal nitrogen (TAN = NH_3+NH_4^+) concentration but the NH_3 emission in the presence of 200 and 400 mM HCO_3^- is 1.7 and 2.5 times higher than emissions from pure AS solutions. Enhancement in NH_3 emissions was not linear and plateaued at 100 mM HCO_3^- in solution. Enhancement of NH_3 emissions at HCO_3^- > 100 mM was related to the loss of CO_2 across the air-liquid interface rather than the presence of excess HCO_3^- increasing the bulk solution pH.

Interaction of soil water evaporation, NH_4^+ redistribution, and NH_3 emissions were studied under differing soil and environmental conditions using a simple flow-through chamber system combined with annular denuder technology. Surface soils (0-10 cm) of differing texture

(loamy sand – BASF-ls; sandy loam – CEFS-sl or DUKE-sl) were tested for water evaporation rate and NH_3 loss and found to adequately reproduce laboratory evaporation rates with no differences among replicates. An air flow rate of 5 LPM was found to be adequately sensitive to the mass of NH_3 captured by the annular denuder tubes and allowed differentiation of the potential stages of water loss. For the non-amended soil (BASF-ls), significant N mineralization occurred during the first 24-hours of the experiment, resulting in ~2x increase of NH4-N in the packed soil column. The response between the calculated integrated average NH_3 concentrations and extractable NH4-N appeared linear with a slope of 0.3 μg NH_3-N m^{-3} per 1μg NH_4-N g^{-1} soil. In conclusion, a simple flow-through column can provide a measure of the direct impact of an increase in NH_4-N on potential NH_3 emissions.

As an index for NH_3 emission, it is important to estimate the magnitude and direction of NH_3 emissions through accurately calculating the soil critical compensation point (X_g). A laboratory approach was designed to compare two methods used in standardizing the calculation of X_g. The first method is determination of the soil NH_4^+ concentration in soil extracts. The second method uses the NH_4^+ adsorption isotherm to calculate the fraction of NH_4^+ in the soil solution that is available for loss to the atmosphere as NH_3. The comparison of NH_4^+ sorption among different soils showed the following trend: DUKE-sl > CEFS-sl,> BASF-ls. The adsorption isotherms allow calculation of the fraction of sorbed NH_4^+ and the fraction of $NH_4^+{}_{(aq)}$ in solution. The results from soil bulk extractions used to estimate the compensation point have higher X_g values compared to the X_g predicted by the adsorption isotherms. In general, the adsorption isotherm approach appears to be a more viable way to correct the extractable NH_4^+ for determining a more realistic compensation point.

Bi-Directional Exchange of Ammonia from Soils in Row Crop Agro-ecosystems

by
Najwa Ibrahim Alnsour

A dissertation submitted to the Graduate Faculty of
North Carolina State University
in partial fulfillment of the
requirements for the degree of
Doctor of Philosophy

Soil Science

Raleigh, North Carolina

2020

APPROVED BY:

Dr. Wayne Robarge Committee Chair	Dr. John Walker
Dr. Joshua Heitman	Dr. Lingjuan Wang Li

DEDICATION

To My Dad and Mom

May God Rest their Souls in Peace

BIOGRAPHY

Najwa Alnsour is a Ph.D. candidate of soil physical chemistry at North Carolina State University. She began her studies in Jordan with a B.S. in Soil and Irrigation from the University of Jordan and earned her first MSc. from Jordan University of Science and Technology in Soil, Water, and Environment. Najwa focused her research on thermodynamics, kinetics, and adsorption of different pollutants onto soil minerals, completing a thesis entitled "Adsorption of Phenol, Chlorinated Phenols, and Chromate onto Jordanian Organoclay: Equilibrium and Kinetics. She earned her second MSc. from Iowa State University in Soil Chemistry, completing a thesis entitled "Organic Matter in Holocene Paleosols at the Farwell Site." In 2013, Najwa started her Ph.D. at NCSU under the supervision of Dr. Wayne Robarge. As an NCSU student, Najwa worked on Bi-Directional Exchange of Ammonia from Soils in Row Crop Agro-Ecosystems.

She possesses more than ten years of research experience in soil science and environmental chemistry. She was a co-author for five published manuscripts in peer-reviewed journals. Najwa worked as a lecturer for a laboratory section at Hashemite University in the Department of Water Management and Environment.

Najwa's career vision is to work in a large and global company to work with a diverse group of people with many different backgrounds. Through these experiences, she aims to empower future professionals and leadership development to achieve career success and satisfaction.

ACKNOWLEDGMENTS

All praise and thanks to Allah Almighty, who gave me focus, strength, and patience to accomplish this work. I would like to express my gratitude to my advisor Dr. Wayne Robarge for his support to unleash my creative energy in writing and a critical thinking, for sharing his knowledge and excellent guidance in my research. I would like to express my sincere appreciation to Dr. John Walker, for sharing his vast knowledge with me, his continuous guidance and expertise helped me throughout this research work. I would also like to thank the other members of my examining committee including Dr. Joshua Heitman and Dr. Lingjuan Wang Li for their contributions to this document and their support and valuable discussions.

I want to express my sincere thanks to all of my professors, colleagues and staff members in the Department of Crop and Soil Sciences at NC State for their help and support.

To my family, I cannot thank you all enough for believing in me and praying for my success as a scientist and my growth as a person. My most heartfelt thanks go to my Husband Ali, who has always supported my ambitions with an unwavering enthusiasm for giving me the confidence, love, and values which allowed me to believe in myself and reach for my dreams and also for being there for me during life's difficult moments. Without them, none of this would have been possible.

TABLE OF CONTENTS

LIST OF TABLES

LIST OF FIGURES

Chapter One

Interaction between Carbonate and Ammonium in Aqueous Buffered Solutions: Implications for the Bi-directional Exchange of Ammonia

1. Introduction

1.1. Ammonia and the Environment

Ammonia (NH_3) is an alkaline gas in the atmosphere and an important component of inorganic particulate matter ($PM_{2.5}$). It plays a major role in removal of acidic gas via formation of aerosols, as well as in the global nitrogen cycle (Walker et al., 2006; Behera et al., 2013). Ammonia deposition is also known as a widespread environmental concern because of potential adverse effects to nutrient sensitive terrestrial and aquatic ecosystems (e.g. surface water eutrophication and soil acidification) (Bash et al., 2013). Agriculture including livestock husbandry, manure, and use of NH_3-based synthetic fertilizers are the biggest sources (80-90%) of NH_3 emissions (Sutton et al., 2008). Industrial processes, cars, cooking wood, humans and natural soils, vegetation and oceans are other sources of NH_3 (Sutton et al., 2008).

Total acid deposition involves wet deposition (e.g. rainwater, hail, sleet, snow, cloud and fog) and dry deposition (e.g. deposition of gases and particles). The National Atmospheric Deposition Program/National Trends Network, known as NADP / NTN, monitors wet deposition at more than 269 locations throughout the United States (http:/nadp.sws.uiuc.edu). The major chemical components of wet deposition include ammonium, sulfate, and nitrate. Wet deposition is calculated as the product of concentrations measured by NADP/NTN and precipitation amount estimated from the PRISM model (Fig. 1.1).

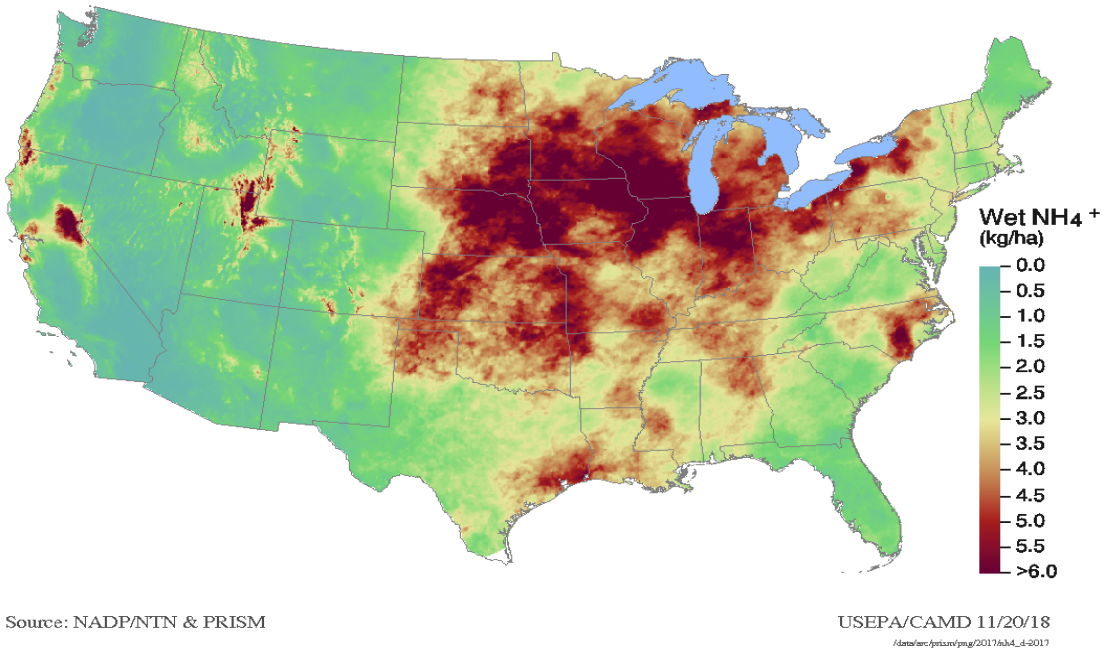

Figure 1.1. Wet deposition of ammonium ion (kg ha^{-1}) in the U.S in 2017. Source: National Atmospheric Deposition Program/National Trends Network (NADP/NTN) (https://www3.epa.gov/castnet/maps/prism/2017/nh4_d-2017.png)

The Clean Air Status and Trends Network (CASTNet) of the EPA tracks air concentrations of inorganic nitrogen and sulfur compounds at around 70 rural locations. Dry deposition of particle ammonium (kg ha^{-1}) in U.S. was estimated from observed CASTNET concentrations and simulated CMAQ deposition velocities and concentrations using TDep hybrid technique (Fig. 1.2) (Schwede and Lear 2014)

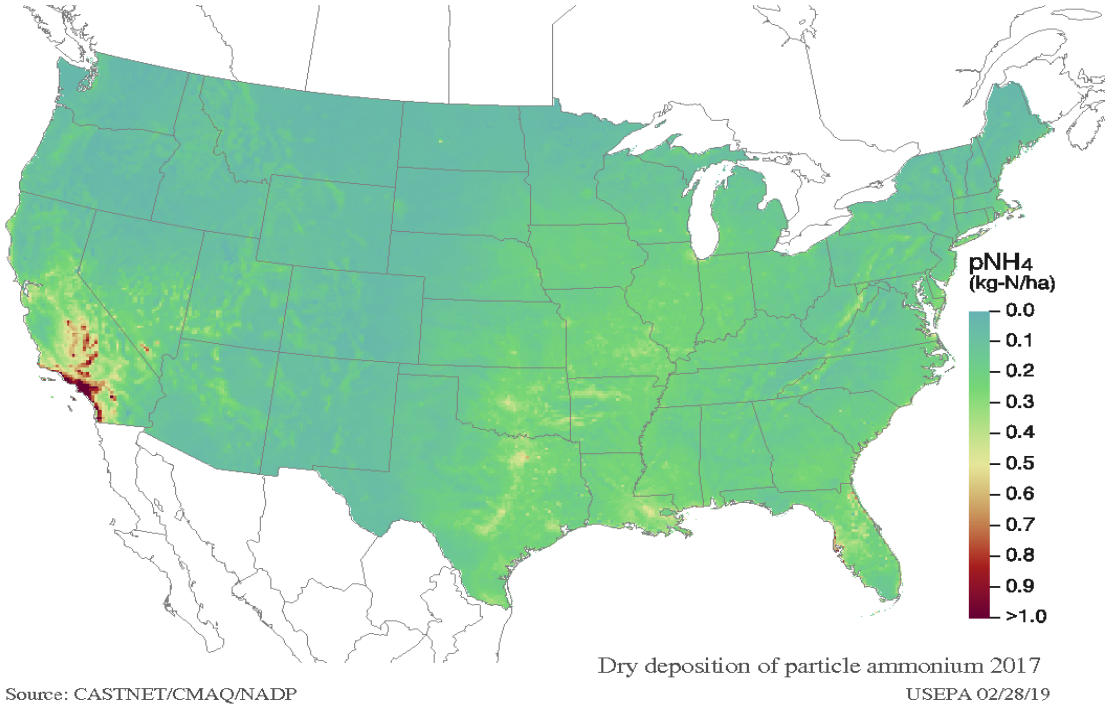

Figure 1.2. Dry deposition of particle ammonium (kg ha^{-1}) in the U.S in 2017. National Atmospheric Deposition Program/National Trends Network (NADP/NTN). (https://www3.epa.gov/castnet/maps/tdep/2017/nh4_dw-2017.png).

Dry deposition refers to the transport of NH_3 gas or particles from the atmosphere to the surface of water, soil, and plant leaves in the absence of rainfall (Duyzer et a., 1992). Various mechanisms involved in dry deposition of NH_3 include NH_3 turbulent transfer, diffusion, and adsorption to wet surfaces. Estimation of NH_3 deposition is dependent on meteorological conditions, and modelling of the boundary layer across differing crop types, forests, and grasslands (Sutton et al., 1993). Atmospheric concentration and deposition velocity are the main parameters used to estimate the deposition flux. Deposition velocities for natural surfaces vary from 10 to > 300 mm s^{-1} based on physical, chemical, and vegetation factors (Fowler et al., 1998; Schrader and Brummer, 2014). Examples of atmospheric concentrations that have been measured in natural environments are 0.20 µg NH_3 m^{-3} for a coniferous forest (Sutton et al., 1993), 0.45 µg NH_3 m^{-3} for Scottish moorland (Fowler et al., 1998), 0.3–0.8 µgNH_3 m^{-3} for a

deciduous forest in the Midwestern USA (Pryor et al., 2001), and 0.28–1.40 μgNH_3 m^{-3} for a mixed forest in the southeastern USA (Sparks et al., 2008).

1.2. Ammonia in the Atmosphere

Ammonia gas (NH_3) has a short residence time in the atmosphere because of its high solubility, stickiness, and high reactivity (Galbally and Roy, 1983). Ammonia is an important contributor to particulate matter ($PM_{2.5}$), which has adverse health effects on humans (Pleim et al., 2013). In the atmosphere, before NH_3 deposits on different surfaces, it can go through different physical and chemical processes such as chemical transformation and dispersal. Deposition on the surface can cause NH_3 gas to be transformed and removed from the atmosphere by reaction with sulfuric acid (H_2SO_4), leading to the formation of ammonium sulfate:

$$2NH_{3(g)} + H_2SO_4 \leftrightarrow (NH_4)_2SO_{4(s)} \quad (1.1)$$

Atmospheric NH_3 also reacts with nitric acid (HNO_3) and hydrochloric acid (HC1) to form ammonium nitrate and ammonium chloride aerosols

$$NH_{3(g)} + HNO_3 \leftrightarrow NH_4NO_{3(s)} \quad (1.2)$$

The reaction with nitric acid is highly dependent on relative humidity and temperature and has been studied in detail (Meng and Seinfeld, 1996; Wexler and Clegg, 2002). Ammonium chloride (NH_4Cl) aerosol can be present in the atmosphere when the relative humidity is below the deliquescent point and temperatures are below 10°C (Pio and Harrison, 1987). The main equilibrium reaction is:

$$NH_{3(g)} + HCl \leftrightarrow NH_4Cl_{(s)} \quad (1.3)$$

1.3 Bidirectional Exchange of Ammonia

The exchange of atmospheric NH_3 with vegetation is bidirectional (i.e. via emission and deposition) (Farquhar et al., 1980; Sutton et al., 1993; Nemitz et al., 2000). Ammonia is considered a sticky gas in that it readily interacts with many differing surfaces. However, unlike other pollutant gases, ammonia can be re-emitted from environmental surfaces under proper conditions. The gaseous NH_3 concentration within leaf stomata is known as the stomatal compensation point, permitting emission and deposition reliant on atmospheric concentrations (Farquhar et al., 1980). Farquhar et al. (1980) was the first to calculate a stomatal compensation point that explained the bidirectional exchange of NH_3. Emission results if the mole fraction of gaseous NH_3 in the air is smaller than the compensation point. Deposition exists where the mole fraction of NH_3 in the air is greater than the compensation point (Wu et al., 2009). Therefore, estimation of compensation point is an important parameter that controls the direction of NH_3 flux above vegetative surfaces (Wu et al., 2009).

The exchange of NH_3 is quantified as the flux in units of mass per unit of area and per unit of time. Flux can be downward, indicating deposition to the surface. These values are given a negative sign by convention. Likewise, upward fluxes indicating emission are positive in value. The stomatal compensation point (X_s) is a function of temperature, NH_4^+ concentration, and pH of the apoplast (Nemitz et al., 2000; Walker et al., 2006), and can be calculated as stated in Nemitz et al. (2000):

$$\chi_s = \frac{161500}{T} \exp\left(-\frac{10380}{T}\right) \frac{[NH_4^+]}{[H^+]} \qquad (1.4)$$

where T is the canopy temperature in Kelvin. The constants 161500 and 10380 are associated with the temperature adjusted Henry's Law coefficient. $[NH_4^+]$ and $[H^+]$ represent the ammonium and hydrogen ion concentration (mol L^{-1}) in the apoplast solution within the stomatal

cavity, respectively. The leaf emission potential $\Gamma_s = [NH_4^+/H^+]$ depends on nitrogen content of the soil and plant. The details of the compensation point derivation are presented in Chapter Three.

A typical form of the bidirectional exchange model includes the stomatal compensation point (X_s), stomatal resistance (R_s), cuticular resistance (R_w), aerodynamic resistance (R_a), boundary layer resistence (R_b), soil or ground resistance (R_g), soil compensation point (X_g), and canopy compensation point (X_c) (Nemitz et al., 2001). The bidirectional models are now implemented in both regional (Pleim et al., 2019) and global (Zhu et al., 2015) chemical transport models (CTMs).

1.4. Bicarbonate Enhancement from Aqueous Solutions

Despite the development of different theories and models for predicting NH_3 emission in the presence of HCO_3^-, detailed information on how elevated CO_2 and the subsequent change in its partial pressure above the air/liquid interface impacts NH_3 emissions/deposition is still far from being well understood, especially in biological systems that may be relatively well buffered as compared to simple aqueous solutions of pure salts.

Various models (static and dynamic) have been focused on quantifying the magnitude of ammonia emissions and to simulate interactions between CO_2 and NH_3 and solution pH from wastewater, aqueous solutions, and manure. These models are based on theories related to the diffusive transport of gases, kinetically limited CO_2 hydration/dehydration reactions, along with equilibrium acid/base reactions in solution (Kirk and Singh, 1992; Hafner et al., 2013; Peterson et al., 2014). A model developed by Peterson et al. (2014) presented a dynamic mathematical model that measures the development of pH gradients over time in the surface of dairy slurry. The model was evaluated by conducting pH measurements at a resolution of 0.1 mm to a depth

of 30 mm in ammonium bicarbonate (NH_4HCO_3) solution. Researchers found that the pH increased near the surface over 24 hours from 8.2 to 9.46 due to concurrent emission of CO_2 and NH_3 from the solution, and the increase of $NH_{3(aq)}$ concentration at the surface (Peterson et al., 2014).

Kirk and Singh (1992) proposed a theory to describe simultaneous transfer of CO_2 and NH_3 emission and their interaction through acid-base reactions in rice fields. In this theory, a two thin layer model was used to describe the diffusion, and chemical reactions for gases and dissolved species. These researchers predicted that ammonia emission in rice field conditions is limited by diffusion in air and aqueous solution, and CO_2 loss is limited by diffusion in solution. With CO_2 and NH_3 emission, a pH gradient near the air-liquid interface is produced, where the pH at the interface is lower than that in the bulk solution (Kirk and Singh, 1992).

Hafner et al. (2013) measured the emission of ammonia from NH_4Cl and NH_4HCO_3 solutions over 7 hours. Emission of NH_3 from the NH_4Cl solution was much lower than from NH_4HCO_3 at same total $NH_{3(aq)}$ concentration and pH. The difference in emissions was caused by an increase in pH near the surface in the NH_4HCO_3 solution due to emission of CO_2. In the presence of NH_4HCO_3, surface pH changed from 7.79 to 8.22, and the pH decreased from 7.82 to 6.87 in the presence of NH_4Cl (Hafner et al., 2013). This model was also used to predict NH_3 emission from manure. Hafner et al. (2013) found during 1 h, NH_3 emission increased by a factor of 4.9 as the pH increased from 6.5 to 8.5, and then decreased by a factor of 1.8 over subsequent 24 h. The decrease in surface pH is related to high flux of NH_3 (Hafner et al., 2013).

Lee et al. (2013) investigated enhanced NH_3 emissions from animal wastewaters and ammonium sulfate solution (AS) at constant pH and temperature. Sodium bicarbonate ($NaHCO_3$) was added to stimulate the potential influence of elevated partial pressure of CO_2. The

enhancement showed a 2x higher magnitude of NH_3 emission from AS solution with rather than without HCO_3^-. The authors proposed that the enhanced NH_3 emission was related to the influence of HCO_3^- and the transport restrictions close the air-liquid interface were kinetically restricted with loss of CO_2 across the interface layer consumed H_2CO_3 and appeared to increase NH_3 emissions.

1.5 Research Objectives

The overall goal of this dissertation research is to better understand the chemical and physical processes that control retention or release of ammonia from soil and to link these processes to emission and deposition fluxes of ammonia. This work focusses on two areas of uncertainty where significant knowledge gaps persist: interaction of bicarbonate and ammonia emission from aqueous solutions, and characterization of the pool of ammonium in soils that actively influences the bi-directional exchange of ammonia. This chapter investigates the processes of NH_3 emission from aqueous solutions. Despite the development of different theories and models for predicting ammonia emission in the presence of bicarbonate, detailed information on how elevated CO_2 and the subsequent change in its partial pressure above the air/liquid interface impacts NH_3 emissions/deposition is still far from being well understood, especially in biological systems that may be relatively well buffered as compared to simple aqueous solutions of pure salts.

Our specific objectives are to explore the potential influence of elevated partial pressure of CO_2 on enhancement of NH_3 emission from buffered ammonium sulfate (AS) solutions. Sodium bicarbonate ($NaHCO_3$) is used as a source of CO_2/HCO_3^- to mimic the linkage between CO_2 and NH_3 processes in natural systems, e.g. soil respiration and photosynthesis. The influence of HCO_3^- on improving NH_3 emissions is investigated through quantitative analysis of

the amount of NH_3 emitted. The main motivation of this study is not only quantifying the magnitude of NH_3 emitted but also to better quantify the reactions and understand the mechanisms that could impact NH_3 emission. This requires exploring the reaction mechanisms of CO_2 with ammonia that are occurring in solution and understanding the chemistry of $NH_4^+/NH_3(aq)$ and CO_2 near the air-liquid interface that are contributing to the enhancement of NH_3 emissions. To achieve these objectives, time integrated measurements of NH_3 emissions were conducted under controlled conditions (stirred glass reaction chamber, constant headspace air flow, depth of solution, pH (phosphate buffer), temperature), and ammonium (NH_4-N) concentration in the absence and presence of HCO_3^- using annular denuder technology. The performance of the reaction chamber was assessed by measuring mass flow rate of NH_3 from buffered AS solution using differing conditions of pH (5.5-8.5), air flow rate (3.0-9.0 LPM), chamber headspace (0.5-2 L), temperature (0.5-35°C), and TAN concentrations (5.0-1000 mg NH_4-N L^{-1}).

2. Material and Methods

2.1.Experimental Apparatus

In order to measure the release of NH_3 from phosphate buffered solutions (0.1 M) of ammonium sulfate (AS) with or without the addition of sodium bicarbonate we used a glass reaction chamber (Pyrex®, 2000 mL, Model No. 6947) in combination with annular denuder technology (URG Inc.) (Fig.1.3). The chamber has an internal volume of 2 L (12.5 cm x 17.5 cm x 9.2 cm) and a surface area of 122 cm^2 at the air-liquid interface with the solution. A glass lid with two inlets (~ 1 cm internal diameter) was attached to the reaction chamber using a metal clamp and two lock springs. To minimize gas leaks from the chamber, electrical tape was first used around the outside of both lid and glass chamber. The glass reaction chamber was placed in a circulating water bath allowing temperature control of < +/- 0.2˚C of the internal solution.

The flat-bottomed glass chamber allowed mixing using a magnetic stirrer (VWR Scientific, Dyla-Dul, model No. 986950) located below the water bath. The solution within the glass chamber was mixed via magnetic coupling, such that there was an absence of a vortex in the solution. Temperature of the water bath was controlled by a digital temperature controller (VWR, Refrigerated Circ, Model No. 1166D). Temperature of the solution in the glass reaction chamber was monitored manually using a digital thermometer with a tolerance of +/- 0.1 ºC (Fisher Scientific Digital Thermometer Model 15-077-8 with external steel probe).

Air flow (~ 6 LPM) through the glass chamber was controlled via a microprocessor- controlled pump (Model No. URG-3000-02BBM) using a digital mass flow controller. Flow rates were confirmed using a BIOS® piston flow meter (S/N 100776; Model Revision 1.08). The chamber inlet was unrestricted but was connected to a common manifold that allowed either ambient or conditioned air into the chamber. For conditioned air, a gas flowmeter (Cole Palmer model No. PMRI-010562) was used to control the flow rate through the external manifold at ~ 8 LPM. Typical sampling times of ~ 1 hr at 6 LPM (60 L = 0.06 m^3) meant background amounts of NH_3 drawn into the headspace of the chamber were insignificant compared to the mass of NH_3 released from the test solutions. Ammonia emission measurements from AS solutions prepared in the presence of a phosphate buffer solution (0.1M) were typically conducted after the solution achieved the desired temperature. While the solution was reaching the designated temperature (~10 min), the air flow through the chamber was maintained at 6 LPM.

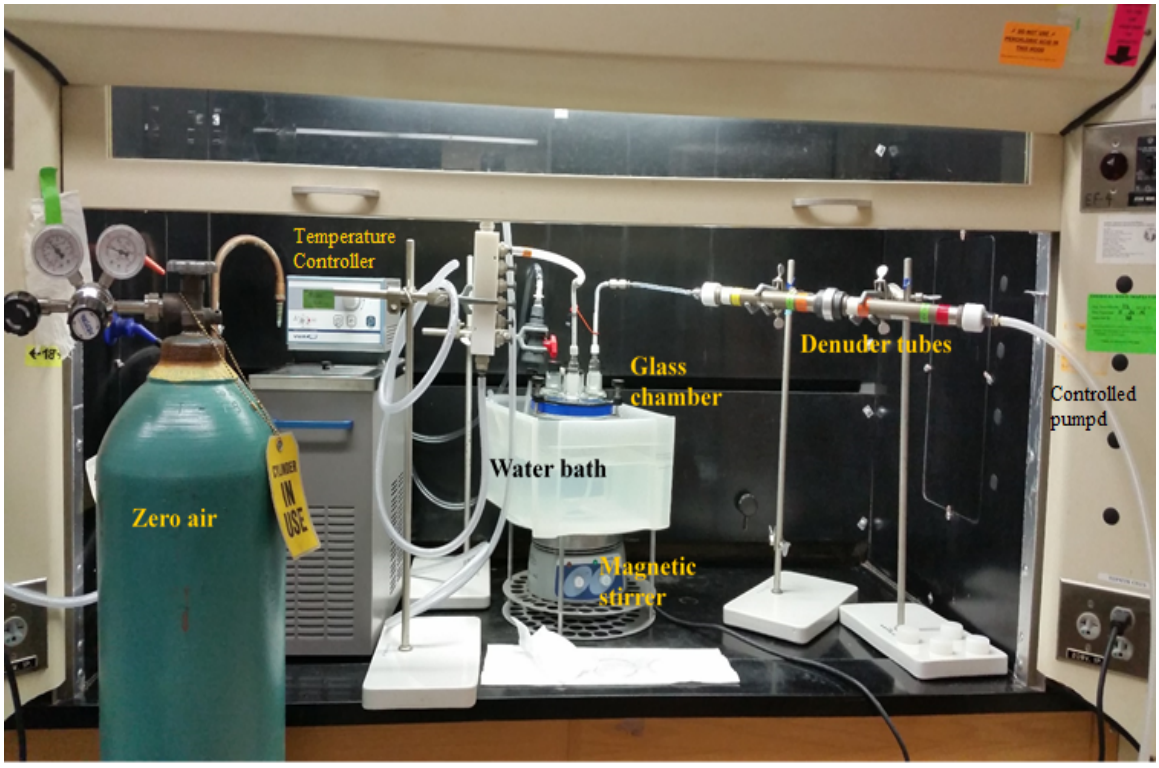

Figure 1.3. Laboratory Experimental Setup

2.2. Annular Denuder Technology

The mass of NH_3 exiting the glass chamber was collected using annular denuder tubes (URG Inc.). The tubes were coated with phosphorous acid (H_3PO_3) (0.5 % w/w) (ACROS, ORGANICS) and then dried with ammonia-free air. Acid-coated denuders were kept in a refrigerator prior to use. The mass of NH_3 released was determined by accounting for the volume used to extract the exposed denuder tube (10 mL of deionized water) multiplied by the concentration of NH_4-N found in the extract. The average mass of NH_4-N from ten blank acid-coated denuder tubes was 0.36µg NH_4-N, with a range of 0.17 to 0.81µg NH_4-N.

2.3. Performance of Experimental Apparatus

We evaluated the performance of our experimental apparatus before conducting experiments. The evaluation included the working concentrations range possible using the annular denuder technology, and the ability of the experimental apparatus to mimic well-known influences of pH, temperature, volume of solution, and air flow rate on NH_3 emissions from solutions containing ammonium.

2.3.1. Retention Capacity of Annular Denuder Tubes

To determine the collection efficiency, paired denuder tubes were used in tandem. The tubes were held in a horizontal position with air flowrate of 6 LPM and exposed for 1 hr. The theoretical collection efficiency for NH_3 using annular denuder tube was calculated using the empirical equation of Ferm (1979). The Ferm Protocol utilizes the mass obtained individually in each tube in order to calculate the collection capacity if two tubes were used in series. Collection efficiency can be expressed as E= 100*(a-b)/a, where a is NH_3 sorbed in the first tube, and b is the amount collected in the second tube. Table 1.1 shows the collection efficiency for NH_3, as a function of NH_4-N concentrations. The reported values are averages of duplicate measurements. For NH_4^+ concentration (5.0-250 mg NH_4-N L^{-1}), the average efficiency of denuders was 98%. As the concentration of NH_4^+ increased to 1000 mg L^{-1}, the apparent collection efficiency for the annular denuder decreased to 89%.

Table 1.1. Ammonia collection efficiency using acid-coated denuder tubes as a function of buffered ammonium concentration containing no bicarbonate, zero air through the chamber was used. Experimental conditions: T (20°C), pH (7.5), air flow rate (6 LPM), volume of solution (2 L), sampling time (1 hr). Efficiency is calculated based on the difference between the amount of NH_3 collected in the first tube and the amount collected in the second tube divided by the amount collected in the first tube X 100 (Ferm, 1979).

TAN (mg NH_4-N L^{-1})	First denuder (µg)	Second denuder (µg)	Efficiency %	RSD (%)
5	5.7	0.5	91.7	1.2
25	23.0	0.5	97.8	5.4
50	52.0	0.4	99.3	1.6
75	74.0	0.6	99.2	0.1
100	99.2	0.5	99.5	0.5
250	219.1	0.3	99.9	6.8
500	377.0	25.8	93.2	2.7
750	572.4	49.6	91.3	5.4
1000	689.7	74.5	89.2	0.8

The total mass of NH_3 collected by the second tube in tandem with the first tube is plotted versus the TAN (mg NH_4-N L^{-1}) concentration (Fig. 1.4). The extent of breakthrough was assessed at higher concentration (500-1000 mg NH_4-N L^{-1}). The mass of NH_3 collected by the paired denuder tubes was combined for the final calculation of an integrated NH_3 flux observed over set period of time. The precision (expressed as %RSD) of the measurements is presented in Table 1.1.

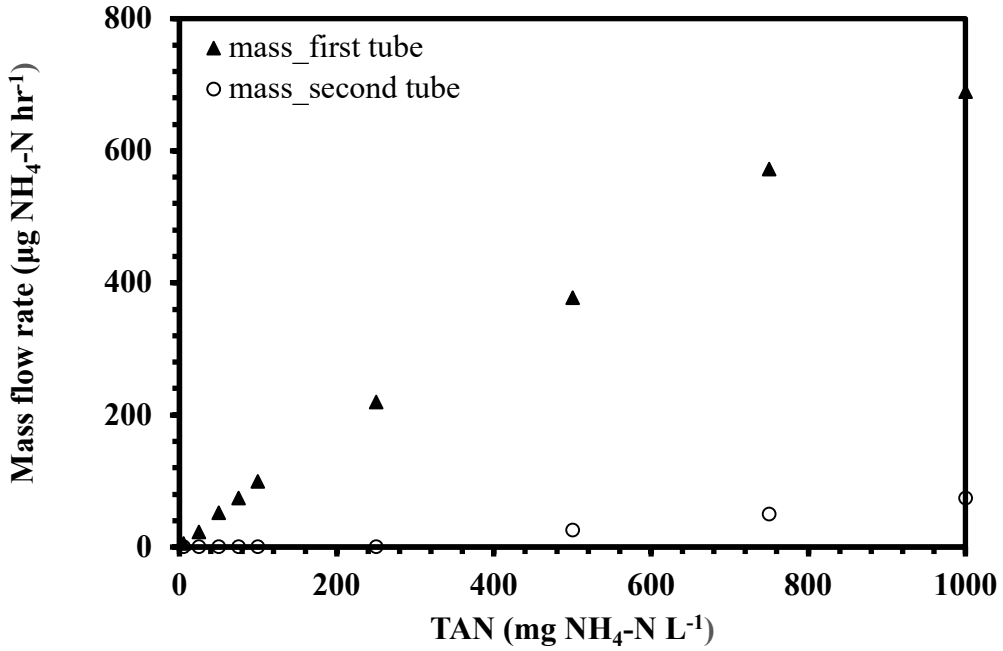

Figure 1.4. Measurement of atmospheric NH_3 release from ammonium sulfate (AS) prepared in phosphate buffered solution (0.1M) using paired denuder tubes as a function of ammonium concentration, zero air through the chamber was used. Experimental conditions in absence of bicarbonate: TAN (5-1000 mg NH_4-N L^{-1}), air flow rate 6 LPM, pH 7.5, temperature 20°C, and volume of solution 2 L.

2.3.2 Airflow/Chamber Headspace

Figure 1.5 illustrates ammonia release from AS solution prepared in phosphate buffer (0.1 M) as a function of airflow rate and temperature. Loss of NH_3 from the buffered AS solution increased with airflow rate through the headspace of the chamber. A value of 6 LPM was chosen for subsequent measurements to ensure adequate sensitivity in the mass of NH_3 captured by the acid-coated annular denuder tubes in a reasonable period of time (typically 1 hr).

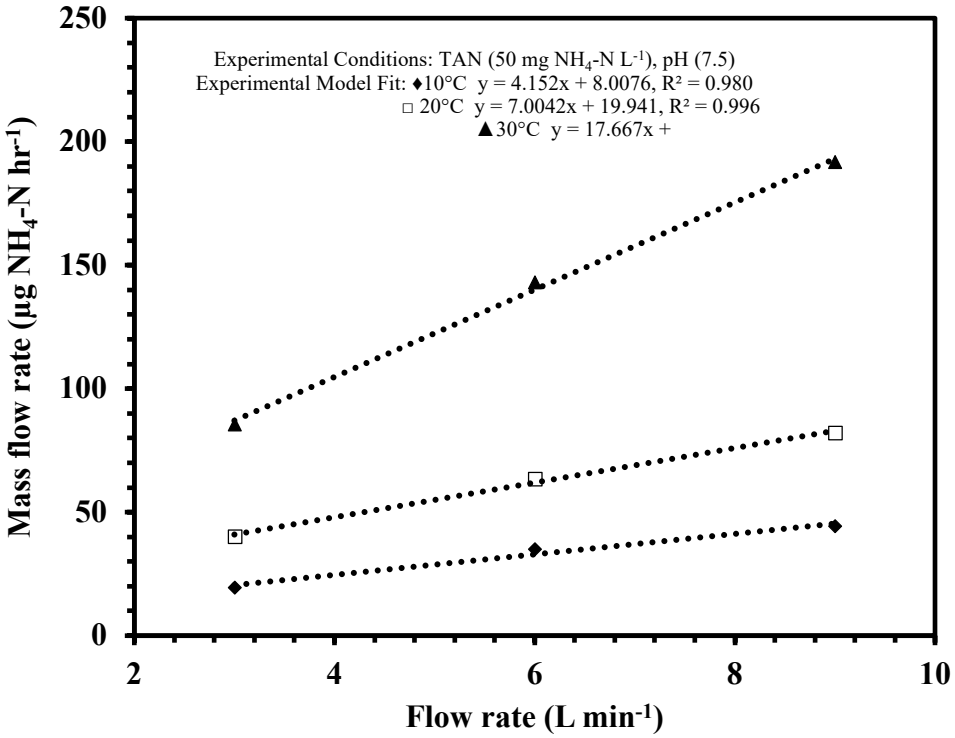

Figure 1.5. Ammonia release from ammonium sulfate (AS) prepared in phosphate buffered solution (0.1 M) as a function of airflow rate and temperature, ambient air has been used for inlet air through the chamber. Experimental condition in absence of bicarbonate: TAN (50 mg NH_4-N L^{-1}), pH 7.5, and volume of solution 2 L. Dashed lines represent linear regression models at different temperatures.

Figure 1.6 presents the NH_3 release as a function of different volumes of solution at different temperatures. The volume of solution in the chamber was varied from 0.5 to 2 L which changed headspace above the solution at fixed air flow rate and residence time from 2 to 0.50 L. As the volume of solution increased from 0.5 to 2 L, the NH_3 flux rate increased by 37%, 59%, and 77%, at 10, 20, and 30 °C respectively. Overall, the volume of the buffered AS solution in the glass chamber was sufficient to maintain steady state conditions during the time of measurements. This allowed for replicate measurements with the same solution formulation. The increase in emissions with increasing solution volume is probably a result of decreasing headspace volume and subsequent increase in air exchange rate within the chamber at fixed flow rates.

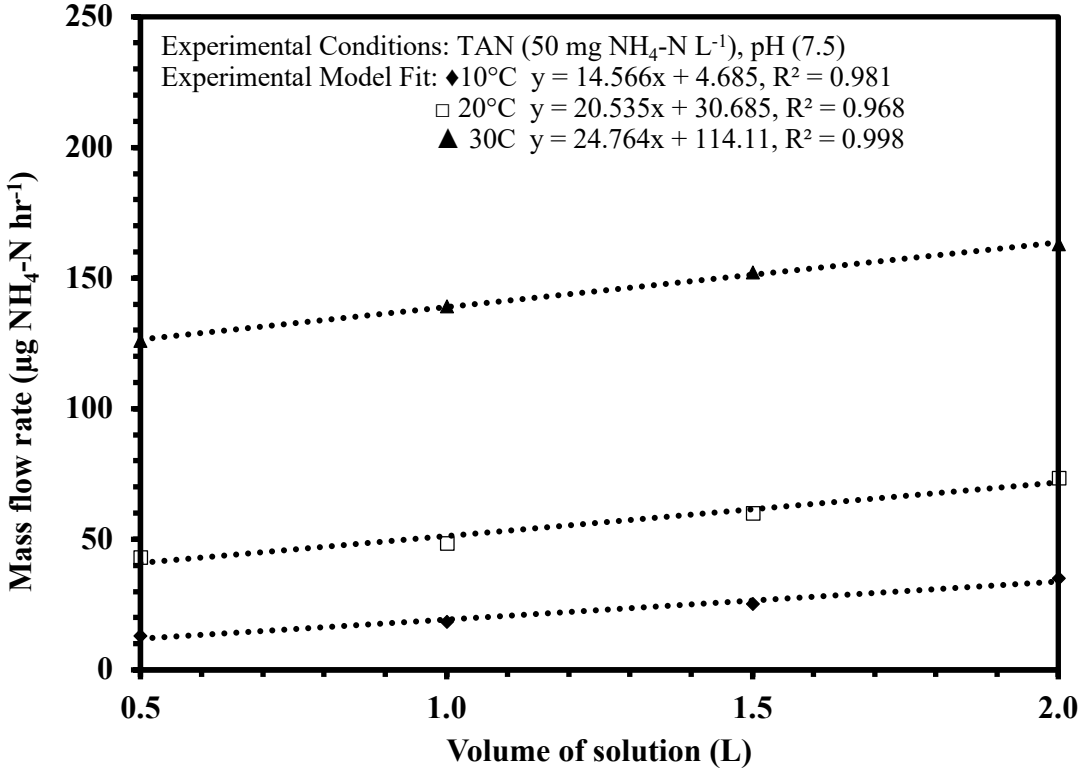

Figure 1.6. Ammonia release from ammonium sulfate (AS) prepared in phosphate buffered solution (0.1 M) as a function of volume of solution within the chamber and temperature, ambient air has been used for inlet air through the chamber. Experimental condition in absence of bicarbonate: TAN (50 mg NH_4-N L^{-1}, pH 7.5, and air flowrate 6 LPM. Dashed lines represent linear regression models at different temperatures.

2.3.3 Influence of Temperature

Figure 1.7 shows the increase in NH_3 emission with temperature from buffered AS solution containing 50 mg NH_4-N L^{-1}. Loss of NH_3 as a function of temperature followed the well-known exponential relationship across the temperature range tested. No condensation of water vapor was observed within the headspace of the glass chamber at either limit of the range of temperatures evaluated. The measured flux of NH_3 increased exponentially with temperature from 2 L of AS from 1.42 at 0.5°C to 14.53 mg m^{-2} hr^{-1} at 35°C. Our results are consistent with observations by Velek and Stumpe (1978), who reported that NH_3 loss from 10 mg L^{-1} N

solution increased exponentially with temperature from approximately 0 at 0°C to nearly 20 mg N/100 cm^{-2} hr^{-1} at 46°C.

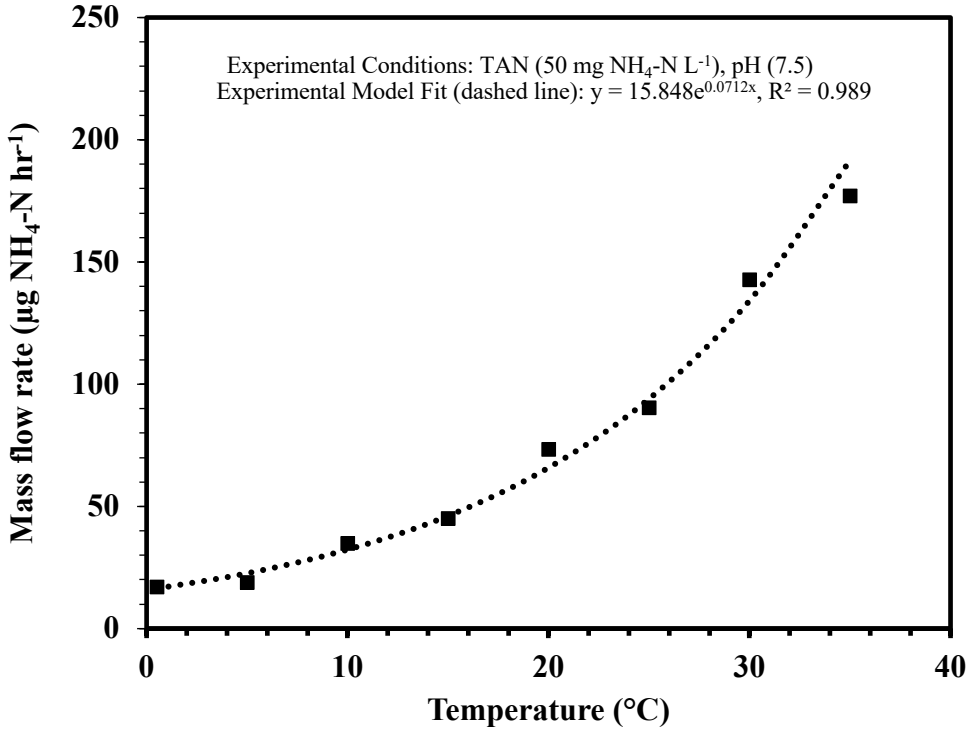

Figure 1.7. Ammonia release from ammonium sulfate (AS) prepared in phosphate buffered solution (0.1M) as a function of temperature, ambient air has been used for inlet air through the chamber. Experimental condition in absence of bicarbonate: TAN (50 mg NH_4-N L^-), pH 7.5, air flowrate 6 LPM, and volume of solution 2 L. Dashed lines represent exponential regression model.

2.3.4 pH and Temperature

Figure 1.8 illustrates, the mass of NH_3 emitted from the AS solutions varied with changes in buffer pH (5.5-8.5) and temperature (10-30°C) using our experimental setup. The TAN concentration of the AS solution was 50 mg L^{-1}. Loss of NH_3 from the AS solution was anticipated to increase exponentially with solution temperature. TAN concentration and pH before and after the experiment duration showed little or no change as the mass of NH_3 lost was not enough to significantly alter total mass of NH_4-N in solution. The NH_4^+/NH_3(aq) relationship

therefore remained constant. During this experiment, manual measurements of temperature revealed the temperature control of the solutions within + /-0.1°C.

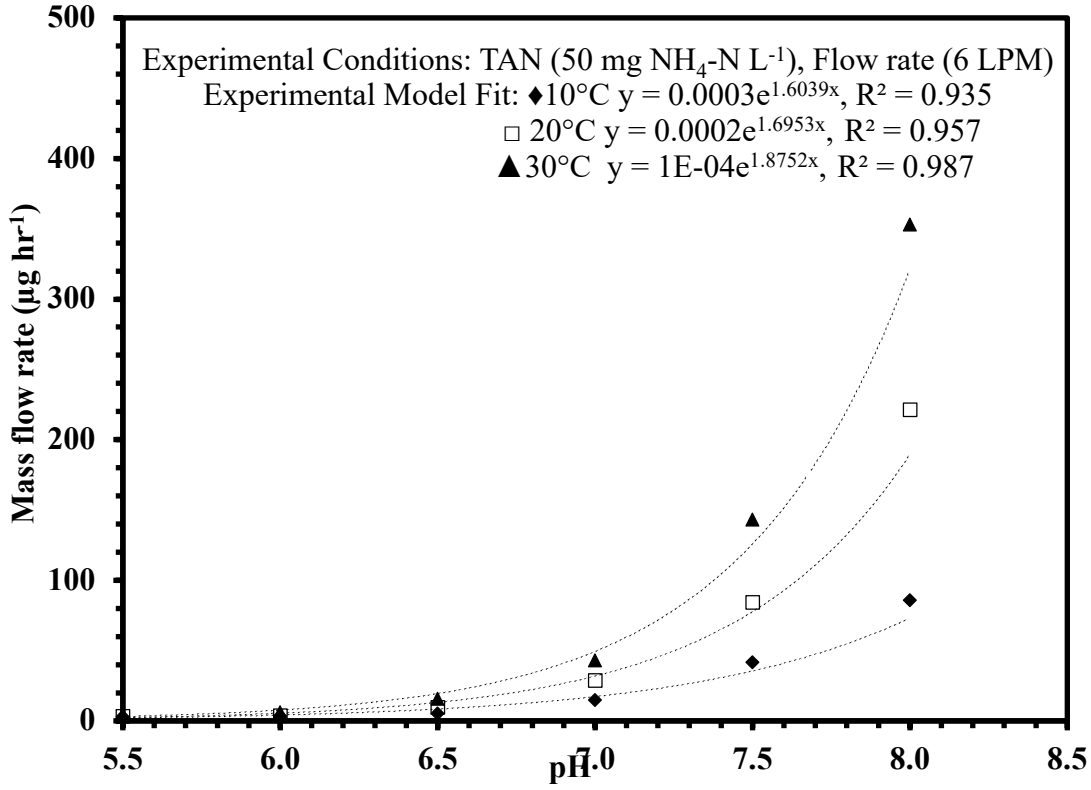

Figure 1.8. Measurements of NH_3 release from ammonium sulfate (AS) prepared in phosphate buffered solution (0.1M) as a function of temperature and pH, ambient air has been used for inlet air through the chamber. Experimental conditions in absence of bicarbonate: TAN 50 mg NH_4-N L^{-1}, air flow rate 6 LPM, and volume of solution 2 L. Dashed lines represent exponential models at different temperature.

The performance of our experimental setup was sufficient to assess NH_3 emission from aqueous solutions. The acceptable range for just TAN in absence of bicarbonate is 5.0-250 mg NH_4-N L^{-1}. The standard parameters chosen to assess the potential impact of bicarbonate on enhancing NH_3 emissions from aqueous solutions were pH 7.5, temperature at 20°C, air flow rate at 6 LPM, and 2 L volume of solution.

2.4. Ancillary Measurements

We stored all denuder extracts at 4ºC until analysis via a flow injection analyzer (Lachat, Quick-Chem 8000, QuikChem Method 10-107-06-2-A- Ammonia in surface water, wastewater 0.10 to 5.0 mg N L^{-1} as NH_3). Pure ammonium sulfate (AS) (ACROS, ORGANICS) solutions and sodium bicarbonate (ACS, Fisher Scientific) were prepared at different concentrations in the presence of a phosphate buffer solution. Additions of AS or sodium bicarbonate were made either from concentrated stock solutions or weighed amounts of solid to a known volume of buffer solution. The pH buffer solutions were prepared using 0.1 M Na_2HPO_4 (ACS, Fisher Scientific) and 0.1 M KH_2PO_4 (ACS, Fisher Scientific). The pH of the final test solution was then checked and adjusted with acid or base as needed to obtain the desired buffer pH value using a pH meter and combination glass electrode (Mettler Toledo) calibrated with NIST-traceable pH standards. Emissions of NH_3 were not measured while the pH of the 2 L of TAN solution was adjusted

For all tests, two denuder tubes in series were used and flux calculations were carried out over a certain time period. The mass of ammonia collected by both tubes was used for the flux calculation in one experiment when the influence of the initial NH_4^+-N concentration was studied in the presence and absence of bicarbonate. Flux calculations for other parameters was based exclusively on the mass of the first denuder tube. In these experiments, the initial NH_4^+-N concentration was 50 mg L^{-1} and the collected mass of NH_3 from the second tube was close to the blank readings. In the study, ambient air was used for inlet air through the chamber to characterize the effect of pH, temperature, solution volume and air flow rate on NH_3 emissions. Zero air was supplied at the chamber inlet to measure NH_3 release in the absence and in presence of bicarbonate.

2.5. Statistics

We used IGORPro® software (WaveMetric, Inc.) for fitting nonlinear standard curves from the Lachat system. Microsoft® Excel software (version 16.22) was used for all statistical analyses. VisualMinteq Version 3.1 was used to calculate the concentration of aqueous inorganic C species as a function of pH and initial HCO_3^- concentrations in test solutions. All constants for the chemical reactions in the discussion section were taken from Stumm and Morgan (1995).

3. Results

3.1. Ammonia Release in Absence of Bicarbonate

Figure 1.9 shows ammonia emissions from pure AS solution as a function of TAN concentration in phosphate buffered solution (0.1M; pH 7.5) in absence of bicarbonate at constant temperature (20°C) in presence of zero air. The emitted NH_3 increases approximately linearly with change in TAN (5-1000 mg NH_4-N L^{-1}). The linear regression equations for the measured NH_3 release as a function of the TAN concentration for the overall range of concentration and lower portion of concentration (5-100 mg NH_4-N L^{-1}) are presented in Eq (1.5) and (1.6), respectively,

TAN: 5-1000 mg NH_4-N L^{-1} $y = 0.74\ (\pm 0.02)x + 15\ (\pm 7.1)$ (1.5)

TAN: 5-100 mg NH_4-N L^{-1} $y = 0.99\ (\pm 0.02)x + 0.6\ (\pm 1.4)$ (1.6)

where y is the measured NH_3 release (μg NH_3-N hr^{-1}) and x is TAN (mg NH_4-N L^{-1}). The overall result of a linear regression is shown in Fig. 1.9A, where the denuder efficiency declines to 89% TAN (5-1000 mg L^{-1}) (Table 1.1). Fig. 1.9B shows a lower portion of the curve from Fig. 1.9A, where the range over denuder efficiency is greater than 99% at concentrations of TAN < 200 mg L^{-1}. The slope of Eq. 1.6 is essentially one and the intercept brackets zero (0.6 ±1.4) with an $R^2 = 0.999$. Figure 1.9B demonstrates that when pH, temperature and flow-rate are

tightly controlled, release of NH_3 from an aqueous solution is linear and a direct function of TAN. Changes in slope, therefore, can be used to measure any enhancement in emissions due to the presence of bicarbonate.

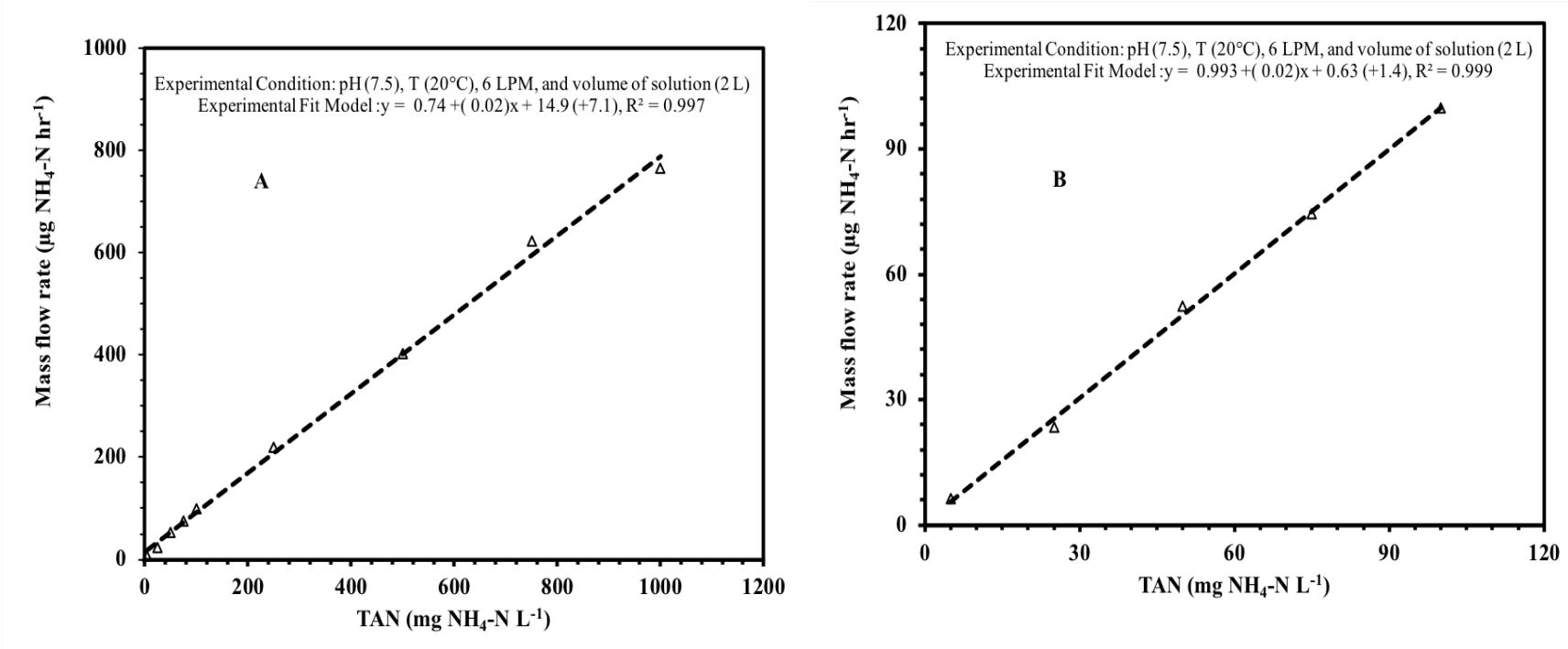

Figure 1.9. Measurement of NH_3 release from buffered AS solutions prepared in phosphate buffered solution (0.1M) as a function of TAN, zero air was used to flush the chamber. Experimental conditions: TAN concentration: A (5-1000 mg NH_4-N L^{-1}), B (5-100 mg NH_4-N L^{-1}), temperature (20°C), pH (7.5), airflow rate (6 LPM), and volume of solution (2 L). Dashed line represents linear regression model. The mass of NH_3 collected by the paired denuder tubes was combined for the final calculation of an integrated NH_3 flux.

As noted, Eq. 1.6 has slope of ~ 1 within experimental uncertainty. This is 1 μg NH_3 per hour per unit of TAN. So, if TAN = 60 mg NH_4-N L^{-1}, the system is emitting 60 μg NH_3-N per hour. Since the airflow rate is 6 LPM, an estimate of an integrated NH_3 concentration that would deliver 60 μg NH_3 in one hour is (60 μg/0.36 m^3 = 167 μg m^{-3}). As noted, the slope actually decreases at higher TAN due to loss of denuder efficiency, thus technically it is possible to derive an average maximum NH_3 concentration expressed as μgNH_3 m^{-3} above which the denuder system is no longer ~ 100% efficient (Table 1.2). The mass of NH_3 collected by the paired denuder tubes was combined for the final calculation of an integrated NH_3 flux observed over set period of time. At NH_4^+ concentration, 5-250 mg NH_4-N L^{-1}, the NH_3 collected in the second tube was similar to the blank reading; no breakthrough was detected. The breakthrough was assessed at higher concentration (500-1000 mg NH_4-N L^{-1}), and the %E decreased to ~89%.

Table 1.2. Average NH_3 concentration expressed as μgNH_3 m^{-3} as a function of TAN when the denuder system is assumed to be operating at ~ 100% efficiency. Zero air was used to flush the chamber.

TAN (mg NH_4-N L^{-1})	First denuder (μg m^{-3})	Efficiency %	RSD (%)
5	16	91.7	1.2
25	64	97.8	5.4
50	144	99.3	1.6
75	206	99.2	0.1
100	276	99.5	0.5
250	609	99.9	6.8

3.2. Impact of Bicarbonate on NH_3 Emissions – Initial Observations

The mass of NH_3 collected per unit time in a well buffered phosphate solution (0.1M) as a function of TAN in the presence of bicarbonate (HCO_3^-) is presented in Fig. 1.10. The linear regressions through the observed data are listed in Eq. 1.7 and 1.8,

For 200 mM HCO_3^- $y = 1.4\ (\pm 0.04)x + 30\ (\pm 10.4)$ (1.7)

For 400 mM HCO_3^- $y = 1.6\ (\pm 0.1)x + 59\ (\pm 1.6)$ (1.8)

where y, and x are defined as for eq (1.5) and (1.6). The magnitude of the measured NH_3 ($\mu g\ hr^{-1}$) differed significantly from the observed pure AS solutions. As indicated by the slope in equations 1.7 and 1.8 versus equation 1.5 and 1.6, the calculated NH_3 emission from 200 and 400 mM HCO_3^- are 1.9 and 2.2 times higher than emissions from pure AS solution at the same pH (7.5) and T (20°C).

Figure 1.10B shows a lower portion of the curve from Fig 1.10A, where the range over denuder efficiency is greater than 99% at concentration of TAN < 200 mg L^{-1}. The linear regressions through the observed data are listed in equations 1.9 and 1.10. Because of resulting slopes, the average efficiency (> 99%) of denuder would be reduced over range of TAN. The calculated uncertainty associated with the intercept in Equations 1.9 and 1.10 are closer to zero, where the efficiency of denuders in collection of ammonia are in the range of > 99%.

For 200 mM HCO_3^- $y = 1.7\ (\pm 0.15)x + 9.5\ (\pm 8.9)$ (1.9)

For 400 mM HCO_3^- $y = 2.5\ (\pm 0.07)x + 1.7\ (\pm 4.1)$ (1.10)

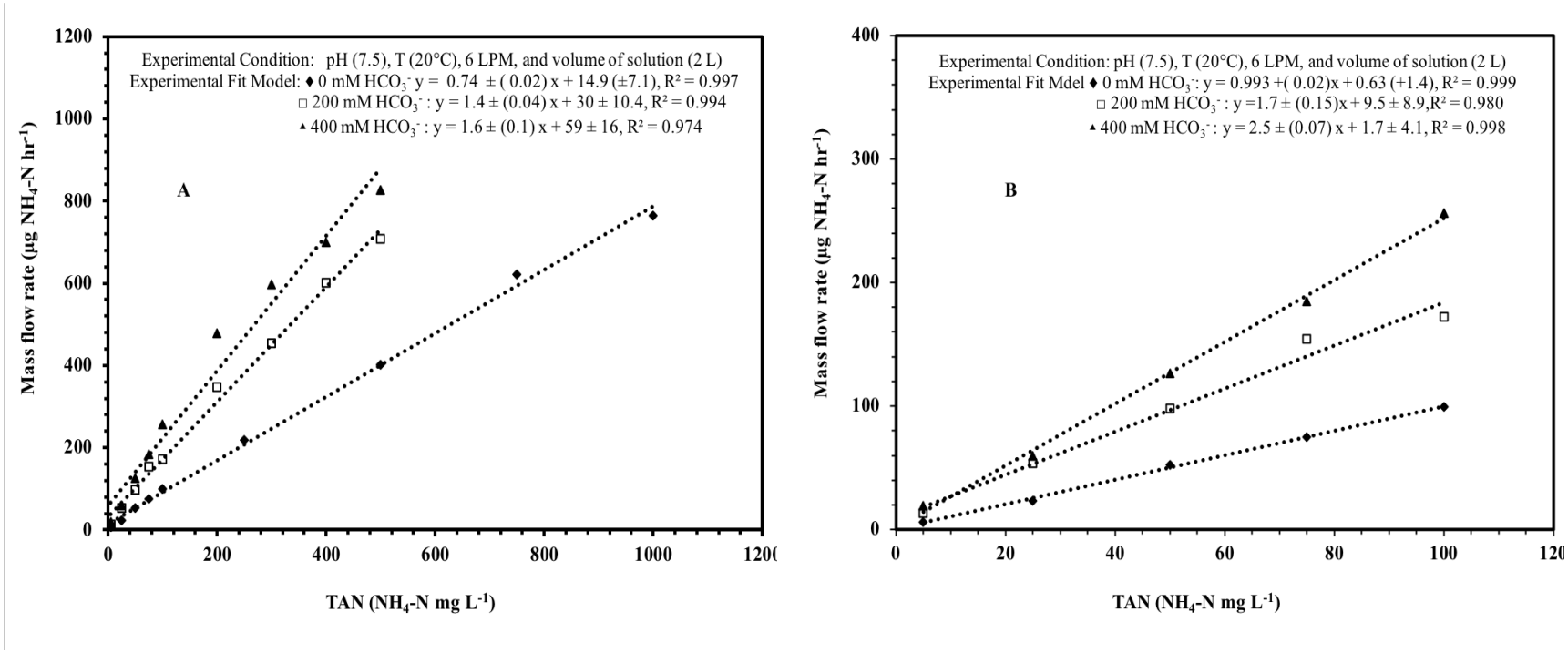

Figure 1.10. Comparison of ammonia release from buffered AS solutions in presence (initial concentration of HCO_3^- is 200 mM and 400 mM) and absence HCO_3^-. Experimental conditions: pH 7.5, temperature 20°C, air flow rate 6 LPM, volume of solution 2 L, zero air was used to flush the chamber. The mass of NH_3 collected by the paired denuder tubes was combined for the final calculation of an integrated NH_3 flux. Dashed lines represent the respective linear regression models.

NH_3 emissions increased significantly in the presence of HCO_3^- (Eq. 1.9 and 1.10). The change in slope is much greater than in the absence of HCO_3^- (Eq. 1.7 vs. Eq.1.5). Breakthrough for the first denuder tube appears to start at a mass flow of 440 μgNH_4-N hr^{-1} (Fig.1.11). The apparent enhancement in emissions by HCO_3^- means the effective average NH_3 concentration at lower TAN values is higher than in the absence of bicarbonate. Thus, it becomes more problematic that the appearance of NH_4-N in the second denuder tube, which serves as the indication of breakthrough in the first tube, is in fact a quantitative measurement of NH_4-N passing through the first denuder tube. As such, the second denuder tube only helps to verify that breakthrough has occurred.

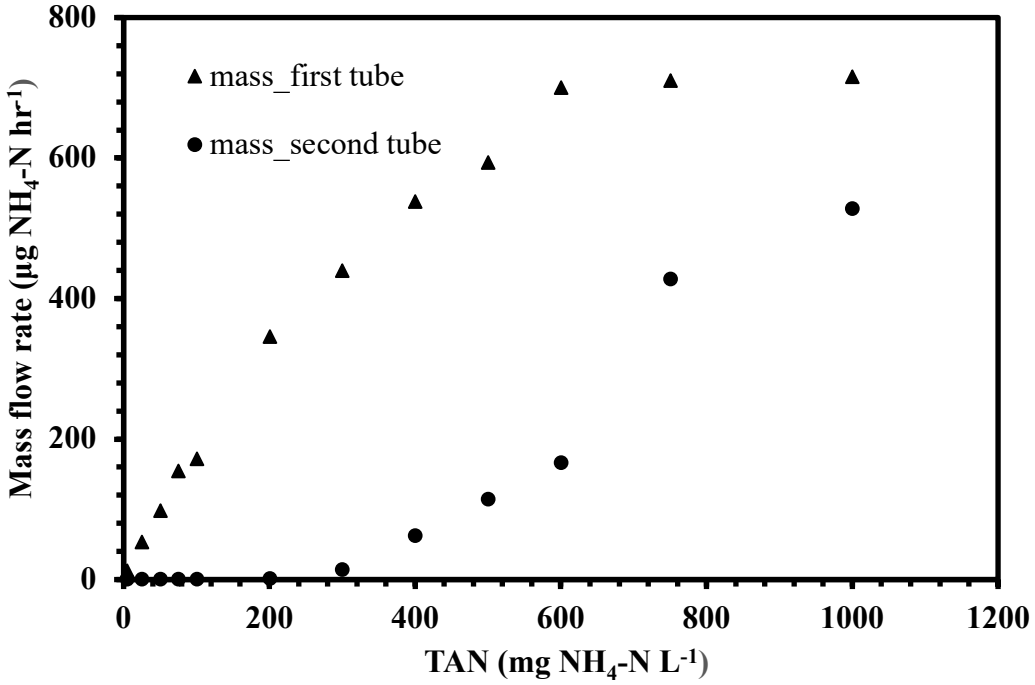

Figure 1.11. Measurement of NH_3 release from ammonium sulfate (AS) prepared in phosphate buffered solution (0.1M) using paired denuder tubes as a function of ammonium concentration in presence of bicarbonate (initial concentration of HCO_3^- is 200 mM), zero air was used to flush the chamber. Experimental conditions: TAN 5-1000 mg NH_4-N L^{-1}, air flow rate 6 LPM, pH 7.5, temperature 20°C, and volume of solution 2 L.

The average efficiencies of the denuders for ammonia in the presence of bicarbonate (200 mM) as a function of TAN concentrations is shown in Fig. 1.12. The first denuder tube was found to have 99.9% collection efficiency at concentration 5-300 (mg NH_4-N L^{-1}), 82% at 400-600 (mg NH_4-N L^{-1}), and 33% at 700-1000 (mg NH_4-N L^{-1}).

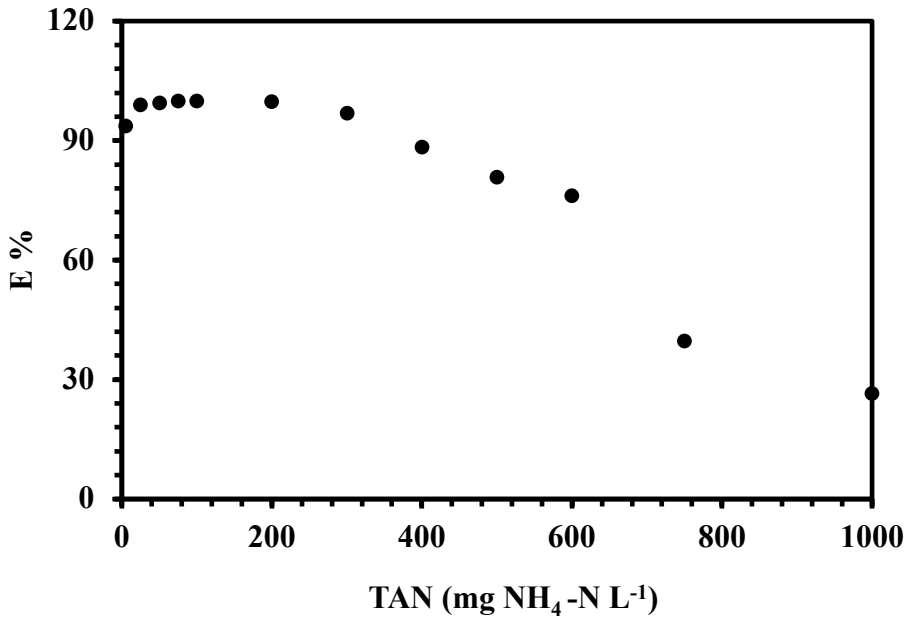

Figure 1.12. The average efficiencies of denuders for NH_3 release from ammonium sulfate (AS) prepared in phosphate buffered solution (0.1M) in presence of bicarbonate (initial concentration of HCO_3^- is 200 mM), zero air was used to flush the chamber. Experimental conditions: TAN 5-1000 mg NH_4-N L^{-1}, pH 7.5, temperature 20°C, air flow rate 6 LPM, and volume of solution 2 L. Collection efficiency was calculated on the first denuder tube.

3.3. Impact of Variable Bicarbonate Concentrations on NH_3 Emissions

Results for testing different concentrations of total inorganic carbon species (TIC) (10-400 mM) on enhancement of NH_3 emissions at initial TAN (5-100 mg L^{-1}) are presented in Fig. 1.13. The results in Fig. 1.13 indicate that the presence of HCO_3^- enhanced NH_3 emissions from buffered AS solutions, but the potential enhancement in NH_3 emissions was detected only when the initial bicarbonate concentrations were greater than 100 mM (1.13A). Any enhancement at

less than an initial concentration of 100 mM HCO_3^- was minor and similar in magnitude to our experimental error (Fig.1.13B).

In this experiment, the addition of HCO_3^- represents the addition of base to the TAN solutions. The sequential increases in initial HCO_3^- additions resulted in eventually overwhelming the buffer capacity of the 0.1M phosphate background matrix. A relatively small amount of acid was needed to adjust the solution pH back to 7.5 when the initial target concentration of HCO_3^- was less than 100 mM HCO_3^-. Above this target initial HCO_3^- concentration, it was necessary to add substantially more acid to lower the pH back to 7.5. As noted in the Materials and Methods section, this adjustment in pH back to 7.5 after initial addition of HCO_3^- was performed before measurements of NH_3 emissions were initiated.

Addition of initial HCO_3^- concentrations of 200 or 400 mM to the 0.1M buffer solution resulted in pH values equal to or greater than 8.5. Thus, adjusting the pH of the solution back to pH 7.5 meant that at the higher HCO_3^- concentrations the buffer solution was supersaturated with respect to the target buffer pH for the experiment. In other words, the solution would continue to degas ($HCO_3^- + H^+ \leftrightarrow CO_2 \uparrow + H_2O$) in response to the 0.1M phosphate buffer holding the pH constant at ~ 7.5. Use of zero air at the chamber inlet would only act to further this reaction as the effective partial pressure of CO_2 was forced toward zero. The observed enhancement in NH_3 emissions, therefore, appeared to be directly related to the loss of CO_2 across the air-liquid interface and not due to the presence of excess HCO_3^- increasing the bulk solution pH.

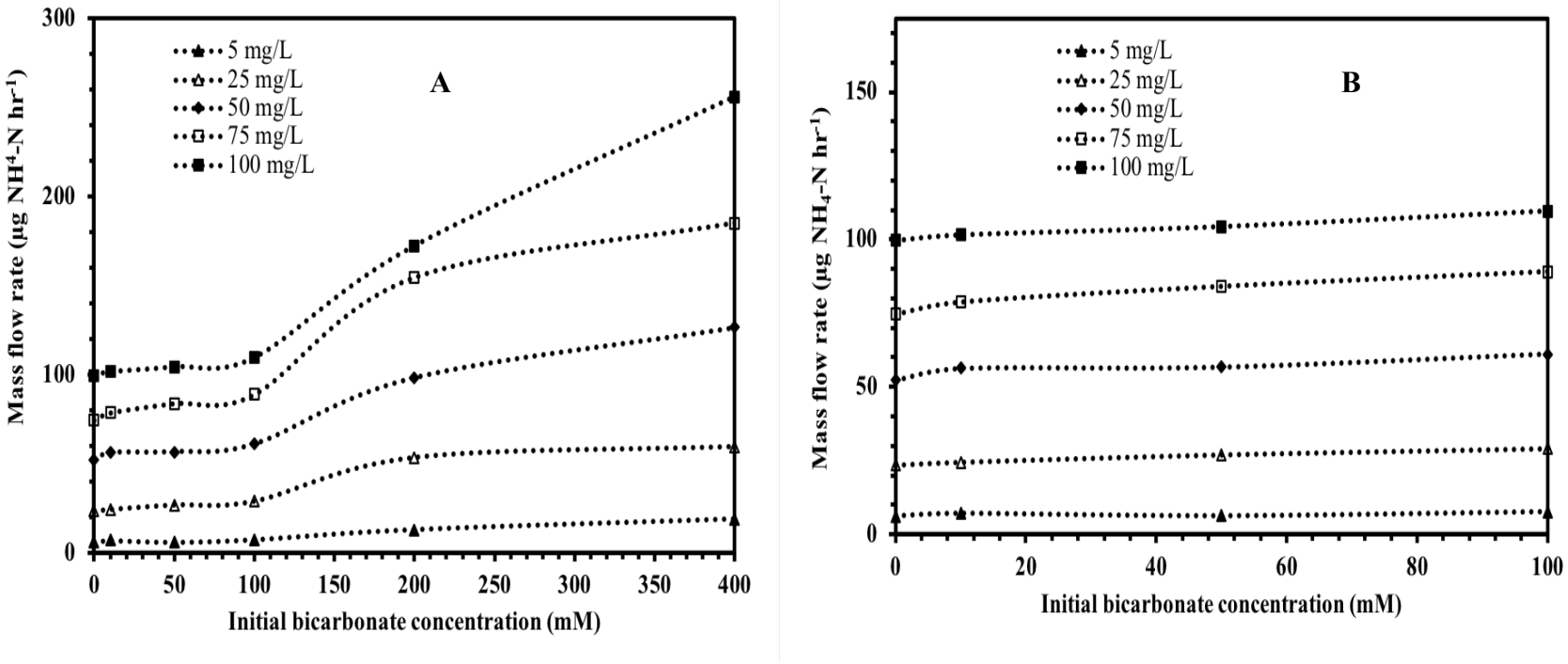

Figure 1.13. Measurement of NH_3 release from ammonium sulfate (AS) prepared in phosphate buffered solution (0.1M) spiked with $NaHCO_3$ as a function of ammonium concentration, zero air flowing through the chamber was used. Experimental conditions: TAN 5-100 mg NH_4-N L^{-1}, air flow rate 6 LPM, pH 7.5, temperature 20°C, volume of solution 2 L, initial HCO_3^- concentration: A: (10-400 mM), B: (0-100 mM). The mass of NH_3 collected by the paired denuder tubes was combined for the final calculation of an integrated NH_3 flux observed over set period of time. Dashed lines are added to better visualize trends in NH_3 emissions.

The experiment was repeated using a phosphate buffer concentration of 1M and a single TAN concentration (Fig. 1.14). The factor of 10 increase in the buffer capacity of the solution matrix was sufficient to accommodate the addition of HCO_3^- and the solution pH remained at 7.5 requiring no further addition of acid. As illustrated in Fig. 1.14, there was no or very modest enhancement in NH_3 emissions across the range in initial HCO_3^- concentrations, even though the solutions were technically super-saturated with HCO_3^- at pH 7.5. This suggested that conditions favoring the enhancement in NH_3 emissions observed using the 0.1M phosphate buffer due to the loss of CO_2 across the air-liquid interface were overwhelmed by the additional buffer capacity of the 1M phosphate concentration. Alternatively, the factor of 10 increase in buffer capacity of the 1M phosphate solution was sufficient to force the loss of CO_2 from solution to equilibrium before the start of the measurement of NH_3 emissions, or the continued loss of CO_2 was minimal compared to the comparable conditions with the 0.1M phosphate buffer solutions.

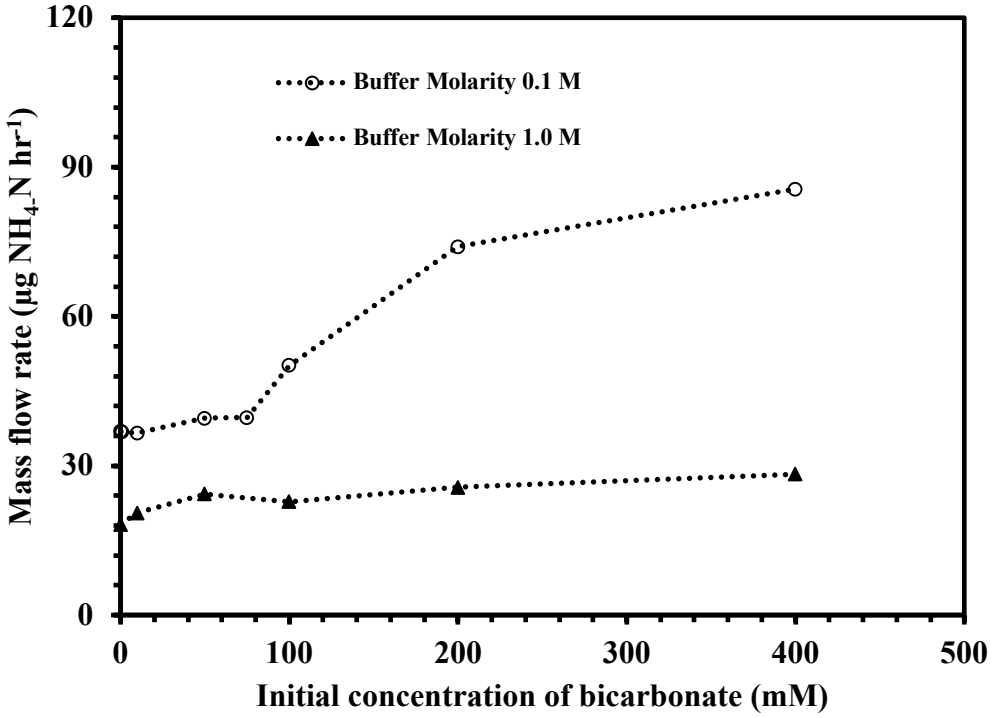

Figure 1.14. Ammonia release from ammonium sulfate (AS) prepared in phosphate buffered solution at two different molarity (0.1 and 1.0 M) in presence of initial HCO_3^- concentration (10-400 mM), zero air was used to flush the chamber. Experimental condition: TAN (50 mg NH_4-N L^{-1}), pH 7.5, and volume of solution 2 L. The mass of NH_3 collected by the paired denuder tubes was combined for the final calculation of an integrated NH_3 flux observed over set period of time. Dashed lines are added to better visualize trend in NH_3 emissions.

4. Discussion

The chamber combined with annular denuder technology used in this research has demonstrated that enhanced NH_3 emissions from buffered ammonium sulfate solutions in the presence of HCO_3^- is possible when solution pH solution is controlled at 7.5. The following chemical reactions characterize the phosphate buffer used in this study:

$$H_3PO_4 \leftrightarrow H_2PO_4^- \qquad \text{-log K = 1.86} \qquad (1.16)$$

$$H_2PO_4^- \leftrightarrow HPO_4^{2-} \qquad \text{-log K = 7.2} \qquad (1.17)$$

$$HPO_4^{2-} \leftrightarrow PO_4^{-3} \qquad \text{-log K =11.5} \qquad (1.18)$$

The only species of relevance are HPO_4^{-2} and $H_2PO_4^-$ as expressed through Eq. 1.17. In this study, the total phosphate concentration was 0.1M. At pH 7.5, this results in concentrations of HPO_4^{-2} and $H_2PO_4^-$ of 0.056 and 0.012M, respectively. The concentration of 0.1M phosphate buffer proved effective in controlling pH for several hours across the range in TAN tested. For example, at TAN 100 mg NH_4-N L^{-1}, if we assume all of the TAN is NH_4^+, the resulting concentration of NH_4^+ is 0.0056 M. This represents the upper limit of the amount of H^+ that could be generated assuming 100% conversion of NH_4^+ to $NH_{3(g)}$. At the buffer concentration of 0.1M, 100% loss of TAN in solution as $NH_{3(g)}$ would only result in conversion of 0.0056M of HPO_4^-, or a change of only ~ 9 % in the conversion of HPO_4^{-2} to $H_2PO_4^-$. However, at TAN concentrations near 1000 mg NH_4-N L^{-1}, the impact on pH from NH_3 emissions may have been sufficient to shift pH slightly lower via Eq. 1.17. Slightly lower pH would lower NH_3 emissions which may explain in part the non-linearity observed in Fig. 1.4. Small changes in pH have a significant impact on NH_3 loss between pH 7 and 7.5 (Fig. 1.8). However, overall the measured pH did not change over the several hours of NH_3 emission measurements reinforcing the conclusion that the amount of NH_3 lost did not significantly change the overall ratio of HPO_4^{-2} to $H_2PO_4^-$ in solution.

If the solutions used in this research were allowed to come to equilibria with the partial pressure of CO_2 in the atmosphere (~ 0.0004 atmospheres), then the concentration of HCO_3^- in solution would be ~0.25 mM at the ionic strength represented by the 0.1M phosphate buffer solution. Any HCO_3^- present above this concentration means that the solution was super-saturated with respect to CO_2. The initial HCO_3^- concentrations used in this study ranged from 10-400 mM, or the initial degree of supersaturation of the solutions with respect to bicarbonate ranged from 40-1600x that expected at pH 7.5, when in equilibrium with the atmosphere. The

degree of supersaturation was further exaggerated by introducing zero air at the inlet of the chamber effectively trying to lower the partial pressure of CO_2 in the head space within the chamber to zero. As such, the experimental conditions used in this study were designed to promote CO_2 emissions of varying degrees to the extent possible while at the same time controlling the bulk solution pH. This differs from previous studies where the enhancement of HCO_3^- on NH_3 emissions was clearly due to the increase in pH of unbuffered systems. The design of this study created non-equilibrium conditions (use of zero air at the inlet of the chamber) even after addition of acid following the initial addition of HCO_3^- to adjust the solution pH back to 7.5. At sufficient relative supersaturations of HCO_3^- in solution (apparently at initial concentrations of 100mM HCO_3^- or greater), there was sufficient CO_2 loss after adjustment back to pH 7.5 to result in the enhancement of NH_3 emissions (Fig. 1.13).

This work was designed in part to imitate natural systems where CO_2 concentrations within the bulk matrix exceed the partial pressure of the ambient atmosphere. This can occur in soils as a result of root and microbial respiration and decreased soil diffusivity (Hanson et al., 2000; Kuzyakov, 2006; Lalonde and Prescott, 2007; Kuzyakov, 2010). Swine lagoon slurries represent another example where CO_2 emissions are a direct function of respiration by the large microbial activity density within the water column and in the bottom sludge. The degree of emissions is a function of temperature, but they are always present unless temperatures drop sufficiently to effectively stop respiration. The loss of CO_2 is not enough to drive bulk pH changes since other reactions can buffer the bulk pH, especially in systems like swine lagoon slurries. Based on the results from this study, the continued loss of CO_2 at the air-liquid interface may enhance NH_3 emissions, depending on the rate of CO_2 lost (related to the degree of super-saturation) and the total amount of TAN present (Fig. 1.13).

The relationship between TAN and relative degree of super-saturation with respect to CO_2 was further investigated by replotting the data in Fig. 1.13 relative to expected NH_3 emissions in the absence of HCO_3^- (Fig. 1.15). The data suggest that there was some enhancement in emissions starting at initial HCO_3^- concentrations of ~ 100 mM. From ~ 100 mM to ~ 400 mM initial HCO_3^- concentration the effect on enhanced NH_3 emissions was varied, although it became somewhat more uniform at the highest concentration of HCO_3^-. Up to ~ 400 mM initial HCO_3^- concentration, however, there appeared to be a definite inverse relationship with TAN. The enhancement of NH_3 emissions was most pronounced at the lowest TAN concentration used in the study (TAN 25 mg L^{-1}). Assuming the results in Fig. 1.15 are not simply due to experimental variation, the data suggest the loss of NH_3 from solution in the presence of HCO_3^- may be via several reactions. One reaction may include the loss of CO_2, while the other may be due to the hydrolysis reaction involving only NH_4^+ and $NH_{3(aq)}$. The inverse dependence with TAN may reflect an upper limit on the degree of enhancement possible from the loss of CO_2, such that with increasing TAN, a greater percentage of NH_3 is lost via a reaction independent of CO_2 emissions. However, as the relative degree of supersaturation with respect to CO_2 increases, a single reaction dominates the loss of NH_3 from solution, irrespective of the concentration of TAN present.

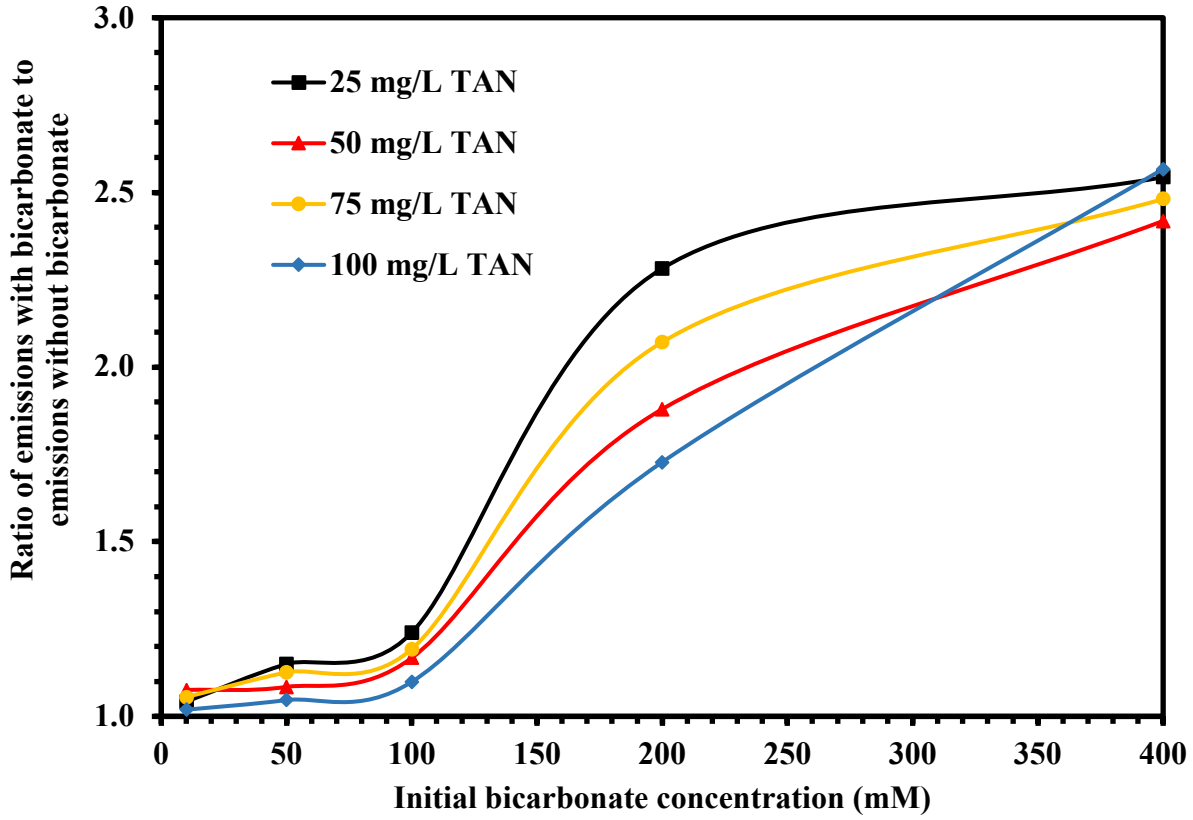

Figure 1.15. Measurement of NH_3 release from ammonium sulfate (AS) prepared in phosphate buffered solution (0.1M) spiked with $NaHCO_3$ as a function of TAN concentration when zero air was used to flush the chamber. Experimental conditions: TAN 5-100 mg NH_4-N L^{-1}, air flow rate 6 LPM, pH 7.5, temperature 20°C, and volume of solution 2 L, initial HCO_3^- concentration: 0-400 mM. The mass of NH_3 collected by the paired denuder tubes was combined for the final calculation of an integrated NH_3 flux observed over set period of time. Lines are added to better visualize trends in NH_3 emissions.

4.1 Potential Mechanisms for NH_3 Emissions

Several possible mechanisms for the enhancement of NH_3 emission from the buffered AS solutions used in this study were explored. The first involves no direct interaction between CO_2 emissions and NH_4^+/NH_3 in solution. The necessary equilibrium reactions that are part of this mechanism are (assumed ionic strength = 0.5M):

$$NH_4^+ + H_2O \leftrightarrow NH_{3(aq)} + H_3O^+ \qquad \log K = -9.4 \qquad (1.19)$$

$$NH_{3(aq)} \leftrightarrow NH_{3(g)} \qquad \log K_H = -1.76 \qquad (1.20)$$

$$HPO_4^{2-} + H^+ \leftrightarrow H_2PO_4^- \qquad \log K = 7.2 \qquad (1.21)$$

These are then combined to yield:

$$NH_4^+ + HPO_4^{2-} \leftrightarrow NH_{3(g)} + H_2PO_4^- \qquad \log K = -3.96 \qquad (1.22)$$

As shown in Fig. 1.9, the emission of NH_3 increased linearly with increasing concentrations of TAN for pure buffered AS solutions. This corresponds with Eq. 1.22 and the assumption that the Henry's Law coefficient is indeed constant as the concentration of dissolved $NH_{3(aq)}$ in solution varies. The linearity in NH_3 emissions in Fig. 1.9A (5-1000 mgNH_4-N L^{-1}) and 1.9B (5-100 mgNH_4-N L^{-1}) further support the assumption regarding the Henry's Law coefficient. By the mechanism described in Eq. 1.22, the change in NH_3 emissions with increasing TAN in Fig. 1.9 is driven exclusively by variations in dissolved $NH_{3(aq)}$ concentrations close the air-liquid interface. The concentration of $NH_{3(aq)}$ in turn is driven by the concentration of NH_4^+. The dependence on the partial pressure of NH_3 (pNH_3) on the NH_4^+ concentration is shown by rearranging Eq. 1.22:

$$pNH_3 = 1.09\ x\ 10^{-4} \left(\frac{[HPO_4^{-2}]}{[H_2PO_4^-]}\right) x\ [NH_4^+] \qquad (1.23)$$

According to Eq. 1.23, NH_3 emissions from the buffered AS solutions are a direct function of TAN (NH_4^+ + $NH_{3(aq)}$). The ratio of $[HPO_4^{-2}]$/$[H_2PO_4^-]$ is held constant at a value of pH 7.5. Thus, pNH_3 is directly dependent on TAN and emissions should reveal a linear relationship. Implicit in Eq. 1.23, is the assumption that the ratio of $[HPO_4^{-2}]$/$[H_2PO_4^-]$ is constant within the thin water layers close to the air-liquid interface and that there is rapid communication with the bulk solution such that the ratio is held constant.

A mechanism demonstrating the potential enhancement in NH_3 emissions due to CO_2 emissions can be approached in a similar fashion. The equilibria concerning $CO_{2(g)}$ and HCO_3^- in solution can be expressed as follows:

$$CO_{2(g)} + H_2O = H_2CO_3^* \qquad \log K = -1.5 \qquad (1.24)$$

$$H_2CO_3^* = H^+ + HCO_3^- \qquad \log K = -6.3 \qquad (1.25)$$

The term $H_2CO_3^*$ represents both $CO_{2(aq)}$ and H_2CO_3 in solution, with the acknowledgement that the conversion of $CO_{2(aq)}$ to $H_2CO_3^*$ is a rate limiting step and represents a modest fraction of the actual amount of dissolved $CO_{2(aq)}$ present. Combing Eq. 1.24 and 1.25 yields the desired relationship between the partial pressure of CO_2 and the concentration of HCO_3^- in solution.

$$CO_{2(g)} + H_2O = H^+ + HCO_3^- \qquad \log K = -7.8 \qquad (1.26)$$

Equation 1.26 in turn can be combined with Eq. 1.21 to substitute the phosphate buffer reaction for the concentration of H^+:

$$CO_{2(g)} + H_2O + HPO_4^{2-} = HCO_3^- + H_2PO_4^- \qquad \log K = -0.6 \qquad (1.27)$$

Rearrangement of Eq. 1.27 to solve for the partial pressure of CO_2 (pCO_2; equation not shown) illustrates that pCO_2 is a direct function of HCO_3^- concentration as long as pH is held constant.

A mechanism involving both pCO_2 and pNH_3 and be derived by combining Eqs. 1.22 and 1.27:

$$NH_4^+ + HCO_3^- = CO_{2(g)} + NH_{3(g)} \qquad \log K = -3.36 \qquad (1.28)$$

Rearrangement of Eq. 1.28 yields the desired result for the possible dependence of pNH_3 on both HCO_3^- and pCO_2:

$$pNH_3 = 4.365x10^{-4} \times [NH_4^+][HCO_3^-]/pCO_2 \quad (1.29)$$

Since in this study there was an apparent enhancement in the loss of NH_3 for the same concentration of TAN in the presence of HCO_3^-, the overall reaction should involve a greater free energy than Eq. 1.23. This is apparent in the calculated log K term in Eq. 1.28, although the increase in free energy is not excessive. Equation 1.29 does maintain the linear dependence of pNH_3 on both the concentration of NH_4^+ and HCO_3^-, but a direct dependence on pH is absent. This is not necessarily surprising, as the purpose of the buffered system in this study was to assess NH_3 emissions when the pH in the bulk matrix is held constant. Equation 1.29 does reveal a potential negative feedback mechanism on pNH_3 through the presence of pCO_2. Here, the pCO_2 term is interpreted to mean the pCO_2 concentration immediately at the air-liquid interface. This pCO_2 concentration would in turn be impacted by the turbulence within the chamber (residence time) as well as the overall gradient in pCO_2 moving away from the air-liquid interface. In using zero air at the entrance to the chamber, and a fixed flow rate, an attempt was made to fix the gradient moving away the air-liquid interface to the extent possible. In other words, the pCO_2 at the air-liquid interface would vary primarily as a function of the HCO_3^- present and subsequent reactions in solution, and thus control the gradient moving away from the air-liquid interface. The ratio of $[HCO_3^-]/pCO_2$ in Eq. 1.29 should not necessarily be considered a predictable constant, as multiple steps are involved in various equilibria that have differing rate constants as discussed further below.

The potential existence in solution of Eq. 1.29 does not mean Eq. 1.23 is not active when HCO_3^- is present. It is best to assume both processes are in play, as well as Eq. 1.27, when attempting to explain the actual observations in NH_3 emissions recorded in this study. However, it is also important to remember that the enhanced NH_3 emissions when HCO_3^- was added to the buffered AS solutions represent non-equilibrium conditions. As already noted, the additions of mM concentrations of bicarbonate used in this study resulted in super-saturated conditions in solution with respect to CO_2 to varying degrees. It is assumed that sufficient HCO_3^- was left in solution at certain mM additions of HCO_3^- after adjustment of pH back to 7.5 to result in CO_2 emissions, and that these subsequent emissions lead to enhanced NH_3 emissions (as was documented for the 200 and 400 mM initial HCO_3^- concentrations). Unfortunately, the presence of dissolved inorganic carbon (DIC) was not confirmed in this study during the measurement periods for NH_3 emissions. Thus, interpretation of Fig. 1.13, for example, using Eq. 1.29 should be approached with caution as it is simply not known whether the lack of any relatively significant enhancement in NH_3 emissions at initial HCO_3^- concentrations < 100 mM is due to a lack of CO_2 emissions or not during the measurement periods.

If it can be assumed that CO_2 emissions were present when the initial HCO_3^- concentration was > 100 mM, then Eq. 1.29 can be applied to Fig. 1.15. The presence of super-saturated conditions was sufficient at the initial HCO_3^- concentration of 200 mM to promote some enhancement in NH_3 emissions, but the fraction of emissions via Eq. 1.29 was less than via Eq. 1.23 as TAN increased. This implies possible rate limiting steps suppressed emissions for the amount of HCO_3^- present. According to Eq. 1.28, if one HCO_3^- molecule is consumed in converting NH_4^+ to dissolved NH_3 this generates one H_2CO_3* molecule, which then must be destroyed via a two-step process. There is also competition for HCO_3^- via Eq. 1.27 which may

act to limit the degree of NH_3 enhancement in emissions. It appears that doubling the initial HCO_3^- concentration to 400 mM overcame these restrictions resulting in the same relative enhancement in NH_3 emissions.

The discussion to this point has assumed that the thickness of the aqueous thin-layer near the air-liquid interface was not influenced by the concentration of HCO_3^-, or by gradients in dissolved species in the bulk solution matrix. The bulk solution was stirred during experiments in an attempt to minimize gradients in dissolved species. If it is assumed that the thickness of the thin layer was constant, then the rates of reactions within the thin-layer were controlled by the diffusion rates of the various chemical species including NH_4^+, HCO_3^-, phosphate species, and the rate of transfer of $CO_{2(g)}$ and $NH_{3(g)}$ across the air-liquid interface. It is not known to what extent the various reactions listed in this Discussion may have interacted and impacted the various reaction steps prior to the individual final equations listed (Eqs. 1.23, 1.27 and 1.29).

4.2. Excess pCO_2 in Soil Systems

The experimental conditions in this study used solutions technically super-saturated with respect to the pCO_2 in the ambient atmosphere. As such, this represented systems at non-equilibrium with respect to pCO_2. The extent to which this can occur in soil systems is explored further.

The concentration of CO_2 in the soil atmosphere of forest, pasture and cultivated soils commonly exceeds 30 to 70 times the levels of CO_2 in the atmosphere (Gunn and Trudgill, 1982; Fernandez and Kosian, 1987; Buyanovsky and Wagne, 1983; Parafit et al., 1997). Concentrations of soil carbon dioxide are regulated by the balance between the production and diffusion rates of CO_2, which in turn are a function of moisture content, texture and soil structure. These variables come together to produce temporal (seasonal) and specific variations

in soil CO_2 concentrations (especially related to soil depth) (Fernández and Kosian, 1987; Castelle and Galloway, 1990; Zabowski and Sletten, 1991). The potential for CO_2 degassing in New Zealand pasture soils is exceptionally high as soil CO_2 concentrations commonly occur in the range 25000 to 50000 μL L^{-1} (or 70 to 140 times atmospheric levels of ~ 356 μL L^{-1}) (Parafitt et al., 1997). Levels as high as 12500 μL L^{-1} have been reported in New England spruce and fir forest soils (Fernandez and Kosian, 1987). Castelle and Galloway (1990) observed CO_2 concentrations in a deciduous Virginia forest as high as 14 000 μL L^{-1}. Soil CO_2 in the upper 25 cm of the French rendzina (Durand, 1980) was recorded as up to 8000 μL L^{-1}, and in the Siberian forest chernozem it exceeded 8000 μL L^{-1} (Vugakov and Popova, 1968). Buyanovsky and Wagner (1983) observed CO_2 concentrations up to 70000 μL L^{-1} > 200 times the concentration of atmospheric CO_2 in the cultivated soil. In this study, initial super-saturated conditions with respect to pCO_2 in the atmosphere ranged from 40-1600x, consistent to some degree with actual pCO_2 levels reported in these soil systems.

5.0. Conclusion

Well known parameters that impact NH_3 emissions are pH, temperature, and wind speed, as well as total ammoniacal nitrogen (TAN). Recently, both experimental and modeling data have demonstrated that the presence of bicarbonate (HCO_3^-) can enhance the emissions of NH_3 from aqueous systems (e.g. Lee et al., 2013). Due to the ubiquitous presence of CO_2 in the environment, the subsequent CO_2 – carbonate (CO_3^-) equilibrium may be impacting NH_3 emissions/deposition thought to be controlled only by the parameters listed. The results from this study indicate that our experimental approach is sufficient to assess the potential impact of HCO_3^- on enhancing NH_3 emissions from aqueous buffered solutions at relatively low concentrations of TAN and bicarbonate in solution. However, our data suggest that any potential

enhancement of HCO_3^- on NH_3 emissions in natural systems in equilibrium with ambient atmospheric CO_2 is modest to potentially non-existent, especially at HCO_3^- solution concentrations ≤100 mM.

Further studies should address the processes controlling DIC speciation and CO_2 reactions in the phosphate buffer solutions. Research is still needed to understand further the linkage of CO_2 and NH_3 processes in natural systems, especially soil respiration and photosynthesis. For example, given soil respiration rates, would we expect CO_2 levels within the soils to be significant enough to enhance NH_3 emissions? In that regard, what would we expect to see at the leaf level with respect to interaction between photosynthesis and reduced nitrogen (NH_4^+/NH_3) assimilation versus chemical equilibrium in the leaf apoplast fluid. It is also important to further delineate when such enhancement reactions should be considered in modeling the bi-directional exchange of NH_3 with soils and other environmental surfaces.

REFERENCES

Bash, J.O., E.J. Cooter, R.L. Dennis, J.T. Walker and J.E. Pleim. 2013. Evaluation of a regional air-quality model with bidirectional NH_3 exchange coupled to an agroecosystem model. Biogeosciences 10:1635-1645.

Behera, S.N., R. Betha and R. Balasubramanian. 2013. Insights into chemical coupling among acidic gases, ammonia and secondary inorganic aerosols. Aerosol Air Qual. Res. 13:1282–1296.

Buyanovsky, G.A. and G.H. Wagne. 1983. Annual cycles of carbon dioxide level in soil air. Soil Sci. Soc. Am. J. 47:1139-1145.

Castelle, A.J. and J.N. Galloway. 1990. Carbon dioxide dynamics in acid forest soils in Shenandoah National Park, Virginia. Soil Sci. Soc. Am. J. 54:252.

Durand, R. 1980. Variations saisonnieres de la concentration des solutions et des gaz du sol en milieu crayeux. Sci. Sol 3:217-229.

Duyzer, J.H., H.L.M. Verhagen, J.H. Weststrate and F.C. Bosveld. 1992. Measurement of the dry deposition flux of NH 3 on to coniferous forest. Environ Pollut. 75:3-13.

Farquhar, G.D., P.M. Firth, R. Wetselaar and B. Weir. 1980. On the gaseous exchange of ammonia between leaves and the environment: Determination of the ammonia compensation point. Plant Physiol. 66:710-714.

Ferm, M. 1979. Method for determination of atmospheric ammonia. Atmos. Environ. (1967) 13:1385-1393.

Fernandez, I.J. and P.A. Kosian. 1987. Soil air carbon dioxide concentrations in a new England spruce-fir forest. Soil Sci. Soc. Am. J. 51:261-263.

Fowler, D., C.R. Flechard, M.A. Sutton and R.L. Storeton-west. 1998. Long term measurements of the land–atmosphere exchange of ammonia over moorland. Atmos. Environ. 32:453-459.

Galbally I.E., C.R. Roy. 1983. The fate of nitrogen compounds in the atmosphere. In: Freney J.R., Simpson J.R. (eds) Gaseous Loss of Nitrogen from Plant-Soil Systems. Developments in Plant and Soil Sciences, vol 9. Springer, Dordrecht.p.265-284

Gunn, J. and S.T. Trudgill. 1982. Carbon dioxide production and concentrations in the soil atmosphere: A case study from New Zealand volcanic ash soils. Catena 81-94:81-94.

Hafner, S.D., F. Montes and C. Alan Rotz. 2013. The role of carbon dioxide in emission of ammonia from manure. Atmos. Environ. 66:63-71.

Hanson, P.J., N.T. Edwards, C.T. Garten and J.A. Andrews. 2000. Separating root and soil microbial contributions to soil respiration: A review of methods and observations. Biogeochemistry 48:115-146.

Kirk, G.J.D. and Rachhpal-Singh. 1992. Simultaneous transfer across an air-water interface of gases that interact through acid-base reactions. Atmos. Environ. 26:1651-1660.

Kuzyakov, Y. 2006. Sources of CO_2 efflux from soil and review of partitioning methods. Soil Biol. Biochem. 38:425-448.

Kuzyakov, Y. 2010. Priming effects: Interactions between living and dead organic matter. Soil Biol. Biochem. 42:1363-1371.

Lalonde, R.G. and C.E. Prescott. 2007. Partitioning heterotrophic and rhizospheric soil respiration in a mature douglas-fir (pseudotsuga menziesii) forest. Can. J. Forest Res. 37:1287-1297.

Lee, S.R., S.R. Yates, W.P. Robarge and S.A. Bradford. 2013. Synergistic ammonia losses from animal wastewater. Atmos. Environ. 71:245-250.

Meng, Z. and J.H. Seinfeld. 1996. Time scales to achieve atmospheric gas-aerosol equilibrium for volatile species. Atmos. Environ. 30:2889-2900.

Nemitz, E., M.A. Sutton, A. Gut, R. San José, S. Husted and J.K. Schjoerring. 2000. Sources and sinks of ammonia within an oilseed rape canopy. Agric. for. Meteorol. 105:385-404.

Nemitz, E., C. Milford and M.A. Sutton. 2001. A two-layer canopy compensation point model for describing bi-directional biosphere-atmosphere exchange of ammonia. Q.J.R. Meteorol. Soc. 127:815-833.

Parfitt, R.L., H.J. Percival, R.A. Dahlgren and L.F. Hill. 1997. Soil and solution chemistry under pasture and radiata pine in New Zealand. Plant Soil 191:279-290.

Petersen, V., R. Markfoged, S.D. Hafner and S.G. Sommer. 2014. A new slurry pH model accounting for effects of ammonia and carbon dioxide volatilization on solution speciation. Nutr. Cycling Agroecosyst. 100:189-204.

Pio, C.A. and R.M. Harrison. 1987. The equilibrium of ammonium chloride aerosol with gaseous hydrochloric acid and ammonia under tropospheric conditions. Atmos. Environ. (1967) 21:1243-1246.

Pleim, J.E., J.O. Bash, J.T. Walker and E.J. Cooter. 2013. Development and evaluation of an ammonia bidirectional flux parameterization for air quality models. J. Geophys. Res. Atmos. 118:3794-3806.

Pleim, J.E., L. Ran, W. Appel, M.W. Shephard and K. Cady-Pereira. 2019. New bidirectional ammonia flux model in an air quality model coupled with an agricultural model. J. Adv. Model Earth Sy. 11:2934-2957.

Pryor, S.C., R.J. Barthelmie, L.L. Sørensen and B. Jensen. 2001. Ammonia concentrations and fluxes over a forest in the midwestern USA. Atmos. Environ. 35:5645-5656.

Schrader, F. and C. Brümmer. 2014. Land use specific ammonia deposition velocities: A review of recent studies (2004–2013). Water Air Soil Poll. 225:1-12.

Schwede, D., and G.C. Lear 2014. A novel hybrid approach for estimating total deposition in the United States Atmos. Environ. 92, 207-220.

Sparks, J.P., J. Walker, A. Turnipseed and A. Guenther. 2008. Dry nitrogen deposition estimates over a forest experiencing free air CO2 enrichment. Global Change Biol. 14:768-781.

Stumm, W., and J.J. Morgan. 1995. Aquatic Chemistry: Chemical Equilibria and Rates in Natural Waters, 3rd Edition, John Wiley & Sons, Inc., 605 Third Avenue, New York, NY.

Sutton, M.A., C.E.R. Pitcairn and D. Fowler. 1993. The exchange of ammonia between the atmosphere and plant communities. Adv. Ecol. Res. 24:301-393.

Sutton, M.A., J.W. Erisman, F. Dentener and D. Möller. 2008. Ammonia in the environment: From ancient times to the present. Environ. Pollut. 156:583-604.

Vlek, P. L. G., and J. M. Stumpe. 1978. Effects of solution chemistry and environmental conditions on ammonia volatilization losses from aqueous systems. Soil Sci. Soc. Am. J. 42: 416-421.

Vugakov, P.S. and Y. Propova. 1968. Carbon dioxide regime in soils of the Krasnoyarsk forest Steppe. Sov. Soil Sci. 6:795-800.

Walker, J.T., W.P. Robarge, Y. Wu and T.P. Meyers. 2006. Measurement of bi-directional ammonia fluxes over soybean using the modified bowen-ratio technique. Agric. for. Meteorol. 138:54-68.

Wexler, A.S. and S.L. Clegg. 2002. Atmospheric aerosol models for systems including the ions H^+, NH_4^+, Na^+, SO_4^{2-}, NO_3^-, Cl^-, Br^-, and H_2O. J. Geophys. Res. Atmos. 107:4207.

Wu, Y., J. Walker, D. Schwede, C. Peters-Lidard, R. Dennis and W. Robarge. 2009. A new model of bi-directional ammonia exchange between the atmosphere and biosphere: Ammonia stomatal compensation point. Agric. for Meteorol. 149:263-280.

Zabowski, D. and R.S. Sletten. 1991. Carbon dioxide degassing effects on the pH of Spodosol soil solutions. Soil Sci. Soc. Am. J. 55:1456-1461.

Zhu, L., D. Henze, J. Bash, G.-. Jeong, K. Cady-Pereira, M. Shephard, M. Luo, F. Paulot and S. Capps. 2015. Global evaluation of ammonia bidirectional exchange and livestock diurnal variation schemes. Atmos. Chem. Phys. 15:12823-12843.

Chapter Two

Use of a Simple Flow-Through Chamber to Assess Ammonia Loss from Soils

1.0. Introduction

Better knowledge of the processes that control gaseous ammonia (NH_3) transport across the soil-atmosphere interface is important for predicting NH_3 deposition, and the overall impact of soils on NH_3 atmospheric chemistry. Specifically, there is a need for better understanding of the interaction of soil water evaporation, ammonium (NH_4^+) redistribution, and ammonia (NH_3) deposition/emissions under differing soil and environmental conditions. Soil water evaporation can drive solute redistribution in soils, especially towards the soil surface. Since NH_4^+ and NH_3 are interrelated through Henry's Law, soil drying represents the potential to elevate NH_4^+ concentrations near the soil surface for several days following rain events. An additional source of NH_4^+ that could enhance NH_3 emissions is mineralization of soil organic matter by soil microbial activities that were stimulated by rainwater inputs. This combination of physical, biological, and chemical processes suggests that use of a simple soil extraction techniques commonly employed for measuring "extractable" NH_4^+ (2M KCl) may in fact provide limited useful information in predicting NH_3 gaseous deposition/emissions from soils, especially soils that routinely do not receive relatively large inputs of reduce N (NH4-N) via commercial fertilizers or animal manures.

This chapter will discuss the evaluation of a simple flow-through chamber technique to study the interaction between soil water evaporation, soil NH_4^+ concentrations and NH_3 emissions. Annular denuder technology is used to capture the mass of NH_3 exiting the chamber

to allow an index of emissions potential without the need for NH_4^+ additions. However, the approach should allow sufficient NH_3 retention capacity via the denuder tubes to allow study of dose-response relationships with additions of NH_4^+ salts. Measurement of soil water loss is straightforward by determining differences in mass from time zero. Multiple soils are included to test potential impacts of texture and to a lesser extent pH. Lastly, air movement across the soil surface is controlled through the design of the chambers and use of mass-flow controllers. Potential problems that arose in the use of the chambers will be discussed, and to what extent these problems may impact the ability of this overall approach to further understand the impact of soil water evaporation on NH_3 emissions.

1.1 Soil Water Content and Ammonia

Factors likely to affect the amount and rate of NH_3 loss from soils include rainfall, antecedent soil moisture content, soil solution NH_4-N concentration, temperature and wind velocity (Mclnnes et al., 1986). Soil water is a critical factor in the transport of NH_3 to the soil surface and is considered partly responsible for high NH_3 losses (Black et al., 1987; Cai 1997; Tian et al., 1998; Sommer and Olesen, 2000). The intensity and frequency of rain events can impact soil emissions: intense rainfall events on dry soil lower emissions, while, higher NH_3 losses have been observed with only modest amounts of rainfall (Freney, 1983; Black et al., 1987). Antecedent soil moisture content is also a factor, as NH_3 loss has been shown to be a function of accumulated rain amounts due to several sequential rainfall events (Sommer and Olesen, 2000). The variation in soil water content has an effect on the stability of soil nitrogen. Drying of the soil increases the concentration of NH_4^+ in soil solution and may enhance the losses of NH_3 (Jewitt, 1942; Kresge and Satchell, 1960; Volk, 1959).

It has been suggested that a simple relationship should exist between soil water content and the rate of NH_3 loss. The NH_4-N concentrations at higher soil moisture contents should be lower than at lower soil water contents, causing lower NH_3 losses from more moist soils (Martin and Chapman, 1951; Wahhab et al., 1957; Fenn and Escarzaga, 1976). In other studies, researchers have observed the opposite (Volk, 1959; Ernst and Massey, 1960; Kresge and Satchell, 1960). Unfortunately, the explanation of these results is often confused by concurrent water loss as soils dry. Loss of water tends to sustain or increase NH_4-N concentrations over time and lead to more significant losses than if no drying of the soil occurred. This appears to have taken place in several studies in which the relationships between water and NH_3 losses were recognized (Jewitt, 1942; Wahhab et al., 1957). Therefore, it has been suggested that moisture loss is necessary for NH_3 loss to occur (Wahhab et al., 1957). However, others have shown that NH_3 may still be lost in substantial amounts under non-drying circumstances (Ernst and Massey, 1960; Terry et al., 1978). The rate of water loss may also affect the amount of NH_3 loss in other ways. It has been suggested that the fast drying of wet soil could produce NH_4^+(aq) concentrations enough to restrain nitrification thereby increasing NH_3 losses (Terry et al., 1978; Lyster et al., 1980). Conversely, the slow drying of soils might allow time for the nitrification process to lessen the NH_4-N concentration and further acidify the system, ending in a net reduction in NH_3 losses (Terry et al., 1978).

The rate of NH_3 loss from aqueous solution at constant temperature is known to be directly proportional to the total NH_4-N concentration at a given constant pH, or when the solution pH is sufficiently high (>10) that all the NH_4-N added exists as $NH_{3(aq)}$ (Vlek and Stumpe, 1978). Thus, the soil buffering capacity may have an impact on determining NH_3 emissions as soils dry. Also, of importance is the cation exchange capacity, as it has a direct

impact on the NH_4^+(aq) concentration present in the bulk soil solution. Several laboratory experiments have shown that coarse-textured (sandy) soils volatilize more of applied NH_4-N than fine-textured soils (Wahhab et al., 1957; Gasser, 1964; Fenn and Kissel, 1976). The lower CEC of the coarse-textured soils means less of the added NH_4^+ cation would be closely associated with cation exchange sites. Therefore, coarse-textured soils would have a higher amount of the NH_4^+ ions in the bulk soil solution compared with fine-textured soils, and this would be reflected in their enhanced ability to volatilize NH_3.

The movement of NH_4^+ within the bulk soil solution is driven by two primary mechanisms: mass flow and ion diffusion. Mass flow occurs when NH_4^+ is transported in the flow of water in response to a potential gradient. During soil evaporation, there is a net upward movement of soil water that results in the upward movement of both dissolved $NH_{3(aq)}$ and NH_4^+ (Gardner, 1960). The net amount of NH_4^+ transported by mass flow of water is highly influenced by the cation exchange capacity, and clay-type and surface area and subsequent impact on water viscosity. Movement of NH_4^+ by diffusion is assumed to follow Fick's laws and occurs in response to a concentration gradient; where NH_4^+ moves from an area of high concentration to one of low concentration. A concentration gradient can arise as a result of NH_4^+ conversion during nitrification, and net NH_3 loss.

The rate of NH_4^+ movement depends on the thickness and tortuosity of soil water films. In unsaturated soils, water can exist as wedge-shaped volumes at points of contact between soil particles. These individual volumes are joined by thin films covering intervening particles surfaces. As soils drain, both the wedge-shaped films and the thin films are depleted, until transport is dominated by only the presence and connection of thin films. In unsaturated soils, the

presence of both wedge-shaped films and thin films presents a tortuous pathway for ion diffusion. In the case of soil water evaporation, the lower portions of soil beneath the surface drying layer will represent a reservoir of water that will move upwards due to potential gradient induced by the drying process. Movement will continue until rate of water movement can no longer match the rate of water loss at the soil surface. Loss of NH_3 during the process may be delayed or slowly increase as the NH_4^+ present near the surface builds (Black et al., 1987).

1.2. Shape of Water Loss Curves

Hillel (2004) has proposed a series of stages for describing soil water evaporation. The shape of the water loss curves varies with either the presence or absence of a water table. In this study, the packed soil columns conform to the scenario of a nonexistent water table with relative constant atmospheric conditions (wind speed = flow rate, temperature, and to some degree relative humidity). In the absence of a water table the three stages proposed by Hillel (2004) are as follows:

1. Stage One – water loss is relatively constant. The soil surface dries slowly as water moves vertically to the soil surface due to the induced gradient as a result of water loss across the soil-atmosphere interface. At this stage, the evaporation rate is controlled by atmospheric conditions (solar radiation, wind, temperature, and humidity) rather than by the properties of the soil profile. The duration of Stage One is relatively short lasting from a few hours to a few days.
2. Stage Two – the rate of water loss rapidly declines. The second state is initiated when the actual evaporation from the soil falls below the potential evaporation induced by the atmospheric parameters listed in Stage One. There is still vertical movement of soil water, but the rate of movement slows, probably as the tortuosity increases for water attempting to

move through the soil matrix. The transition between Stage One and Stage Two can be distinct, and Stage Two may last considerably longer than Stage One.

3. Stage Three – soil surface is completely dry. Water loss at Stage Three is largely by vapor diffusion through the soil matrix. This stage can persist for days, weeks, or even months. The transition between Stage Two and Stage Three is not readily apparent, other than the appearance of the air-dry soil surface.

A general schematic of water loss stages for soils of different texture as described by Hillel (2004) is illustrated in Fig. 2.0. Since water movement through the soil matrix is a factor in both Stage One and Two, soil texture can have a direct influence on the intensity and duration of the actual rates of water loss observed, with finer textured soils having higher overall water content than coarse textured soils as well (Fig. 2.0). Under similar external conditions, Stage One lasts longer in a clay textured soil (curve 4, Fig. 2.0) than in sandy soil (curve 1, Fig. 2.0). The other two factors limiting the length of the initial stage of evaporation are permeability and matric potential gradient (Hill, 2004). If permeability is too low, water cannot flow easily to the zone of the evaporating surface. If the matric potential gradient is also small, water will not move toward to the surface. Soils with high permeability, such as the sands (curve 1, Fig. 2.0), have low gradient capillary pressure curves. Soils with low permeability, such as the clays (curve 4, Fig.2.0), have high gradient capillary pressure curves. For loamy soils, there is a mix of high permeability and high capillary pressure gradients (curves 2 and 3, Fig. 2.0) (Hillel 2004).

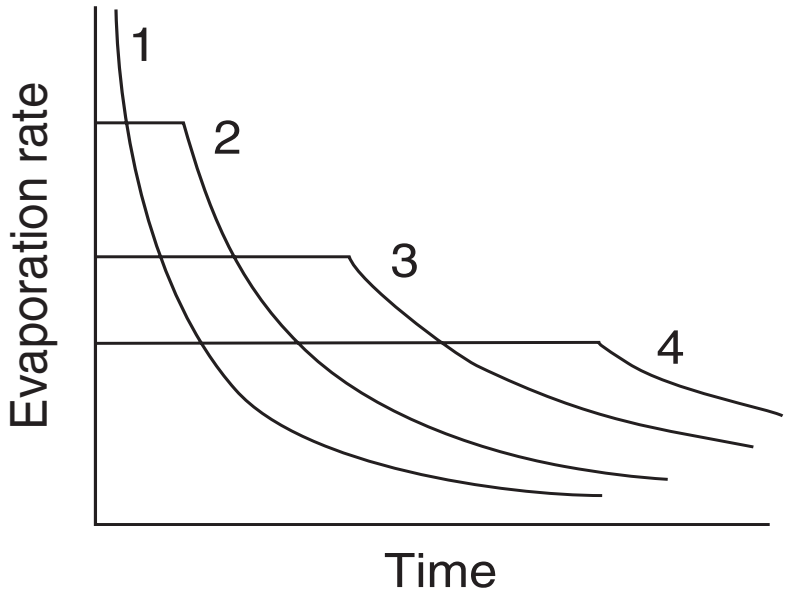

Figure 2.0. Proposed stages of soil evaporation as a function of soil texture. (Curve 1 = sandy texture; Curve 2 = loamy with relatively high permeability; Curve 3 = loamy with relatively low permeability; Curve 4 = clayey texture). Taken from Hillel (2004).

1.3. Chamber Methods

There are many varieties of chamber techniques that have been used for the measurement of NH_3 emission from soils. The primary characteristic for all chamber methods is that chambers cover a relatively small surface area compared to field scale treatments. Chambers restrict the communication between the headspace of the emitting surface and the rest of the atmosphere (Denmead and Raupach, 1993). In general, chamber techniques are portable and relatively versatile. Because of their relatively small footprint, chamber techniques are often a more cost-effective way to do process studies and treatment comparisons than micrometeorological techniques. Chambers can be separated into two groups: static chambers and flow-through chambers (Hutchinson and Livingston, 1993).

1.3.1 Simple Static Chamber Concept/Limitations

The static chamber (SC) is a simple low-cost method for estimating the gas emissions from the soil surface. Static chambers are commonly used to measure non-reactive gas emissions (carbon dioxide - CO_2, nitrous oxide - N_2O, methane - CH_4) usually from areas less than 1 m^2. The time span for a set of measurements typically ranges from minutes to possibly a few hours. The most common approach is to sample the headspace within the chamber over time and then plot the resulting change in concentration as a function of sampling interval. The sensitivity of the method to detect changes in the headspace gas concentration is a function of the analytical instrumentation used to analyze the gas samples (typically gas chromatography with a suitable detector), ambient atmospheric levels of the gas of interest at time zero - placement of the chamber into position, and time to allow gases to accumulate in the chamber headspace.

The SC approach is not suitable for NH_3 due to the reactive nature of NH_3 itself, unless an internal trap for NH_3 is used within the chamber (Miola et al., 2015). Use of internal NH_3 traps, however, usually lack adequate sensitivity to measure NH_3 loss over relatively short time intervals (minutes), unless the soil has been amended with NH4-N containing fertilizers. Prolonged placement of static chambers can result in relatively high humidity and condensation on internal chamber surfaces as well as the enclosed soil and possibly vegetation. For a reactive gas such as NH_3, condensation results in additional adsorptive surfaces that compete with an internal NH_3 trap (Aita et al., 2014). This can lead to a negative bias in the estimated soil flux.

The magnitude of this bias varies with the nature of the emitting surface covered by the chamber (Hudson et al., 2009), and the duration of a set of measurements (Miola et al., 2015). Ammonia recovery when using SCs is generally always less than 100% (Misselbrook et al., 2005; Van Der Weerden et al., 1996). Another limitation in the use of SCs is that the calculated

soil flux for the gas of interest only represents a single flux estimate in time and space. Use of multiple chambers can address the spatial variability in soil flux, but application to understanding temporal variability is limited to the resolution of generally hours, if not days.

1.3.2. Simple Flow Through Chambers

Flow-through chambers employ a sealed chamber with controlled inlets and outlets for a continuous stream of air passing through the chamber headspace. Changes in the emission of gases can be determined in real time by monitoring the change in the concentration of the gas of interest in the flowing air stream exiting the chamber (Mulvaney et al., 2008). Alternatively, the mass of the gas of interest can be scrubbed from the exiting air-stream and an integrated average gas concentration can be calculated for the time interval sampled (Menneer et al., 2008; Zaman and Blennerhassett, 2010). The measurement process can also be interrupted for short periods of time allowing measurement of other parameters.

Flow-through chamber methods based on the concept of a continuously stirred tank reactor (CSTR) employ an impeller to ensure adequate mixing of air flowing into the chamber with the chambers internal contents including gases released from the emitting surface (Aneja, 2006). The chamber with an open bottom is placed onto a stainless-steel ring, which is then inserted into the soil (Hill et al., 1978). The soil flux measurements begin ~ one hour after placing the ring into the soil when steady-state conditions within the chamber are typically achieved. The flux rate (F_{NH3}, μg N m^{-2} h^{-1}) is estimated using the following mass balance equation (Eq.2.1)

$$\frac{dC}{dt} = \left(\frac{q(C_{air})}{V} + \frac{JA}{V}\right) - (C)\left(\frac{LA_w}{V} + \frac{q}{V}\right) - R \qquad (2.1)$$

where C is the gas concentration within the chamber (ppbv), Cair is the gas concentration in air (ppbv), q is the air flow rate through the chamber (LPM), V is the chamber volume (L), A

is area of soil covered by chamber (m^2), A_W is an internal surface area of the chamber (m^2), L is the total loss of gas per unit area (m min^{-1}) due to reaction with walls of the chamber, J is the gas emission per unit area per unit time (μg m^{-2} h^{-1}); and R is the potential reaction of gas in the chamber.

Equation 2.1 can be simplified by the use of zero air as the carrier gas allowing C_{air} and R to be set to a value of zero. The concentration of C within the chamber can be assumed to be constant due to the use of an impeller. At steady state, dC/dt is zero and Eq. (2.1) reduces to:

$$\frac{J}{h} = C_{eq}\left(\frac{LA_w}{V} + \frac{q}{V}\right) \qquad (2.2)$$

The loss term L within the chamber can be calculated from the slope of the plot Eq. 2.3 (Kaplan et al., 1988):

$$-\ln\left[\frac{C_{eq} - C(t)}{C_{eq} - C_o}\right] versus\ time\ (t) \qquad (2.3)$$

where Co is the initial concentration of gas measured at a constant flow rate (LPM). C_{eq} is the concentration of gas measured at different flow rate (LPM). C(t) is the concentration of gas at any time t. With the value of the slope from Eq. 2.3, L is determined by Eq. 2.4 (Kaplan et al., 1988):

$$L = \left(slope - \frac{q}{V}\right)\left(\frac{V}{A_w}\right) \qquad (2.4)$$

where the parameters have the same meaning as described for equation 2.1.

A simpler variation in the flow-through chamber design is to trap the gas of interest exiting the chamber over a given time interval. Either scrubbing the inlet gas stream of the gas of interest, or assuming a known fixed inlet concentration over the measurement time interval,

provides the means to calculate the net mass of the gas released from the emitting surface. This then allows an estimate of the average flux by dividing the net mass collected by the surface area of the chamber in contact with the emitting surface, and the time of collection. An average net concentration of the gas within the chamber can also be calculated if the flow rate through the chamber is known to sufficient accuracy.

1.3.3. Simple Flow-Through Chambers: Advantages and Limitations

Chamber measurements are advantageous due to their simplicity, low cost, ease of installation, and maintenance. They can be used in laboratory experiments and with small field plots. One of the primary limitations that requires caution when using flow-through chambers arises from the impact of the flowing air-stream on the atmospheric pressure within the chamber. Pressure differences arise because of resistance to air-flow at the outlets/inlets of the chamber (Rolston, 1986). Failure to account for possible pressure differences in the chamber can result in a bias in calculated fluxes – typically positive. The differences in pressure can be reduced by maximizing the area for the inlet gas stream into the chamber versus the inlet (Rolston, 1986).

Soil gas emissions across the soil-air interface are sensitive to small changes in atmospheric pressure. This happens whether the inlet gas stream is either drawn into or blown through the chamber (Fang and Moncrieff, 1996). When air is drawn out of a chamber there can be a pressure deficit inside the chamber, whereas positive pressure can be when air is blown in. Another disadvantage of the simple flow-through chamber system is that flowing gas through the chamber acts to dilute the gas emitted into the chamber headspace. This can make it difficult to detect small changes in gas concentration in the flowing stream exiting the chamber, depending on the sensitivity of the analytical instrumentation in use (Rolston, 1986). It is apparent that for

some gases, such as NH_3, there is an interaction between flow-rate of gas through the chamber and ability to detect net changes in NH_3 concentration in the air stream, especially if not trapping the NH_3 exiting the chamber. High flow-rates increase the exchange rate of the volume of air within the chamber and act to lessen the chances of condensation of moisture on the internal surfaces of the chamber. However, higher flow-rates can induce negative atmospheric pressure, artificially increasing flux from the emitting surface. Lower flow-rates lessen the chance of inducing negative atmospheric pressure within the chamber but increase the residence time for a given volume of air, effectively increasing the probability of gases such as NH_3 being adsorbed by other surfaces. Use of a flow-through chamber, therefore, in many instances, may represent a compromise between selected flow-rates through the chamber, the strength of the source term, and analytical techniques available to measure the gas of interest in the output stream.

1.4. Measurement of Ammonia

Techniques commonly used to measure the presence/concentration of NH_3 in the atmosphere/flowing gas streams can be divided into two categories: intensity measurements which measure NH_3 concentration in ~ real time, and mass measurements which capture or strip NH_3 via an infinite sink from which integrated (average) concentrations can be calculated with appropriate ancillary data. Both approaches have positives and negatives when combined with flow-through chambers to assess NH_3 emissions from different sources. Intensity measurements are usually based on optical methods employing spectroscopy. Mass measurement devices can be both passive and active in design.

1.4.1 Optical Methods

Modern analytical instruments for measuring NH_3 concentrations in the atmosphere were initially designed based on chemiluminescence. Chemiluminescence is the release of light due to a chemical reaction. Chemiluminescence-based instruments determine NH_3 by converting it to nitric oxide (NO) at high temperatures (750-800°C) in the presence of a catalyst (Phillips et al., 2001, Ammann et al., 2012; Bruemmer et al., 2013; Marx et al., 2012). The technique is very sensitive (a few ppt for NO and 1 ppb for NH_3), fast (the response time down to 0.1second), and relatively flexible. The technology has been the basis for routine atmospheric monitors used by state and federal regulatory agencies. The main limitations to this instrumentation are the necessity for regular calibration and maintenance. Although the instrumentation itself is now relatively modest in cost, the equipment does require adequate shelter and control of environmental parameters with constant sources of electrical power.

An emerging replacement technology for the generation of analytical instrumentation based on chemiluminescence are those employing Fourier transform infrared spectroscopy (FTIR). This technology uses a modulated source of infrared light from which are isolated specific frequencies that are absorbed by the gaseous species of interest. An alternative is to use a select (filtered) portion of the infrared spectrum that contains the frequency specific to the gas of interest together with a detector with enough resolution to generate an absorption spectrum that can be compared to a known reference (Loh et al., 2008). The advantages of this approach are its relative simplicity in design and use, plus overall robustness. Detection limits typically range from < 1 ppmv to percent levels depending on the combination of light source, optical path length and detector built-in to the instrument. Instrumentation techniques based on FTIR also can be reduced in size making them mobile and able to be operated for relatively long periods of

time on portable power sources. The main limitation for the FTIR-based approach is spectral overlap between the gaseous species of interest and other volatile species present in the atmosphere being sampled (especially water vapor). Typically, FTIR instruments are provided with spectral libraries that together with modern microprocessor technology and spectral manipulation software allow accurate determination of the concentration of the gas species of interest (Hassouna et al., 2013; Zhao et al., 2012). Despite the continued evolution of FTIR-based instruments, they are still relatively costly compared to those using chemiluminescence.

Techniques using lasers as a light source have also been evolving with the current generation largely using Cavity Ring-Down Spectroscopy (CRDS). In this technique, a laser is used to excite a gas sample within a holding area inside the instrument. The holding area of cavity contains reflective mirrors, substantially increasing the effective path-length of the instrument by orders of magnitude, increasing the percentage of the gas of interest excited by absorption of light from the laser source. When the laser source is turned off, the decay of the excited species, the so-called "ring-down time", is measured and recorded. The "ring-down time" for each gas depends on the absorption coefficient at the wavelength emitted by the laser (Baer et al., 2002; O'Keefe et al., 1999). The technique can be highly specific, even allowing differentiation of the natural isotopic composition of the gaseous species present (e.g. separation of N^{14} from N^{15} dominant fractions). Overall, CRDS-based instruments are relatively robust, highly sensitive, selective, and generally easy to use (O'Keefe et al., 1999). The instruments do require adequate shelter and control of environmental parameters, proper calibration protocols, and currently are very expensive compared to chemiluminescence-based technology, usually an order of magnitude in cost when required ancillary pumps and calibration equipment are included.

1.4.2 Mass Measurement Devices

Mass measurement devices for NH_3 in the atmosphere or a flowing gas-stream employ an "infinite-sink" that is designed to ensure 100% removal of NH_3 coming in contact with components of the device. Simple acid-based scrubbers (bubblers) are best known as an easy and cost-effective way to strip NH_3 from a gas stream. A non-volatile acid, such as sulfuric acid, is used to strip NH_3 from the air-stream as it is pulled through the scrubber. Connecting scrubbers in sequence allows testing for break-through when the capacity of the bubbler, or the combination of air-flow rate and NH_3 concentration present at the scrubber inlet do not provide sufficient residence time for 100% capture efficiency for the first scrubber in line. While the use of scrubbers is relatively inexpensive, they do require precise handling of acid solutions of varying volume due to evaporation of water due to continuous flow of gas through the scrubber. In addition, capture of the NH_3 is due to a simple acid-base reaction, thus other gaseous species that react with the acid in the scrubber will result in a false-positive bias in the analysis. There is also an underlying limit in the sensitivity of the approach as the amount of NH_3 captured is determined as a difference, and there is a finite practical limit in regards the strength of the acid used in simple scrubbers.

Two designs that are similar to the simple acid-scrubber approach, but simplifier to use with possibly better sensitivity are passive samplers and annular denuder technology. Passive samplers have long been used to measure the concentrations of gaseous NH_3 over a period of time at ambient levels (Ferm, 1991). According to Fick's law, the gas diffuses from the ambient air (a zone of relatively higher concentration) to the acid-coated collection filter medium (an "infinite" sink for NH_3). The presence of a turbulence barrier on the filter is used to ensure the

NH_3 is transported to the acid-coated filter via diffusion process only and not by convective transport. A virtual flow for the passive sampler is calculated using Eq. (2.5):

$$m_{NH3} = \frac{D_{NH3}\, x\, A}{\Delta x} \qquad (2.5)$$

where m_{NH3} is the virtual flow rate of passive sampler ($cm^3\ min^{-1}$), D_{NH3} is the diffusion coefficient ($cm^2\ min^{-1}$), A is the cross-sectional area (cm^2) of the sampler and Dx is the distance from the turbulence barrier to the acid-coated filter paper – the diffusion distance (cm). The ambient concentration of NH_3 determined by the passive sampler depends on the mass of NH_3 adsorbed by the filter, duration of exposure, and diffusion coefficient (which is temperature dependent). The amount of adsorbed NH_3 by the filter (Q_{NH3}) is:

$$Q_{NH3} = (c_e - c_v)v \qquad (2.6)$$

where c_e is the filter extract concentration of NH_4^+ ($\mu g\ mL^{-1}$), c_v is the concentration of an accompanying travel blank ($\mu g\ mL^{-1}$), and v is the volume of the extracting solution (mL).

The advantages of using the passive sampler technique are that it is a simple, relatively inexpensive device that is easy to set up in the field and operate as it requires no power and only a simple weather shelter. A major limitation of the approach is that its sensitivity is a direct function of the expected ambient levels of NH_3 in the atmosphere to be sampled, and the time of required exposure (Namiesnik et al., 2005). Typically, exposure times are measured in weeks or at least days to ensure sufficient accumulation of mass of NH_3 to differentiate from the associated blanks. In addition, working in an NH_3 free atmosphere to be extent possible during the preparation of the acid-coated filters is an absolute requirement in order to measure changes in ambient NH_3 concentrations (typically in range of 0.5 – 3 $\mu gNH_3\ m^{-3}$). Lastly, the strength of the acid used to coat the filters should also be approached with caution, as most non-volatile inorganic acids are also hydroscopic and too high acid concentrations used to coat the filters can

result in condensation of water on the filter in the field and loss of sample as passive samplers are often deployed in an inverted position.

An alternative to the passive filter concept that is essentially based on the same approach is annular denuder technology. Denuders are acid coated tubes used to trap NH_3 or other gases from a flowing gas stream (Leuning et al., 1985; Ni and Heber, 2008; Phillips et al., 2001; Schjoerring et al., 1992). The NH_3 gas diffuses and adsorbs to the internal wall of the acid coated tube and then is transformed to a stable molecule (NH_4^+) in association with a non-volatile acid anion. The denuder tubes are constructed to allow laminar flow through the denuder tube assembly, optimizing the probability to capture NH_3 molecules from the flowing gas stream. Unlike the passive sampler design, annular denuder technology is designed for 100% capture efficiency, effectively reducing the time of exposure necessary to capture measurable masses of NH_3 from days to hours, although longer exposure periods are also possible. Annular denuder technology provides greater flexibility for obtaining multiple sampling points during a given time interval. The overall capture efficiency of a single acid-coated denuder tube can also be tested as a function of NH_3 levels to be measured and sampling flow rate.

There are a number of limitations to the approach. The individual denuder tubes are relatively expensive to purchase and repair, since they are somewhat fragile. Their use requires a pump(s) that maintains precise flow-rates (typically using mass-flow controllers) in order to allow an accurate calculation of an average NH_3 concentration for a given exposure period. Lastly, preparation of the acid-coated denuders requires paying attention to potential sources of NH_3 contamination, especially during the drying step for coating the internal glass surfaces of the denuder tubes. However, annular denuder technology is considered more accurate and precise than using passive filters.

1.5. Research Objectives

For the purposes of this research project, a technique was required that would provide sensitive, accurate and replicated measurements of the potential emission of NH_3 from soils, especially non-amended NH_4-N soils, while at the same time allowing an assessment of soil water loss following different conditions of initial soil water content. Measurements of NH_3 loss must be sensitive enough to detect relatively small differences over time. For this study, a simple flow-through chamber with packed soil columns in combination with annular denuder technology was selected for observing NH_3 release. Knowing the potential limitations of flow-through chambers as outlined above, measurements of NH_3 will serve primarily as an index of conditions which can impact NH_3 emissions during soil water loss due to evaporation, rather than trying to relate actual calculated average NH_3 concentrations directly to amounts of extractable NH_4-N present in the soil column. The specific objectives of this portion of the study include: (i) to design a simple flow-through chamber system combined with annular denuder technology that affords both precision and sensitivity in measuring soil water loss and measured NH_3 emissions; (ii) to determine the best flow-rate to use with simple flow-through chamber to avoid condensation of water within the chambers and loss of NH_3 to internal surfaces while at the same time attempting to differentiate the potential Stages of water loss (Fig. 2.1); and (iii) to assess the sensitivity of the flow-through chamber combined with annular denuder technology to delineate dose-response relationships as a result of NH_4-N addition to the whole soil or layers of soil in the packed soil columns.

2.0. Methods and Materials

2.1. Flow-Through Chamber

A glass reaction chamber (Pyrex®, 2000 mL, Model No. 6947) was chosen in combination with annular denuder technology (URG Inc.) as the flow-through chamber design for use in this study (Fig.2.1). The glass chamber has an internal volume of 2 L (12.5 cm x 17.5 cm x 9.2 cm) and a cross-sectional area of 122 cm^2. The glass lid of the reaction chamber has 4 openings. Two of the openings were sealed with 3/8-inch John Guest® NPTF connectors. Each NPTF fitting was connected to vacuum polyethylene tubing (¼ inch ID, max 250 psi at 70°F). The other end of the vacuum tubing had a stainless-steel fitting 3/8- inch NPTM that was inserted into a Teflon screw cap (URG Corporation, Chapel Hill, NC) that was placed on one end of a denuder tube. One of these two openings was designated the chamber outlet, and the other the chamber inlet. Air flow leaving the chamber through the outlet passed through one or two denuder tubes before the connection to the mass flow controller. Air entering the chamber was drawn through a denuder tube to remove ambient ammonia from entering the chamber. One of the remaining two openings on the glass lid was sealed using a rubber stopper and epoxy resin. The last opening, located in the middle of the lid, was closed with a rubber stopper to form an air-tight seal. The rubber stopper allowed access to the internal portion of the chamber without the need for removing the entire lid (e.g. for adding water through the course of a given experiment).

Air flow (1-, 3-, 5-, 6-, and 8- LPM) through the glass chamber was controlled via a micro-processor-controlled pump (URG Corporation, Chapel Hill, NC, Model # URG-3000-02N) using a digital mass flow controller (Fig. A3). Flow rates were confirmed at the chamber

inlet and outlet using a BIOS DryCal® DC-Lite primary flow meter (S/N 100776; Model Revision 1.08).

2.2 Chamber Assembly

Two 8.2-cm long open top PVC columns with 10.1 cm inside diameter and cross-sectional area of approximately 80.1 cm^2 were placed inside a chamber. The bottom one was inverted, and its internal volume was to a large degree isolated from the air-exchange inside the glass chamber (Fig. 2.1). The top PVC column insert was filled with soil. The chamber has a total internal volume of 2.0 L, and the net internal volume after accounting for the volume occupied by the PVC containers was ~ 1 L, leaving ~ 1 L of the actual open space inside the chamber. The corresponding exchange rate of air using different flow rates inside the chamber is shown in Table 2.1. The design attempts to reach a compromise of not allowing the soil to dry out so quickly as to make observations of treatment effects difficult, while at the same time limiting to the extent possible the interaction of NH_3 with the internal surfaces of the glass chamber.

The chamber glass lid was affixed to the top of the chamber using electrical tape. At the lid edge in contact with the body of the glass chamber, strips of electrical tape were placed around the outer edge. A continuous strip of electrical tape was then run twice around the circumference to form the air-tight seal. Use of the electrical tape avoided the need for using other sealants such as silica gel which may be acidic in nature and act as an absorption surface for NH_3 inside the sealed chamber. In addition, use of the electrical tape avoided the need for a clamp to hold the glass lid in position during the course of an experiment. The final configuration of the assembled chamber included use of at least two 3-channel annular denuder tubes (30 mm x 242 mm length): one to scrub NH_3 entering a chamber, and one to collect NH_3

exiting the chamber (Fig. 2.1). Up to four chambers were operated at one time. Three were run from a three-channel mass flow controller. A second single channel mass flow controller was used for a fourth chamber. Air-flow was checked at the start and end of each experiment.

Table 2.1. Exchange rate of air using different flow rates inside the chamber

Air Flow rate (LPM)	Effective exchange rate of air (Vol min^{-1})
1	0.9
3	2.7
5	4.5
6	5.4
8	7.2

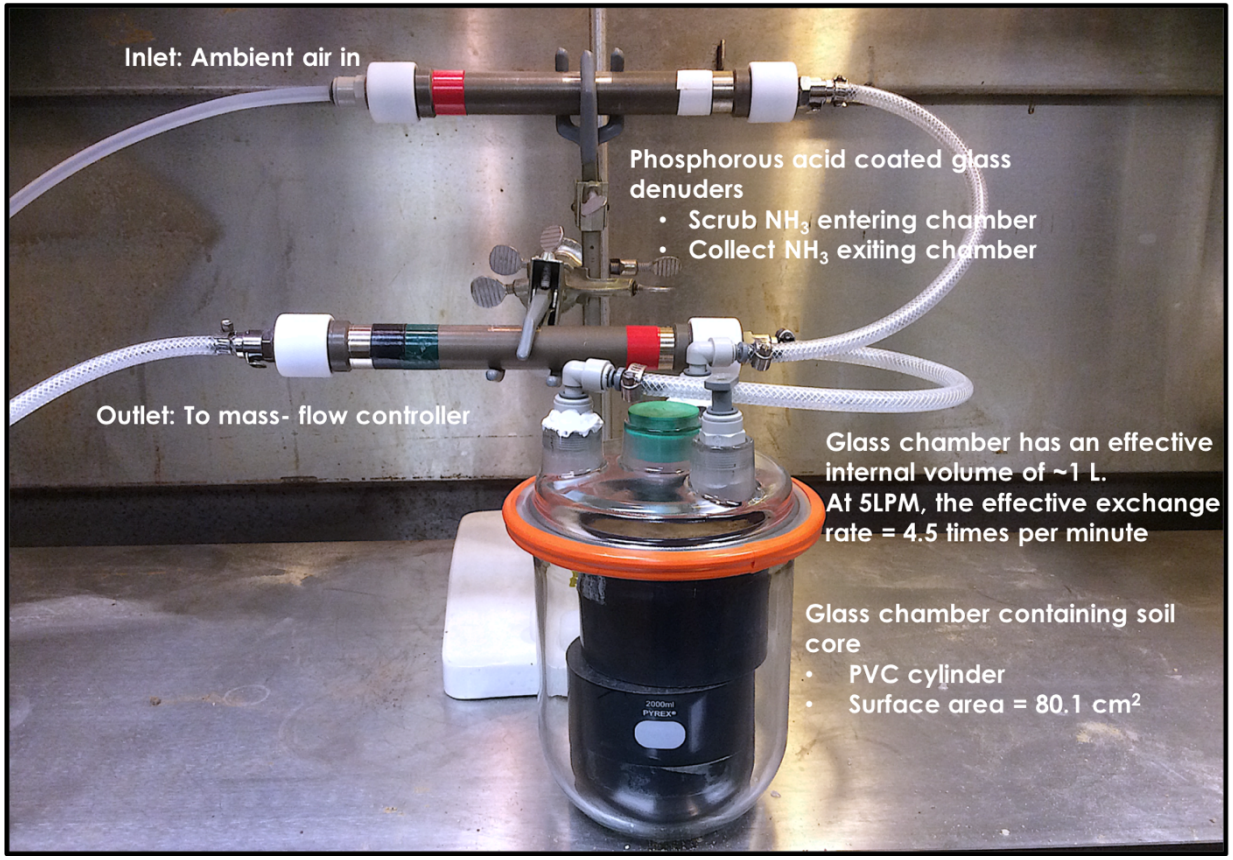

Figure 2.1. Experimental setup for simple flow-through chamber

2.3. Annular Denuder Technology

The three-channel annular denuder tubes (30 mm x 242 mm length) used in this study consisted of borosilicate concentric glass tubes (Appendix, Fig. A1) with an outer stainless-steel shell. The concentric glass tubes have a ~ 2 mm annular spacing. At one end, the concentric glass tubes are offset 25 mm from one end of the stainless-steel shell. This end is called the flow straightening end. The flow straightening end functions to convert the inlet air stream to laminar flow. When not in use, the prepared or exposed denuder tubes are equipped with Teflon caps.

Details for preparing the annular denuders as described by Purdue et al. (1992) are outlined in Appendix A. The mass of NH_3 collected using the annular denuder technology was determined by accounting for the volume used to extract the exposed denuder tube (10 mL of deionized water) times the concentration of NH_4-N found in the extract. All denuder extracts were stored at 4ºC until analysis via a flow injection analyzer (Lachat, Quick-Chem 8000, QuikChem Method 10-107-06-2-A- Ammonia in surface water, wastewater 0 to 20 mg N L^{-1} as NH_3). An integrated average NH_3-N concentration for a set time interval is obtained from the net mass of NH_3-N collected divided by total volume of air pulled through the glass chamber. The total volume of air sampled is equal to the product of the time for a given sampling period and the set volumetric air flow rate maintained by the mass-flow controller.

It is possible to observe breakthrough using annular denuder technology when the combination of NH_3 emissions and flow rate exceed the capacity of the annular denuder tube to strip NH_3 from the air stream. The retention capacity of the denuder tubes was tested in Chapter one. For the conditions for this portion of the overall study, rates of NH_3 loss were deemed not sufficient to challenge the assumption of 100% retention of NH_3 by a single annular denuder tube.

For each batch of prepared annular denuder tubes, laboratory blanks were set aside to determine back ground levels of NH_4-N introduced during the various handling steps for an individual annular denuder tube. The average mass of NH_3-N recovered from the laboratory blanks for the annular denuder tubes ranged from 0.02 to 0.39 μg NH_4-N.

2.4. Soils

Surface soils (0-10 cm) of differing soil texture were collected for use in this study. Loamy sand and clay loam textured soils were obtained from a tilled, fallow field at the BASF The Chemical Company Research Farm located near Holly Springs, NC. The clay loam soil actually originated from Illinois (Drummer soil series) and was transported to NC by BASF personnel to conduct field and greenhouse experiments. Soils with a sandy loam texture and differing soil organic matter contents were obtained from two sites: The Center for Environmental Farming System (CEFS) located at the Cherry Research Station near Goldsboro, NC, and a former pasture/grassy field at the Duke Forest, near Durham, NC. For this study, the soils were designated as follows in tables and figures: loamy sand – BASF-ls; clay loam – BASF-cl; sandy loam – CEFS-sl or DUKE-sl.

The collected soils were air-dried for about 6 to 8 weeks at room temperature, passed through a 2-mm sieve, mixed, and stored in a large bucket in the laboratory environment. Soil pH in water and 0.01M $CaCl_2$ was measured using standard procedures (Peech, 1965) (Table 2.2). Soil pH in the presence of 0.01M $CaCl_2$ provided a relative index of the presence of exchangeable acidity in the soil that will act to buffer soil pH. With a large pool of exchangeable acidity, it is unlikely that changes in soil pH will be seen over time. The cation exchange capacity (CEC) was determined by 1.0 M NaOAc buffered at pH 7 (Chapman, 1965). Soil texture was determined using the hydrometer method described by Gee and Bauder (1986). Soil

water retention data were collected using a pressure plate apparatus (Klute, 1986). Extraction of NH_4^+ from soil samples with 2M KCl was determined using the procedure described in Mulvaney (1996).

Table 2.2. Physical and chemical properties of soils used in the study

	(BASF-ls)	(CEFS-sl)	(DUKE-sl)	(BASF-cl)
pH (H_2O) (1:2.5)	6.57	5.41	5.77	6.34
pH ($CaCl_2$) (1:2.5)	5.88	4.70	5.07	5.89
CEC ($cmol_c\ kg^{-1}$)	1.7	10.3	14.5	25.9
Sand %	84.5	68.3	52.7	24.0
Silt %	12.5	25.4	42.4	40.0
Clay %	3.0	6.4	4.9	36.0
Texture class	loamy sand	sandy loam	sandy loam	clay loam
Water content at FC capacity $m^3\ m^{-3}$	0.14	0.30	0.36	0.36
NH_4-N ($\mu g\ g^{-1}$)	2.2	7.9	35.8	4.4

2.5. Soil Columns

Table 2.3 summarizes the laboratory experiments undertaken to measure water and NH_3 loss using flow-through chamber combined with annular denuder technology. According to the objectives of the experiment, the soil was prepared as follows prior to beginning measurements.

Preparation of soil column

Three portions of ~ 216.5 g air-dried soil were packed into PVC cylinder columns in 2-cm deep increments. Distilled water in 10 mL increments was applied uniformly on top of each depth increment or the whole soil column using an automatic pipette (Rainin® Model E4 XLS) set at speed 1 (slow). Water was added in increments to achieve 80% of field capacity (FC) as determined from the individual soil's moisture retention curve (Appendix, Table B1). Following addition of water, and placement into the glass chamber, a packed soil column was allowed to equilibrate up to 30 min before commencing measurements. The mass of water loss was determined as the difference between sequential weighing of the assembled chamber (Mettler

Toledo, Model XS6001M, SNR 1129160413) every time the denuder tubes were replaced. At the end of experiment, the soil columns were dissected into three layers of 0-2, to 2-4, and 4-6 cm. Each soil layer was analyzed for 2M KCl extractable NH_4-N and NO_3-N, soil moisture content, and pH.

Fumigation procedure

In certain experiments, soil fumigation using chloroform was employed to control soil microbial activity. Distilled water was added to the soil to achieve approximately 50% of FC. A small portion of moist soil (originally 50 g air-dried soil) was placed into thirteen 200 mL wide glass bottles and the bottles set into a glass vacuum desiccator lined with wet Kimwipes® to maintain ~ 100% relative humidity. The desiccator also contained ~75 mL ethanol-free chloroform ($CHCl_3$) in a 125 mL Erlenmeyer flask with a few boiling chips. The glass desiccator was placed under vacuum for 1 minute, which accelerated saturation of the interior atmosphere with $CHCl_3$. The evacuated desiccator was then placed in a dark cabinet at room temperature (22°C) for 10 days. The flask of $CHCl_3$ was then removed and the desiccator evacuated 5 times. The thirteen increments of fumigated soil were then mixed and used to pack a soil column.

Table 2.3. Description of experiments carried out using simple flow-through chambers

Experiment	Objective	Experimental Conditions
1. Impact of different soil textures on water and NH_3 loss	Examine the impact of different soil textures on water and NH_3 loss.	Soil water and NH_3 loss were measured during 120-hour period. The effective exchange rate 4.5 times per min. The soil conditions were: BASF-ls (650 g), depth (60 mm), 80% FC (60 mL) CEFS-sl (650 g), depth (70 mm), 80% FC (140 mL) DUKE-sl (550 g), depth (65 mm), 80% FC (160 mL) BASF-cl (650 g), depth (70 mm), 80% FC (162 mL)
2. Impact of different flow rates on water and NH_3 loss	Investigate the impact of different air flow rates on water and NH_3 loss.	ǂ Three portions of ~ 216.5 g air-dried BASF-sl soil were packed into PVC cylinder columns in depth increments of 4-6 cm, 2-4 cm, and 0-2 cm. A fixed amount of water was added to each depth increment (20 mL) for a total of 60 mL H_2O. The duration of an experiment is 156 hours.
3. Redistribution of solute due to water loss	Measure the redistribution of NH_4^+ following the spiked addition of NH4-N to a layer of soil within a packed soil column	ǂ BASF-sl soil was packed similar to non-amended soil. 66 µg NH4-N/g soil was added to lower 2/3 of soil column. The total NH_4-N content in the three depth increments at time zero was: 0-2 cm = 446 µg NH_4-N; 2-4 cm = 14300 µg NH_4-N; 4-6 cm = 14300 µg NH_4-N. The duration of an experiment is 144 hours.
4. Impact of wetting and drying on NH_3 loss from fumigated non- amended soil	Comparing the NH_3 loss during cycles of successive wetting and drying periods and quantifying the total mass of NH_3 that can be detected over given period of time. Fumigated soil was used to eliminate biological processing of the N pool.	††Chloroform fumigated BASF-ls soil was packed into PVC cylinder columns (n = 4 per experiment) to a bulk density of approximately 1.4 g cm^{-3}. Distilled water was added to compensate for water loss. The duration of an experiment was 30 days.
5. Dose response curve	Evaluate performance of simple design in characterizing NH_3 loss from soil with varying additions of NH4-N	††NH_4-N was added to BASF-sl soil at rate of 2x, 5x, 10x, and 20x of the initial soil content of NH_4-N. The duration of the experiment was 120 hours.

† Soil column conditions: BASF-ls (650 g), depth (60 mm), and 80% FC, effective exchange rate (4.5 times per min).

†† Initial water content of each column was set at ~ 80% FC and flow rate was set at 6 LPM (effective exchange rate of (5.4 times per min). Water was added to the individual columns every ~ 24 hours to bring them back to the initial water content of ~ 80% FC.

2.6. Laboratory Room Air NH_3 Concentrations

The chamber inlet annular denuder tubes were used as a measure of the ambient NH_3 concentration in the laboratory room air for the period 9/22/2016 to 3/18/2018 (Fig.2.2). The range in laboratory room air NH_3 concentrations varied as a function of year. The calculated mean values for 2016, 2017 and 2018 were 1.49, 1.71, 1.24 μg NH_3-N m^{-3}, respectively. The presence of NH_3 reflects the fact that there are multiple sources of NH_3 in most modern buildings – these include floor waxes and cleaners, bathrooms and bathroom cleaners, as well as the use of reagents in other laboratories. Additionally, a fume hood was kept on continuously during an experiment to help control temperature in the room. Thus, the room where the experiment was conducted was under negative pressure and drew in air from other parts of the building. The measured ambient NH_3 levels illustrate that any exposed surfaces to ambient air within most buildings are continuously exposed to NH_3. Any exposed surface, dry and especially wet, will attempt to equilibrate with the partial pressure of NH_3 in the room atmosphere. This includes any air-dry soil that was stored in the room unless it had an air tight lid.

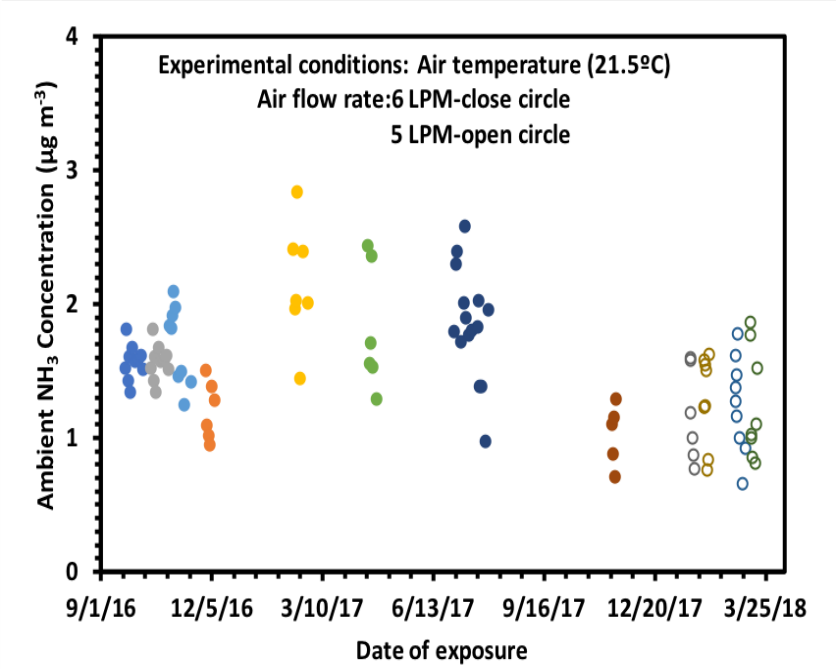

Figure 2.2. Ambient NH_3 concentrations as a function of date measured under laboratory room conditions from 9/22/2016 to 3/18/2018 using annular denuder tube technology. Dates of exposure correspond to individual experiments.

Precondition the chamber

The presence of significant amounts of NH_3 in the laboratory atmosphere suggested that the internal surface of the flow-through chamber may release NH_3 at the start of an experiment when exposed to essentially NH_3-free air entering the chamber. This would result in a potential significant positive bias in the mass of NH_3 collected and assumed released by the soil in the packed columns. We assessed the potential for this positive bias in our measurements by running empty chambers (no soil) with accompanying annular denuder tubes (Fig. 2.3). We assumed that any measurable NH_3 captured in the exit annular denuder tube in the outlet stream originated from the interior walls of the chamber unless there were significant leaks in the chamber design allowing air to enter the chamber, by-passing the annular denuder tube on the inlet.

Measurable amounts of NH_3 were apparently released from the internal surfaces of the glass chamber and empty PVC columns during the first ~ 100 hours of the experiment (Fig. 2.3). The shape of the release curve appeared to mirror the changes in average NH_3 concentration in the room. Either NH_3 was being pulled into the chamber and by-passing the inlet annular denuder when the average ambient concentrations exceeded 1μg NH_3-N m^{-3}, or the trends in the data for the inlet and outlet concentrations are just a coincidence for this one experiment. In any event, a decision was made to precondition the chamber before starting subsequent experiments. The empty chamber system was assembled and kept running with an annular denuder tube on the inlet to each chamber for at least 24 hours prior to starting an experiment. A "pre-conditioned" chamber was then loaded with a packed soil column and sealed as quickly as possible at the start of each experiment. For the remainder of this study it was assumed that all the NH_3 captured by the outlet denuder tube was derived for emission of NH_3 from the soil surface.

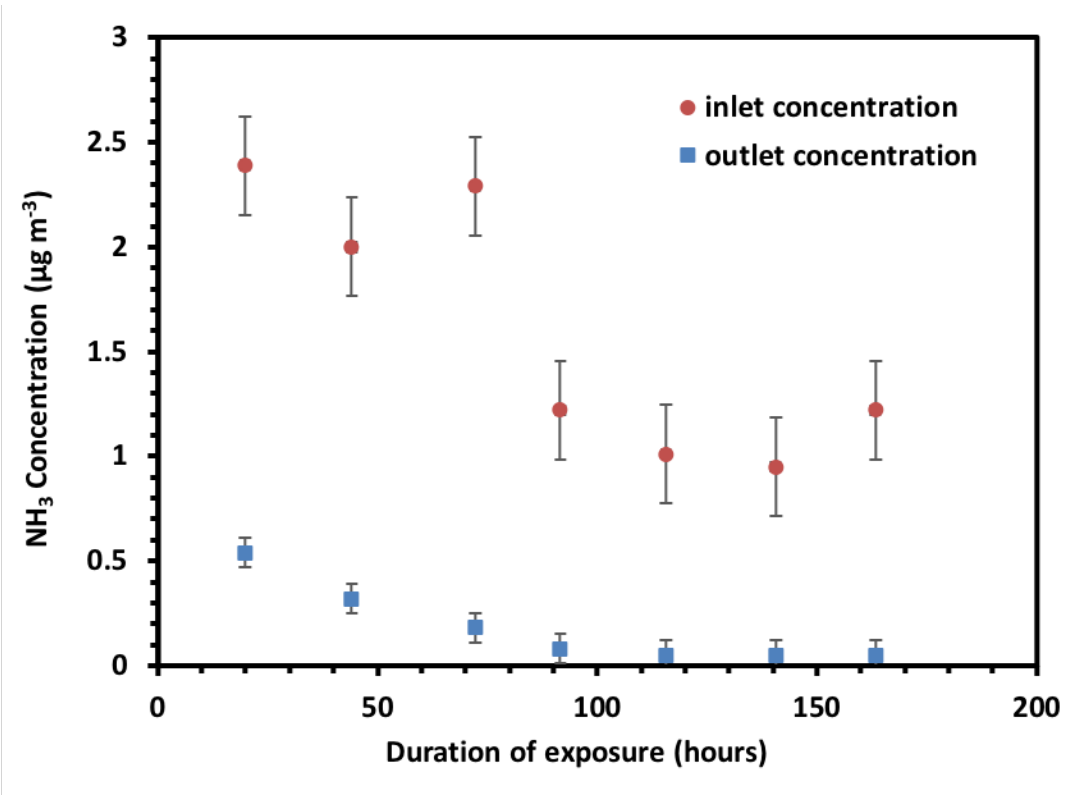

Figure 2.3. Inlet and outlet NH_3 concentrations for an empty chamber as a function of duration of exposure (hours). Vertical bars denote the standard error of the mean (n = 4). Experimental conditions: Date: 4/4/2017 to 4/10/2017; Temperature (23ºC); Effective exchange rate (5.4 times per min). (Air flow rate 5 LPM).

Laboratory Blank

Laboratory blanks were set aside for each batch of prepared annular denuder tubes and extracted along with exposed annular denuder tubes that were attached to the chambers. The average mass of NH_3-N from 24 laboratory blanks extracted from 2016 through 2018 was 0.16 µg NH_3-N. Approximately 36% of the laboratory blanks contained between 0 to 0.09 µg NH_3-N, 36% contained between 0.1 to 0.3 µg NH_3-N, and the remaining 14% contained between 0.3 to 0.4 µg NH_3-N.

Limit of Detection (L_D) was evaluated based on the standard deviation of laboratory blanks as reported by Currie (1999):

$$L_D = 2t_{1-\alpha,\upsilon}\sigma_o \quad \text{Eq. (2.7)}$$

where t is two-tailed student's t value, υ is degrees of freedom, α= 0.05 probability, and σ_o is the standard deviation of laboratory blanks. The standard deviation for the laboratory blanks was 0.12 µg N. The value of 2t was based on 23 degrees of freedom and a t value = 2.069 for 0.05 level at the 95% probability level. This yielded a minimum detection value of 0.50µg N.

2.7 Ancillary Measurements

Soil pH was measured in a 1:2.5 (soil: deionized water mixture) using a pH meter and combination glass electrode (Accumet® Model BASIC AB15; Thermo-Fisher Scientific) calibrated with NIST-traceable pH standards. Temperature and relative humidity were measured in the laboratory room using an EL-USB-2LCD RH/TEMP DATA LOGGER. Gravimetric soil moisture was determined by mass loss after heating 10 g of soil for 48 hours at 60 °C with a detection limit on the order of 0.01g H_2O g^{-1} fresh soil.

Soil NH_4-N and nitrate-N (NO_3-N) extraction: Five grams of soil was mixed with 25 mL 2M KCl solution in 50 mL screw cap centrifuge tubes (Corning®, Inc.). The mixture was shaken for two hours on a rotating shaker (Glas-Col®,LLC. Model: 099A RD4512, Ser. No. 11327320), and then centrifuged at 2500 rpm for 20 min (IEC Model K Centrifuge. Serial No. 71652652) to obtain a clear supernatant solution. The solution was then passed through Whatman No.42 filter paper and collected into a 15 mL screw cap PVC conical centrifuge tube and stored until analysis at 4°C. Results of soil extractions are expressed on an oven-dry mass basis. Oven dry mass was determined based on separate measurements of moisture content. Soil NH_4-N and denuder

extracts were analyzed via a flow injection analyzer (Lachat, Quick-Chem 8000). A representative standard curve for NH_4-N and NO_3-N solutions prepared in 2M KCl are shown in Appendix C1. Analyses were carried out using 9-point standard curve from 1 to 20 μg NH_4^+ per mL plus calibration checks. Data for the standard curves were fitted using a second-order polynomial via IGORPro® software (WaveMetric, Inc.) to calculate the concentrations of NH_4-N and NO_3-N in each extract (Appendix C1 and C2).

2.8. Statistics

Scatter, histogram, and non-linear graphs were generated using Microsoft® Excel software (version 16.22) or via IGORPro® software (WaveMetric, Inc.). Statistical analysis was performed using also Microsoft® Excel software.

3.0 Results and Discussion

3.1 Water Loss from Packed Columns

Influence of soil texture

The rate of water loss observed as a function of soil texture at a flow rate of 5LPM is shown in Fig. 2.4. In general, none of the soils exhibited Stage 1 water loss as described by Hillel (2004). This indicates that at 5LPM, and an initial water content of ~ 80% FC, the soils used in this study will start at Stage 2 water loss at time zero. As suggested by Hillel (2004), the differences in the rate of water loss between the soils is controlled largely by differences in soil texture. This is evident in Fig. 2.4, where the BASF-cl has the highest rates of water loss, the CEFS-sl had the lowest observed rates, and the BASF-ls falls in between. The exception is the DUKE-sl, which exhibited water loss rates comparable to the BASF-cl. One explanation for this exception is the apparent higher soil organic matter content of the DUKE-sl, versus the other

soils obtained from the surface of tilled fields. Beyond ~ 120 hours, the four soils appeared to enter into Stage 3 water loss. Actual loss from the CEFS-sl neared zero, again reflecting the influence of soil texture on overall soil water content.

Addition of water

The BASF-ls soil was used to investigate the potential effect of the method of addition of water to the soil column may have had on the rate of water loss. In one trial, water was added to the top of the dry packed soil columns in 10 mL increments (total 60 mL). Each succeeding 10 mL increment was added only after the previous increment had penetrated into the soil. The wetted soil columns were then allowed to stand 15 minutes before starting measurements. In the second trial, the soil column was packed in 2-cm increments and DI water added to each 2-cm increment (10 mL intervals, total 20 mL per packed layer) before adding the next layer of soil. The cumulative water loss for the different methods of water addition as a function of time are shown in Fig. 2.5.

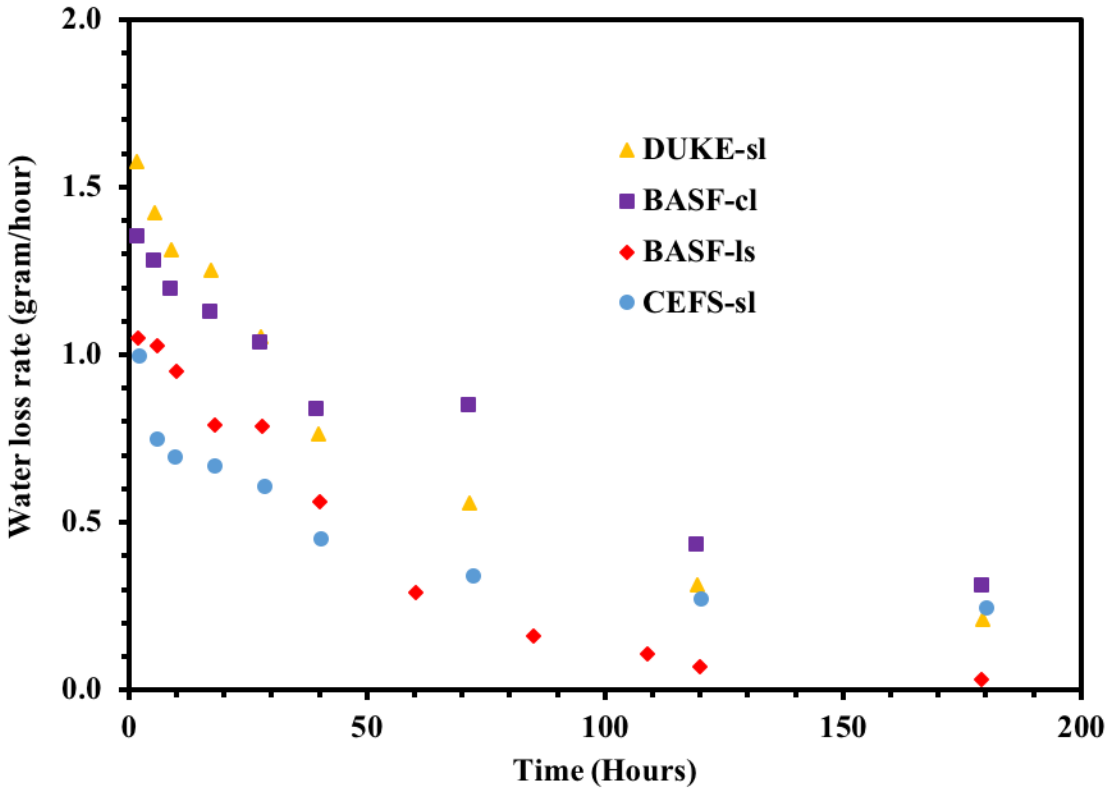

Figure 2.4. Water loss rate (gram/hour) versus time (hour) for soils of different texture. Experimental conditions: Air flow rate = 5LPM, 80% FC; BASF-ls (650 g, 5.5 cm depth); CEFS-sl (650 g, 7.0 cm depth); DUKE-sl (550 g, 6.5 cm depth); BASF-cl (650 g, 7.0 cm depth).

Overall, the rates of water loss between the two methods of adding water were similar. During the first 20 hours of the experiment, the rate of water loss appears nearly linear, then gradually slows, especially after 30 hours. Approximately the same amount of water was lost from either method of water addition by 50 hours after the start of the experiments. The largest variation in results was observed within the individual trials, especially for adding all the water to the top of the entire packed soil column (Fig. 2.5a). The differences between replicates within a trial start to become evident around 5 – 10 hours after initiation of the individual experiments. The large deviation observed for the one chamber where all the water was added to the top of the packed soil column probably resulted from a combination of how the soil column was packed and the resulting influence on the redistribution of the added water within the column.

Movement of the added water deeper within the individual column would act to slow water loss over time. Adding water to packed soil increments appears to result in more even distribution of water within the packed column at time zero.

Chamber Position

The results in Fig. 2.6 might also be explained by the physical placement of the individual chambers on the laboratory bench. To test the influence of physical placement of individual chambers, a total of three positions were sampled along the laboratory bench. The chambers and the microprocessor-controlled pump were placed on the same bench. The prepared chambers were placed at distances of ~100, 50, and 30 cm (named as positions 1, 2, and 3, respectively) from microprocessor-controlled pump. The physical placement of Chambers 1 and 2 on the bench top placed them relatively closer to the room wall-mounted HVAC units and the windows located along the south wall. The individual soil columns were packed in 2-cm depth increments and water added (20 mL total) to each increment as described for Fig. 2.5b. Total loss of water was 50.3, 49.00, and 50.60 g for chambers in positions 1, 2 and 3, respectively (Fig. 2.6). The maximum difference of total loss among three chambers was 1.6 g. The overall average total loss was 49.97±0.85 g (1.7% RSD) or ~ 83% of the water added in ~ 125 hours. Though chamber differences in total loss after 120 hours were small, larger differences between one of the chambers and the other two were observed during the first 24 hours. The maximum variation between replicates occurred between 6 and 32 grams of water loss, especially for Chamber 1, which was positioned closest to the room HVAC units and windows. This suggests that placement within the room may have had an impact of rates of water loss during the first ~ 40 hours of an experiment. However, the overall variation was similar in magnitude to that observed in Fig. 2.5b and may also have been largely due to packing

of the soil increments within that particular soil column. Overall, the temporal trend in water loss was consistent across all three chambers and all three reached approximately the same total water loss by the end of the experiment.

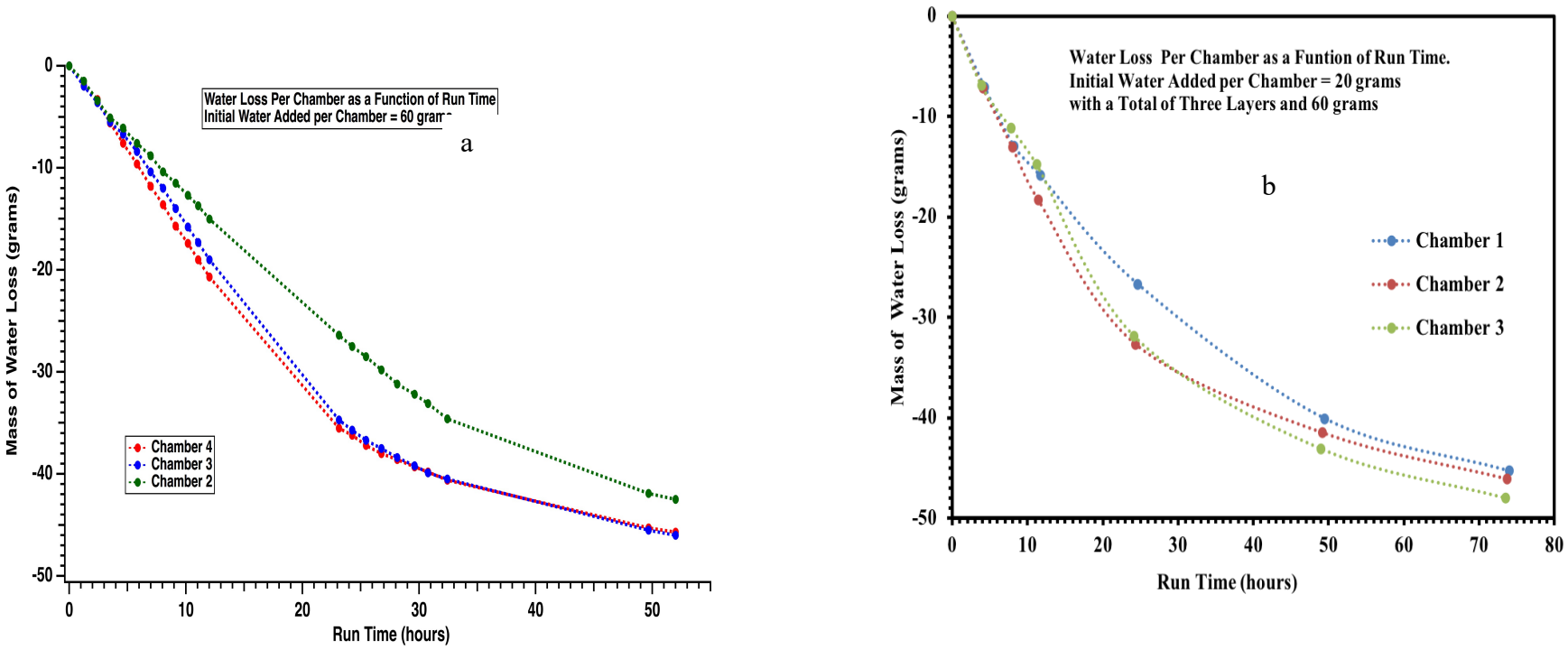

Figure 2.5. Water loss curve for BASF-ls soil as a function of run time. Experimental conditions: (a) Water was added to top of dry column in 10 mL increments to a total of 60 mL per chamber. (b) Water was added per 2-cm packed layer (20 grams per packed layer, 60 grams total). Air exchange rate = 4.5 vol/min, FC (80%), soil (650 g, 6.0 cm soil depth)

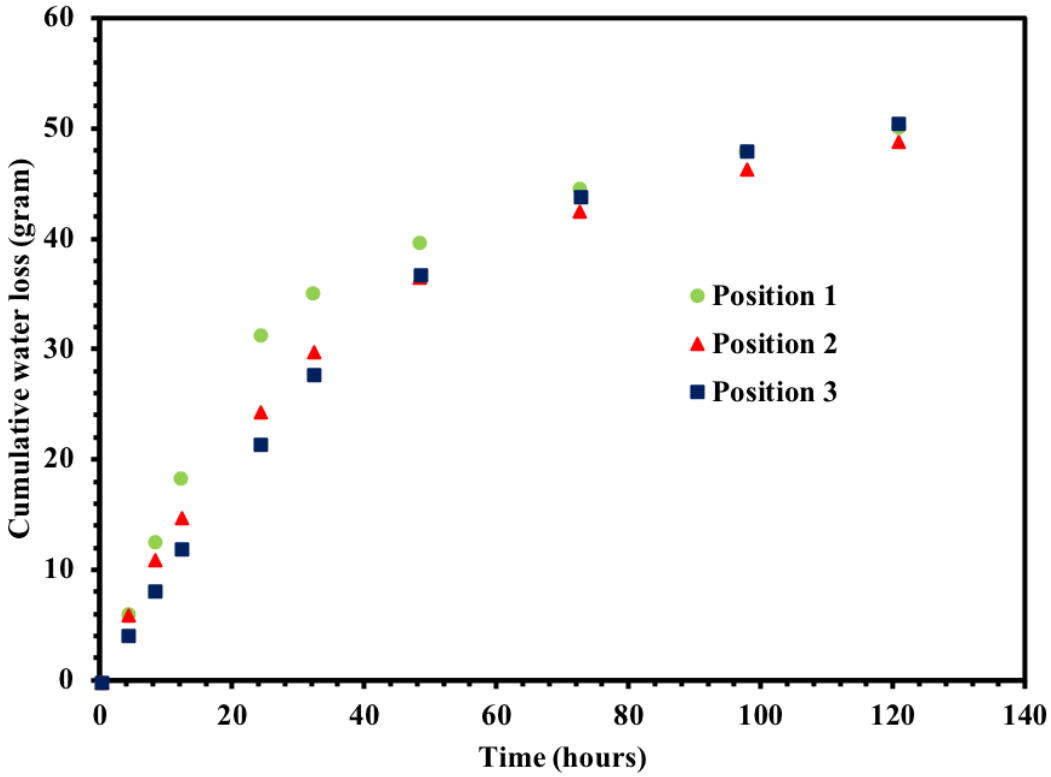

Figure 2.6. Cumulative water loss measured for BASF-ls soil using a simple through-dynamic chamber as a function of chamber position and a function of time. Experimental conditions: soil mass (650 g, depth 6.0 cm), FC (80%), and exchange rates (4.5 vol/min), Date of experiment (01/31/2018-02/05/2018).

Influence of temperature and relative humidity

Temperature and relative humidity (%RH) in the laboratory air can have a marked impact on water loss using the simple flow-through chambers. A summary of the range of room temperatures and %RH values observed during three experiments (Jan. 17-19, 2018, Jan. 31 to Feb. 5, 2018, April 10-16, 2018) are provided in Table 2.4. Overall, temperature control in the laboratory was very good as the mean temperature for each period only varied by 1.6˚C and the minimum and maximum temperatures were basically the same. The largest differences observed were for %RH between the three experimental periods, with changes in %RH being driven by changes in the outside weather. The values of %RH during the period January 17 to January 19

were low and nearly constant (6.5% to 8.5% from t = 0 to t = 27 hours), then increased to 28% at t = 52 hours (data not shown). The trend in %RH during the second period from January 31 to February 5 increased from 17% at t = 0 to 31% at t = 28 hours and then decreased to 12% at t = 60 hours. It again increased to 37% at t = 85 hours with a final value of 20% at t = 109 hours. For the last period from April 10 to April 16, %RH was relatively constant at 28% from time zero to t = 32 hours and then increased to 59% at t = 106 hours (data not shown). Changes in %RH did impact the strength of water loss during certain time periods within an experiment, but not the overall patterns in cumulative water loss. The variation in %RH would also not be responsible for the differences observed between chambers within a given trial.

Table 2.4. Descriptive summaries of air temperature and percent relative humidity during measurement period. Experimental conditions: BASF-ls soil, soil mass (650 g), FC (80%), and exchange rate (4.5 vol/min).

Period	Jan. 17 – 19, 2018	Jan. 31-Feb. 5, 2018	April 10-16, 2018
Ambient Air Temperature (ºC)			
Mean	20.6	21.5	22.1
Std. Dev.	0.80	0.41	0.23
Minimum	19.1	20.5	22.0
Maximum	21.6	22.0	22.5
Percent Relative Humidity (%)			
Mean	11.1	22.3	35.6
Std. Dev.	6.9	7.5	13.4
Minimum	6.50	12.0	27.0
Maximum	28.0	37.0	59.0

Impact of exchange rate (flow-rate)

The effect of exchange rate on water loss curves using the BASF-sl soil is shown in Fig. 2.7. Measurements of water loss were taken every 4 hours for the first 12 hours, and then every 24 hours for five days. At the lowest exchange rates (0.9 and 2.7 vol/min), the moisture loss curves appeared to follow Stage 1 water loss as described by Hillel (2004). Stage 1 water loss appeared to last at least 40 hours at 0.9 vol/min, and at least 24 hours for 2.7 vol/min. There is a suggestion that Stage 1 water loss even occurred for a few hours at 4.9 vol/min. At the highest exchange rate of 7.2 vol/min, the rate of water loss immediately fell into the Stage 2 category. The rate of water loss among the 5 different exchange rates began to merge at the ~ 80 hour mark (Fig. 2.7).

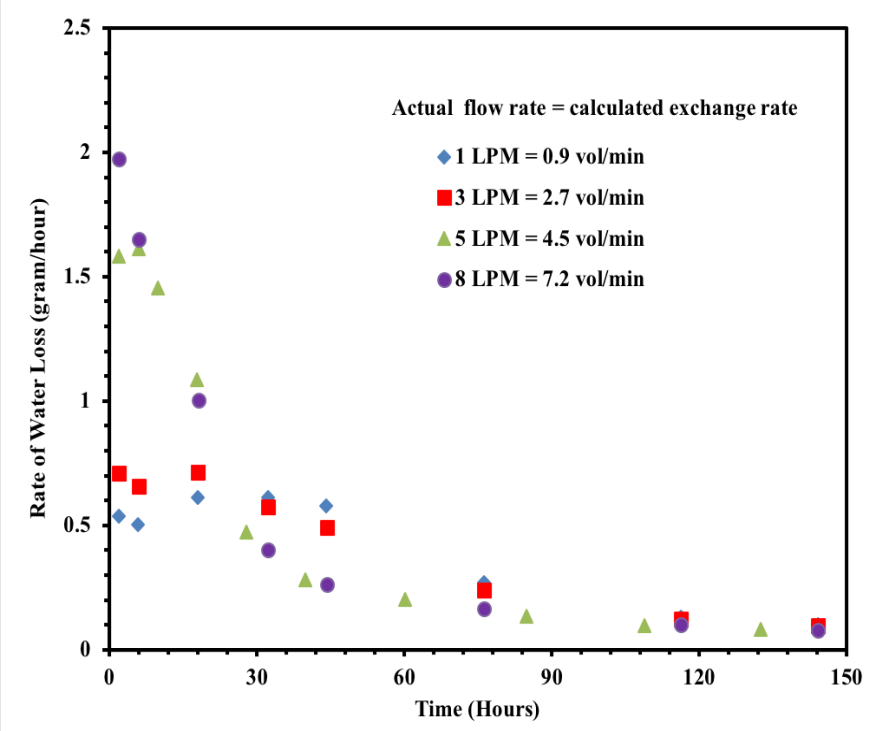

Figure 2.7. Water loss rate (gram/hour) versus time as a function of air exchange rate for BASF-sl soil. Experimental conditions: soil mass (650 g), FC (80%). A fixed amount of water was added to each depth increment (20 mL) to a total of 60 mL water. The flow rates 1, 3, 8 LPM were run at the same time from 03/12/2018 to 03/18/2018. The flow rate at 5 LPM was run from 04/10/2018 to 04/16/208.

The cumulative loss data at each flow rate are shown in Fig. 2.8a. To facilitate comparisons between the 4 flow rates, the cumulative loss from each flow rate was fit using a regression model and the results plotted in Fig. 2.8b. The results suggest that overall cumulative water loss at flow rates of 3 LPM or less result is the same after 150 hours. At flow rates of 5 LPM or higher, there is a tendency to increase total loss as flow rate increases, but the resultant total loss by 150 hours is similar.

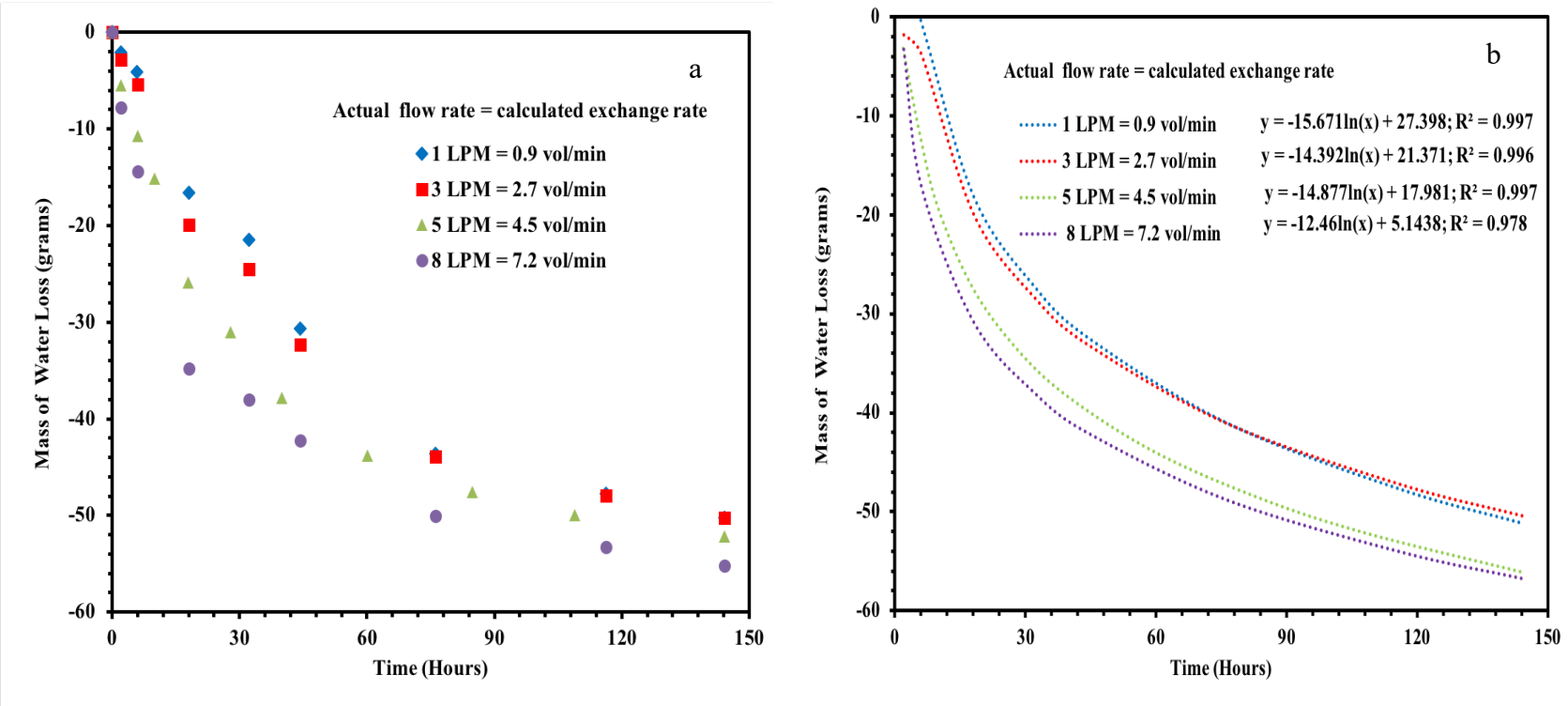

Figure 2.8. Comparison between (a) a measured water loss and (b) estimated water loss using a nonlinear function for BASF-ls soil at different air exchange rate. Three portions of ~ 216.5 g air-dried soil were packed into PVC cylinder columns to a depth of and 4-6 cm, 2-4 cm, and 0-2 cm. A fixed amount of water was added to each depth increment (20 mL) to a total of 60 mL water. The flow rates 1, 3, 8 LPM were run at the same time from 03/12/2018 to 03/18/2018. The flow rate 5 LPM was run from 04/10/2018 to 04/16/2018.

3.2. Redistribution of Solute due to Water Loss

The impact of water movement on solute transport within the columns during evaporation was evaluated using both non-amended and amended un-fumigated soil (BASF-ls) with nitrogen added as ammonium sulfate. Extractable (2M KCl) NH_4-N and NO_3-N was determined at time zero, and then at 24, 48, 72 and 144 hours after the start of the experiment. With only 4 chambers, each time period sampled represents a single packed soil column. For these experiments, the soil was packed in 2-cm increments and water, or water plus NH_4-N added to each increment as needed.

Non-Amended Soil

The results for the 2M KCl extracts of the individual soil columns for the non-amended soil are summarized in Table 2.5. Total inorganic N present at time zero was 980 µg-N. It is readily apparent that during the first 24-hour period of the experiment there was substantial mineralization of N resulting in ~ 2x increase in NH_4-N within the packed soil column. There is also a noticeable increase in the NO_3-N content, suggesting both conversion of NH_4-N to NO_3-N as well as potential transport of NO_3-N toward surface of the packed column. There was actually an apparent slight decrease of NO_3-N in the 4 – 6 cm depth at time=24 hours (Table 2.5).

Assessing potential solute redistribution using the data in Table 2.5 is not straightforward because of the compounding presence of N-mineralization and conversion of NH_4-N to NO_3-N. The first step was to assess whether the total N within the entire packed column varied over time, possibly due to continued mineralization or denitrification due to the presence of increased NO_3-N. After the initial burst in mineralized N during the initial 24 hours of the experiment, total-N within the packed soil column appeared to remain relatively constant for the remaining duration of the experiment (Fig. 2.9), suggesting mineralization was essentially complete within 24 hours

and there were no other losses of inorganic N. There was a consistent, nearly linear increase in NO_3-N at the expense of NH_4-N (Fig. 2.9). When viewed for each packed depth increment, there was a definite shift of the total-N present to the surface 0 – 2 cm depth increment (Fig. 2-10). This shift was in part at the expense of the deeper depth increments, with loss from the 4 – 6 cm increment always greater than loss from the 2 – 4 cm depth increment. This shift in the distribution of total-N within the packed column did not follow the change in water loss due to evaporation. The change in the distribution of total-N is only a few percent between depth increments by the 24-hour mark, even though total water loss from the packed column had already reached 40% of the amount of water added (Fig. 2.10). This relatively small redistribution of total-N during the period of highest rate of water loss maybe compounded by the fact that NH_4-N was doubling within the packed column due to mineralization.

Table 2.5 Distribution of 2M KCl extractable NH_4-N and NO_3-N found in packed non-amended soil (BASF-ls) columns as a function of depth increment and time.

Time	NH_4-N	NO_3-N	Sum
- hours -	- µg N -	- µg N -	- µg N -
Depth Increment: 0 – 2 cm			
0	430	550	980
24	1097	695	1792
48	1023	891	1914
72	886	1027	1913
144	861	1615	2476
Depth Increment: 2 - 4 cm			
0	430	550	980
24	1061	618	1679
48	1054	655	1709
72	902	697	1599
144	428	1137	1565
Depth Increment: 4- 6 cm			
0	430	550	980
24	1080	535	1615
48	1112	568	1680
72	987	587	1574
144	395	994	1389

A measure of the relative percent change within each depth increment for NH_4-N and NO_3-N as a function of time is shown in Figs. 2.11 and 2.12, respectively. The data in these figures represent the relative percent distribution of total NH_4-N or NO_3-N within each depth increment as compared to the percent distribution of total NH_4-N or NO_3-N at time zero. The solid lines connecting the individual data points are added to see the overall trend in the relative percent distribution of NH_4-N or NO_3-N found, and do not necessarily indicate movement of N. As indicated in Fig. 2.10, there was relatively little change among the 3 depth increments in the relative distribution of NH_4-N up to the 72-hour mark. In other words, even though the total amount of NH_4-N in the column was decreasing (Fig. 2.9), the relative distribution of NH_4-N within the packed column did not change. The small change in relative amounts of NH_4-N suggest there was little impact of water loss on NH4-N redistribution within the packed column

for the non-amended soil. There was a significant change in percent relative distribution of total NH_4-N by time = 144 hours, indicating that of the total NH_4-N present, ~ 20% more was in the 0 – 2 cm depth increment, while there was a corresponding loss of ~ 10% in the lower two depth increments (Fig. 2.11). This relative change in the distribution of NH_4-N occurred during the period of slowest rate of water loss when the packed column was at the end of Stage 2 and moving into Stage 3 water loss.

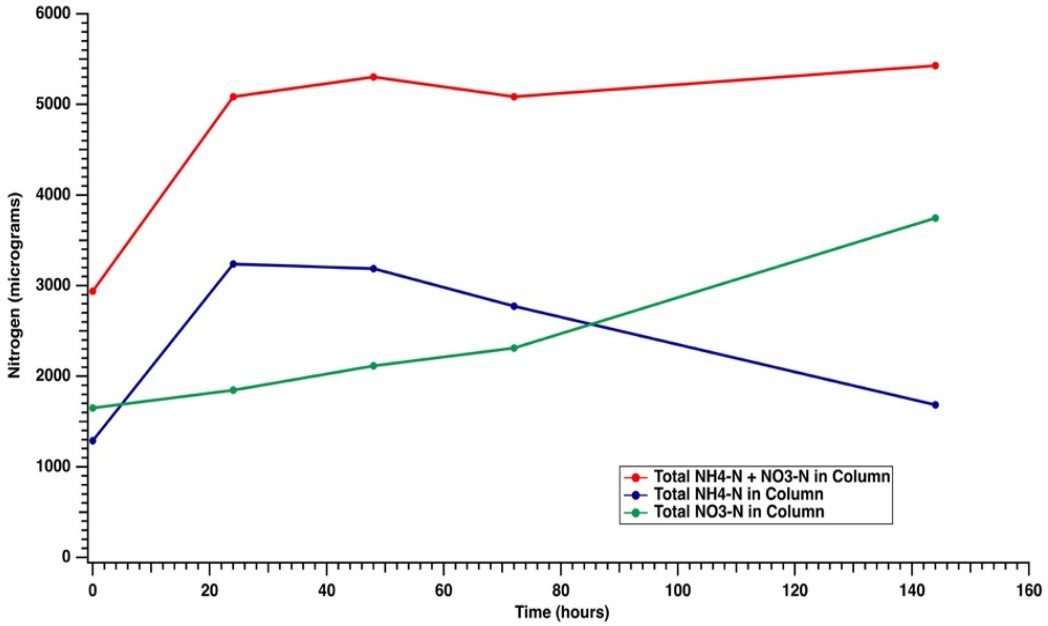

Figure 2.9. Amount of 2M KCl extractable total NH_4-N and NO_3-N and their sum in non-amended packed soil (BASF-ls) column as a function of time. Solid lines added as a visual aid to show over trend in the data.

The relative changes in NH_4-N within the packed column are, for the most part, explained by the corresponding relative changes in the distribution of NO_3-N within the packed column (Fig. 2.12). Compared to time zero, there was a consistent increase in NO_3-N within the 0 – 2 cm depth increment and 2 – 4 cm depth increment throughout the experiment (Fig. 2.12). This change was due in part to mineralization of NH_4-N present, but the data also suggest this change

was driven by consistent loss of NO_3-N from the 4 - 6 cm depth. This relative loss appeared to end at time = 72 hours, when rate of water loss slowed to its minimum value.

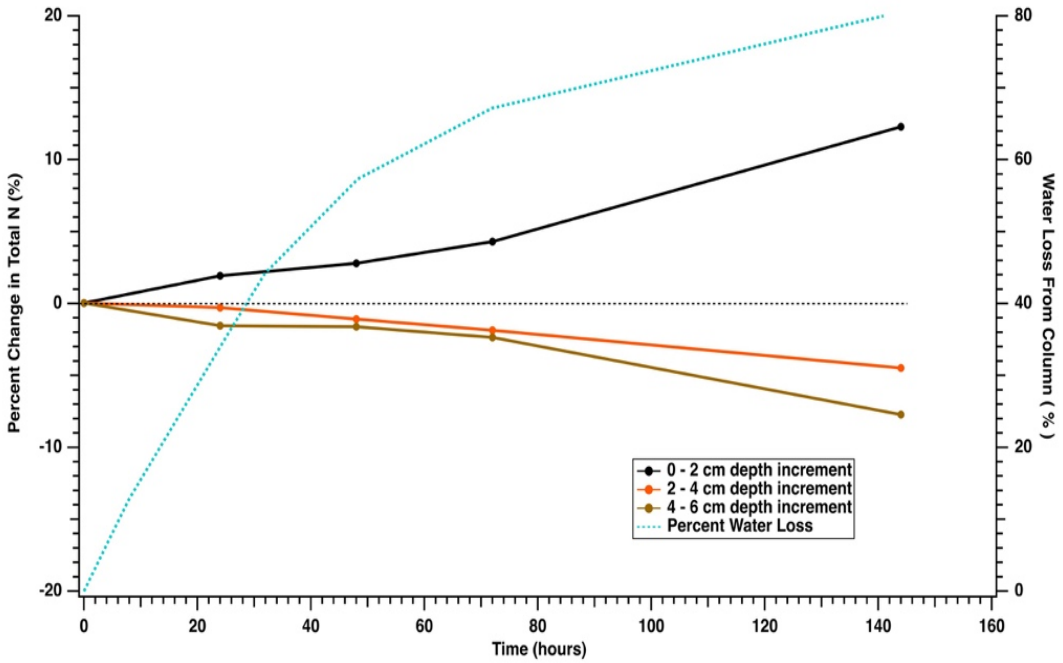

Figure 2.10. Percent change in proportion of total-N present in each depth increment for a non-amended soil (BASF-ls) as a function of time as compared to percent of water loss. Solid or dashed lines added as a visual aid to show over trend in the data.

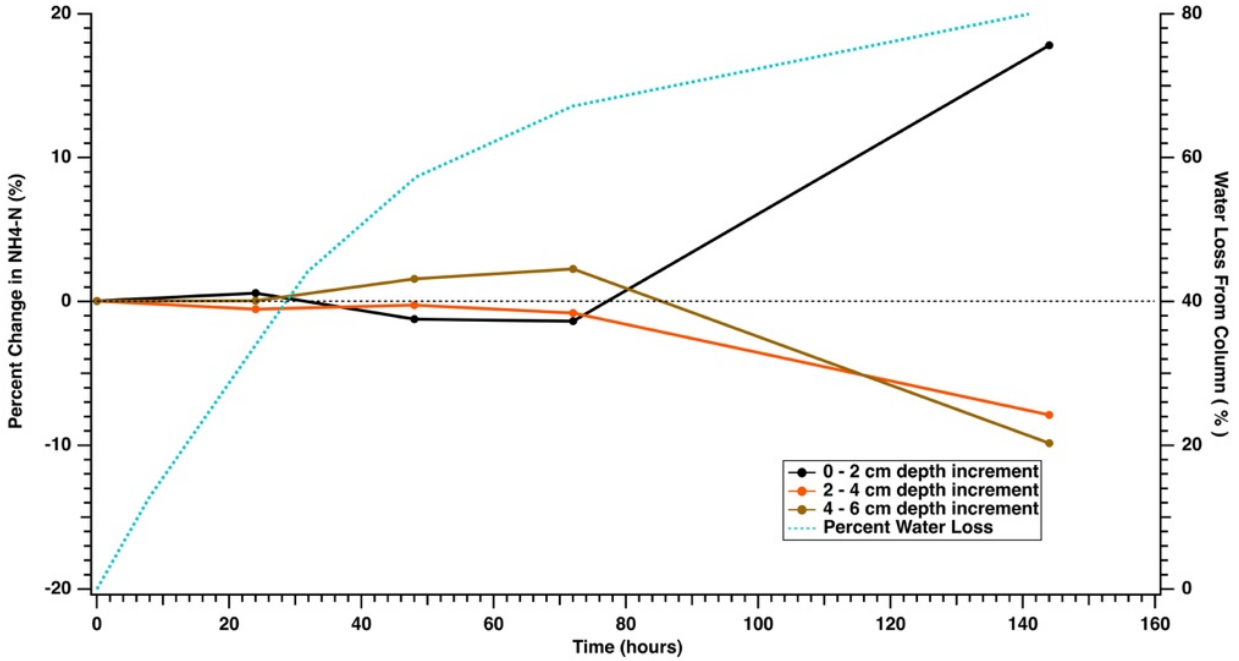

Figure 2.11. Relative percent change in the distribution of NH_4-N for a given depth increment for a packed non-amended soil (BASF-ls) column as a function of time as compared to percent of water loss. The data points represent the change in percent NH4-N within each depth increment as a function of total NH_4-N present relative to the same percent distribution of NH_4-N at time zero. Solid or dashed lines added as a visual aid to show over trend in the data.

When looking at the change in total-N within each depth increment across 144 hours, approximately 291 µg-N was lost from the 4 – 6 cm depth increment, and 144 µg-N from the 2 – 4 cm depth increment, for a total of 435 µg-N (Table 2.5). The gain in total-N in the 0 – 2 cm depth increment was 1496 µg-N. Of this, ~ 812 µg-N was due to mineralization within the first 24-hours, assuming that the increase in NO_3-N during this time period in the 0 – 2 cm depth was due to nitrification within that depth increment. This leaves an apparent net increase in total-N in the 0 – 2 cm depth increment of ~ 684 µg-N, of which only 435µg-N can be accounted for by the calculated loss of N from the lower two depth increments. This suggests that mineralization of N continued within the packed soil column beyond the 24-hour period indicated in Fig. 2.9, and that the relatively small loss in NH_4-N in the 0 – 2 cm depth increment (Table 2.5) was not due to NH_4-N transport from the deeper increments within the packed column but was due to

continued mineralization. The apparent loss of NH_4-N from the deeper two increments was not due to transport but was due primarily to nitrification. Across all three depth increments, the apparent degree of nitrification appeared to be greatest between 72 and 144 hours, when the soil column has already lost ~ 70% of the water added.

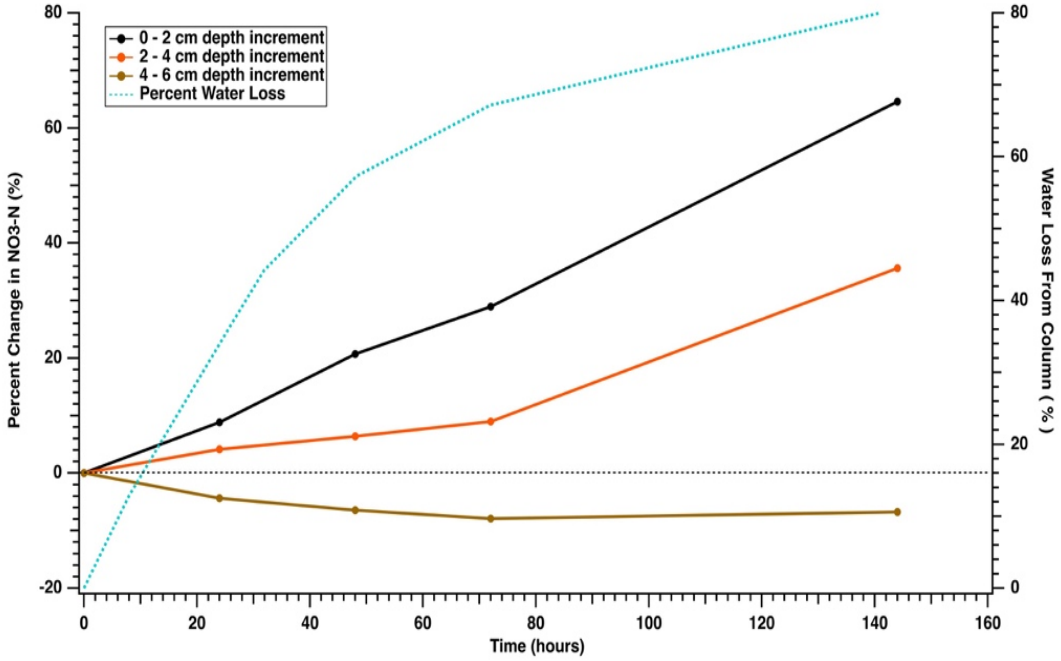

Figure 2.12. Relative percent change in the distribution of NO_3-N for a given depth increment for a packed non-amended soil (BASF-ls) column as a function of time as compared to percent of water loss. The data points represent the change in percent NO_3-N within each depth increment as a function of total NO_3-N present relative to the same percent distribution of NO_3-N at time zero. Solid or dashed lines added as a visual aid to show over trend in the data.

NH_4-N Amended Soil

For the NH_4-N amended soil (BASF-ls), NH_4-N was added to only the lower two depth increments. The target addition rate was ~ 7.5x the amount of 2M KCl extractable NH_4-N found for the non-amended soil at time = zero. The added NH_4-N (as a solution) was applied to each of the lower two depth increments as they were packed and amended with water. At time zero, the amount of NH4-N in 0 – 2 cm depth was 446 µg-N, and 4591 µg-N in the 2-4 cm and 4-6 cm

depths. As for the non-amended soil, each time period sampled represents a single packed soil column.

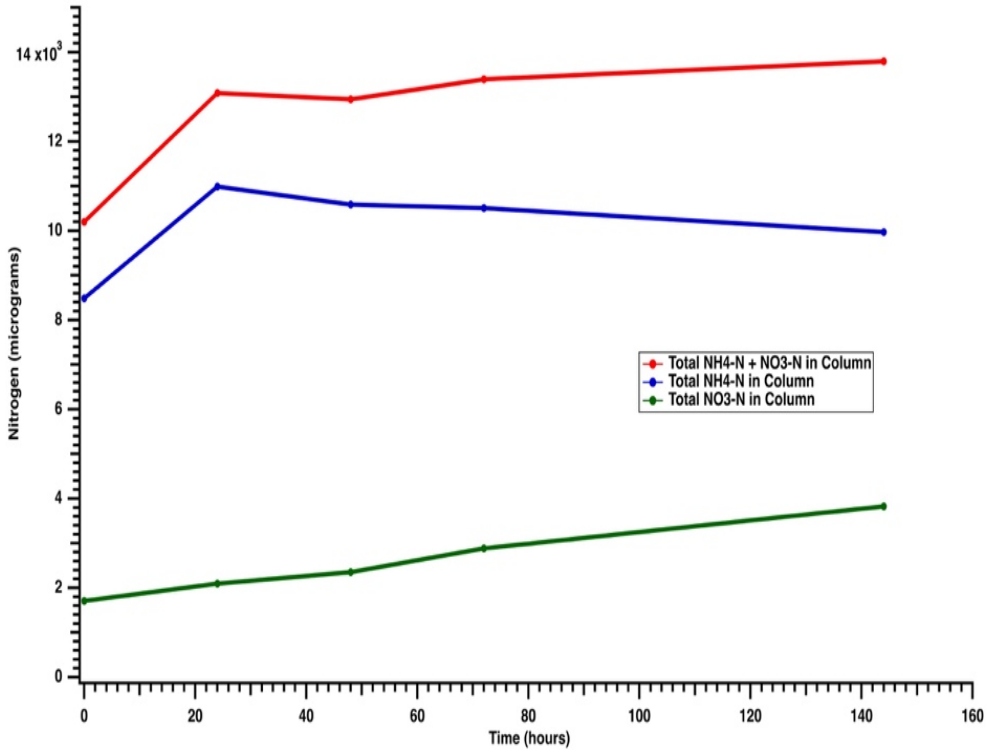

Figure 2.13. Amount of 2M KCl extractable total NH_4-N + NO_3-N and their sum in NH_4-N amended packed soil (BASF-ls) column as a function of time. Solid lines added as a visual aid to show over trend in the data.

The results for the 2M KCl extracts of the individual soil columns for the amended soil are summarized in Table 2.6. The plot of total N (NH_4-N + NO_3-N) and total NH_4-N and NO3-N in the packed column as a function of time is provided in Fig. 2.13. As was apparent for the non-amended soil, there was a significant amount of mineralization of NH_4-N within the first 24 hours, especially in the 0 – 2 cm depth increment. The apparent increase in NH_4-N was actually greater than that observed for the non-amended soil, even assuming some redistribution of NH_4-N during this first 24 hour period. Overall, the total N in the packed column continued to increase during the experiment going from an initial value of ~ 10,200 µg-N at time zero to ~ 13,800 µg-N at time = 144 hours. There was a noticeable increase in total N between time = 72

hours (13,400 μg-N) and time = 144 hours, which suggested as the soil columns became substantially drier mineralization of NH_4-N continued, but not at the rate noted during the first 24 hour period. Overall, NO_3-N increased within the column in almost a linear fashion with a corresponding linear decrease in NH_4-N after the first release of NH_4-N from mineralization (Fig. 2.13). Throughout the course of the experiment, however, the amount of NH_4-N present was substantially greater than NO_3-N.

When viewed for each packed depth increment, the substantial release of mineralized NH_4-N influenced the percent distribution of total-N between the three depth increments (Fig. 2.14). However, there was also a decline in total-N in the lower two depth increments which was due in part to loss of NH_4-N (Table 2.6). This decline is also more consistent with the water loss curve (Fig. 2.14) and appears to slow, or in the case of the 2 – 4 cm depth, stop as rate of water loss slows. Unfortunately, the overall magnitude of the decline in the lower two depths is made to appear more significant than warranted because of the substantial amount of mineralized NH_4-N released during the first 24 hours of the experiment, primarily in the 0 – 2 cm depth. This also influenced attempts of look at the relative percent distribution of total NH_4-N within each depth increment as compared to the percent distribution of total NH_4-N at time zero (Fig. 2.15). The plot essentially mirrored the percent of total N distribution in Fig. 2.14, due to the dominant contribution of NH_4-N to total N and the amount of mineralized N released in the 0 – 2 cm depth.

A plot of the relative percent change within each depth increment for NO_3-N as a function of time is shown in Figs. 2.16. The data in these figures represent the relative percent distribution of total NH_4-N or NO_3-N within each depth increment as compared to the percent distribution of total NH_4-N or NO_3-N at time zero.

Table 2.6. Distribution of 2M KCl extractable NH_4-N and NO_3-N found in packed NH_4-N amended soil (BASF-ls) columns as a function of depth increment and time

Time	NH_4-N	NO_3-N	Sum
- hours -	- µg N -	- µg N -	- µg N -
Depth Increment: 0 – 2 cm			
0	446	570	1016
24	2600	794	3394
48	3291	1087	4378
72	3710	1443	5153
144	4061	1591	5652
Depth Increment: 2 – 4 cm			
0	4021	570	4591
24	3916	692	4608
48	3832	693	4525
72	3673	772	4445
144	3488	1151	4639
Depth Increment: 4 – 6 cm			
0	4021	570	4591
24	4475	610	5085
48	3465	575	4040
72	3124	671	3795
144	2423	1081	3504

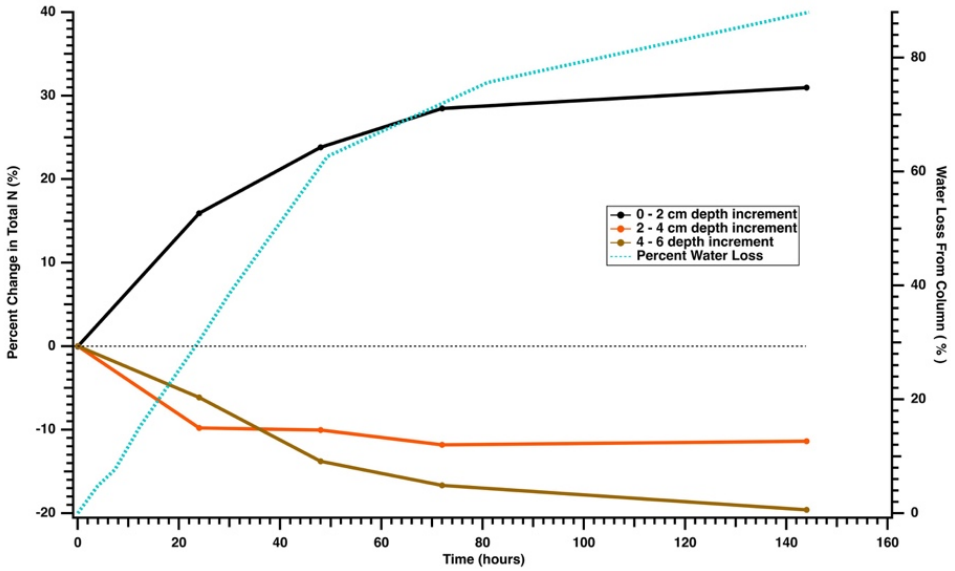

Figure 2.14. Percent change in proportion of total-N present in each depth increment for a NH4-N amended soil (BASF-ls) as a function of time as compared to percent of water loss. Solid or dashed lines added as a visual aid to show over trend in the data.

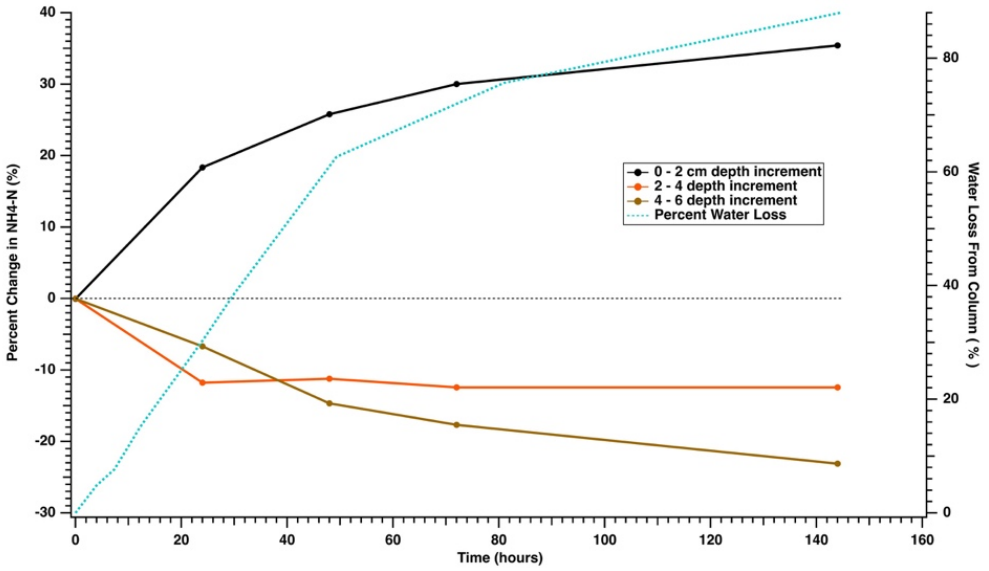

Figure 2.15. Relative percent change in the distribution of NH_4-N for a given depth increment for a packed NH_4-N amended soil (BASF-ls) column as a function of time as compared to percent of water loss. The data points represent the change in percent NH4-N within each depth increment as a function of total NH_4-N present relative to the same percent distribution of NH_4-N at time zero. Solid or dashed lines added as a visual aid to show over trend in the data.

Figure 2.16 indicates that there was a continuing shift in the relative distribution of total NO3-N within the packed column to the top 0 – 2 cm increment at the expense of the lower two depths till the 72 hour mark. Beyond 72 hours, nitrification in the lower 2 depth increments substantially increased, showing the apparent decrease the in the relative percentage of NO_3-N in the 0 – 2 cm depth increment. The absolute data in Table 2.6 indicates that NO_3-N actually did continue to increase slowly in the 0 – 2 cm depth increment, but not at the apparent rate exhibited by the lower two depths.

By comparing the total N present in each depth increment at 144 hours (Table 2.6) versus the calculated time=zero values, the 4 – 6 cm depth increment net N loss was ~ 1580 µg-N, while the 0 – 2 cm depth increment net N gain was ~ 4640 µg-N. The 2 – 4 cm depth appeared to gain ~ 190 µg-N. Assuming no new N was transported into the 4 – 6 cm depth, the ~ 1580 µg-N lost was transported into the overlying 2 – 4 cm depth, and then ~ 1390 µg-N was transported

further into the 0 – 2 cm depth by time =144 hours. This leaves a difference for the 0 – 2 cm depth of ~ 3250 µg-N that was apparently generated *in situ*. The maximum amount of mineralized N in the non-amended soil was ~ 640 µg-N per depth increment (Table 2.5). Assuming the mineralization of N was comparable between the two experiments and all the mineralized N from the lower two depths was transported to the 0 – 2 cm depth, this could only account for ~ 1280 µg-N. Furthermore, this transport would have had to occur in the first 24 hours, and still leaves a deficit of ~ 1970 µg-N. While the data in Table 2.6 support the conclusion that some transport of N was present in the NH-N amended packed column, the actual impact this transport had on N distribution is equaled or even exceeded by N mineralization, especially in the 0 – 2 cm depth increment. It is not known whether the addition of NH_4-N to the lower two depth increments acted to stimulate mineralization of N in the amended packed soil column, or whether some other combination of variables acted to produce the observed results.

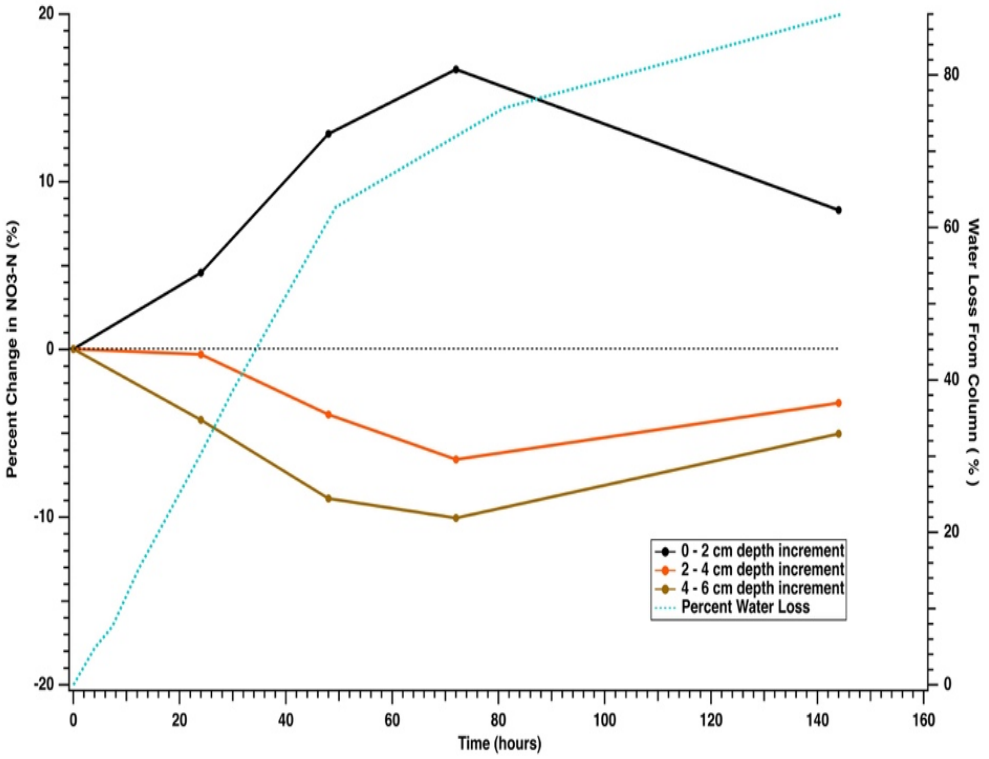

Figure 2.16. Relative percent change in the distribution of NO_3-N for a given depth increment for a packed NH_4-N amended soil (BASF-ls) column as a function of time as compared to percent of water loss. The data points represent the change in percent NO_3-N within each depth increment as a function of total NO_3-N present relative to the same percent distribution of NO_3-N at time zero. Solid or dashed lines added as a visual aid to show over trend in the data.

3.3 Loss of Ammonia from Soil Cores

The ability of the simple flow-through chamber to provide an index of potential NH_3 emissions was tested in a series of experiments. As illustrated in the previous section, attention was paid to the inorganic-N mass balance within the prepared soil columns due to the potential interaction between any applied variables and mineralization of N during the course of an experiment.

Preliminary Time Series Experiment

A preliminary experiment was conducted over a substantial period of time (~ 720 hours) in order to test the effect of wetting and drying cycles on potential NH_3 emissions and also to determine if the fraction of NH_4-N present that could contribute to NH_3 emissions could be

depleted. A non-amended fumigated soil (BASF-ls) was used in this experiment in an attempt to control microbial activity, especially mineralization of N. The wetting cycles (~ 4 days in length) consisted of adding water to the individual columns after ~ 24 hours to bring them back to the initial water content of ~ 80% FC. The drying cycles (~ 7 – 10 days in length) were initiated in each case after the packed columns were brought back to ~ 80% FC. Individual packed soil columns were sacrificed at 216, 384, 504 and 720 hours during the course of the experiment. Therefore, data generated from this preliminary experiment represents varying degrees of replication or simply single observations.

Use of the fumigated soil was successful in stopping nitrification, but not mineralization (Table 2.7). Extractable (2M KCl) NO_3-N was essentially constant during the 720 hours of observation (~ 900 (+/- 20) µg N), while extractable NH_4-N in a packed soil column increased from a value of ~ 4880 µg N at time zero to ~ 13,800 µg N at time = 504 hours. Assuming from time = 384 hours that the total amount of NH_4-N present in a packed column was constant and differences in NH_4-N at > 384 hours represent variation among individual columns, then the total NH4-N reached within the packed columns was ~ 13,200 (+/- 500) µg N or roughly 2.7x the initial value of NH_4-N present at time zero.

Table 2.7. Extractable (2M KCl) NH_4-N and NO_3-N from individual fumigated soil (BASF-ls) packed columns subjected to wetting and drying cycles.

Time	**NH_4-N**	**NO_3-N**	**Sum**
- hours -	- µg N -	- µg N -	- µg N -
0	4882	918	5,800
216	7149	864	8,013
384	13142	907	14,049
504	13778	902	14,680
720	12737	910	13,647

The cumulative loss of NH_3 as a function of time and wetting or drying cycles throughout the experiment is shown in Fig. 2.17. Figure 2.17 illustrates that NH_3 emissions were always present during the course of study, resulting in ~ 650 µg N lost as NH_3-N by time = 720 hours. The most intense NH_3 emissions were during the wetting cycles with the daily addition of water to bring the packed columns back to ~ 80% FC. Across each wetting cycle that was 4 days in length, the observed average rate of NH_3 emitted was 1.0, 1.6 and 1.2 µg N hr^{-1}, respectively. Although reduced in magnitude, NH_3 emissions did not stop during the dry down periods, averaging across each dry down cycle values of 0.56, 0.76 and 0.67 µg N hr^{-1}, respectively. The calculated integrated average concentrations of NH_3-N for all the observations ranged from 1.5 – 4.9 µg N m^{-3} (data not shown).

The plot of cumulative NH_3 loss in Fig. 2.17 also suggests that the increase in NH_4-N within the packed soil columns (Table 2.7.) became noticeable at the ~ 216 hour mark when there is a substantial shift in the overall magnitude of NH_3 loss, before the total NH_4-N present within the packed columns became relatively constant at time = 384 hours. Overall, the amount of NH_3 recovered as NH_3 emissions was ~ 13% of the 2M KCl NH_4-N measured at time zero, which was < 5% of the NH_4-N present in the packed soil column by time = 720 hours. Even if a protocol could be applied that inhibited both mineralization and nitrification within the soil columns, it appears unrealistic to assume that continued measurements of NH_3 emissions to assess the amount of NH_4-N present contributing to NH_3 loss is practical, unless soil parameters where further artificially manipulated to induce volatilization of NH_3.

Dose-Response Relationship

The apparent response of NH_3 emissions to increased presence of NH_4-N suggested in Fig. 2.17, was tested further using packed columns composed of unfumigated soil (BASF-ls). The concentration of NH_4-N in the soil at time zero (~2.2 µg NH_4-N g^{-1}) was used to calculate the total amount of NH_4-N to be added. The NH_4-N was added at rates of 2x, 5x, 10x, and 20x the amount present at time zero, resulting in values of total NH_4-N present of ~ 2,860, 7,150, 14,300, and 28,600 µg N per 650 g of air-dry soil. The soil was spread in a thin layer on a flat tray and ammonium sulfate solution applied evenly over the soil in 10 mL increments (total = 50 mL) using a calibrated digital pipette. The soil was mixed after each 10 mL addition and then spread out again on the tray. At time zero, after addition of the aliquots of ammonium sulfate to the bulk soil, the calculated NH_4-N content (initial + added N) was 4,290, 8,580, 15,730, and 30,030 µg N, respectively. Initial water content of each column was set at ~ 80% FC and flow rate was set at 6 LPM. Calculated integrated average NH_3 concentrations were derived for each 24-hour period. Water was then added daily to bring the packed columns back to the water content at time zero for the next 24-hour measurement period.

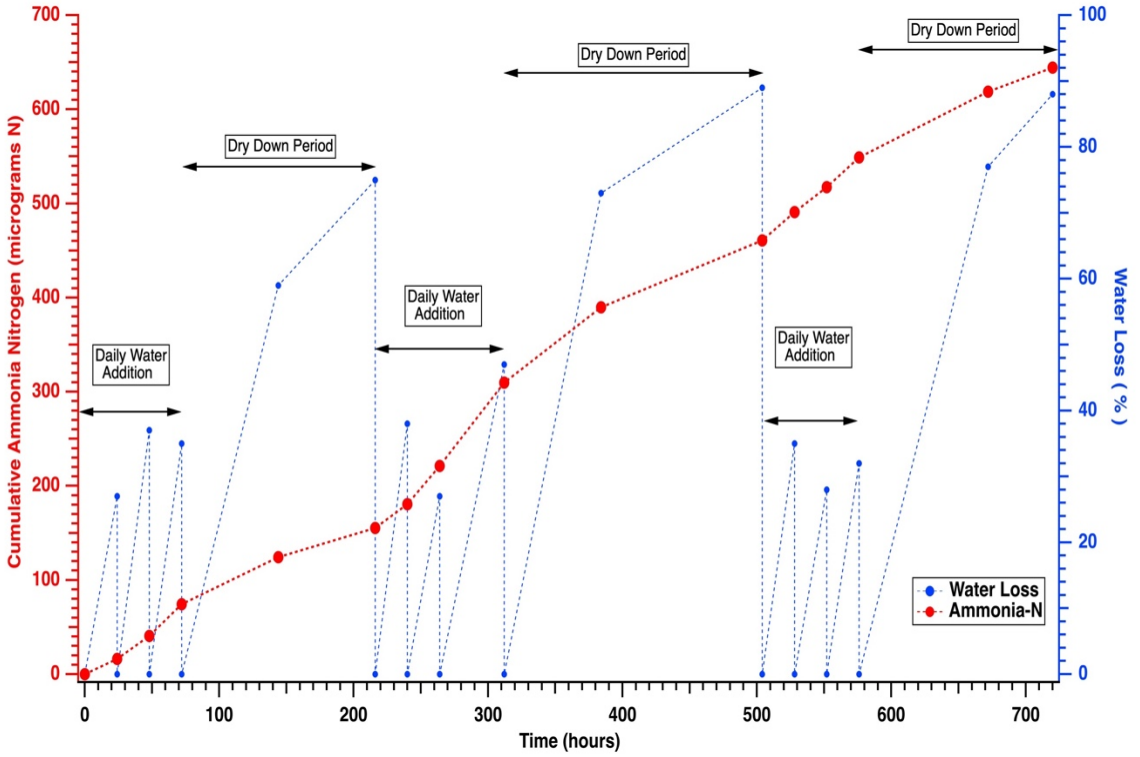

Figure 2.17. Time series measurement for cumulative NH_3 loss from fumigated non-amended BASF-ls packed soil columns as a function of time and alternating wetting and drying cycles. During wetting cycles soil water content was adjusted to 80% of FC after 24 hours. Flow rate: 6 LPM. Packed columns were sacrificed at 216, 384, 504, and 720 hours resulting in data points representing mean of decreasing observations over time. Dashed lines added to help visualize overall trends in the data.

The calculated integrated average NH_3 concentrations as a function of time and rate of NH_4-N addition are shown in Fig. 2.18. There is definite response in NH_3 emitted as a function of NH_4-N added, which in general remained relatively constant throughout the course of the experiment. These results are similar to those in Fig. 2.17 for the wetting cycles, indicating that conditions resulting in NH_3 emissions were fairly reproducible for the individual 24-hour measurements followed by addition of water to restore the columns to initial water content at time zero. Overall, the largest changes in NH_3 emissions appeared to be between the first and second set of observations, perhaps due to continued NH_4-N redistribution in the packed columns after the first wetting cycle.

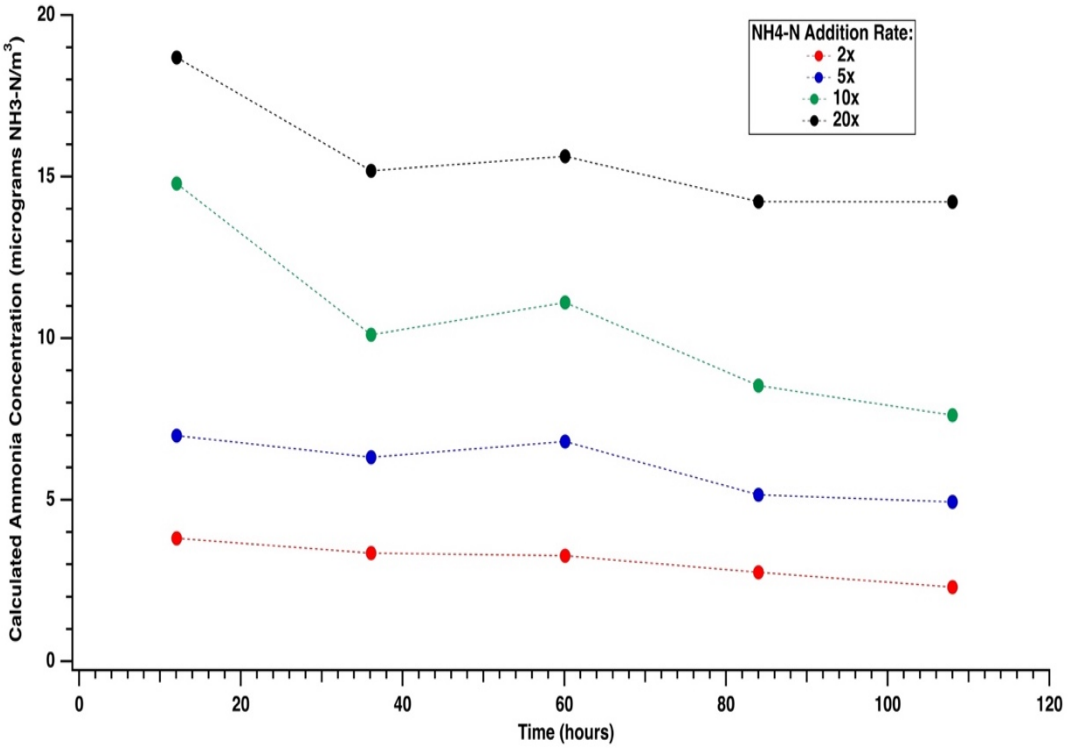

Figure 2.18. Calculated average NH_3 concentration per each 24-hour period as a function of time and rate of NH_4-N addition to unfumigated packed soil (BASF-ls) columns. Rate of NH4-N addition based on initial NH_4-N concentration of ~ 2.2 µg N g^{-1}. Individual data points are plotted at mid-point of each 24-hour measurement period and represent single observations. The dashed lines are added to help visualize overall trends in the data.

The relationship between calculated average NH_3 concentrations and NH_4-N concentration in the entire packed soil columns at time=120 hours is shown in Fig. 2.19. The measured extractable (2M KCl) NH_4-N concentrations at time=120 hours were plotted along the x-axis to account for the increase in NH_4-N due to mineralization which occurred sometime during the course of the experiment. In general, the response between the calculated integrated average NH_3 concentrations and extractable NH4-N appeared linear with a slope of ~ 0.3 (+/- 0.1) µg NH_3-N m^{-3} per 1µg NH_4-N g^{-1} soil, where the uncertainty associated with the µg NH_3-N m^{-3} value is at the 95% confidence level. The strength of the linear relationship was more apparent for measurements when time > 24 hours (data not shown). The relationship demonstrated in Fig. 2.19, however, is based on estimates of NH_4-N in the entire packed column,

and probably does not reflect actual concentration of NH_4-N responsible for the observed NH_3 emissions. Figure 2.19 does illustrate that the simple flow-through column can provide a measure of the direct impact of an increase in NH_4-N on potential NH_3 emissions.

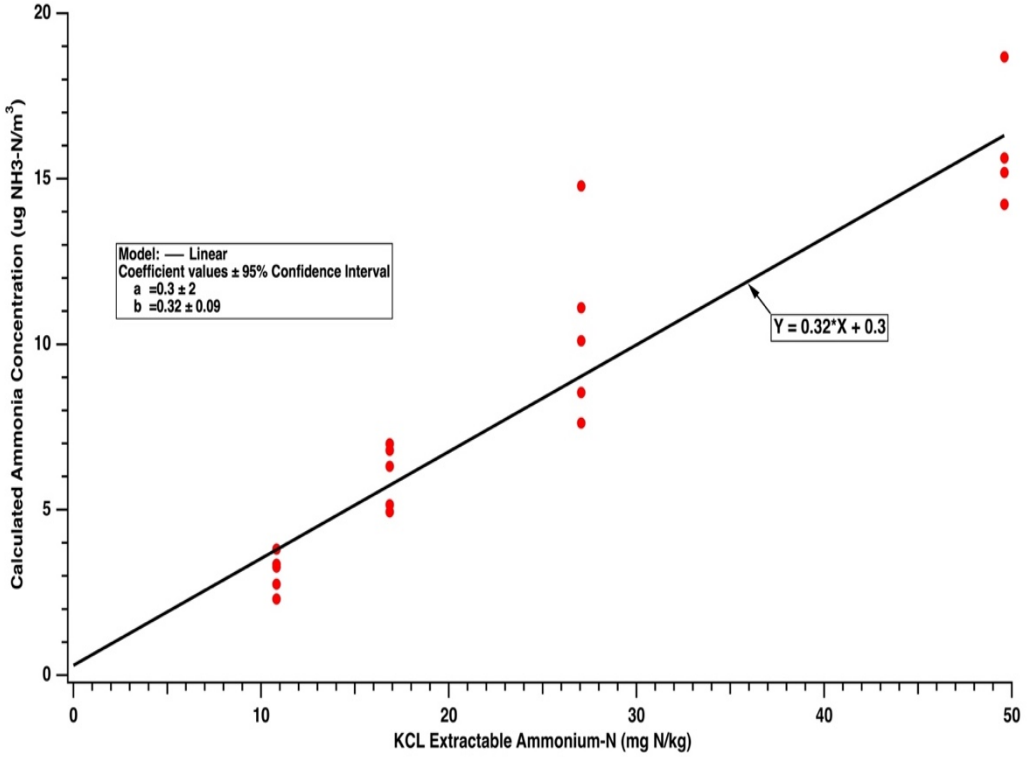

Figure 2.19. Calculated average NH_3 concentration per each 24-hour period plotted as a function of extractable (2M KCl) NH_4-N in entire unfumigated packed soil (BASF-ls) columns at time=120 hours.

The rates of NH_4-N addition used in this experiment can be placed in further context by comparison of the amount NH_4-N added to the measured cation exchange capacity of the BASF-ls soil (Table 2.2). The calculated NH_4-N content (initial + added N) was 4,290, 8,580, 15,730, and 30,030 µg N at time zero. These quantities are ~ 0.31, 0.61, 1.12 and 2.14 meq of NH_4-N in the form of NH_4^+. For the total soil mass of 650 grams, these values translate to 0.048, 0.094, 0.17 and 0.33 meq of charge per 100 grams of soil. Using the value of 1.7 meq/100 grams for the CEC of the BASF-ls soil (Table 2.2), means that the total NH_4-N present at time zero for this experiment ranged from ~ 2.8 to 19.4 % of the CEC. The calculations illustrate that increased

additions of NH_4-N can impact the cation exchange equilibrium in the soil, especially mineral soils with relatively low CEC capacities such as those typically found in the southeastern U.S. These calculations also indicate that even modest levels of NH_4-N present (e.g. < 3 % of the measured CEC) can impact measured NH_3 emissions.

Water Loss Impacts on NH_3 Emissions – No N Addition

Another series of experiments were conducted to further investigate the apparent impact of water loss on NH_3 emissions as suggested during the wetting and dry down cycles in Fig. 2.17. The first experiment in this group used non-amended unfumigated packed soil (BASF-ls) columns where the soil was placed in the column in 2-cm increments and water (20 mL) was added to each depth increment. Using this approach, the finished columns (N = 3) were set at ~ 80% FC and then allowed to dry down over 120 hours at a flow rate of 5 LPM. Measurements of NH_3 loss were conducted at variable time periods during the dry down period in order to provide more detail in observed NH_3 loss than originally observed in Fig. 2.17.

The nitrogen mass balance for the columns used in this experiment is summarized in Table 2.8. At time zero, the mean NH_4-N + NO_3-N mass in the columns was 3546 µg N. At time-120 hours, the mean mass of NH_4-N + NO_3-N had increased to 6632µg N, or nearly doubled due to mineralization of N.

Expressed as a percentage, the net increase in the mass of N in the columns (~ 3086 µg N) was present as 65.6% NO_3-N and 34.4% NH_4-N. Within the soil columns, ~ 6% of N present had shifted from both the lower two depth increments to the surface 0 – 2cm layer (Table 2.8). The source of the new nitrogen in the columns was the result of mineralization of N and then subsequent nitrification to form NO_3-N. As suggested in Fig. 2.9, the bulk of mineralization of N may have been completed within the first 24 hours of the experiment. If it is assumed that

mineralization was uniform throughout the entire depth of the columns, then ~ 1029 µg N was generated in each depth interval. By time =120 hours, a portion of this new N accounts for the observed increase in NH_4-N in each depth interval. The remainder was converted to NO_3-N, a portion of which then was redistributed within the columns as they continued to dry down. Continuation of this scenario results in a net gain of ~ 800 µg N in the surface 0 – 2 cm depth increment. This increase came equally from the lower portions of the packed columns. It is likely that this net gain in N involved some movement of NH_4-N, but probably a substantial percentage was in the form of NO_3-N.

The calculated average NH_3 concentrations for the emitted NH_3 during the experiment as a function of time are shown in Fig. 2.20 along with the mean cumulative percent water loss. There was an apparent increase in the integrated average NH_3 concentration up to ~ time = 30 hours, or when ~ 55% of the water present had been lost due to evaporation. During this period the rate in water loss was ~ linear, suggesting a direct impact of water loss on the release of NH_3. At the 40 hour mark, the integrated average NH_3 concentrations decreased and became essentially constant while loss of water continued but slowed (Fig. 2.20).

Table 2.8. Mean Extractable (2M KCl) NH_4-N and NO_3-N from individual unfumigated non-amended soil (BASF-ls) packed columns (N=3) subjected to one drying cycle ~120 hours in length. Initial water content set at ~ 80% FC.

Depth Increment	NH_4-N	NO_3-N	Sum	Percent Distribution
- cm -	- µg -N -	- µg -N -	- µg -N -	- % -
Time = 0 hours				
0 – 2	446	736	1182	33.3
2 – 4	446	736	1182	33.3
4 – 6	446	736	1182	33.3
Totals=	**1338**	**2208**	**3546**	**100.0**
Time = 120 hours				
0 – 2	1073	1949	3022	45.5
2 – 4	680	1054	1734	26.2
4 – 6	645	1231	1876	28.3
Totals=	**2398**	**4234**	**6632**	**100.0**

The cumulative loss of NH_3 for each of the three columns is plotted in Fig. 2.21. As suggested by the preliminary data in Fig. 2.17, the loss of NH_3 as the columns dried appeared to segregate into two distinct periods. The first lasted up to approximately the ~ 47 hour mark and appeared to be consistent between the three columns. This corresponds to a cumulative water loss of ~ 60% (Fig. 2.20). Beyond this point, the apparent rate of loss slows and the individual variations between the columns becomes more distinct. In this experiment, the apparent rate of loss of NH_3 was roughly 0.25 µg N hr^{-1} up to time=47 hours. Beyond 47 hours, the rate of loss varied with a particular column ranging from roughly 0.07 – 0.2 µg N hr^{-1}.

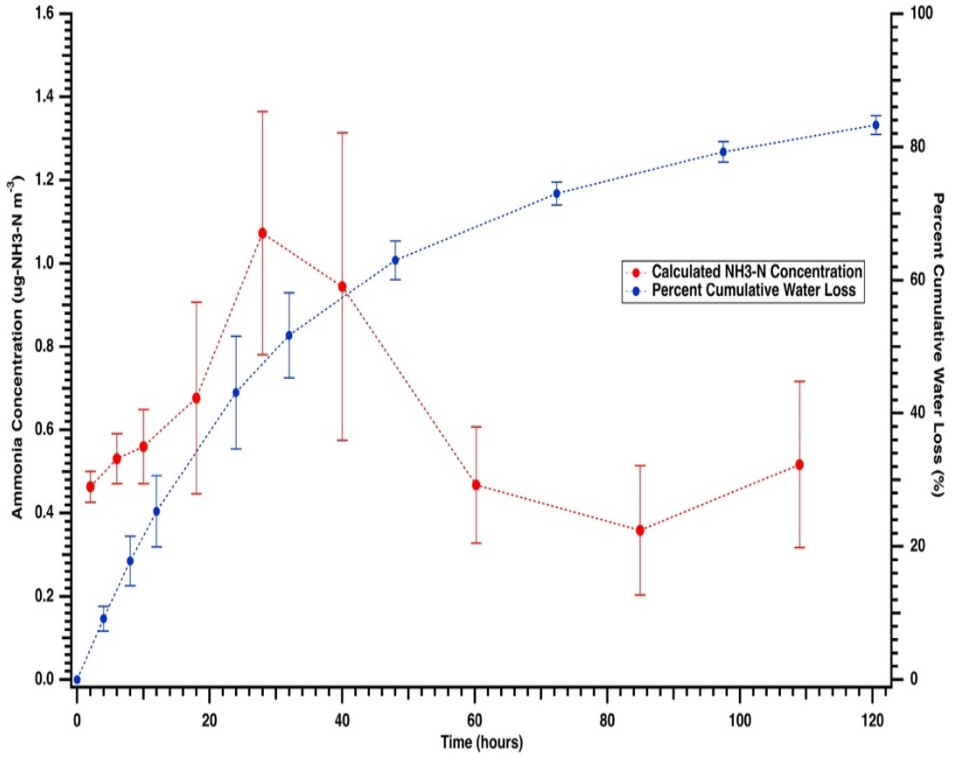

Figure 2.20. Calculated average NH_3 concentration (N=3) per each measurement period and cumulative percent water loss as a function of time. Error bars represent standard deviation. Average NH_3 concentrations are plotted at mid-point of each measurement period. Cumulative water loss is plotted at the end of each measurement period. The dashed lines are added to help visualize overall trends in the data.

Since it appeared NH_3 loss was more a function of water loss in the first ~ 50 hours of the experiment, the cumulative NH_3 loss per column was plotted as a function of the percent cumulative water loss (Fig. 2.22). This further analysis of the dataset indicates that at up to ~ 40% cumulative water loss, NH_3 loss from each column basically fell along the same linear line. This suggests variations introduced through packing of the individual columns were minimal during this period and ability to emit was NH_3 was directly dependent on the conditions driving the rate of water loss within the chambers. To some degree this corresponds to Stage 1 drying of the soil as described by Hillel (2004). It is also apparent that the actual total cumulative loss of NH_3 during this period accounts for a smaller % of total loss than suggested by Fig. 2.21. Less

than 5µg N was lost before reaching ~ 40% of the cumulative water loss from the columns, or from Fig. 2.20, within the first ~ 24 hours of the experiment.

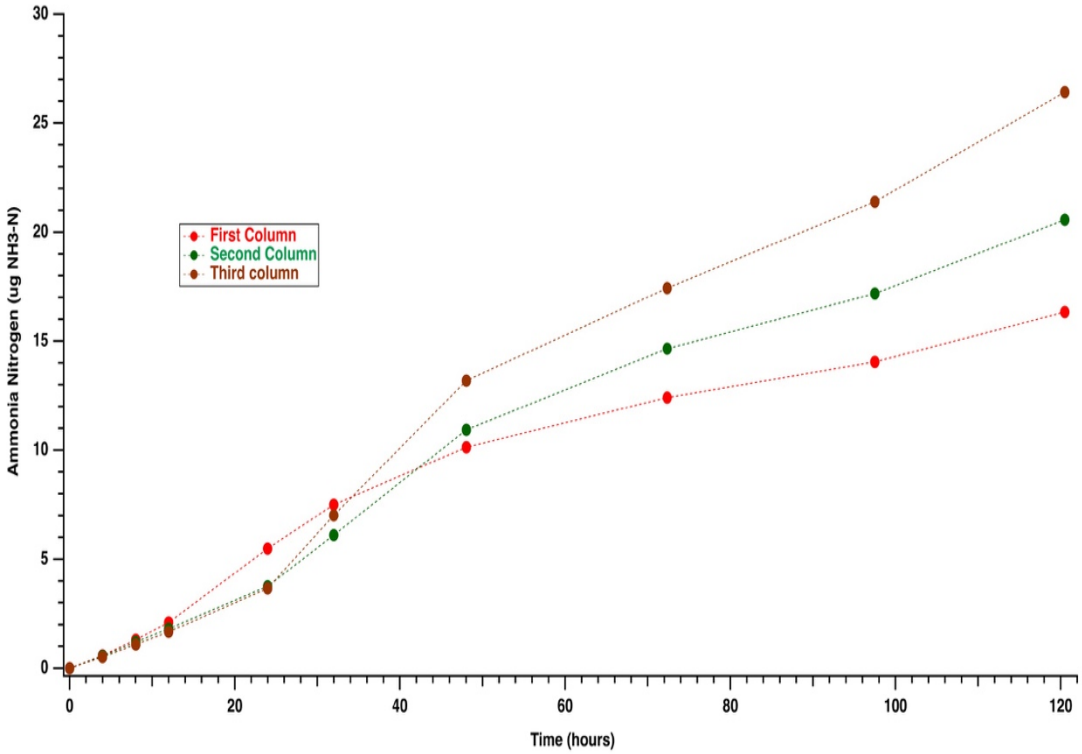

Figure 2.21. Cumulative NH_3-N loss from individual soil (BASF-ls) columns as a function of time. The dashed lines are added to help visualize overall trends in the data.

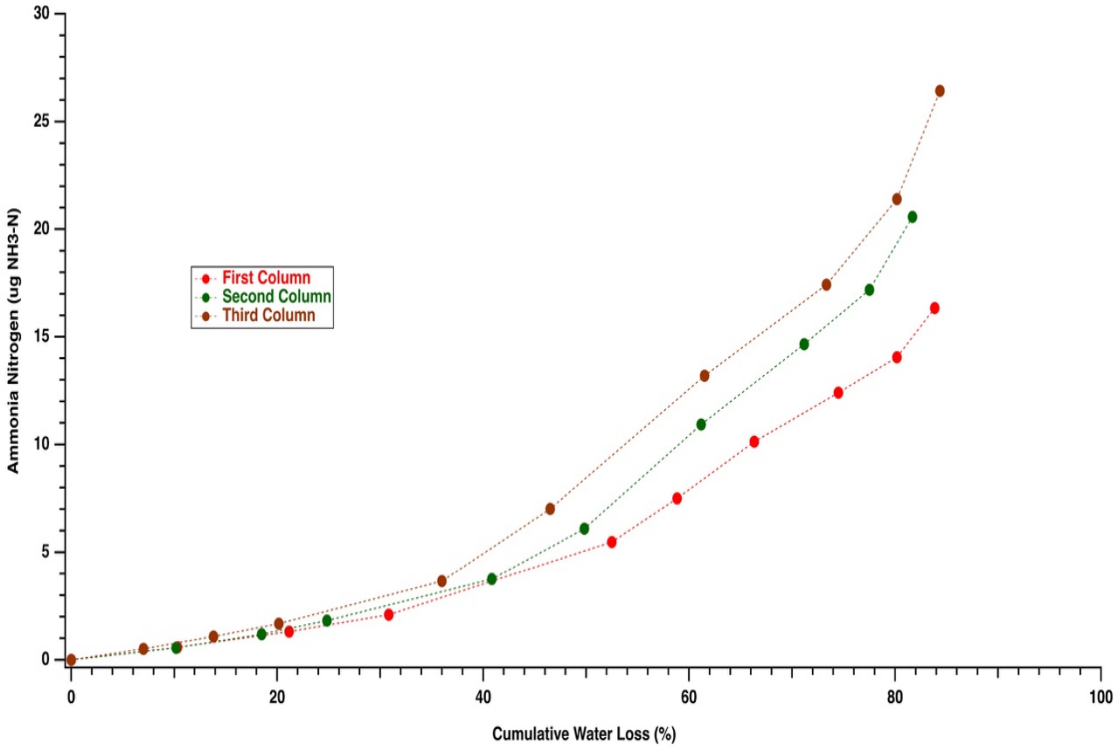

Figure 2.22. Cumulative NH_3-N loss from individual soil (BASF-ls) columns as a function of percent cumulative water loss from each column. The dashed lines are added to help visualize overall trends in the data.

Water Loss Impacts on NH_3 Emissions – N Addition

The experiment as described above was repeated using N amended soil (BASF-ls). Three columns were again packed in depth increments with ammonium sulfate added to the 4 – 6 and 2 – 4 cm increments but not to the 0 – 2 cm increment. Water content was adjusted to ~ 80% FC at time zero. In addition to these three columns which were placed in the simple flow-through chambers, two additional columns were prepared in the same manner, but covered with aluminum foil and let stand at room temperature for 2 hours. These two columns were then sacrificed and the extractable (2M KCl) NH_4-N and NO_3-N determined on the respective depth increments. The nitrogen mass balance for the three columns placed in the chambers is summarized in Table 2.9. The nitrogen balance for the two soils columns left to equilibrate for 2 hours in provided in Table 2.10.

Table 2.9. Mean Extractable (2M KCl) NH_4-N and NO_3-N from individual unfumigated N amended soil (BASF-ls) packed columns (N=3) subjected to one drying cycle ~72 hours in length. Initial water content set at ~ 80% FC. Flow rate: 5 LPM.

Depth Increment	NH_4-N	NO_3-N	Sum	Percent Distribution
- cm -	- µg-N -	- µg-N -	- µg-N -	- % -
Time = 0 hours				
0 - 2	446	736	1182	3.6
2 - 4	14776	736	15512	48.2
4 - 6	14776	736	15512	48.2
Totals =	**29998**	**2208**	**32206**	**100.0**
Time = 72 hours				
0 - 2	13921	3219	17140	43.4
2 - 4	10063	1609	11672	29.6
4 - 6	9099	1542	10641	27.0
Totals=	**33083**	**6370**	**39453**	**100.0**

After 72 hours the mean total N found in the three chambers placed in the simple flow-through chambers was 39453µg N, versus the mean value of 32206 µg N at time zero (Table 2.9). The additional 7247 µg N due to mineralization was spilt between the NH_4-N and NO_3-N fractions. Approximately 42.6% was in the NH_4-N fraction (3085 µg N), the remaining 57.4% was in the NO_3-N fraction (4162 µg N). As noted for other instances when the soil is amended with N, the majority of N present remained in the NH_4-N fraction, with a substantial fraction of this shifting to the 0 – 2 cm depth increment (43.4%). While there is some nitrification, compared to the total N present at 72 hours, the net increase in NO_3-N is only 10.6%.

Review of the N balance for the two additional columns incubated and then sacrificed after 2 hours provided further insight into rate of mineralization with the N amended BASF-ls soil (Table 2.10). After only 2 hours the mean total N found in the two columns was 39171µg N for a net increase of 6965 µg N, or ~ 96% of the net increase in N found after 72 hours. Furthermore, although there was some nitrification, the actual increase in NO_3-N was only 1461 µg N, the majority of which was in the lower two depth increments (Table 2.10).

Table 2.10. Mean Extractable (2M KCl) NH_4-N and NO_3-N from individual unfumigated N amended soil (BASF-ls) packed columns (N=2) subjected left standing for 2 hours. Initial water content set at ~ 80% FC.

Depth Increment	NH_4-N	NO_3-N	Sum	Percent Distribution
- cm -	- µg-N -	- µg-N -	- µg-N -	- % -
Time = 0 hours				
0 - 2	446	736	1182	3.6
2 - 4	14776	736	15512	48.2
4 - 6	14776	736	15512	48.2
Totals =	**29998**	**2208**	**32206**	**100.0**
Time = 2 hours				
0 – 2	5827	848	6675	17.0
2 – 4	12363	1489	13852	35.4
4 – 6	17312	1332	18644	47.6
Totals =	**35502**	**3669**	**39171**	**100.0**

The two columns incubated for 2 hours and then sacrificed were covered with aluminum foil, effectively stopping soil water loss by evaporation. Therefore, changes in N content within the depth increments most probably reflect changes *in situ*, or due to diffusion. The increase in NO_3-N reflects nitrification of NH_4-N, therefore the net increase in NO_3-N reflects part of the total NH_4-N produced or present after 2 hours. Assuming this is correct, the total NH_4-N in the 4 – 6 cm depth including N mineralized was 17908 µg N. For the 2 – 4 cm depth this figure is 13116 µg N. Totaling these two estimates yields a value of 31,024 µg N. At time zero, the estimated total NH_4-N in these two depth increments was 29552 µg N for a difference of 1472 µg N. This is only 21.1% of the additional N found after 2 hours (6965 µg N), leaving 5493 µg N unaccounted for and part of the 5827 µg NH_4-N in the 0 – 2 cm depth after 2 hours. Correcting for the original 446 µg N present at time zero and including the net increase of 112 µg in NO_3-N yields the desired total of 5493 µg N.

These calculations illustrate that the increase in NH_4-N in the 0 – 2 cm depth was due to mineralization of N *in situ*, indicating that the presence of increased NH_4-N in the lower depth

increments did act to suppress mineralization. The subsequent further increase in NH_4-N in the 0 – 2 cm depth in the three chambers in the flow-through chambers was due to NH_4-N transport as the soils dried. Much of this additional NH_4-N came from both the 2 – 4 cm and 4 – 6 cm depths. Assuming the rate of mineralization in the 0 – 2 cm depth was the same in all the prepared columns, then ~ 8094 μg NH_4-N was moved to the 0 – 2 cm depth in the columns exposed to conditions favoring water loss. This transport was mostly likely enhanced by the presence of the sulfate anion. Assuming 215 grams of soil in the 0 – 2 cm depth increment, the concentration of NH_4-N was ~ 65 μg NH_4-N g^{-1} soil at 72 hours in the packed soil columns inside the chambers.

The presence of the increased concentrations of NH_4-N in the packed soil columns was reflected in the mean calculated integrated average NH_3 concentrations measured during the 72 hour period (Fig. 2.23). As observed for the non-amended soil (Fig. 2.20), there was an increase in observed NH_3 concentration with water loss that appeared to reach a maximum at about 40 hours and 60% cumulative total water loss from the columns. However, the data suggest that the NH_3 concentration remained constant and did not decline as observed in Fig. 2.20.

Plotting the cumulative NH_3-N loss for each column as a function of time reinforced the conclusion that the initial loss of water from the columns starting from ~ 80% FC appear to fall along the same linear relationship and that differences among the columns do not become apparent till after ~ 24 hours (Fig. 2.24). However, when the cumulative NH_3 loss data is plotted against the individual measured cumulative water loss for each column, the variation between columns is much less than observed for the non-amended soil (Fig. 2.25). One explanation for this observation as opposed that observed in Fig. 2.21, is that the relatively rapid increase of NH_4-N in the packed columns, especially in the 0 – 2 cm depth, exerts the dominant influence on NH_3 emissions once the cumulative water loss is > 30%. Above 50% cumulative water loss, the

increase in porosity in the 0 – 2 cm depth increment must be such as to favor a substantial increase in NH_3 emissions, since the cumulative NH_3 loss increase by ~ a factor of 4 (Fig. 2.25).

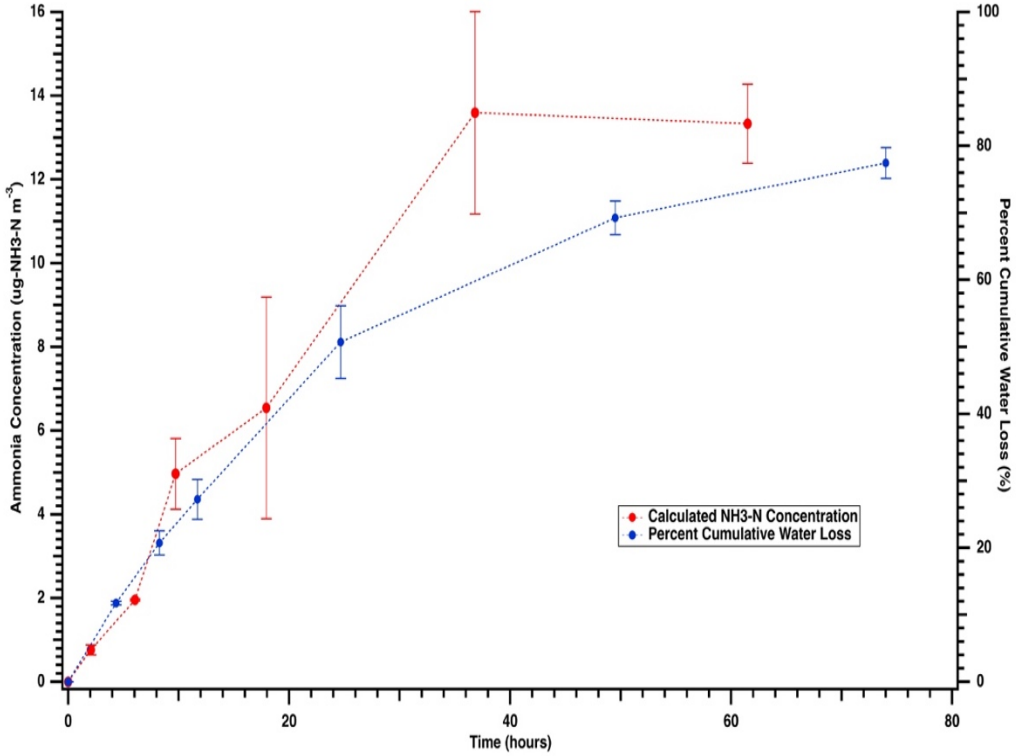

Figure 2.23. Calculated average NH_3 concentration (N=3) per each measurement period and cumulative percent water loss as a function of time for N amended soil (BASF-ls). Error bars represent standard deviation. Average NH_3 concentrations are plotted at mid-point of each measurement period. Cumulative water loss is plotted at the end of each measurement period. The dashed lines are added to help visualize overall trends in the data.

The results from these two sets of experiments demonstrate the ability of the simple flow-through chamber to discern changes in NH_3 emissions induced by changes in water content within the packed columns as well as demonstrating the impact of added NH_4-N, either from mineralization within the packed soil columns or added as an ammonium salt. However, the intensity of NH_3 emissions as a function of time is potentially controlled by the initial moisture content of the soil column, and not necessarily strictly by soil pH and NH_4-N concentration in equilibria with NH_3 within the soil.

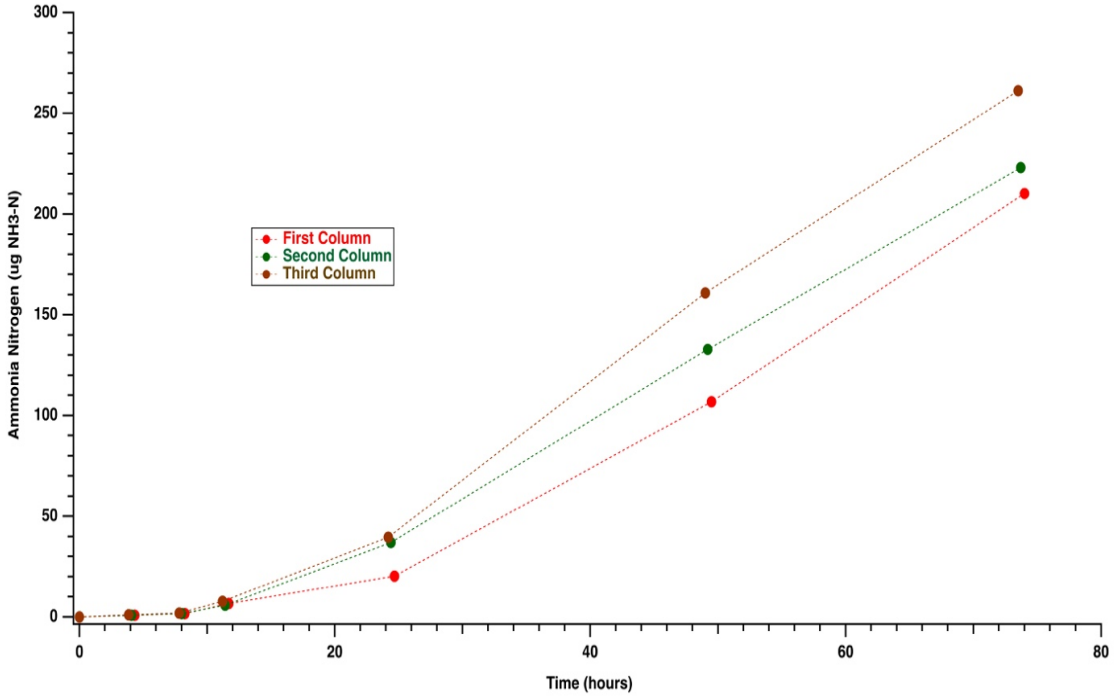

Figure 2.24. Cumulative NH_3-N loss from N-amended individual soil (BASF-ls) columns as a function of time. The dashed lines are added to help visualize overall trends in the data**.**

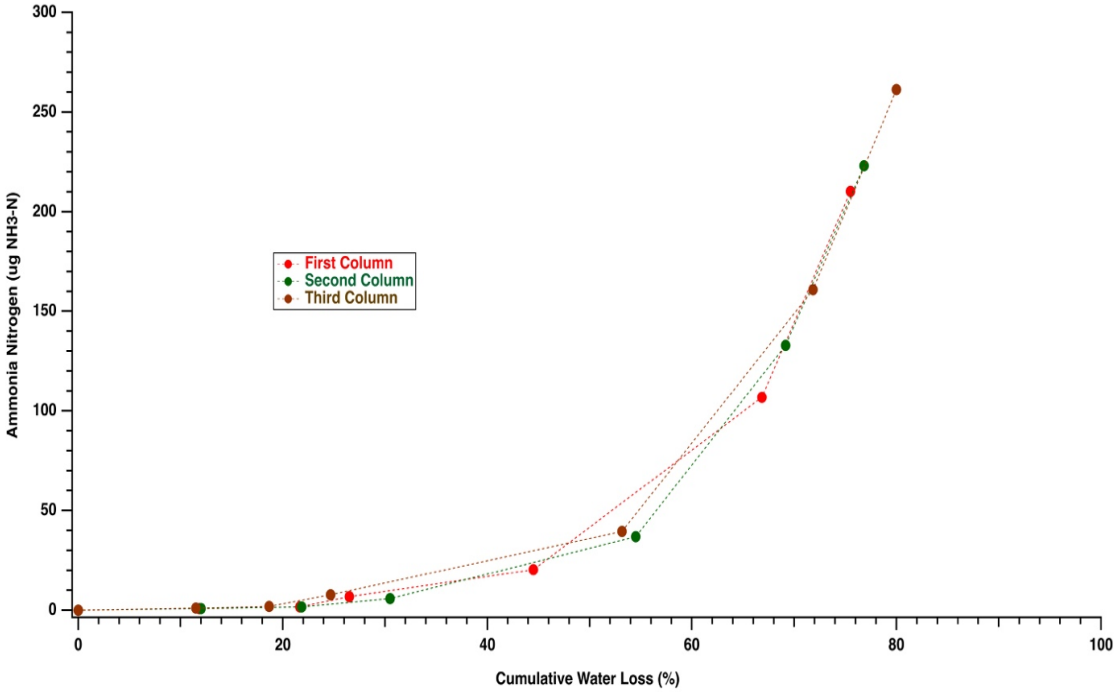

Figure 2.25. Cumulative NH_3-N loss from N-amended individual soil (BASF-ls) columns as a function of percent cumulative water loss from each column. The dashed lines are added to help visualize overall trends in the data.

4.0 Summary

For the purposes of this research project, a technique was required that would provide sensitive, accurate and replicated measurements of the potential emission of NH_3 from soils, especially non-amended NH_4-N soils, while at the same time allowing an assessment of soil water loss following different conditions of initial soil water content.

Water loss measured using a simple flow-through chamber showed very similar in water loss patterns in all experiments. Two methods for adding water in the soil columns: adding water to the top of the entire packaging column vs. adding water to each 2 cm increment. The largest variation in water loss rate across chambers was observed within the individual trials, especially for adding all the water to the top of the entire packed soil column (Fig. 2.5a). The differences between replicates within a trial start to become evident around 5 – 10 hours after initiation of the individual experiments. The large deviation observed for the one chamber where all the water was added to the top of the packed soil column probably resulted from a combination of how the soil column was packed and the resulting influence on the redistribution of the added water within the column. Movement of the added water deeper within the individual column would act to slow water loss over time. Adding water to packed soil increments appears to result in more even distribution of water within the packed column at time zero. The placement of chambers within the room may have had an impact of rates of water loss during the first ~ 40 hours of an experiment. However, the overall variation was similar in magnitude to that observed in Fig. 2.5b and may also have been largely due to packing of the soil increments within that particular soil column. Overall, the temporal trend in water loss was consistent across all three chambers and all three reached approximately the same total water loss by the end of the experiment.

Air flow rate of value 5 LPM was chosen to use with simple flow-through chamber for three reasons due to: (i) adequate sensitivity in the mass of NH_3 captured by the acid coated annular denuder tubes in a reasonable period of time, (ii) lessen the chances of condensation of moisture on the internal volume of the chamber and loss of NH_3 to internal surfaces, (iii) the ability to differentiate the potential Stages of water loss (Fig. 2.1).

The sensitivity of the flow-through chamber combined with annular denuder technology was assessed to delineate dose-response in NH_3 emissions as a result NH_4-N addition to the soil in the proper time frame and efficiency of the denuder tubes. The calculated integrated average NH_3 concentrations as a function of time and rate of NH_4-N addition indicate there was positive response in NH_3 emitted, which in general remained relatively constant throughout the course of the experiment. In general, the response between the calculated integrated average NH_3 concentrations and extractable NH4-N appeared linear with a slope of ~ 0.3 (+/- 0.1) µg NH_3-N m^{-3} per 1µg NH_4-N g^{-1} soil, where the uncertainty associated with the µg NH_3-N m^{-3} value is at the 95% confidence level. The strength of the linear relationship was more apparent for measurements when time > 24 hours. in conclusion, simple flow-through column can provide a measure of the direct impact of an increase in NH_4-N on potential NH_3 emissions.

REFERENCES

Aita, C., R. Gonzatto, Ezequiel C C Miola, Daniela B dos Santos, P. Rochette, D.A. Angers, M.H. Chantigny, S.B. Pujol, D.A. Giacomini and S.J. Giacomini. 2014. Injection of dicyandiamide-treated pig slurry reduced ammonia volatilization without enhancing soil nitrous oxide emissions from no-till corn in southern brazil. J. Environ. Qual. 43:789.

Ammann, C., V. Wolff, O. Marx, C. Brümmer and A. Neftel. 2012. Measuring the biosphere-atmosphere exchange of total reactive nitrogen by eddy covariance. Biogeosciences 9:4247-4261.

Aneja, V.P., J. Blunden, C.S. Claiborn and H.H. Rogers. 2006. Dynamic chamber system to measure gaseous compounds emissions and atmospheric-biospheric interactions. In: Environmental simulation chambers: application to atmospheric chemical processes. Springer, Netherlands, pp 97–109. ISSN:1568–1238

Baer, D.S., J.B. Paul, M. Gupta and A. O'Keefe. 2002. Sensitive absorption measurements in the near-infrared region using off-axis integrated-cavity-output spectroscopy. Applied Physics B Lasers and Optics 75:261-265.

Black, A.S., Sherlock, R.R., and Smith, N.P. 1987. Effect of timing of simulated rainfall on ammonia volatilization from urea, applied to soil of varying moisture content. Journal of Soil Science 38, 679-687

Brümmer, C., O. Marx, W. Kutsch, C. Ammann, V. Wolff, C.R. Flechard and A. Freibauer. 2013. Fluxes of total reactive atmospheric nitrogen ([sigma]nr) using eddy covariance above arable land. Tellus 65:19770-20.

Cai, G.X. 1997. Ammonia volatilization. In: Zhu, Z.L., Wen, Q.X., Freney, J.R. (eds.), Nitrogen in soils of china. Kluwer academic publishers, Dordrecht/Boston/London, pp. 193–213.

Cassel, D. K., and D.R., Nielsen. 1986. Field Capacity and Available Water Capacity: In Methods of soil analysis: Part 1. Physical and mineralogical methods, 2nd Edition. Klute, A. (Ed.), ASA-SSSA, Madison, WI, USA. pp. 901-926.

Chapman, H.D., 1965. Cation exchange capacity. In: Black CA (ed) Methods of soil analysis. Amer Soc Agron Inc., Madison. pp 891-901.

Currie, L.A. 1999. Nomenclature in evaluation of analytical methods including detection and quantification capabilities: (IUPAC recommendations 1995). Anal. Chim. Acta 391:105-126.

Denmead, O.T., and M.R. Raupach, 1993. Methods for measuring atmospheric gas transport in agricultural and forest systems. In: Harper, L.A., Mosier, A.R., Duxbury, J.M., Rolston, D.E. (Eds.), Agricultural Ecosystem Effects on Trace Gases and Global Climate Change. ASA Special Publication, vol. 55. American Society of Agronomy, Madison, WI, pp. 19–43

Ernst, J. W. and H. F. Massey. 1960. The effects of several factors on volatilization of ammonia from urea in the soil. Soil sci. Am. Proc. 24: 87-90.

Fang, C. and J.B. Moncrieff. 1996. An improved dynamic chamber technique for measuring CO_2 efflux from the surface of soil. Funct. Ecol. 10:297-305.

Fenn, L.B. and D.E. Kissel. 1976. The influence of cation exchange capacity and depth of incorporation on ammonia volatilization from ammonium compounds applied to calcareous Soils1. Soil Sci. Soc. Am. J. 40:394.

Fenn, L.B. and R. Escarzaga. 1976. Ammonia volatilization from surface applications of ammonium compounds on calcareous soils: V. soil water content and method of nitrogen Application1. Soil Sci. Soc. Am. J. 40:537.

Ferm, M. 1991. A sensitive diffusional sampler. Report B-1020, Swedish environmental Research Institute, Gothenburg, Sweden. pp.12

Freney, J. R., J. R. Simpson, and O. T. Denmead. 1983. Volatilization of ammonia. In J. R. Freney & J. R. Simpson (Eds.), Gaseous Loss of Nitrogen from Plant-Soil Systems (Vol. 9, pp. 1-32): Springer Netherlands.

Gardner, W.R. 1960. Dynamic aspects of water availability to plants. Soil Sci. 89:63-73.

Gasser, J. K. R. 1964. Some factors affecting losses of ammonia from urea and ammonium sulphate applied to soil. J. Soil Sci. 15: 258-272.

Gee, G.W., and J.W. Bauder, 1986. Particle -size analysis. In Methods of soil analysis: Part 1. Physical and mineralogical methods, 2nd Edition. Klute, A. (Ed.), ASA-SSSA, Madison, WI, USA. pp. 383-409.

Hassouna, M., B., P. Grandpierre, and N. Guingand. 2013. "A Test-Bench for Infrared Photoacoustic Analyzers Used to Measure Gas Emissions from Animal Houses and Manure Storage. ISAH Conference, Nanjing, China, 2013.

Hill, F.B., V.P. Aneja and R.M. Felder. 1978. A technique for measurement of biogenic sulfur emission fluxes. Journal of Environmental Science and Health. Part A: Environmental Science and Engineering 13:199-225.

Hillel, D. 2004. Introduction to environmental soil physics. Elsevier Science & Technology, Burlington.

Hudson, N., G.A. Ayoko, M. Dunlop, D. Duperouzel, D. Burrell, K. Bell, E. Gallagher, P. Nicholas and N. Heinrich. 2009. Comparison of odour emission rates measured from various sources using two sampling devices. Bioresour. Technol. 100:118-124.

Hutchinson, G.L., G.P. and Livingston. 1993. Use of chamber systems to measure trace gas fluxes. In: Agricultural ecosystem effects on trace gases and global climate Change (eds L.A. Harper, A.R. Mosier, J.M. Duxbury & D.E. Rolston), pp. 63-78. Special Publication No 55, American Society of Agronomy/Crop Science Society of America/Soil Science Society of America, Madison, WI.

Jewitt, T.N. 1942. Loss of ammonia from ammonium sulfate applied to alkaline soils. Soil Sci. 54:401-410.

Kaplan, W.A., S.C. Wofsy, M. Keller and J.M. Da Costa. 1988. Emission of NO and deposition of O_3 in a tropical forest system. J. Geophys. Res. 93:1389.

Klute, A. 1986. Water retention: Laboratory methods. In Methods of soil analysis: Part 1. Physical and mineralogical methods, 2nd Edition. Klute, A. (Ed.), ASA-SSSA, Madison, WI, USA. pp. 635-660.

Kresge, C.B. and D.P. Satchell. 1960. Gaseous loss of ammonia from nitrogen fertilizers applied to soils. Agron. J. 52:104.

Krupa, S.V. 2003. Effects of atmospheric ammonia (NH 3) on terrestrial vegetation: A review. Environ. Pollut. 124:179-221.

Leuning, R., J.R. Freney, O.T. Denmead and J.R. Simpson. 1985. A sampler for measuring atmospheric ammonia flux. Atmos. Environ. (1967) 19:1117-1124.

Loh, Z., D. Chen, M. Bai, T. Naylor, D. Griffith, J. Hill, T. Denmead, S. McGinn and R. Edis. 2008. Measurement of greenhouse gas emissions from Australian feedlot beef production using open-path spectroscopy and atmospheric dispersion modelling. Aust. J. Exp. Agric. 48:244.

Lyster, S., M.A. Morgan, and P. O'Toole. 1980. Ammonia volatilization from soils fertilized with urea and ammonium nitrate. J. Life Sci. R. Dubl. Soc. 1: 167-175.

Martin, J.P. and H.D. Chapman. 1951. Volatilization of ammonia from surface-fertilized soils. Soil Sci. 71:25-34.

Marx, O., C. Brümmer, C. Ammann, V. Wolff and A. Freibauer. 2012. TRANC - a novel fast-response converter to measure total reactive atmospheric nitrogen. Atmos. Meas. Tech. 5:1045-1057.

McInnes, K.J., R.B. Ferguson, D.E. Kissel and E.T. Kanemasu. 1986. Ammonia loss from applications of urea-ammonium nitrate solution to straw Residue1. Soil Sci. Soc. Am. J. 50:969.

Menneer, J.C., S. Ledgard and M. Sprosen. 2008. Soil N process inhibitors alter nitrogen leaching dynamics in a pumice soil. Aust. J. Soil Res. 46:323-331.

Miola, E., C. Aita, P. Rochette, M.H. Chantigny, D.A. Angers, N. Bertrand and M.O. Gasser. 2015. Static chamber measurements of ammonia volatilization from manured soils: Impact of deployment duration and manure characteristics. Soil Sci. Soc. Am. J. 79:305-313.

Misselbrook, T.H., F.A. Nicholson, B.J. Chambers and R.A. Johnson. 2005. Measuring ammonia emissions from land applied manure: An intercomparison of commonly used samplers and techniques. Environ. Pollut. 135:389-397.

Mulvaney, M.J. 1996. Nitrogen-Inorganics Forms. In Methods of soil analysis: Chemical methods. Part 3. ASA-SSSA, Madison, WI 53711, USA. pp. 1123-1184.

Mulvaney, M.J., K.A. Cummins, C.W. Wood, B.H. Wood and P.J. Tyler. 2008. Ammonia emissions from field-simulated cattle defecation and urination. J. Environ. Qual. 37:2022-2027.

Namieśnik, J., B. Zabiegała, A. Kot-Wasik, M. Partyka and A. Wasik. 2005. Passive sampling and/or extraction techniques in environmental analysis: A review. Anal. Bioanal. Chem. 381:279-301.

Ni, J. and A.J. Heber. 2008. Sampling and measurement of ammonia at animal facilities. p. 201-269. *In* Elsevier Science & Technology.

O'Keefe, A., J.J. Scherer and J.B. Paul. 1999. Cw integrated cavity output spectroscopy. Chem. Phys. Lett. 307:343-349.

Peech, M. 1965. Hydrogen Ion Activity. In: Black, C.A., et al., Eds., Methods of Soil Analysis, Part 2, American Society of Agronomy, Madison, 914-926.

Phillips, V.R., D.S. Lee, R. Scholtens, J.A. Garland and R.W. Sneath. 2001. A review of methods for measuring emission rates of ammonia from livestock buildings and slurry or manure stores, part 2: Monitoring flux rates, concentrations and airflow rates. J. Agric. Eng. Res. 78:1-14.

Purdue, L.J., 1992. Determination of the strong acidity of atmospheric fine-particles (<2.5 μm) using annular denuder technology. Standard Method. Enhanced Method. EPA/600/R-93/037 (NTIS PB93-178234). US EPA, Atmospheric Research and Exposure Assessment Laboratory, Research Triangle Park, NC.

Rolston, D., 1986. Gas Flux: Laboratory methods. In Methods of soil analysis: Part 1. Physical and mineralogical methods, 2nd Edition. Klute, A. (Ed.), ASA-SSSA, Madison, WI, USA. pp. 1103-1119.

Schjoerring, J.K., S.G. Sommer and M. Ferm. 1992. A simple passive sampler for measuring ammonia emission in the field. Water Air Soil Pollut. 62:13-24.

Sommer, S.G. and J.E. Olesen. 2000. Modelling ammonia volatilization from animal slurry applied with trail hoses to cereals. Atmos. Environ. 34:2361-2372.

Terry, R.E., D.W. Nelson, L.E. Sommers and G.J. Meyer. 1978. Ammonia volatilization from wastewater sludge applied to soils. Journal (Water Pollution Control Federation) 50:2657-2665.

Tian, G.M. J.L. Cao, Z.C. Cai, L.T. Ren. 1998. Ammonia volatilization from wheat field top-dress with urea. Pedosphere, 8: 331-336

van der Weerden, T. J., J.F. Moal, J. Martinez, B.F. Pain and F. Guiziou. 1996. Evaluation of the wind-tunnel method for measurement of ammonia volatilization from land. J. Agric. Eng. Res. 64:11-13.

Vlek, P.L.G. and J.M. Stumpe. 1978. Effects of solution chemistry and environmental conditions on ammonia volatilization losses from aqueous systems. Soil Sci. Soc. Am. J. 42:NP.

Volk, G.M. 1959. Volatile loss of ammonia following surface application of urea to turf or bare soils. Agron. J. 51:746.

Wahhab, A., M.S. randhawa and S.Q. ALAM. 1957. Loss of ammonia from ammonium sulphate under different conditions when applied to soils. Soil Sci. 84:249-256.

Zaman, M. and J.D. Blennerhassett. 2010. Effects of the different rates of urease and nitrification inhibitors on gaseous emissions of ammonia and nitrous oxide, nitrate leaching and pasture production from urine patches in an intensive grazed pasture system. Agr. Ecosyst. Environ. 136:236-246.

Zhao, Y., Y. Pan, J. Rutherford and F.M. Mitloehner. 2012. Estimation of the interference in multi-gas measurements using infrared photoacoustic analyzers. Atmosphere 3:246-265.

Chapter Three

Detailed Investigation into Evaluation of Critical Compensation Point Applied to Soils

1.0. Introduction

This research is devoted to better understanding the chemical and physical processes that control retention or release of NH_3 from soil and linking these processes to predicting the emission potential (Γ) and critical compensation point (X_g) of NH_3 from non-amended soil. As presented in chapter two, the dynamic flow-through chamber in combination with annular denuder tube technology allows measurements of soil NH_3 emission at ambient levels of NH_3 while concurrently monitoring soil water evaporation. To derive NH_3 loss from non-amended soils, a more reasonable, realistic, and accurate critical compensation point has to be determined, which requires an estimation of soil emission potential (Γ). A better understanding of the mechanisms regulating the dynamics of Γ regarding NH_4^+ concentration and pH is needed, which requires in part a better assessment of the adopted chemical extraction methods used for determination of NH_4^+. The following sections will further explore these existing processes and how this research contributes to an improved understanding of predicting NH_3 emissions from soil.

1.1.Theoretical Background of the Soil Compensation Point

A better understanding of bi-directional exchange is needed to more accurately predict the magnitude of NH_3 emission and deposition to surfaces (Farquhar et al., 1980; Sutton et al., 1995). Ammonia is considered a sticky gas in that it readily interacts with many differing surfaces (Schilt et al., 2004). However, unlike most other inorganic gases, NH_3 can be re-emitted from environmental surfaces under the proper conditions.

The exchange of NH_3 between the atmosphere and a surface is a bidirectional process (Farquhar et al., 1980; Sutton et al., 1995). Ammonia may, according to the "compensation point" for the underlying surface, be emitted from or deposited into the soil, plant, and water (Walker et al., 2014). The soil compensation point designated as X_g (Dawson, 1977; Nemitz 2001) is established by the equilibrium between NH_3 gas in the soil pores and NH_4^+ ion in the soil solution. At an ambient atmospheric NH_3 concentrations above the point of compensation, NH_3 is absorbed by the soil. Ammonia is lost to the atmosphere at a concentration below the point of compensation (Walker et al., 2014).

Temperature and concentrations of NH_4^+ and H^+ in soil solution together control the compensation point (X_g) of NH_3 (Nemitz et al., 2000b). The potential for NH_3 emissions can be defined as $\Gamma_g = [NH_4^+]/[H^+]$, which as expected, has direct dependence on the amount of NH_4^+ present and being cycled within the soil. For instance, fertilized soils that have a high value of Γ_g will be a source of NH_3, whereas forest soils, which have relatively small values of Γ_g, may fluctuate throughout the year between being a source or a sink for NH_3 (Walker et al., 2006; Walker et al., 2008; Cooter et al., 2010).

The emission/deposition of NH_3 in soil-plant environments has been shown to be an important aspect of the nitrogen cycle (Raven et al., 1993; Krupa, 2003). Estimates of NH_3 emission in various ecosystems ranges from -140 ng m^{-2} s^{-1} (deposition) (Phillips et al., 2004) to + 4 ng m^{-2} s^{-1} (emissions) (Wichink Kruit et al. 2007).

Reduced nitrogen (either as NH_3 or NH_4^+) following deposition can have serious economic and ecological impacts (Schjoerring et al., 1993). These potential impacts include eutrophication, soil acidification, nutrient leaching and enhanced crop response to certain stresses such as ozone, drought, forest and fungal disease (Yamulki et al., 1996). The acidification of soils as well as the

acidification of freshwaters are partly driven by nitrification of deposited NH_3 and NH_4^+ (Schjoerring et al., 1993). Enhanced N-deposition into N-deficient terrestrial ecosystems destabilizes them resulting in loss of biodiversity, replacing slow-growing plant species with fast-growing grasses (Heil and Bruggink, 1987). Deposition of NH_3 and NH_4^+ to aquatic ecosystems can result in eutrophication leading to algal blooms with subsequent death of fish (Schjoerring et al., 1993).

Direct measurement of the exchange of NH_3 between the soil and atmosphere is challenging, especially in non-nitrogen fertilized soils. Static measurements of different soil parameters, such as extractable inorganic N species also provide limited information and do not account for biological processes that are always active in soils. The magnitude and even the sign of the NH_3 exchange is therefore difficult to predict. Many investigators have applied compensation point (X_g) models to predict NH_3 exchange magnitude and direction (Nemitz et al., 2000b; Massad et al., 2010; Zhang et al., 2010; Twigg et al., 2011; Stratton et al., 2018). Use of these compensation point models provides an inexpensive alternative to direct measurement of flux. Accurate X_g models currently suffer from a lack of process-based information of NH_3 soil-atmosphere exchange mechanisms and how these mechanisms vary with environmental conditions.

1.2. Compensation Point and Resistance Approach for Estimating NH_3 Flux

The NH_3 flux (F_g) between the soil and atmosphere at some distance (z) above the soil surface can be represented as the gradient in NH_3 concentration divided by the total resistance to transport within the soil and through the atmosphere (Eq. 3.1).

$$F_g = \frac{X_g - X_z}{R_{bg} + R_{soil}} \tag{3.1}$$

Here, X_z is the measured NH_3 concentration at height z, X_g is concentration of NH_3 in the soil layer, R_{bg} is the air-side boundary layer (laminar) resistance at the soil surface and R_{soil} is the soil resistance. The resistance terms have unit of s m^{-1}. Application of Eq. 3.1 requires derivation of solutions for the various terms in the equation.

1.2.1. Theory

The compensation point is derivative from Henry's law for NH_3 dissolution and the acid dissociation coefficient of NH_4^+. A general link between the gaseous NH_3 concentration and the NH_4^+ concentration and pH in a solution can be obtained by combining the temperature response of the Henry's law equilibrium (Eq. 3.2) and the equilibrium between NH_4^+/NH_3 (aq) dissociation in solution (Eq. 3.3).

$$NH_{3(g)} \overset{K_H}{\leftrightarrow} NH_{3(aq)} \tag{3.2}$$

$$NH_4^+ + H_2O \overset{KNH_4^+}{\longleftrightarrow} NH_{3(aq)} + H_3O^+ \tag{3.3}$$

The partitioning of NH_3 between the gaseous and solution phases varies markedly with temperature. Dasgupta and Dong (1986) provided an expression for the variation of the Henry's law constant (K_H) with temperature:

$$\ln K_H = \frac{4092}{\mathrm{T}} - 9.70 \quad (3.4)$$

At standard atmospheric pressure, the temperature dependence of K_H is expressed (Dasgupta and Dong, 1986) as the ratio between the dissolved molar (M) concentration of NH_3 in pure water and the partial pressure of NH_3 (Eq. (3.5).

$$K_H = \frac{[NH_{3(aq)}]}{P_{NH_3}} = 5.527.10^{-4} \exp\left(4092\left(\frac{1}{T} - \frac{1}{298.15}\right)\right) \quad (3.5)$$

where K_H is the Henry's law constant (mol L^{-1} atm^{-1}), $p$$NH_3$ is the partial pressure of NH_3 (atm) and [NH_3(aq)] is the dissolved molar concentration of NH_3, and T is the absolute temperature (˚K).

The dissociation coefficient (K_{NH4^+}, mol L^{-1}, Eq. 3.6) is calculated based on work by Bates and Pinching, (1949).

$$K_{NH_4^+} = \frac{[NH_{3(aq)}][H^+]}{[NH_4^+]} = 5.67.10^{-10} \exp\left(-6286\left(\frac{1}{T} - \frac{1}{298.15}\right)\right) \quad (3.6)$$

Here, the [$NH_{3(aq)}$] is the concentration (mol L^{-1}) of dissolved NH_3 in the solution, and [NH_4^+] and [H^+] represent the ammonium and hydrogen ion concentrations (mol L^{-1}) in the solution, respectively. From Eq.3.5 and 3.6 the relationship at the interface between an aqueous surface and the atmosphere can be described as

$$\chi = P_{NH_3} = \frac{K_{NH_4^+}\,[NH_4^+]}{K_H\,[H^+]} \quad (3.7)$$

where χ is defined as the surface compensation point and is a function of soil NH_4^+ and H^+ concentrations, and the equilibrium constants K_H and $K_{NH_4^+}$. Both equilibrium constants (K_H and

$K_{NH_4^+}$) are highly temperature- dependent, causing temperature the main driver for X. Eq. 3.7 can be rewritten as:

$$X = [NH_{3(g)}] = \frac{2.75\ x\ 10^{15}}{T} \exp\left(\frac{-1.04\ x10^4}{T}\right).\Gamma_g \quad (3.8)$$

The Γ_g term is the ratio of $[NH_4^+]$ to $[H^+]$ concentrations in the soil solution (unitless), and T is the soil temperature (˚K). Nemitz et al. (2000b) derived the stomatal compensation point χ_{sto} (similar to the Eq. 3.8) as being a function of temperature (K) and the emission potential of the stomata (Γ_{sto} = ratio of the NH_4^+ and H^+ concentrations (mol L^{-1}) in the apoplastic fluid in the stomatal cavity). The soil compensation point (X_g) (μg m^{-3}) (Eq. 3.9) is very similar in theory to that of stomatal compensation point X_{sto} (Nemitz et al., 2001).

$$X_g = \frac{161500}{T_{soil}} \exp\left(\frac{-10380}{T_{soil}}\right) \frac{[NH_4^+]}{[H^+]} \quad (3.9)$$

1.3. Implications of Soil Emission Potential (Γ_g) ($[NH_4^+/H^+]$)

The magnitude of Γ_g dictates the tendency for a soil to emit NH_3. Unfertilized soil has been rarely shown to have a relatively large value of Γ_g (Schjoerring et al., 1993 ; Sutton et al., 1993; Nemitz et al., 2000a), while fertilized soils have an elevated emission potential especially following application of N-bearing fertilizers (e.g. urea or manures) (Ge´nermont et al., 1998; Søgaard et al., 2002; Meyers et al., 2006; Sintermann et al., 2012). Approximately 30–40% of the entire NH_3 emissions to the atmosphere are thought to derive from all fertilizer application to soils (Sintermann et al., 2012, and citations therein). Typically, soil Γ_g values increase by several orders of magnitude following application of manure slurries to agricultural fields (Flechard et al., 2010).

There are other sources of N that can influence Γ_g other than manures and N-containing fertilizers. In a grassland study, David et al., (2009) noted that the underlying soil was only a relatively high potential source of NH_3 emissions after the grass had been mowed. For a short period of time, the emission potential of the soil was ~ three times lower than the leaf litter. The impact of litter on Γ_g can be especially strong in the autumn (Hansen et al., 2013). A detailed model analysis by Zhang et al. (2010) has shown that Γ_g values in unfertilized soils (primarily grasslands) fell within the range of 20–1000 (Zhang et al., 2010). Walker et al. (2008) reported a single measurement of Γ_g for a forest soil of $\Gamma_g = 20$ that may have been affected by a neighboring swine animal feeding operation (Walker et al., 2008). Stratton et al. (2018) calculated an average Γ_g of 117 ± 49 based on n = 7 observations for the forest soils in their study.

1.4. Soil Processes involved in the Determination of NH_3 Compensation Point (X_g)

Description and quantification of NH_3 exchange processes at the soil-atmosphere interface is an essential step in understanding the mechanisms behind the determination of X_g. Initial soil pH, NH_4^+ content, pH buffer capacity, temperature and soil moisture are important considerations for determining the extent of NH_3 emissions (Nathan and Malzer, 1994).

1.4.1. Soil pH

In theory, the compensation point for the soil NH_3 can be calculated for any temperature and by considering the concentration of NH_4^+ and H^+ in the soil solution. Reactions induced by soil amendments that lead to an increase in soil pH can result in an increase in NH_3 emissions (He et al., 1999). The effect of soil pH on NH_3 emissions has been documented by many researchers (Wahhab et al., 1957; Wagner and Smith, 1958; Watkins et al., 1972; Mills et al., 1974; Ryan et al., 1981). Below pH 7, < 1% of TAN ((TAN = NH_3+NH_4^+) is available as $NH_{3(aq)}$

and the potential for emission of NH_3 is much reduced. As the pH rises, there can be a sharp increase in NH_3 loss (Cai, 1997). Jewitt (1942) observed NH_3 reductions of 87%, 13% and zero when applying ammonium sulfate to soil of pH 10.5, 8.6 and 7.0, respectively.

The pH surrounding microsites containing NH_4^+ salt granules may be more crucial than the general soil pH (Nelson, 1982; Stumpe et al., 1984) in promoting NH_3 emissions. Hargrove (1988) found that the soil's pH buffering capacity is perhaps more critical in controlling NH_3 emissions than the original soil pH. If the soil pH buffer capacity is significant the effective $[H^+]$ concentration in soil solution will not change, meaning that emissions become primarily a function of soil temperature and the $[NH_4^+]$ present.

1.4.2. pH Buffering Capacity

Ammonia loss from solution releases H^+ (Eq. 3.3) and therefore is an acidification process (Avnimelech and Laher, 1977; Sharp and Harper, 1995). In the absence of a strong pH buffer capacity, the $NH_{3(aq)}$ percentage in solution shifts (Eq. 3.3) until a new equilibrium is established (Koelliker and Kissel, 1988). Basic soils with free carbonates or other types of alkalinity can have a relatively high soil pH buffer capacity. Many researchers who used ammonium-based fertilizers have experienced large losses in $NH_{3(g)}$ from calcareous soils (Fenn and Kissel, 1973, 1974, 1975, 1976; Fenn, 1975; Fenn and Escarzaga, 1976, 1977; Feagley and Hossner, 1978; Fenn et al., 1981a, b, c).

The significance of initial soil pH, buffer capacity and concentrations of $[NH_4^+]$ from additions of ammonium salts to an alkaline soil on the NH_3 emissions was assessed by Avnimelech and Laher (1977). They found that initial soil pH is of primary significance when the buffer capacity is high or when the NH_4^+ concentrations in the soil solution are low (e.g. if the soil's cation exchange capacity is relatively large). Depending on the initial soil pH, NH_3 loss

increased as buffer capacity increased. If the soil buffer capacity is relatively small, the proportional losses of NH_3 are reduced even as the NH_4^+ concentration increases.

Hydrogen ions originating from nitrification reactions usually decrease soil pH (as well as the $[NH_4^+]$ in soil solution). If the initial soil pH is > 7.5, and there is sufficient soil pH buffering capacity to maintain this higher pH range, then NH_3 emissions will continue for some time before soil pH is sufficiently decreased by nitrification reactions to lower NH_3 release (Ferguson et al., 1984; Hargrove, 1988). In general, in calcareous soils with sufficient buffering capacity a reduction in pH (primarily from nitrification) will not be a major inhibiter of NH_3 emissions, while in non-calcareous soils with lower pH buffering capacity, hydrolysis of urea can significantly increase soil pH leading to an increase in emissions (Hargrove, 1988).

1.4.3. Soil Temperature

He et al. (1999) observed that NH_3 emissions increased two fold as the temperature increased from 5 to 25°C and tripled as the temperature rose from 25 to 45°C. As noted in Eq. 3.5, there is an exponential relationship between temperature and NH_3 emissions. However, He et al. (1999) concluded that the significantly enhanced NH_3 emissions at 45°C were also due to an inhibition of the nitrification process thus increasing NH_4^+ accessibility to promote NH_3 emissions. Hargrove (1988) highlighted the effects of temperature on the equilibrium of $NH_4^+/NH_{3(g)}$ and shifts in $NH_{3(aq)}$ in solution. Increased temperature increases the proportion of $NH_{3(aq)}$ to NH_4^+, decreases the solubility of $NH_{3(g)}$, and increases NH_3 diffusion in soil. Hence, the higher the temperature, the higher the NH_3 loss. Temperature also influences the fertilizer solubility and the rate of NH_3 conversion by microbes. These multiple impacts have been described by Martin and Chapman (1951); Fenn and Kissel (1974); Wahhab et al. (1957); Prasad (1976); and Farquhar et al. (1980).

1.4.4. Soil Water Content

In Chapter Two (Section 1.1), the effect of soil water content on soil NH_3 emission was discussed in depth. As reported from laboratory research, the impact of soil moisture content on NH_3 emission suggests that a low moisture content results in the greatest NH_3 emission (Demeyer et al., 1995). The impact of the soil moisture content on NH_3 emission is complicated and hard to determine in the field due to daily variations in soil water content as water and water vapor moves vertically in response to soil evaporation. The presence of dew and its formation (serving as a adsorptive surface for NH_3) and subsequent evaporation (serving as a release mechanism for NH_3 back to the atmosphere) further compounds attempts to understand NH_3 emissions (Hargrove, 1988). Both the increase in temperature during the daytime and the potential redistribution of NH_4^+ in the soil solution due to soil evaporation can combine to alter the NH_3 partial pressure gradient at the soil surface and increase NH_3 emissions (Lightner et al., 1990; Nathan and Malzer, 1994; Hargrove, 1988).

1.5. Uncertainties Related to Parameters of Soil Compensation Point Model

The primary uncertainties associated with the soil compensation point model and deriving values for X_g are the $[NH_4^+]$ in soil solution and soil pH. Both of these parameters are described in more detail in the following sections.

1.5.1. Uncertainty in Measurement of Soil pH

Although soil pH is one of the most often used measurements to describe soils, the actual measurement process of obtaining a value for soil pH is operationally defined. The ratio of soil to solution used in the measurement, the electrolyte concentration of the solution, and even the positioning of the pH electrode all can influence the measured value (Thomas, 1996). Reported

soil pH values may have been measured in background electrolytes of just deionized water (i.e. salts inherent in the soil sample control the ionic strength), 0.01M $CaCl_2$, or 1M KCl, at soil to solution ratios ranging from 1:1, 1:2 or 1:5 (Soil Survey Staff, 2009; Libohova et al., 2013; GlobalSoilMap, 2015). Values of pH measured in water are generally 0.2 to 0.5 units greater than pH values determined in salt solutions like 0.01M $CaCl_2$, and especially in 1M KCl (Brady and Weil, 1999). It is often argued that use of salt solutions more typically represents the ionic composition of the soil solution (especially in agricultural soils) and the equilibria among the other cations on the soil exchange surfaces such as H^+ and Al^{3+} (Brady and Weil, 1999; Kissel et al., 2009), which dictate the amount of soil acidity present in most mineral soils. Measurement of soil pH in the presence of salt solutions should be more consistent throughout the year as well (Kissel et al., 2009).

Soil pH values are known to vary with season and are influenced by the timing and application rates of fertilizer and other soil amendments, the degree of soil microbial activity, and proximity to the root environment (rhizosphere) (Murdock and Call, 2006). Soil pH has been reported to be higher in winter and lower in late summer (Slattery and Ronnfeldt, 1992). Soil pH may vary from spring to fall by more than one pH unit for the same relative location (Angima, 2010). Lastly, localized changes in soil pH due to fluctuations in soil moisture content may arise as a result of changes in ionic strength as soils dry or wet (Thomas, 1996; Kissel et al., 2009), further compounding deriving the best estimate of pH to use in estimating X_g.

1.5.2. TAN versus $[NH_4^+]$ in Soil Solutions

In studies of cation exchange equilibria with soils (Paliwal and Maliwal, 1966; Paliwal and Maliwal, 1970), the suitability of many equations such as the Gapon equation (Eq 3.10 and

3.11) was examined to explain the distribution of ions between the soil and soil solution. The NH_4^+ exchange reactions with other ions at exchange sites determine how NH_4^+ is partitioned between the exchange sites and the soil solution (Gaspard et al., 1983; Lin and Wu, 1996; Singh and Prasad, 1997; Demir et al., 1998). Consequently, when NH_4^+ is strongly partitioned to exchange sites, the NH_4^+ in the soil solution will decrease and the production of NH_3 will then be decreased (Kissel et al., 2008).

$$NH_4^+{}_{(aq)} + Ca_{0.5} - Soil = (NH_4^+) \text{-}Soil + 0.5Ca^{2+}{}_{(aq)} \quad (3.10)$$

The equilibrium constant of the reaction as described by Gapon (1933) between NH_4^+ and Ca^{2+} is shown in Eq. 3.11.

$$K_G = [(NH_4^+) \text{-}Soil] [Ca^{2+}]^{1/2} / (Ca - Soil) [NH_4^+] \quad (3.11)$$

The limitation inherent in Eq. 3.10 is that we do not have a routine test for just determining the $[NH_4^+]$ in soil solution. In addition, Eq. 3.10 implies a rapid exchange between $[NH_4^+]$ in soil solution and $[NH_4^+]$ on the exchange surface. As such, a measurement of the total amount of NH_4^+ present might be a more valid estimate of the NH_4^+ acting to control NH_3 in soil solution and X_g. This total can be defined as TAN and therefore measurements of TAN might be more representative of NH_4^+ fraction in soil we need to characterize to derive X_g.

Intensive study has been undertaken to develop appropriate methods for measurement of TAN using different salt solutions (Li et al., 2012). Nearly all aqueous extraction methods have extracted TAN in the form of NH_4^+ ions (Hrdina et al., 2019). The method of soil bulk extraction is presently used for determining NH_4^+ and NO_3^- ions where ions are quantitatively displaced from the soil sample by an extractant. Water or a salt solution (KCl or $CaCl_2$) are among the more prevalent extractants (Bremner and Keeney, 1966; Keeney, 1982; Brodrick et al., 1987;

Antisari and Sequi, 1988; Esala, 1994; Yang et al., 1998; Khan et al., 2000; Castro and Korn, 2004). The inherent assumption with the KCl or $CaCl_2$ extractants is that they combine the ions in the soil solution with a fraction or all of the ions the soil exchange sites, whereas water extracts only non-adsorbed ions in the soil solution.

A number of studies have proved the variation in the quantity of extractable NH_4^+ that results from differences in the concentration of the extracting solution and the selection of extracting salt cation (Neftel, 2013). Hanway et al. (1957) described adequately how the concentration of the cation extraction solution influences NH_4^+ extraction. They carried out research with different concentrations of NaCl solutions on the liberation of NH_4^+ from NH_4^+ - saturated Montana vermiculite and Wyoming bentonite. Their study showed that the volume and concentration of NaCl employed was not strongly correlated to NH_4^+ release. The total millimoles of NaCl per gram of clay mineral added was the dominant factor related to NH_4^+ extraction and substantially improved the regression between NH_4^+ and the NaCl-based extracting solutions.

Flechard et al. (2013) pointed to a study by Sterckeman and Ciesielski (1991) for an assessment of NH_4^+ measurement. The authors compared the extraction efficiency of NH_4^+ using 1M KCl and NaCl, and various KCl solution concentrations (0, 0.1, 0.25, 0.5, 0.75, or 2 M) versus 1M KCl. They also evaluated distinct ratios of soil weight to extraction volume and shaking time protocols. For three silty loam soils, the NH_4^+ efficiency of extraction of the 1M NaCl solution was 35% versus 65% for 1M KCl. The extraction efficacy of NH_4^+ for all three soils was higher with 2M KCl. Scott et al. (1958) showed that additional NH_4^+ can be removed from vermiculite if NH_4^+ is continuously removed from the extraction solution by either alkaline solutions or successive extraction techniques. This finding is consistent with the dynamic

equilibrium proposed by Lamm and Nadafy (1973) for K^+ and developed by Nommik and Vahtras (1982) for NH_4^+.

Allison et al. (1953) and Allison and Roller (1955) have estimated the NH_4^+ in soil using the Kjeldahl-N technique by leaching exchangeable NH_4^+ with either KCl or $CaCl_2$. The findings of their studies showed a substantial difference in soil NH_4^+ content depending on whether KCl or $CaCl_2$ was used for leaching. Leaching with KCl led to consistently greater values than leaching with $CaCl_2$.

Beauchamp (1982) examined native release and release of added K^+ and NH_4^+ from two Ontario soils during an extended experiment (166 days) using 0.01M $CaCl_2$ leaching for periods of 7 days or longer. In the 10 to166 day period, the K^+ release rate was constant and was not influenced by NH_4^+ supplementation. Nonetheless, adding K^+ delayed NH_4^+ release from day 10 through to the end of the experiment. The K^+ overriding effect on NH_4^+ release could be due to the low $CaCl_2$ leaching concentration. Most experiments performed by Méngel and Scherer (1981) and Keerthisighe et al. (1984,1985) on the sorption and release of NH_4^+ have used 0.5M $CaCl_2$ to extract exchangeable NH_4^+ rather than 1M KCl to prevent contraction of clay minerals by K^+. Chen et al. (1989) demonstrated alike effects of different salt solutions (Ca and K) on the removal of NH_4^+ in a field incubation experiment on Texas Gulf Coast Soil. Feigenbaum et al. (1994) have observed a significantly boosted liberation of KCl extractable N from recently sorbed beidellite-$^{15}NH_4^+$. They found release of 30% of NH_4^+ sorbed in Ca-saturated beidellite as compared to 6.5% of K-saturated beidellite. Felber et al. (2012) have shown that the complete recovery of ammonium with slurry cannot be obtained with either 0.01M $CaCl_2$ or concentrations of up to 2M KCl.

Cooter et al. (2010) stated that the standard KCl extraction method (1-2 M KCl) would not be the best method for deriving Γ_g as the NH_4^+ extracted is greater than would exist in soil solution, which could overestimate the amount of NH_3 loss to the atmosphere. They assessed their hypothesis by contrasting 1M KCl extractable NH_4^+ to extractions with 0.01 M $CaCl_2$ and deionized water from a Lillington, NC field site. Cooter et al. (2010) compared extractions from moist soil of 0.25g H_2O/g soil and after drying to 0.01g H_2O/g soil. They noticed that a decrease of ionic strength of the extraction solution resulted in less NH_4^+ extraction. For wet and dry soil respectively, 0.01M $CaCl_2$ collected 64% and 55% of the quantity obtained with KCl, and 49% and 46% respectively with deionized water. They concluded the calculated Γ_g should be lowered by 45% in order to get a compromise between modelled flux and measurement flux data for wheat stubble.

Research to this point, as pertaining to Γ_g, is not yet developed enough to provide guidelines on the most suitable technique of extraction of NH_4^+ for advancing the estimate of Γ_g. The analytical difficulties in terms of soil extractable NH_4^+ and pH issues and the resulting uncertainty in soil Γ_g values were reported in Neftel (2013). Fundamental research must be carried out, which is a high priority for the further advancement of the NH_3 emission models for agricultural soils. While regional and global NH_3 modeling advances, more use will be seen in soil chemistry data from long-term ecological sites and farming stations. To effectively apply these results, a better understanding of the relationships between extractable NH_4^+ and soil Γ will be needed.

Since the amount of total extractable NH_4^+ removed from soils using traditional extraction protocols is grossly overestimating the fraction of soil NH_4^+ that is available for the soil-atmosphere exchange of NH_3. A more realistic estimate of the relationship between [NH_4^+]

in soil solution and NH_4^+ sorbed on the soil exchange surface is needed for estimating Γ_g. Adsorption isotherms are one method that could be used to calculate the fraction of NH_4^+ present in soil solution as a function of NH_4^+ loading to the soil exchange surface. This may lead to a more realistic soil compensation point to be used in soil-air exchange modeling.

A sorption isotherm relates the solution phase to loading onto sorption surface, which for NH_4^+ is the exchange (CEC) complex (Sparks, 1996; Hinz, 2001; Zarabi and Jalali, 2018). Venterea et al. (2015) used this approach to determine the amount of NH_4^+ sorbed onto the soil surface (NH_4^+(ex)) versus the concentration of NH_4^+ in the soil solution ($NH_4^+{}_{(aq)}$). The amount of sorbed NH_4^+ was calculated from the change in $NH_4^+{}_{(aq)}$ at the start and end of equilibration and also accounting for the initial 2M KCl-extractable NH_4^+ content of the soil. The resulting NH_4^+ sorption isotherms allowed Venterea et al. (2015) to calculate the fraction of sorbed NH_4^+ in equilibrium with NH_4^+ in solution ($NH_4^+{}_{(aq)}$). Knowledge of $NH_4^+{}_{(aq)}$ allows an evaluation of $[NH_4^+]/[H^+]$, which is the soil emission potential value in the compensation point model. Measures of the relationship between $NH_4^+{}_{(aq)}$ and sorbed NH_4^+ via an adsorption isotherm could be used to correct total extractable NH_4^+ values (TAN) for use in compensation point modeling.

1.6. Research Objectives

As an index for NH_3 emission, it is important to estimate the magnitude and direction of NH_3 fluxes through accurately calculating the soil critical compensation point (X_g) (the tendency of a soil to absorb or release NH_3). Accurate measurements of soil pH and the concentration of NH_4^+ in soil solution afford a means of determining the NH_3 compensation point as opposed to carrying out accurate measurements of NH_3 exchange in the field. Critical soil parameters that need to be considered include soil pH, soil texture, cation exchange capacity, soil moisture, and

soil organic matter content. The main goal of this study is to assess/develop a method to determine the fraction of NH_4^+ concentration in the soil solution that is actually involved in the estimation of soil emission potential (Γ_g) and thus in predicting the NH_3 compensation point. A laboratory approach was designed to compare two methods used in standardizing the calculation of X_g. The first method is based on the determination of the soil NH_4^+ concentration (TAN) in soil extracts together with standard measurements of soil pH. The second method uses the adsorption isotherm approach to calculate the fraction of NH_4^+ concentration in soil solution as a function of NH_4^+ loading on the exchange complex. The chamber design outlined in Chapter Two provided the means to actually assess $NH_{3(g)}$ emissions from soils selected for use in this study. This information is then combined to explore possible improvements in determining a soil's $NH_{3(g)}$ compensation point.

The specific objectives of this portion of the study include: (i) estimation of soil NH_3 compensation point based on a measure of extractable NH_4^+ using traditional methods of extraction for TAN (2M KCl, 0.01M $CaCl_2$, and water); (ii) development of NH_4^+ adsorption curves for a fumigated and unfumigated soils with a range of soil texture, CEC, N and C content; (iii) calculation of the fraction of NH_4^+ in the liquid phase that contributed to NH_3 emission via models of the NH_4^+ isotherms; (vi) quantification of an appropriate reduction factor that could be applied to values obtained for TAN using different chemical extractants (2M KCl, 0.01M $CaCl_2$, and water) to estimate the X_g; (v) demonstration of the relationship between the concentration of the extractable N and the change in the amount of NH_3 emissions using dose-response curves.

2.0 Material and Methods

2.1. Soils

Surface soils (0-10 cm) of differing soil texture were collected for use in this study. Loamy sand textured soils were obtained from a tilled, fallow field at the BASF The Chemical Company Research Farm located near Holly Springs, NC. Soils with a sandy loam texture and differing soil organic matter contents were obtained from two sites: The Center for Environmental Farming System (CEFS) located at the Cherry Research Station near Goldsboro, NC, and a former pasture/grassy field at the Duke Forest, near Durham, NC. For this study, the soils were designated as follows in tables and figures: loamy sand – BASF-ls; sandy loam – CEFS-sl or DUKE-sl.

The collected soils (BASF-ls and CEFS-sl) were air-dried for about 6 to 8 weeks at room temperature, passed through a 2-mm sieve, mixed, and stored in a large bucket in the laboratory environment. DUKE-sl soil was kept in the freezer immediately after collection from the field with no drying treatment prior to use. Soil pH in water and 0.01M $CaCl_2$ was measured using standard procedures (Peech, 1965; Table 3.1). Soil pH in the presence of 0.01M $CaCl_2$ provided a relative index of the presence of exchangeable acidity in the soil that will act to buffer soil pH. With a large pool of exchangeable acidity, it is unlikely that changes in soil pH will be seen over time. The cation exchange capacity (CEC) was determined by 1.0 M NaOAc buffered at pH 7 (Chapman, 1965). Soil texture was determined using the hydrometer method described by Gee and Bauder (1986). Soil water retention data were collected using a pressure plate apparatus (Klute, 1986).

Table 3.1. Physical and chemical properties of soils used in the study.

	(BASF-ls)	(CEFS-sl)	(DUKE-sl)
pH (H_2O) (1:2.5)	6.57	5.41	5.77
pH ($CaCl_2$) (1:2.5)	5.88	4.70	5.07
CEC ($cmol_c\ kg^{-1}$)	1.7	10.3	14.5
Sand %	84.5	68.3	52.7
Silt %	12.5	25.4	42.4
Clay %	3.0	6.4	4.9
Texture class	loamy sand	sandy loam	sandy loam
Water content at FC capacity $m^3\ m^{-3}$	0.14	0.30	0.36

2.2. Fumigation Procedure

For certain experiments, soil fumigation using chloroform was employed to control soil microbial activity. Distilled water was added to the soil to achieve approximately 50% of FC. A portion of moist soil (originally 50 g air-dried soil) was placed into each of thirteen 200 mL wide glass bottles. The bottles were then set into a glass vacuum desiccator lined with wet Kimwipes® to maintain ~ 100% relative humidity. The desiccator also contained ~75 mL ethanol-free chloroform ($CHCl_3$) in a 125 mL Erlenmeyer flask with a few boiling chips. The glass desiccator was placed under vacuum for 1 minute, which accelerated saturation of the interior atmosphere with $CHCl_3$. The evacuated desiccator was then placed in a dark cabinet at room temperature (22°C) for 10 days. The flask of $CHCl_3$ was then removed and the desiccator evacuated 5 times. The thirteen increments of fumigated soil were then mixed and used to pack a soil column.

Table 2.7 (Chapter 2) shows that fumigated soil inhibited the formation of NO_3^- within the packed columns but appeared not to inhibit mineralization. This relatively rapid increase in NH_4^+ with the initial addition of water further confounded attempts to quantify NH_4^+ redistribution within the packed columns due to evaporation. Although NH_4^+ increased in the surface 0 – 2 cm increment during the course of an experiment, careful consideration of N mass

balance for the inorganic N (NH_4^+ and NO_3^-) within the packed column suggested that a substantial portion of the increase in NH_4^+ could have been generated *in situ*.

2.3. Extraction NH_4^+ and NO_3^- from Soil

Five grams of soil (fumigated or un-fumigated) was mixed with 25 mL extractant (2M KCl, 0.01M CaCl2, or water) in 50 mL screw cap centrifuge tubes (Corning®, Inc.). The mixture was shaken for two hours on a rotating shaker (Glas-Col®,LLC. Model: 099A RD4512, Ser. No. 11327320), and then centrifuged at 2500 rpm for 20 min (IEC Model K Centrifuge. Serial No. 71652652) to obtain a clear supernatant solution. The solution was then passed through Whatman No.42 filter paper and collected into a 15 mL screw cap PVC conical centrifuge tube and stored until analysis at 4°C. Results of soil extractions are expressed on an oven-dry mass basis. Oven dry mass was determined based on separate measurements of the soil moisture content. Soil NH_4^+ and NO_3^- extracts were analyzed via a flow injection analyzer (Lachat, Quick-Chem 8000). Representative standard curves for NH_4^+ and NO_3^- prepared in 2M KCl are shown in Appendix C1. Analyses were carried out using 9-point standard curve from 1 to 20 μg NH_4^+ or NO_3^- per mL plus calibration checks. Data for the standard curves were fitted using a second-order polynomial via IGORPro® software (WaveMetric, Inc.) to calculate the concentrations of NH_4^+ or NO_3^- in each extract. Table 3.2 and 3.3 provide measures of extractable NH_4^+ and NO_3^- using 2M KCl, 0.01 M $CaCl_2$, and water for the un-fumigated and fumigated soils used in this study.

Table 3.2 Soil extraction for NH_4^+ and NO_3^- of un-fumigated soils with 2M KCl, 0.01 M $CaCl_2$, and water extractants

Extractant	(BASF-ls)	(CEFS-sl)	(DUKE-sl)
	---------- μg NH_4^+ g^{-1} soil ----------		
2M KCl	2.54	7.71	35.8
0.01 M $CaCl_2$	1.05	6.01	31.1
Water	0.65	2.46	9.74
	---------- μg NO_3^- g^{-1} soil ----------		
2M KCl	3.40	2.96	7.37
0.01 M $CaCl_2$	1.26	3.14	7.47
Water	0.95	2.53	1.00

Table 3.3 Soil extraction for NH_4^+ and NO_3^- of fumigated soils with 2M KCl, 0.01 M $CaCl_2$, and water extractants

Extractant	(BASF-ls)	(CEFS-sl)	(DUKE-sl)
	---------- μg NH_4^+ g^{-1} soil ----------		
2M KCl	5.36	15.05	37.17
0.01 M $CaCl_2$	3.45	17.18	31.91
Water	2.78	4.20	17.44
	---------- μg NO_3^- g^{-1} soil ----------		
2M KCl	1.13	2.11	0.98
0.01 M $CaCl_2$	1.15	1.77	1.10
Water	0.53	1.30	0.35

In general, the DUKE-sl soils had higher extractable NH_4^+ and NO_3^- than the BASF-ls and CEFS-sl soils. The low extractable N in the BASF-ls soil as compared to those of soil CEFS-sl and DUKE-sl relates to its low CEC and lighter texture. The results showed the following increasing order of NH_4^+ extraction magnitude: 2M KCl > 0.01 M $CaCl_2$ > water (**Table 3.2, 3.3**). In these solutions, the 2M KCl is expected to extract all different forms of NH_4^+ from different pools that are present in the soil. The 0.01M $CaCl_2$ method recorded less total NH4-N in the extracts (1.05μg NH_4^+ g^{-1}) compared to the 2M KCl (2.54μg NH_4^+ g^{-1}) for BASF-ls soil. The NH_4^+ extraction by water being 3.9x, 3.1x, and 3.7x lower than KCl for unfumigated soil BASF-ls, CEFS-sl, and DUKE-sl, respectively, and 1.6x, 2.4x, and 3.2x lower than $CaCl_2$ extraction for unfumigated soil BASF-ls, CEFS-sl, and DUKE-sl, respectively. There were slight differences in the amounts of NO_3^- extracted by the two extractants (KCl and $CaCl_2$) in

unfumigated soils 2.54 and 1.26μg NO_3 g^{-1} for BASF-ls soil, 2.96 and 3.14μg NO_3^- g^{-1} for CEFS-sl soil, and 7.37 and 7.47μg NO_3^- g^{-1} for DUKE-sl soil.

2.4. Ammonium Adsorption Isotherms

All the adsorption isotherm experiments were conducted at room temperature (T=22ºC). For each experiment, 30 g of soil sample were mixed with 30-mL of the ammonium sulfate solution in 50-mL screw cap centrifuge tubes (Corning®,Inc.). The initial concentrations of NH_4^+ used with un-fumigated soils were 6, 10, 30, 50, 100, 200, 300, 400, 500 mg NH_4^+/L. The initial concentrations of NH_4^+ solution tested with fumigated soil were 6, 10, 30, 50, 100, 200, 300, 400, 500, 600, 800, and 1000 mg NH_4^+/L. Similarly, a separate sample was prepared using the NH_4^+ solution without the soil sample. All solutions used in this study were diluted with distilled water as required to arrive at solid:solution ratio of 1:1. The tubes were shaken for 24 hours on a rotating shaker with the speed of 40 rpm. Samples were then centrifuged at 2500 rpm for 20 min (IEC Model K Centrifuge. Serial No. 71652652). The supernatants were filtered through Whatman No. 42 filter paper and analyzed for NH_4^+-N and NO_3^--N using a flow injection automated ion analyzer (Lachat, Quick-Chem 8000). The amount of NH_4^+ ions sorbed was calculated as the difference between the initial and final NH_4^+ concentrations in the supernatants using the following expression:

$$Q_e = \frac{(C_o - C_e)V}{m} \qquad (3.12)$$

where Q_e is the amount (mg kg^{-1}) of adsorbed species, C_o is the initial concentration of the NH_4^+ in solution (mg L^{-1}), C_e is the equilibrium concentration of the NH_4^+ in solution (mg L^{-1}), V is the solution volume (L), and m is the mass of air-dried soil (g) and then corrected to oven dry mass based on separate measurements of moisture content. The experiments were carried out in duplicate or triplicate for unfumigated and fumigated soils, respectively.

2.5. Ammonia Emission from Soil

The simple flow- through chamber combined with annular denuder technology was used to measure the release of NH_3 from soil (Fig. 2.1, Chapter Two). Use of the annular denuder technology allowed for the determination of both the total mass of NH_3 released in a given time period, as well as calculation of an integrated average NH_3 concentration in the air stream during the span of the same time interval. Air flow through the chamber was controlled via a microprocessor-controlled pump and a digital mass flow controller. Flow rates at 5 LPM (effective exchange rate of air = 4.5 Vol min^{-1}) were confirmed using a BIOS® piston flow meter. Annular denuder tubes were coated with 0.5% phosphorous acid solution and then dried with NH_3-free air. Paired denuder tubes were used for each chamber, one used to scrub NH_3 from the air entering the chamber and a second denuder to capture the mass of NH_3 exiting the chamber. Table 2.3 (Chapter Two) summarizes the laboratory experiments undertaken to measure soil water evaporation, NH_4^+ redistribution, and NH_3 loss using flow-through chamber combined with annular denuder technology.

2.6. Ancillary Measurements

Soil pH was measured using a 1:2.5 soil: solution ratio (distilled water or 0.01M $CaCl_2$) using a combination glass electrode (Accumet BASIC AB15) (Fisher Scientific) calibrated with NIST-traceable pH standards with an accuracy of roughly 0.01 pH units. Gravimetric soil moisture was determined by weight loss after heating 10 g of soil for 48 hours at 60 °C with a detection limit on the order of 0.01g H_2O g^{-1} fresh soil. Temperature was measured in the laboratory room using EL-USB-2LCD RH/TEMP DATA LOGGER.

3.0. Results

3.1. Adsorption Isotherms for NH_4^+ Using Fumigated and Un-Fumigated Soils

Figure 3.1 presents the NH_4^+ adsorption isotherms for fumigated and unfumigated soils. The capacity for NH_4^+ adsorption relies on cation exchange capacity, clay content, and soil organic matter (Rosenfeld, 1979; Boatman and Murray, 1982; Raaphorst and Malschaert, 1996). Ammonium (NH_4^+) adsorption mechanisms in fumigated and unfumigated soil may occur through physical adsorption mechanisms as well as through NH_4^+ ion exchange at cation-exchange locations with Na^+, K^+, and Ca^{2+} ions (Ranjbar and Jalali, 2013).

The comparison of NH_4^+ sorption among different unfumigated soils showed the following trend: DUKE-sl > CEFS-sl,> BASF-ls. The difference in the NH_4^+ sorption between soils is likely due to the differences in chemical and physical characteristics (Table 3.1). Compared with CEFS-sl and DUKE-sl soils, the BASF-ls soil contains a lower clay content and has a lower CEC, resulting in a lower potential sorption maximum for NH_4^+. The maximum sorption capacity of the examined unfumigated soils as calculated by the Langmuir isotherm and adjusted for initial extractable NH_4^+ with 2M KCl is as follows (Table 3.4, 3.6, 3.8): 138 ± 7, 200 ± 15, 425 ± 49 mg g^{-1} for BASF-ls, CEFS-sl, and DUKE-sl, respectively, which indicates a predominance of CEC on the sorption capacity of the soils. Similar differences in the sorption capacities, reliant on the soil type, were observed by Fernando et al. (2005), Venterea et al. (2015), and Sieczka and Koda (2016). The NH_4^+ distribution from the concentrated source into the soil were studied by Gurovich and Avnimelech (1977). A modification of the Freundlich equation was used to describe the isotherm data. They found the quantity of NH_4^+ sorbed and CEC are closely correlated. Elmaci et al. (2002) evaluated NH_4^+ sorption in certain agriculturally soils and found that the sorption ranges from 7% to 49% and has a positive and negative

relationship with silt and sand content, respectively. Two important factors contributing to NH_4^+ adsorption are the clay type and its content. Zhang et al. (2007) found that the amount of NH_4^+ sorbed has a positive correlation with the amount of clay and the CEC. The estimates also showed the percentage of sorbed NH_4^+ in paddy soils ranged from 6 ± 4 to 17 ± 5 and in upland soils from 6 ± 2 to 40 ± 18. Yu et al. (2011) examined NH_4^+ adsorption and desorption in wetland soils with adsorption ranging from 5 to 58. They also noted that soils with a higher CEC content and clay had a higher capacity to adsorb NH_4^+. Murray et al. (1978) stated that the adsorption of NH_4^+ increased as the alkalinity concentration increased. Rosenfeld (1979) demonstrated that in the exchangeable NH_4^+ in the soils is usually linked to organic matter and not to clay.

In order to isolate the effect of the chemical and physical processes on NH_4^+ sorption, attempts were made to eliminate the influence of microbiological processes through a chloroform-fumigation technique. The pattern of NH_4^+ sorption was similar for the fumigated and unfumigated soils (Fig 3.1). The fumigated soils showed greater adsorption due to different initial concentrations of NH_4^+ partly because a greater range in initial NH_4^+ additions was used with these soils. At the higher equilibrium NH_4^+ concentrations in solution, the NH_4^+ ion was more effective in displacing the other remaining counter cations (i.e. the mole fraction of NH_4^+ in solution was greater). The maximum sorption capacity of the fumigated soils as calculated by the Langmuir isotherm corrected for extractable NH_4^+ with 2M KCl was found to be as follows (Table 3.4, 3.6, 3.8): 307 ± 29, 489 ± 63, and 673 ±76 mg g^{-1} for BASF-ls, CEFS-sl, and DUKE-sl, respectively.

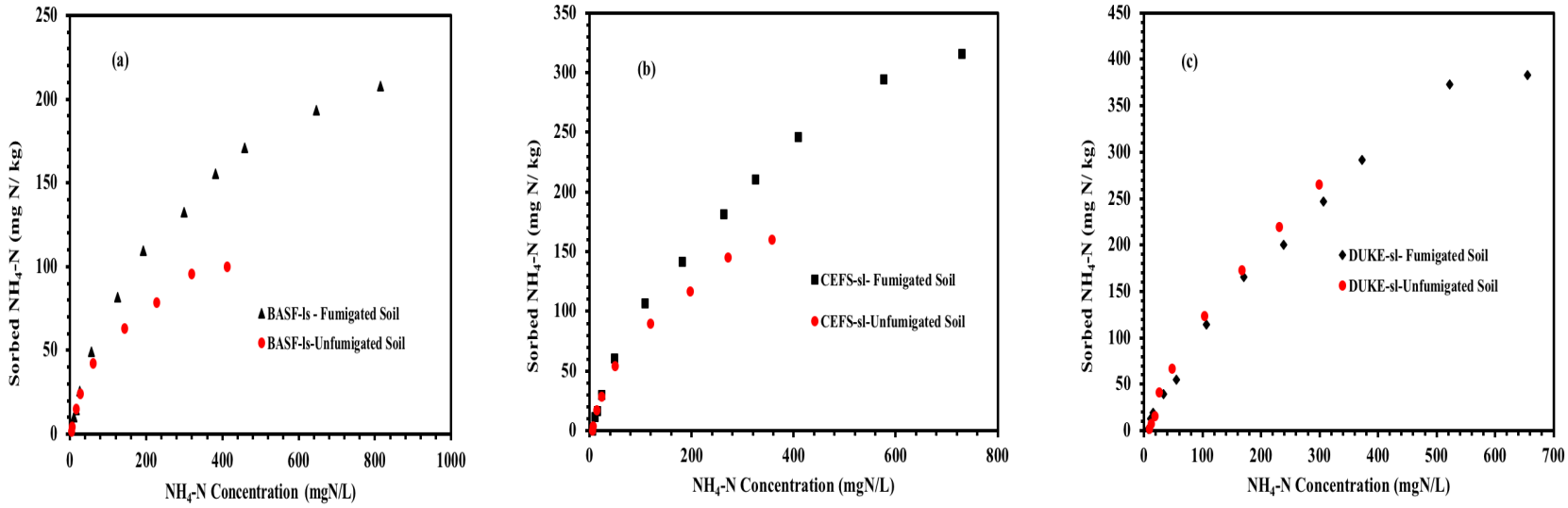

Figure 3.1. Adsorption isotherms for NH_4^+ by fumigated and unfumigated (a) BASF-sl, (b) CEFS-sl, and (c) DUKE-sl soils

The Langmuir equation (Langmuir, 1918) and an equation developed by Venterea (Venterea et al., 2015) were used to describe the sorption of NH_4^+ and to calculate the soil compensation point. The adsorption isotherms allow calculation of the fraction of sorbed NH_4^+ and the fraction of $NH_4^+{}_{(aq)}$ in solution. The fraction of $NH_4^+{}_{(aq)}$ in solution corresponds to the $[NH_4^+]$ term in the ratio of $[NH_4^+]$ /$[H^+]$ which equivalent to the NH_3 emission potential in the compensation point model (Eq. 3.9).

The Langmuir isotherm model (Eq. 3.13) assumes that homogeneous monolayer surface sorption occurs, and that once an adsorbate molecule occupies a site, no further adsorption can take place at that site. Therefore, a saturation value is reached beyond which no further sorption can take place. One form of the Langmuir isotherm equation can be written as follows:

$Q_e = \frac{Q_m K_L C_e}{1 + K_L C_e}$	(3.13)

where C_e is the equilibrium concentration of the adsorbate (mg L^{-1}), Q_m (mg Kg^{-1}) and K_L (L mg^{-1}) are the Langmuir sorption constants related to the maximum sorption capacity and the binding energy of sorption, respectively.

A modification of the Langmuir equation derived by Venterea et al. (2015) (Eq. 3.14) was used to calculate the amount (mg Kg^{-1}) of sorbed NH_4^+ by soil ($srNH_4^+$):

$srNH_4^+ = \frac{\mu\,(slNH_4^+)}{K + (slNH_4^+)}$	(3.14)

where μ (mg N Kg^{-1}) is the maximum sorption capacity and K (mg N L^{-1}) is the concentration of NH_4^+ in solution at which *sr*NH_4^+ equals one-half of μ.

The two sorption isotherms basically describe the relationship between the amount of NH_4^+ (mg Kg^{-1}) retained on the soil surface versus TAN in equilibrium solution, where TAN is defined as sum of $NH_4^+{}_{(aq)}$ + $NH_{3(aq)}$, ignoring any other form of NH_3 present in solution.

Venterea et al. (2015) makes a specific focus in their equations of relating NH_4^+ sorbed to NH_4^+ in solution rather than TAN. An example of the calculation of $NH_4^+{}_{(aq)}$ and $NH_{3(aq)}$, for BASF-ls soil using Venterea's approach is shown in Appendix D.

The entire range and just the low end of the isotherms for each soil were considered when curve fitting the data. The full range covers concentrations of 0-500 and 0-1000 mg NH_4^+ L^{-1} for the unfumigated (Fig. 3.2-3.6) and fumigated soils (Fig. 3.7-3.12), respectively. The low end includes concentrations < 250 mg NH_4^+ L^{-1}. Both the Langmuir isotherm and Venterea's equation have two constants. The isotherm data were fitted using the IGORPRO® program using a least squares fitting procedure in which the value of one constant was assigned as an option thereby forcing the fit to find the best value for the remaining constant. Initial data points of 0,0 were added to the sorption isotherm data to account for the NH_4^+present at time zero. The mass of NH_4^+ present at time zero was estimated by using one of the following three extraction matrices: 2M KCl, 0.01 M $CaCl_2$, or deionized water. The amount of NH_4^+ founding using one of the extractants was added to the initial total NH_4^+ added at time zero and the amount of sorbed NH_4^+ recalculated. The amounts added were usually small compared to the range in TAN used to construct the isotherms: e.g. the NH_4^+ extracted with 2M KCl, 0.01M $CaCl_2$, and water for unfumigated BASF-ls soil were 2.54, 1.05, and 0.65 mg kg^{-1}, respectively. If the sorbed mass is determined based only on the difference in solution concentration from added TAN, then the background NH_4^+ is not accounted for and the amount sorbed may be underestimated by approximately 2%, 0.80%, and 0.5%, when extracted with 2M KCl, 0.01M $CaCl_2$, and water, respectively. This effect is more pronounced at the low end of the sorption isotherms which are more representative of the amount of NH_4^+ in unamended soil.

It is noted that there is hardly any difference in the determined fits whether the Langmuir (Fig.3.2-3.4) or Venterea et al. (2015) equation (Fig. 3.5-3.6) was used. Curves for unfumigated soils fit the data better, in general, than fumigated soils (Fig. 3.7-3.12). The reason is that the soil samples were not dried. Instead, they were maintained at approximately 50% of FC during the fumigation-incubation period. Therefore, soil moisture could make a difference in the sorption of NH_4^+ between fumigated and unfumigated soils

The values of the adsorption parameters determined from Langmuir isotherm and Venterea's equation are shown in Tables (3.4-3.9). The estimated maximum adsorption capacity of NH_4^+ determined by the Langmuir isotherm was assumed to be equivalent to an estimate of the CEC (meq/100g) and was compared to what was measured independently. This assumes the amount of TAN added was sufficient to saturate the CEC. The fraction of CEC accounted for by retention of NH_4^+ over the entire range, and the low end of equilibrium NH_4^+ concentrations was also calculated for each soil, as shown in Tables (3.4-3.9).

Cation-exchange capacity and diffusion-controlled adsorption have been suggested as the primary mechanisms that determine the characteristics of the NH_4^+ sorption isotherms (Chang and Donahue, 2007). Sorption of NH_4^+ is attributable to exchange reactions with cations (Na^+, K^+, Ca^{+2}, Mg^{+2}) present on the exchange sites on the soil. Soils with higher CEC values (e.g. the DUKE-sl soil; 14.5 meq/100 g) have more exchange sites to sorb NH_4^+ from solution. Additional important processes (Chang and Donahue, 2007) other than high CEC are diffusion-controlled adsorption, which can take five stages (Kithome et al., 1998): (1) diffusion of NH_4^+ through a solution to soil particles; (2) NH_4^+ diffusion into soil particles; (3) exchange of NH_4^+ with other cations in soil particles; (4) the diffusion of the displaced cations outside the soil particles (5)

diffusion of the removed cation from the soil particles by soil solution. The soil diffusion process is based on the heterogeneity and tortuosity of soil samples.

Water is so important in increase the sorption capacity for NH_4^+ especially for fumigated soils. Water molecules is tending to form clusters (Hu et al., 1995; Verdaguer et al., 2006), clusters tend to coalesce, forming monolayers (Hu et al., 1995; Ewing, 2006; Verdaguer et al., 2006) and flat multilayering (Verdaguer et al., 2006). Water is thus retained as a few layers of high-energy molecules which create changes in the structure and arrangement of water molecules that affect the dielectric properties of the soil and surface interactions (Jury and Horton, 2004; Kelleners and Verma, 2010), but this study does not prove it. This new research appears to have potential for the future as a new study.

The competition between cations for sites of sorption depends on the concentration, ionic and ionic charges (hydrated radius) (Chang and Donahue, 2007). In particular, when NH_4^+ is present as a high mole fraction in the solution, NH_4^+ may prevail at the sorption sites – it has more chances of occupying the sites than other existing cations. Potassium and Na^+ are replaced by cation competition and lower concentration gradients compared to NH_4^+. The ions of Ca^{2+} (0.412 nm) and Mg^{2+} (0.428 nm) are more hydrated than those of NH_4^+ (0.331 nm) or K^+ (0.331 nm) (Volkov and others, 1997). The largest ions cannot be percolated into the soil particles with the adsorbed NH_4^+ and K^+ and released to solution (Lumbanraja and Evangelou 1994). The presence of K^+ in solution can also cause NH_4^+ to be preferred at adsorption sites (Chang and Donahue, 2007). Whereas NH_4^+ and K^+ have the same hydration range, NH_4^+ sorption was increased in the presence of K^+ as it shown by James and Harward (1964) and Mortland (1968). Adsorbed NH_4^+ continues to expand the interlayer of soil, allowing it to diffuse the trapped interlayer K^+ on a surface and displacing structural K^+ (Lumbanraja and Evangelou, 1994).

(a) BASF-ls un-fumigated soil: Concentration (0-500 mg NH_4^+ L^{-1})

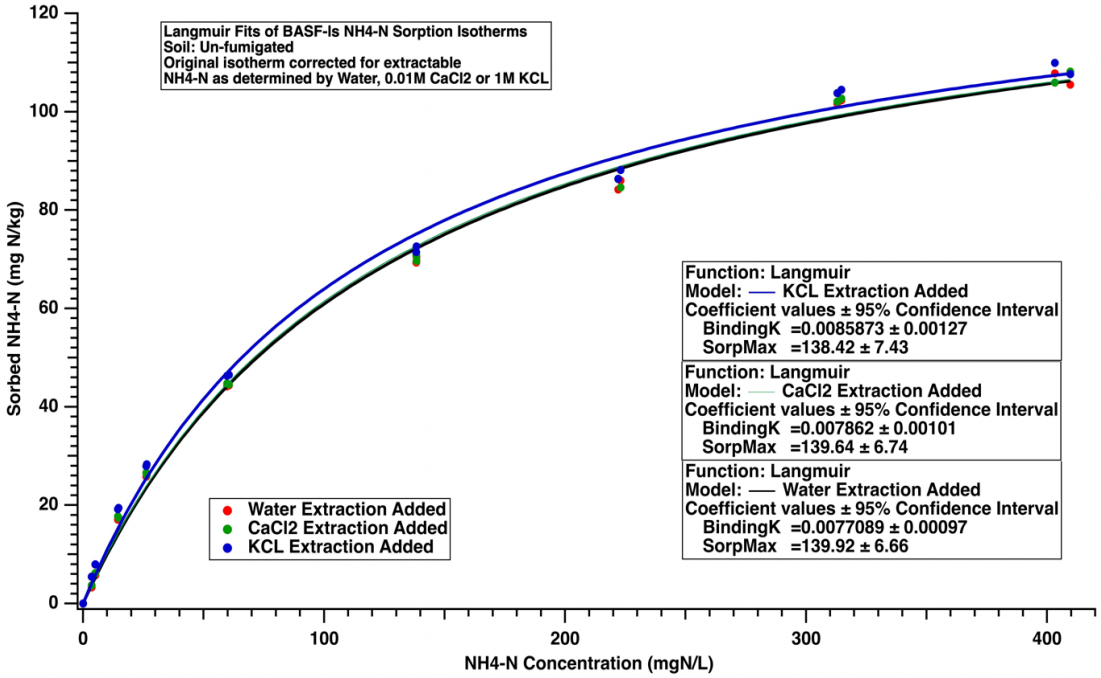

(b) BASF-ls un-fumigated soil: Concentration (<250 mg NH_4^+ L^{-1})

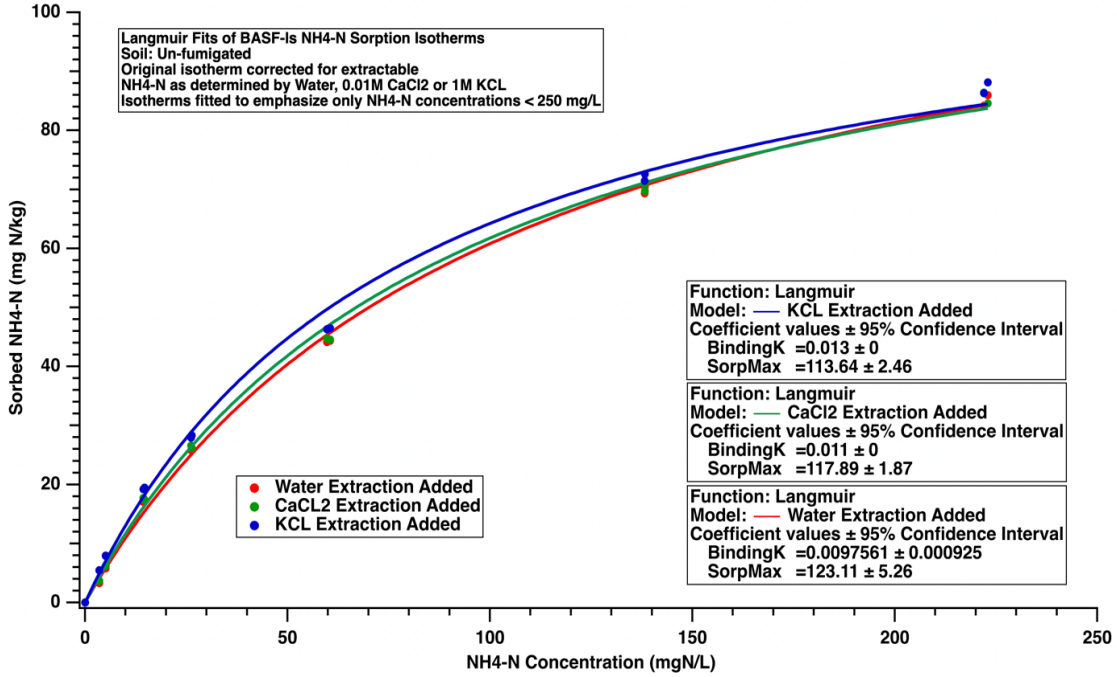

Figure 3.2. Langmuir Adsorption isotherms for un-fumigated BASF-ls soil corrected for extractable NH_4^+ as determined by 2M KCl, 0.01M $CaCl_2$, and water. (a) adsorption isotherm for (0-500 mg NH_4^+ L^{-1}), (b) adsorption isotherm for <250 mg NH_4^+ L^{-1}).

a) CEFS-sl unfumigated soil: concentration (0-500 mg NH_4^+ L^{-1})

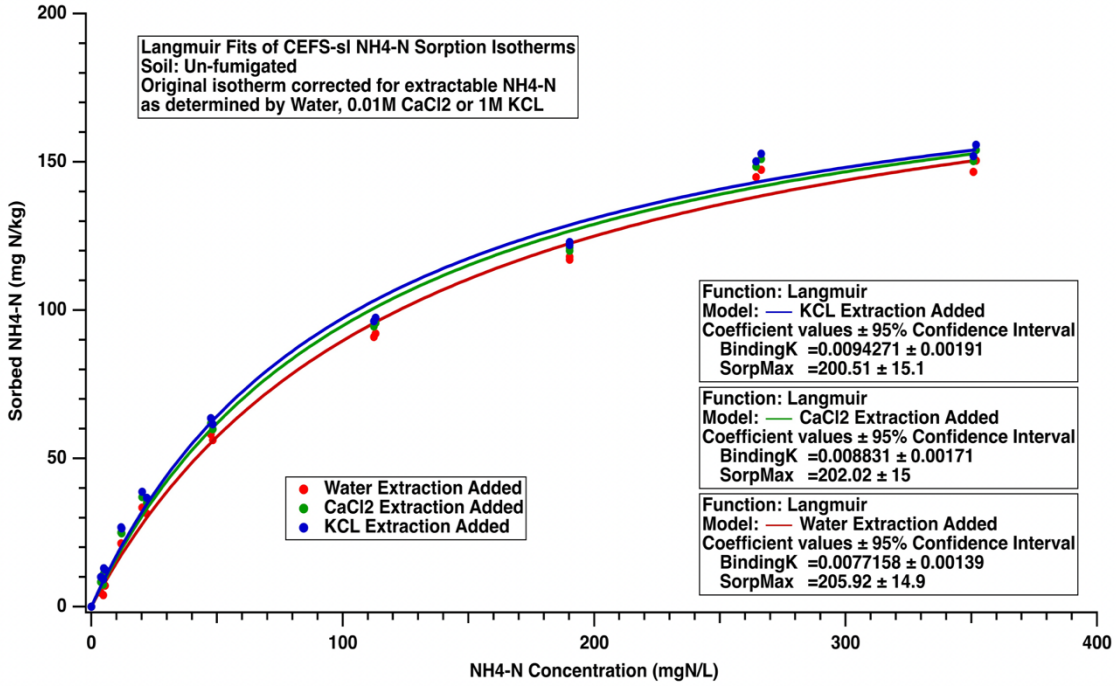

(b) CEFS-sl unfumigated soil: concentration (<200 mg NH_4^+ L^{-1})

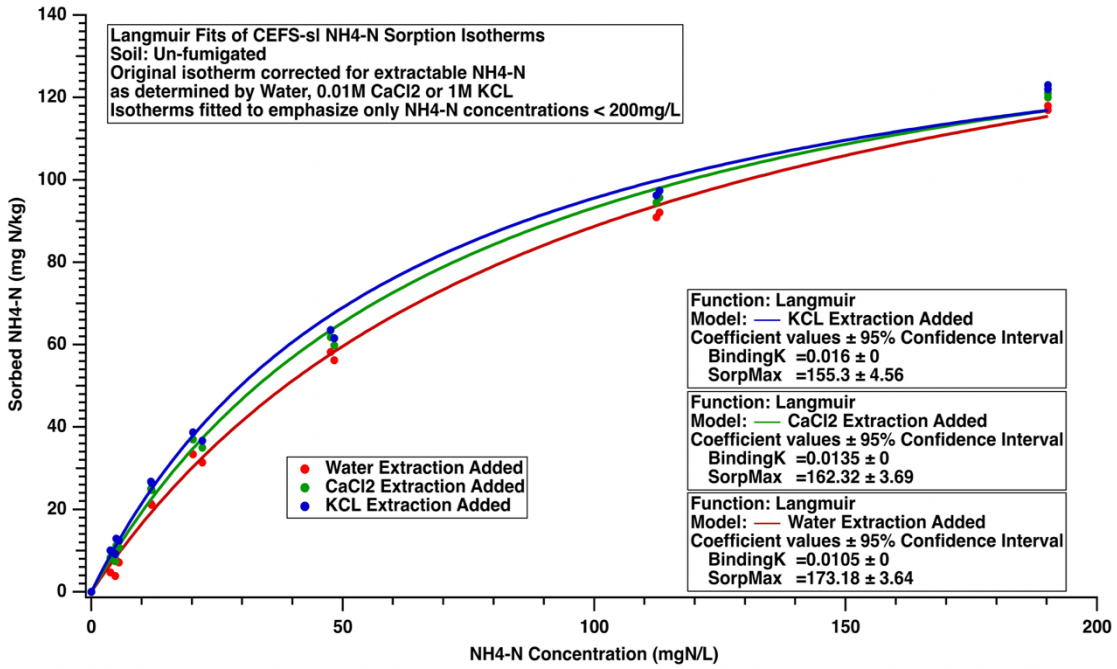

Figure 3.3. Langmuir Adsorption isotherms for un-fumigated CEFS-sl soil corrected for extractable NH_4^+ as determined by 2M KCl, 0.01M $CaCl_2$, and water. (a) adsorption isotherm for (0-500 mg NH_4^+ L^{-1}), (b) adsorption isotherm for <200 mg NH_4^+ L^{-1}).

(a) DUKE-sl un-fumigated soil: concentration (0-500 mg NH_4^+ L^{-1})

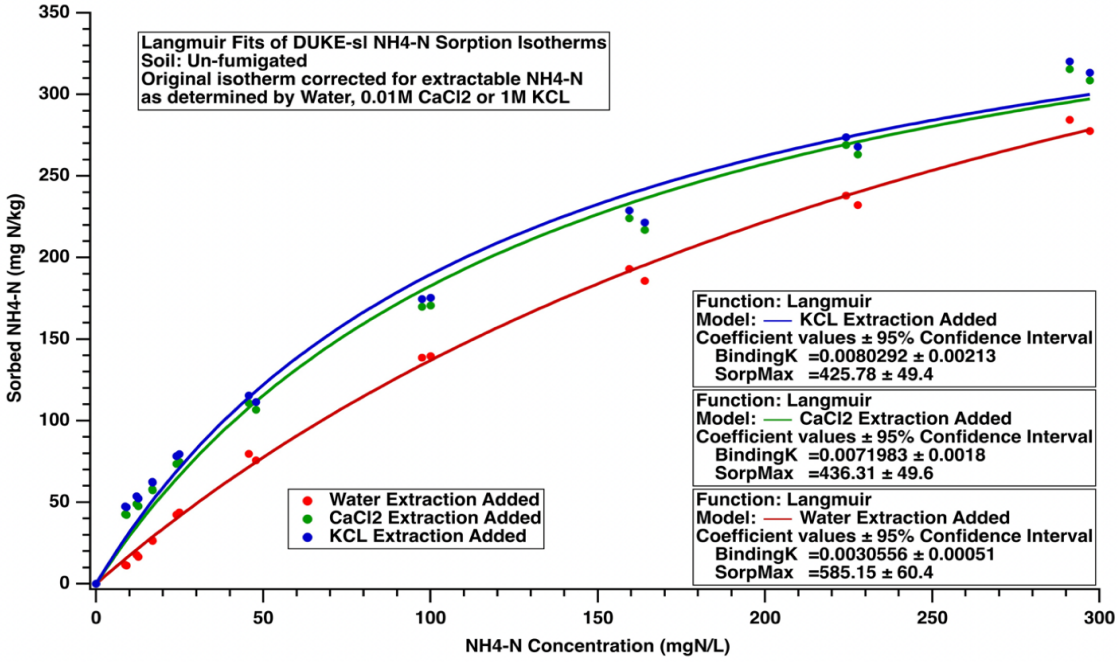

(b) DUKE-sl un-fumigated soil: concentration (<200 mg NH_4^+ L^{-1})

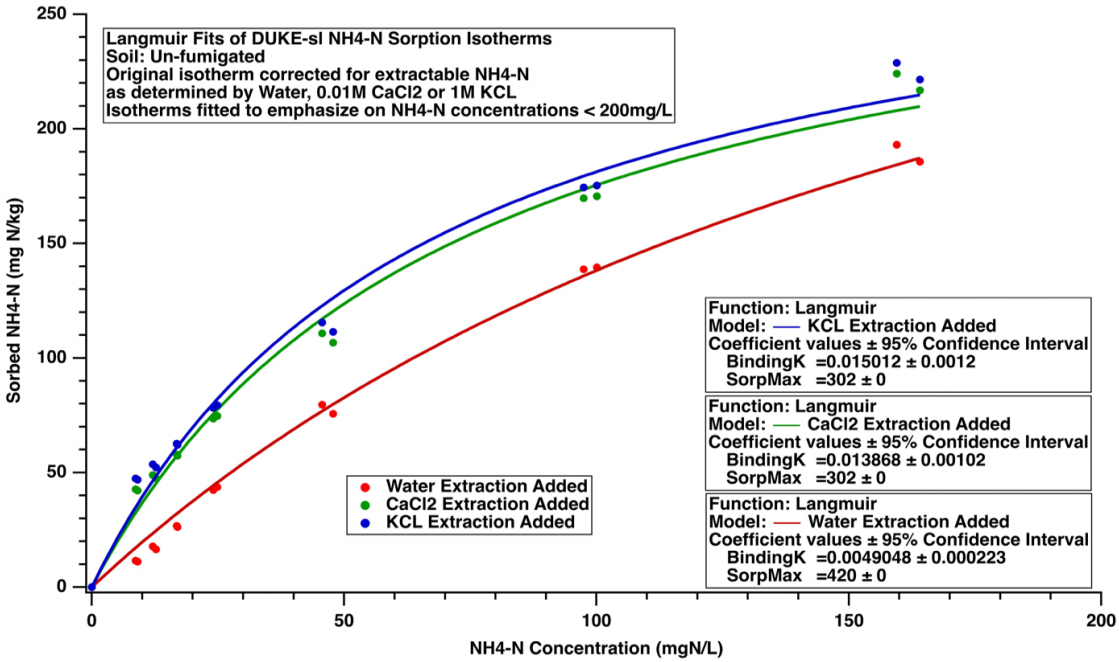

Figure 3.4. Langmuir isotherms for un-fumigated DUKE-sl soil corrected for extractable NH_4^+ as determined by 2M KCl, 0.01M $CaCl_2$, and water. (a) adsorption isotherm for (0-1000 mg NH_4^+ L^{-1}), (b) adsorption isotherm for <250 mg NH_4^+ L^{-1}).

(a) BASF-ls un-fumigated soil: Concentration (0-500 mg NH_4^+ L^{-1})

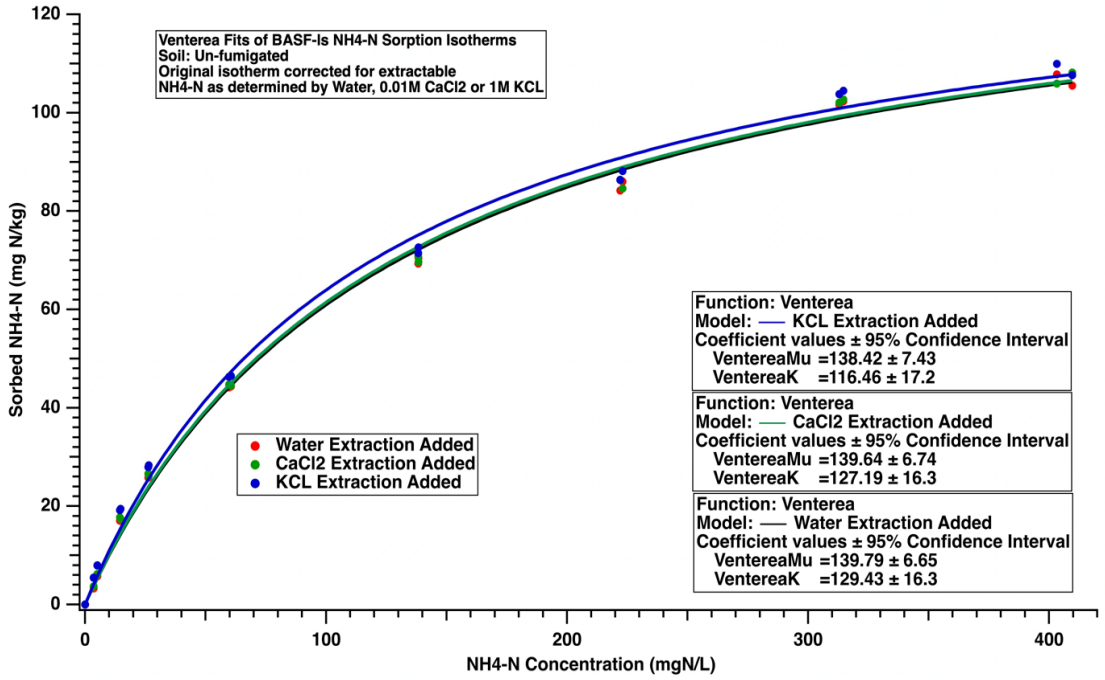

(b) BASF-ls un-fumigated soil: Concentration (<250 mg NH_4^+ L^{-1})

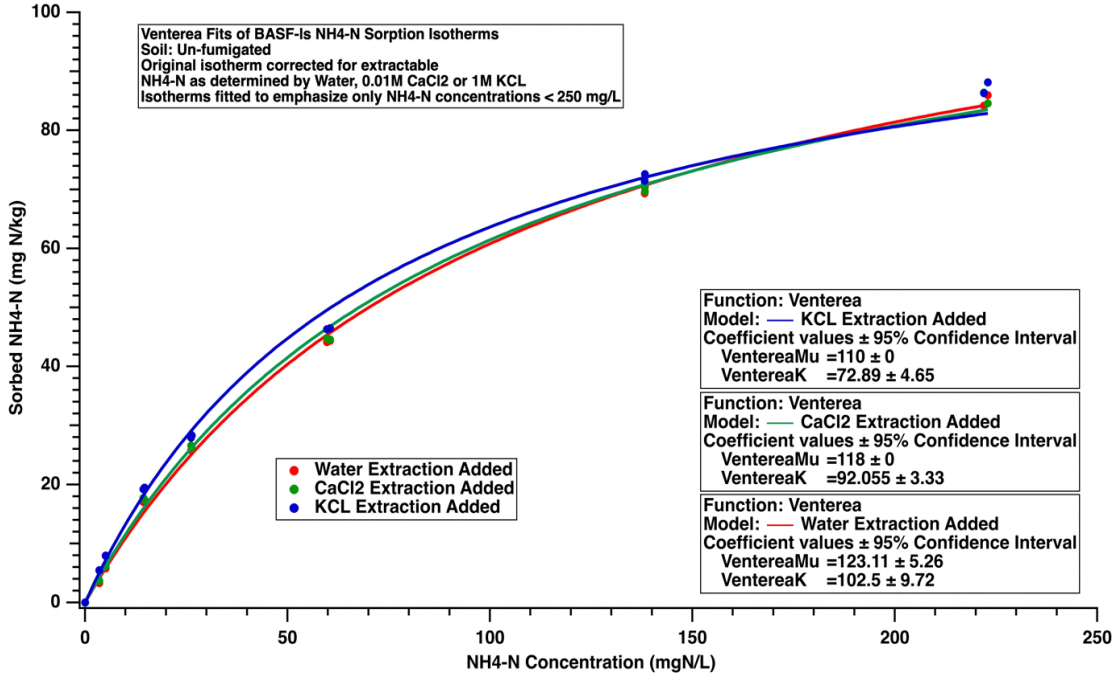

Figure 3.5. Venterea isotherms for un-fumigated BASF-ls soil corrected for extractable NH_4^+ as determined by 2M KCl, 0.01M $CaCl_2$, and water. (a) adsorption isotherm for (0-500 mg NH_4^+ L^{-1}), (b) adsorption isotherm for <250 mg NH_4^+ L^{-1}).

(a) CEFS-sl un-fumigated soil: Concentration (<200 mg NH_4^+ L^{-1})

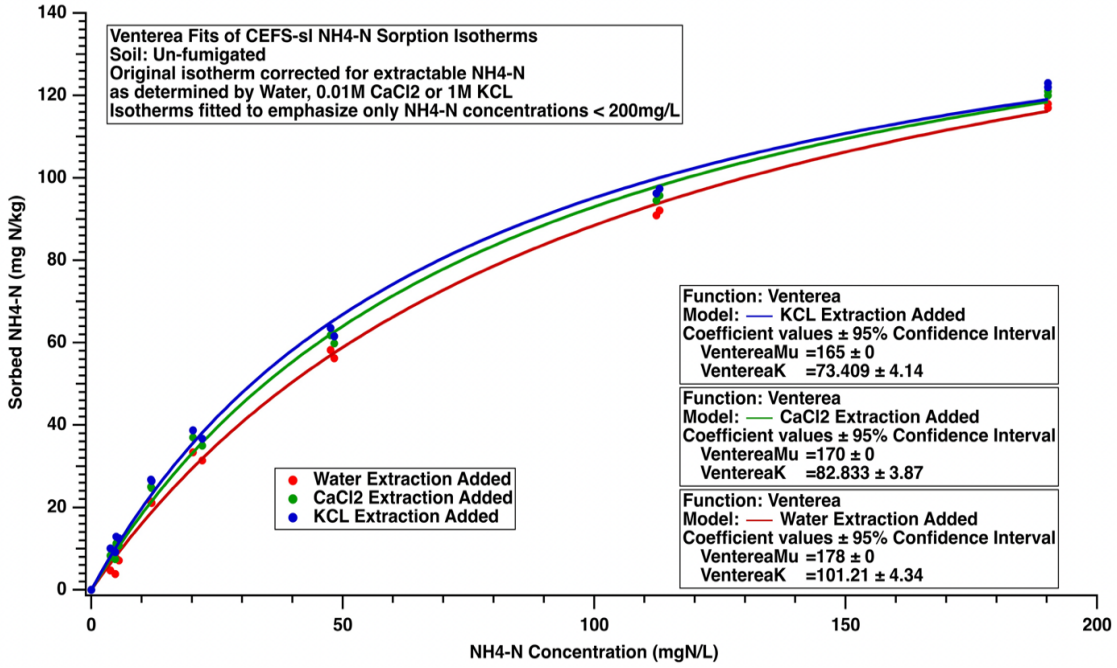

(b) DUKE-sl un-fumigated soil: concentration (0-500 mg NH_4^+ L^{-1})

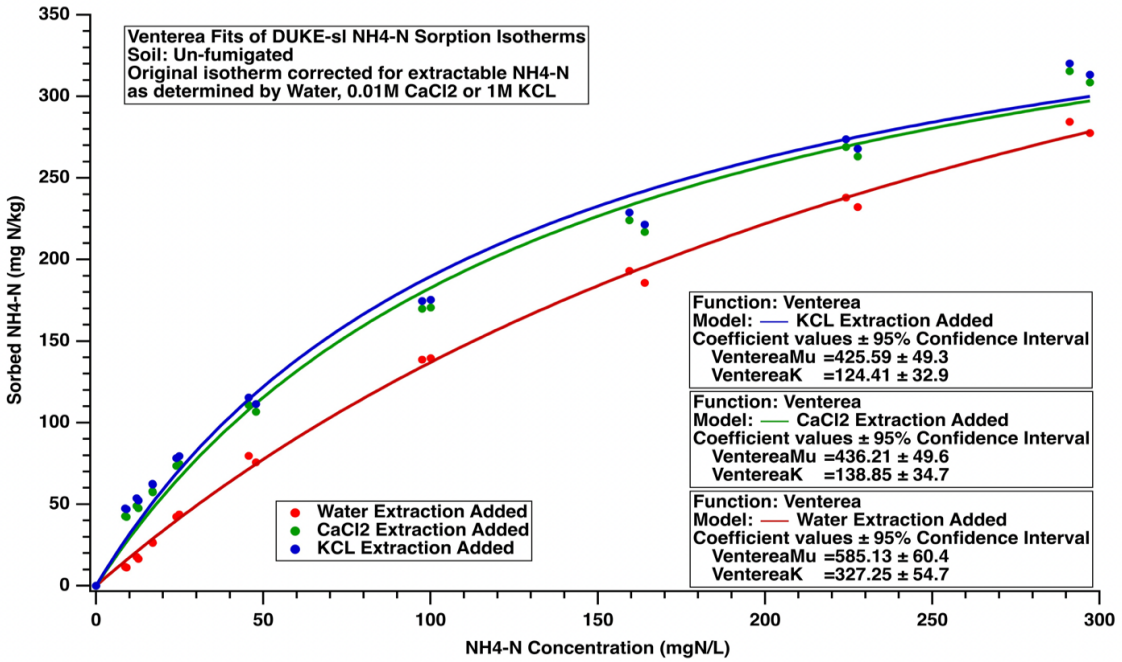

Figure 3.6. (a) Venterea isotherms for (a) un-fumigated CEFS-sl: concentration (<200 mg NH_4^+ L^{-1}) and (b) un-fumigated DUKE-sl soil: concentration (0-500 mg NH_4^+ L^{-1}). Isotherm corrected for extractable NH4-N as determined by 2M KCl, 0.01M $CaCl_2$, and water.

(a) BASF-ls fumigated soil: Concentration (0-500 mg NH_4^+ L^{-1})

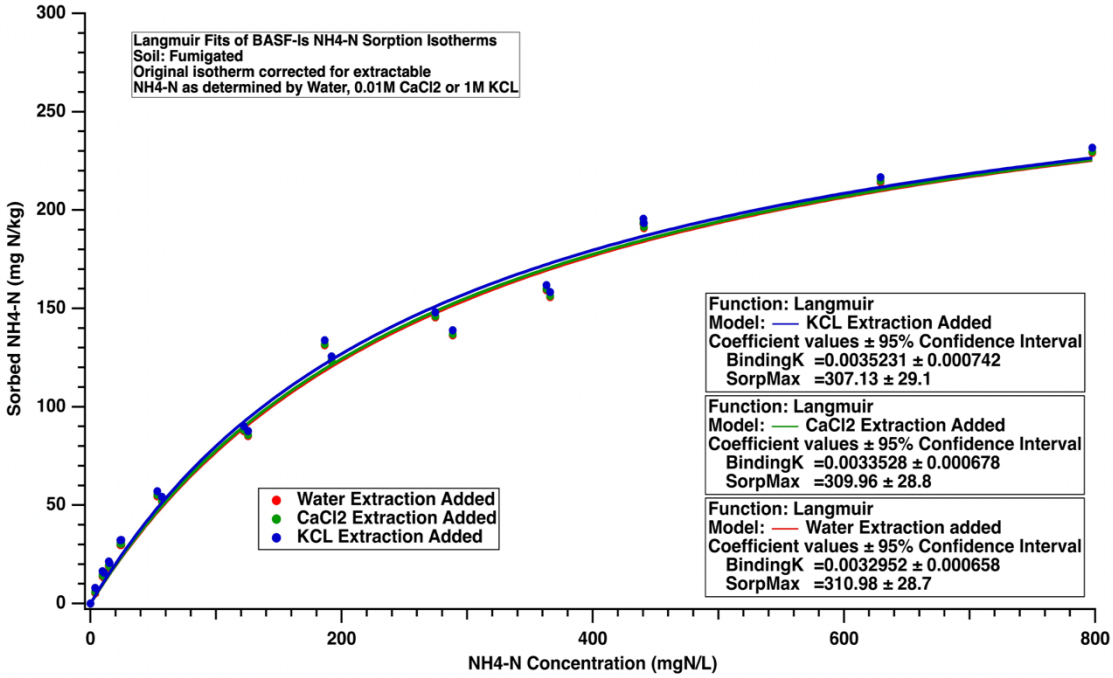

(b) BASF-ls fumigated soil: Concentration (<250 mg NH_4^+ L^{-1})

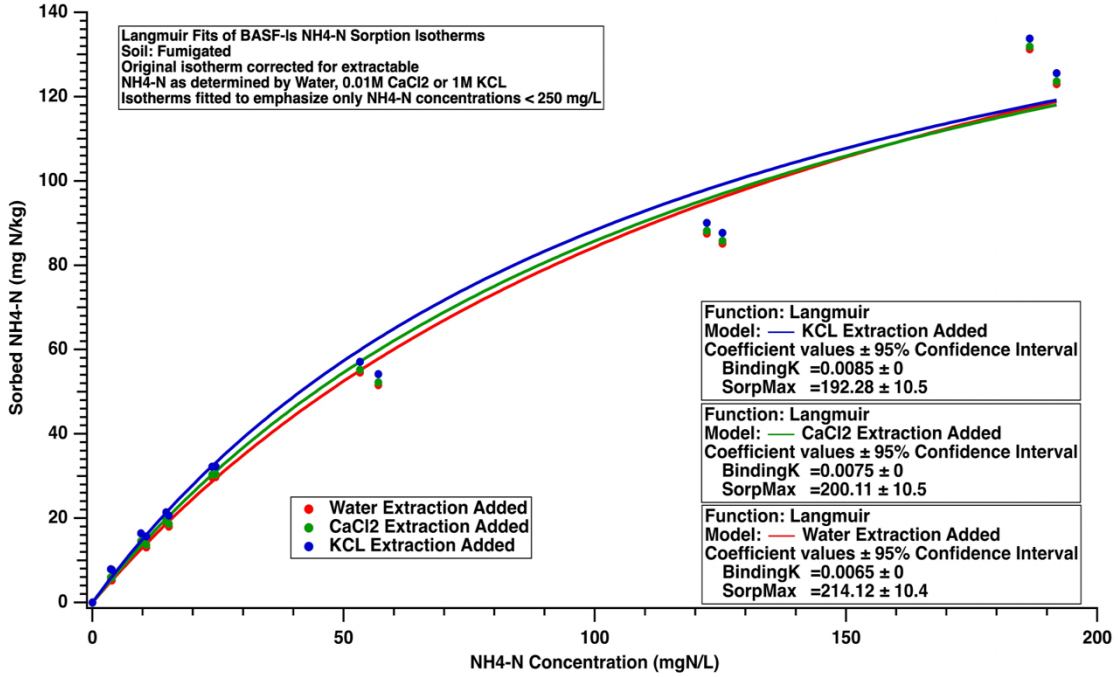

Figure 3.7. Langmuir Adsorption isotherms for fumigated BASF-ls soil corrected for extractable NH_4^+ as determined by 2M KCl, 0.01M $CaCl_2$, and water. (a) adsorption isotherm for (0-500 mg NH_4^+ L^{-1}), (b) adsorption isotherm for <250 mg NH_4^+ L^{-1}).

(a) CEFS-sl fumigated soil: Concentration (0-1000 mg NH_4^+ L^{-1})

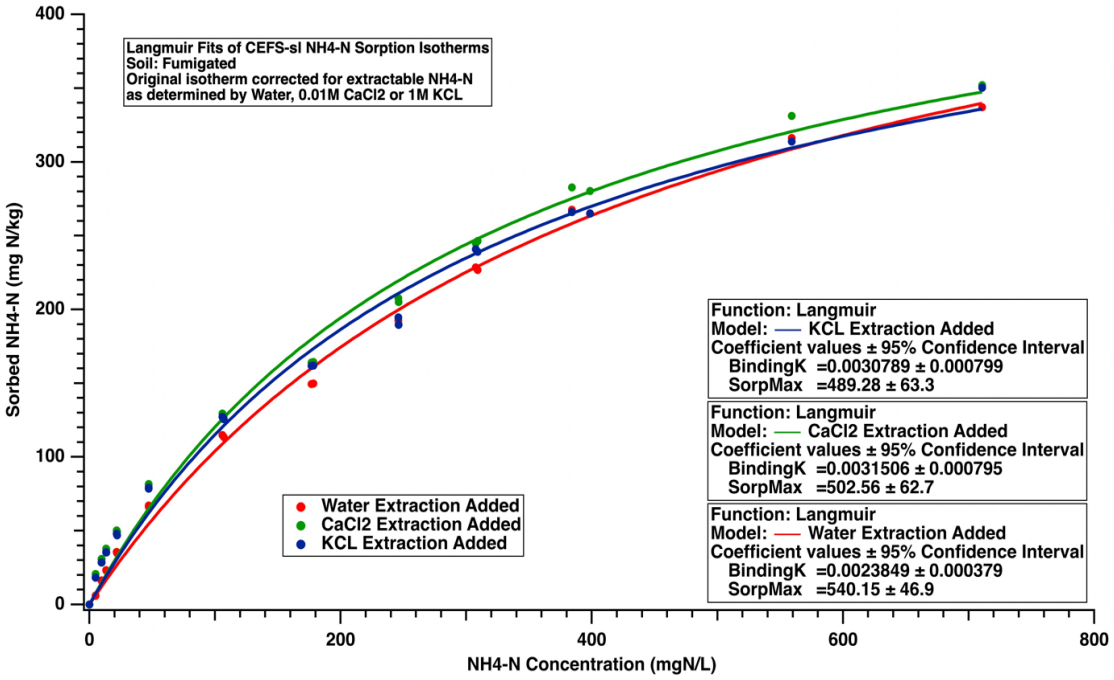

(b) CEFS-sl fumigated soil: Concentration <250 mg NH_4^+ L^{-1}

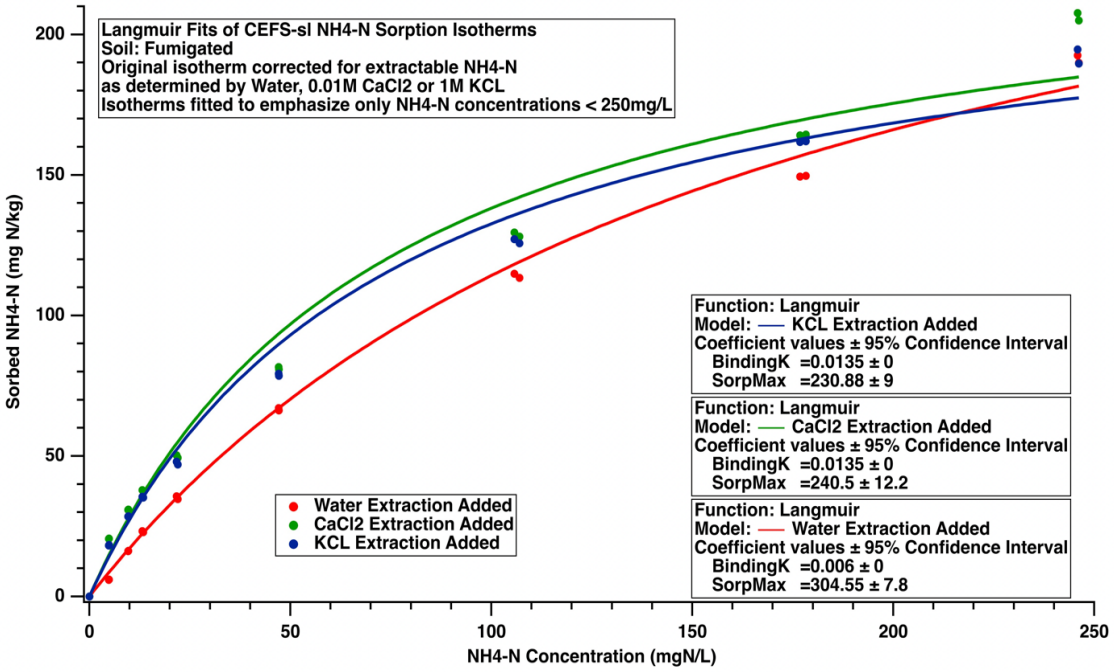

Figure 3.8. Langmuir Adsorption isotherms for fumigated CEFS-sl soil corrected for extractable NH_4^+ as determined by 2M KCl, 0.01M $CaCl_2$, and water. (a) adsorption isotherm for (0-1000 mg NH_4^+ L^{-1}), (b) adsorption isotherm for <250 mg NH_4^+ L^{-1}).

(a) DUKE-sl fumigated soil: Concentration (0-1000 mg NH_4^+ L^{-1})

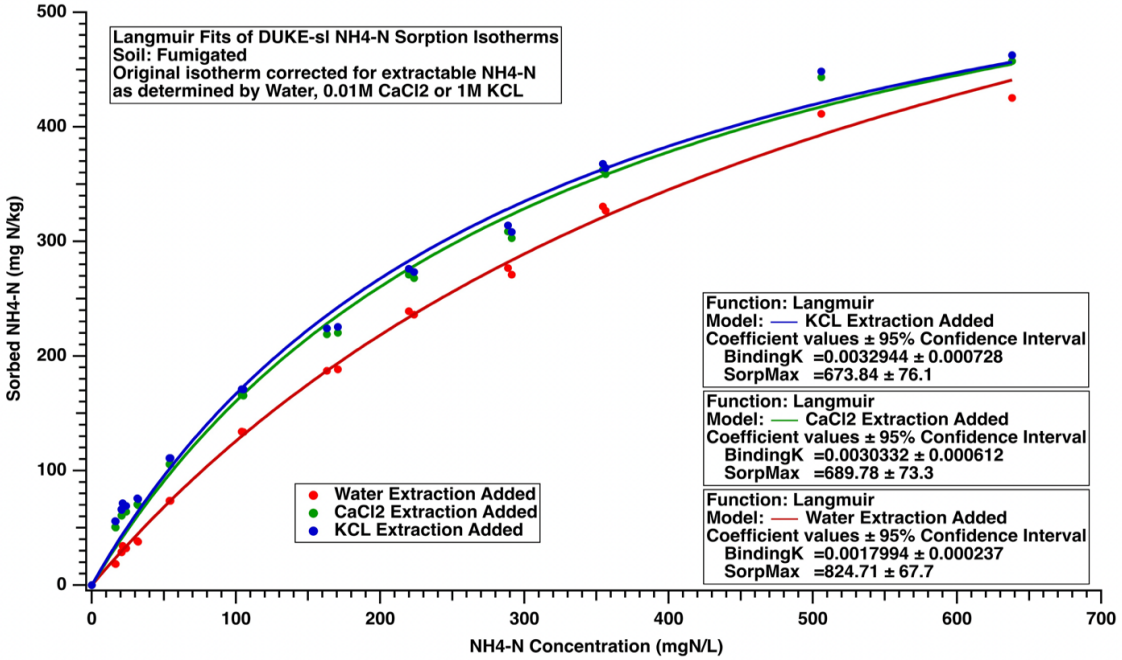

Figure 3.9. Langmuir isotherms for fumigated DUKE-sl soil corrected for extractable NH_4^+ as determined by 2M KCl, 0.01M $CaCl_2$, and water. adsorption isotherm for (0-1000 mg NH_4^+ L^{-1}).

(a) BASF-ls fumigated soil: Concentration (0-500 mg NH_4^+ L^{-1})

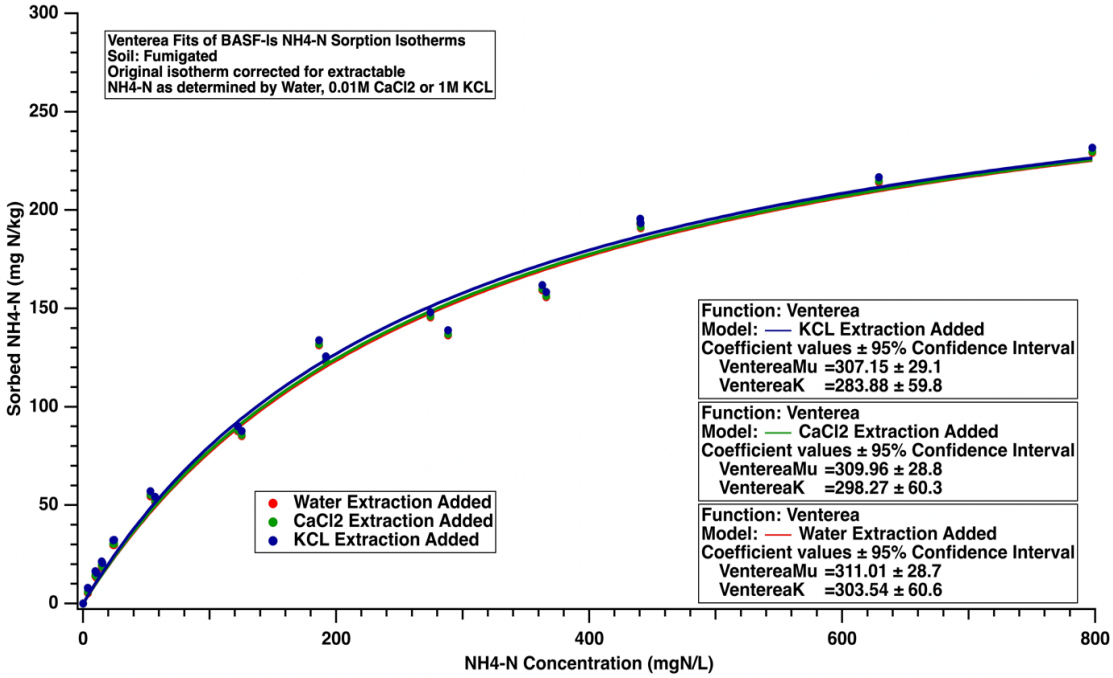

(b) BASF-ls fumigated soil: Concentration (<250 mg NH_4^+ L^{-1})

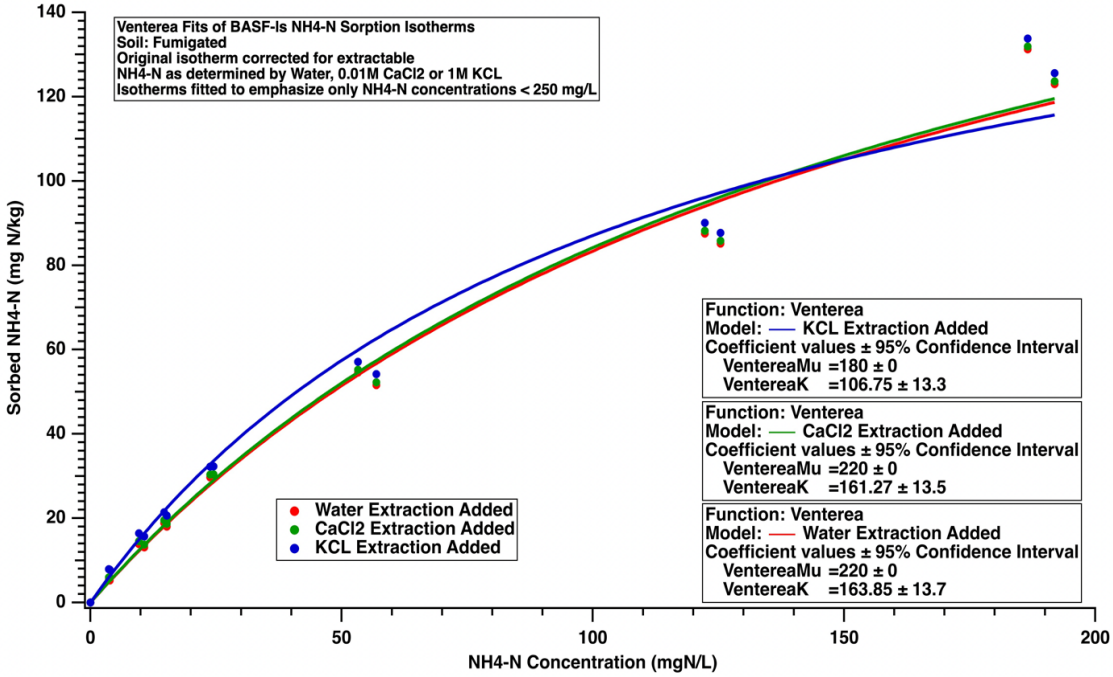

Figure 3.10. Venterea isotherms for fumigated BASF-ls soil corrected for extractable NH_4^+ as determined by 2M KCl, 0.01M $CaCl_2$, and water. (a) adsorption isotherm for (0-500 mg NH_4^+ L^{-1}), (b) adsorption isotherm for <250 mg NH_4^+ L^{-1}).

(a) CEFS-sl fumigated soil: concentration (0-1000 mg NH_4^+ L^{-1})

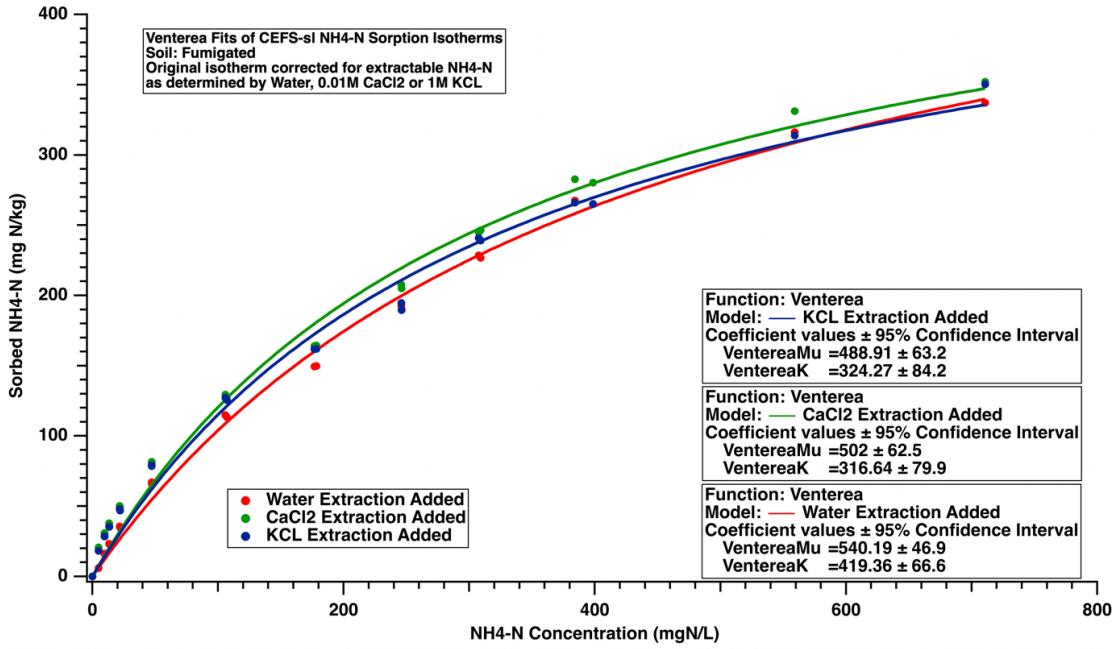

(b) CEFS-sl fumigated soil: concentration (<250 mg NH_4^+ L^{-1})

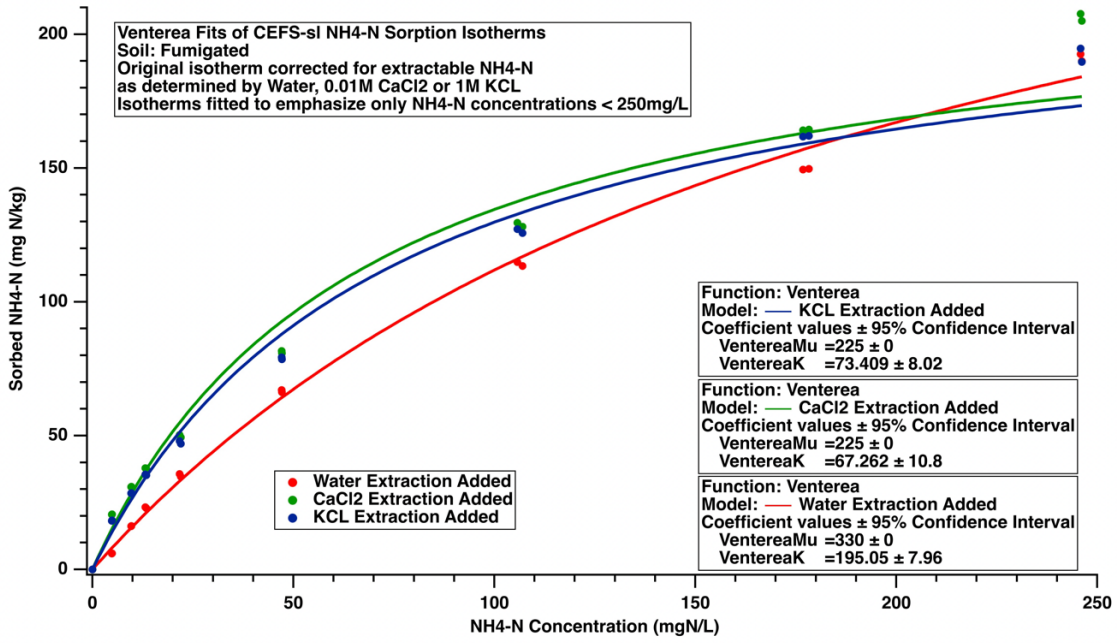

Figure 3.11. Venterea isotherms for fumigated CEFS-sl soil corrected for extractable NH_4^+ as determined by 2M KCl, 0.01M $CaCl_2$, and water. (a) adsorption isotherm for (0-1000 mg NH_4^+ L^{-1} (b) adsorption isotherm for <250 mg NH_4^+ L^{-1}).

DUKE-sl fumigated soil: concentration (0-1000 mg NH_4^+ L^{-1})

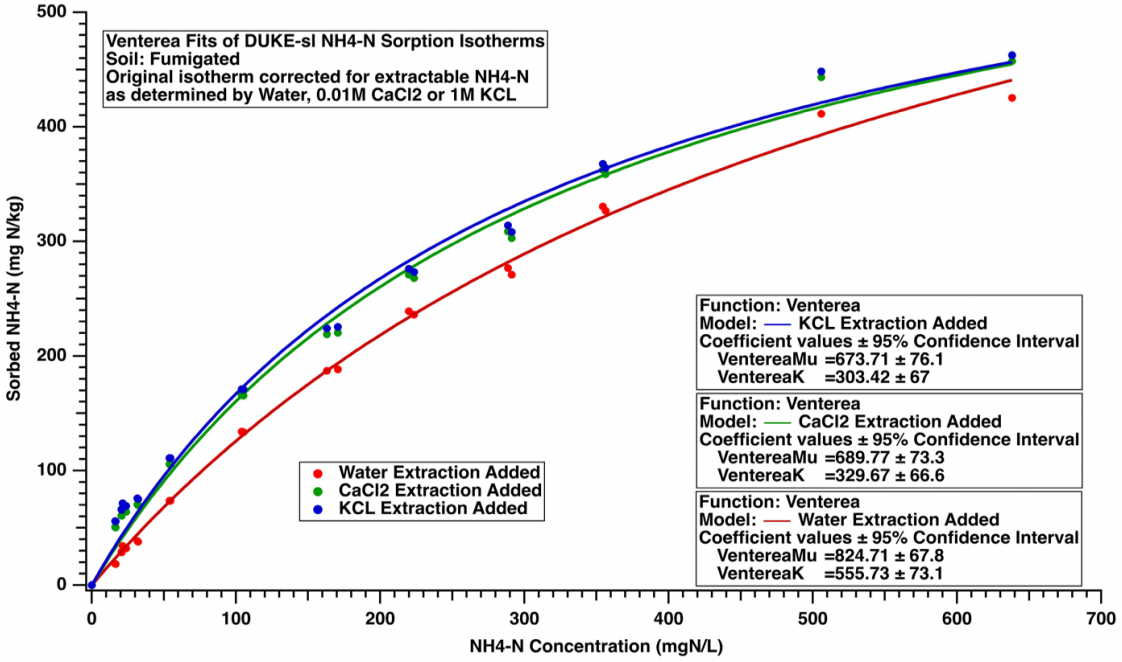

Figure 3.12. Venterea isotherms for fumigated DUKE-sl soil corrected for extractable NH_4^+ as determined by 2M KCl, 0.01M $CaCl_2$, and water. adsorption isotherm covers all the entire range of concentration (0-1000 mg NH_4^+ L^{-1}).

Table 3.4. Parameters of the Langmuir isotherm corrected for extractable NH_4^+ as determined by 2M KCl, 0.01M $CaCl_2$, and water obtained by nonlinear regression for the un-fumigated and fumigated BASF-ls soil.

Treatment	Q_{max} (mg Kg^{-1})	K_L (L mg^{-1})	†CEC (meq/100g)	†% Fraction of CEC
Un-Fumigated BASF-ls Soil				
…… NH_4^+ concentration (0-500 mg L^{-1}) ……				
KCl extraction added	138 ± 7	0.008 ± 1.0E-03	0.99	58
$CaCl_2$ extraction added	140 ± 7	0.008 ± 1.0E-03	1.00	59
Water extraction added	140 ± 7	0.008 ± 1.0E-03	1.00	59
…… NH_4^+ concentration < 250 mg L^{-1}……				
KCl extraction added	113 ± 2	0.013	0.81	47
$CaCl_2$ extraction added	118 ± 2	0.011	0.84	50
Water extraction added	123 ± 5	0.009 ±1.0E-03	0.88	52
Fumigated BASF-ls Soil				
…… NH_4^+ concentration (0-1000 mg L^{-1}) ……				
KCl extraction added	307 ± 29	0.009 ± 3.0E-04	2.19	128
$CaCl_2$ extraction added	310 ± 29	0.003 ± 7.0E-04	2.20	130
Water extraction added	311 ± 29	0.003 ± 7.0E-04	2.22	130
…… NH_4^+ concentration < 250 mg L^{-1}……				
KCl extraction added	192 ±11	0.085	1.37	80
$CaCl_2$ extraction added	200 ±11	0.075	1.43	84
Water extraction added	214 ± 10	0.0065	1.53	89

†The CEC determined from the Langmuir sorption isotherm (Q_{max}, mg Kg^{-1}), and the % fraction of CEC is the ratio of the sorption determined CEC versus independently measured CEC X100.

Table 3.5. Parameters of the Venterea's equation corrected for extractable NH_4^+ as determined by 2M KCl, 0.01M $CaCl_2$, and water obtained by nonlinear regression for the un-fumigated and fumigated BASF-ls soil.

Treatment	μ (mg Kg^{-1})	K (L mg^{-1})	†CEC (meq/100g)	†% Fraction of CEC
Un-Fumigated BASF-ls Soil				
…… NH_4^+ concentration (0-500 mg L^{-1}) ……				
KCl extraction added	138 ± 7	116 ± 17	0.99	58
$CaCl_2$ extraction added	140 ± 7	127 ± 16	1.00	59
Water extraction added	140 ± 7	129 ± 16	1.00	59
…… NH_4^+ concentration < 250 mg L^{-1}……				
KCl extraction added	110	73 ± 5	0.79	46
$CaCl_2$ extraction added	118	92 ± 3	0.84	50
Water extraction added	123 ± 5	103 ± 10	0.88	52
Fumigated BASF-ls Soil				
…… NH_4^+ concentration (0-1000 mg L^{-1}) ……				
KCl extraction added	307 ± 29	284 ± 60	2.19	128
$CaCl_2$ extraction added	310 ± 29	298 ± 60	2.20	130
Water extraction added	311 ± 29	304 ± 61	2.22	130
…… NH_4^+ concentration < 250 mg L^{-1}……				
KCl extraction added	189	107 ± 13	1.35	79
$CaCl_2$ extraction added	220	161 ± 14	1.57	92
Water extraction added	220	164 ± 14	1.57	92

†The CEC determined from the Langmuir sorption isotherm (Q_{max}, mg Kg^{-1}), and the % fraction of CEC is the ratio of the sorption determined CEC versus independently measured CEC X100.

Table 3.6. Parameters of the Langmuir isotherm corrected for extractable NH_4^+ as determined by 2M KCl, 0.01M $CaCl_2$, and water obtained by nonlinear regression for the un-fumigated and fumigated CEFS-sl soil.

Treatment	Q_{max} (mg Kg^{-1})	K_L (L mg^{-1})	†CEC (meq/100g)	†% Fraction of CEC
Un-Fumigated CEFS-sl Soil				
…… NH_4^+ concentration (0-500 mg L^{-1}) ……				
KCl extraction added	201± 15	0.009 ± 2.0E-03	1.43	13.9
$CaCl_2$ extraction added	202 ±15	0.009 ± 2.0E-03	1.44	14.0
Water extraction added	206 ± 15	0.008 ± 1.0E-03	1.47	14.3
…… NH_4^+ concentration < 250 mg L^{-1}……				
KCl extraction added	155 ± 5	0.016	1.11	10.8
$CaCl_2$ extraction added	162 ± 4	0.0135	1.16	11.3
Water extraction added	173 ± 4	0.0105	1.24	12.0
Fumigated CEFS-sl Soil				
…… NH_4^+ concentration (0-1000 mg L^{-1}) ……				
KCl extraction added	489 ± 63	0.003 ± 8.0E-04	3.49	33.9
$CaCl_2$ extraction added	503 ± 63	0.003 ± 8.0E-04	3.56	34.9
Water extraction added	540 ± 47	0.002 ± 4.0E-04	3.86	37.5
…… NH_4^+ concentration < 250 mg L^{-1}……				
KCl extraction added	231 ± 9	0.014	1.65	16.0
$CaCl_2$ extraction added	241 ± 12	0.014	1.72	16.7
Water extraction added	305 ± 8	0.006	2.18	21.1

†The CEC determined from the Langmuir sorption isotherm (Q_{max}, mg Kg^{-1}), and the % fraction of CEC is the ratio of the sorption determined CEC versus independently measured CEC X100.

Table 3.7. Parameters of the Venterea's equation corrected for extractable NH_4^+ as determined by 2M KCl, 0.01M $CaCl_2$, and water obtained by nonlinear regression for the un-fumigated and fumigated CEFS-sl soil.

Treatment	Q_{max} (mg Kg^{-1})	K_L (L mg^{-1})	†CEC (meq/100g)	†% Fraction of CEC
Un-Fumigated CEFS-sl Soil				
…… NH_4^+ concentration < 250 mg L^{-1}……				
KCl extraction added	1654	73 ± 4	1.11	10.8
$CaCl_2$ extraction added	170	83 ± 4	1.16	11.3
Water extraction added	178	101 ± 4	1.24	12.0
Fumigated CEFS-sl Soil				
…… NH_4^+ concentration (0-1000 mg L^{-1}) ……				
KCl extraction added	489 ± 63	324 ± 84	3.49	33.9
$CaCl_2$ extraction added	502 ± 63	317 ± 80	3.56	34.9
Water extraction added	540 ± 47	419 ± 67	3.86	37.5
…… NH_4^+ concentration < 250 mg L^{-1}……				
KCl extraction added	225	73 ± 8	1.65	16.0
$CaCl_2$ extraction added	225	67 ± 11	1.72	16.7
Water extraction added	330	195 ± 8	2.18	21.1

†The CEC determined from the Langmuir sorption isotherm (Q_{max}, mg Kg^{-1}), and the % fraction of CEC is the ratio of the sorption determined CEC versus independently measured CEC X100.

Table 3.8. Parameters of the Langmuir isotherm corrected for extractable NH_4^+ as determined by 2M KCl, 0.01M $CaCl_2$, and water obtained by nonlinear regression for the un-fumigated and fumigated DUKE-sl soil.

Treatment	Q_{max} (mg Kg^{-1})	K_L (L mg^{-1})	†CEC (meq/100g)	†% Fraction of CEC
Un-Fumigated DUKE-sl Soil				
…… NH_4^+ concentration (0-500 mg L^{-1}) ……				
KCl extraction added	426 ± 49	0.008 ± 2.0E-03	3.04	21.0
$CaCl_2$ extraction added	436 ± 50	0.007 ± 2.0E-03	3.12	21.5
Water extraction added	585 ± 60	0.003 ± 5.0E-04	4.18	28.9
……NH4-N concentration < 200 mg/L……				
KCl extraction added	302	0.015 ± 1.0E-03	2.16	14.9
$CaCl_2$ extraction added	302	0.014 ± 1.0E-03	2.16	14.9
Water extraction added	420	0.049 ± 2.0E-04	3.00	20.7
Fumigated DUKE-sl Soil				
…… NH_4^+ concentration (0-1000 mg L^{-1}) ……				
KCl extraction added	674 ± 76	0.003 ± 7.0E-04	4.81	33.2
$CaCl_2$ extraction added	690 ± 73	0.003 ± 6.0E-04	4.93	34.0
Water extraction added	825 ± 68	0.002 ± 2.0E-04	5.90	40.6

†The CEC determined from the Langmuir sorption isotherm (Q_{max}, mg Kg^{-1}), and the % fraction of CEC is the ratio of the sorption determined CEC versus independently measured CEC X100.

Table 3.9. Parameters of the Venterea's corrected for extractable NH_4^+ as determined by 2M KCl, 0.01M $CaCl_2$, and water obtained by nonlinear regression for the un-fumigated and fumigated DUKE-sl soil.

Treatment	μ (mg Kg^{-1})	K (mg L^{-1})	†CEC (meq/100g)	†% Fraction of CEC
Un-Fumigated DUKE-sl Soil				
……NH_4^+ concentration (0-500 mg L^{-1}) …….				
KCl extraction added	426 ± 49	124 ± 33	3.04	21.0
$CaCl_2$ extraction added	436 ± 50	139 ± 35	3.12	21.5
Water extraction added	585 ± 60	327 ± 55	4.18	28.9
Fumigated DUKE-sl Soil				
…… NH_4^+ concentration (0-1000 mg L^{-1}) ……				
KCl extraction added	674 ± 76	303 ± 67	4.81	33.2
$CaCl_2$ extraction added	690 ± 73	330 ± 67	4.93	34.0
Water extraction added	825 ± 68	556 ± 73	5.90	40.6

†The CEC determined from the Langmuir sorption isotherm (Q_{max}, mg Kg^{-1}), and the % fraction of CEC is the ratio of the sorption determined CEC versus independently measured CEC X100.

3.2. Soil Compensation Point Calculations

3.2.1. Comparison of Compensation Point Derived from Soil Extractions and Adsorption Isotherms

The soil compensation point (the concentration of NH_3 gas in soil pore air) (Dawson, 1977; Langford et al., 1992) was calculated from the NH_4^+ concentration and pH of soil extracts and from adsorption isotherms in relationship to the amount of NH_4^+ in solution. The amount of NH_4^+ found with each batch extraction solution (2M KCL, 0.05M $CaCl_2$, water) was paired with its respective adsorption isotherm. The amount of NH_4^+ found was marked on the y-axis and the corresponding NH_4^+ concentration in solution as predicted by the respective isotherm was read from the x-axis. Using the adsorption isotherm to estimate soil solution NH_4^+ concentration is a more empirical but perhaps physically more realistic method of compensation point determination. Compared to bulk extractions using KCl and $CaCl_2$, this method provides an estimate of the amount of NH_4^+ in the soil solution, which reflects the portion of the total amount

of NH_4^+ in the soil that is available for loss to the atmosphere as NH_3. The NH_4^+ sorption isotherms described by Venterea et al. (2015) allowed them to calculate the fraction of sorbed NH_4^+ and the fraction of NH_4^+ in solution ($NH_4^+{}_{(aq)}$). In their framework, $[NH_4^+]/[H^+]$ is equivalent to the soil emission potential (Γ_g) value in the compensation point model (Eq. 3.9).

Based on the parameters of the Langmuir isotherm (Q_{max}, K_L) and Venterea Isotherm (μ, K) parameters (Table 3.4-3.8), and the extractable NH_4^+ data presented in Tables 3.2 and 3.3, the concentrations of NH_4^+ in the solution for entire range and low end isotherms for fumigated and unfumigated soils (Tables 3.10 and 3.11) were calculated from the non-linear Langmuir and Venterea equations. The concentration of NH_4^+ from the low end isotherms was lower than the concentration obtained from the entire range of isotherm for both un-fumigated and fumigated soils. The concentration of NH_4^+ in fumigated soil solution was found to also be lower than in unfumigated soil.

Table 3.10. Predicted concentrations of NH_4^+ using Langmuir adsorption isotherm parameters from the entire range of isotherms and at the low end of the isotherms for the un-fumigated and fumigated soils.

Treatment	Un-Fumigated Soil		Fumigated Soil	
	……mgNH_4^+ L^{-1}……			
	All range of isotherms	Low end of the isotherms	All range of isotherms	Low end of the isotherms
BASF-ls Soil				
KCl extraction added	2.18	1.77	1.81	0.34
$CaCl_2$ extraction added	0.96	0.82	3.36	0.23
Water extraction added	0.61	0.54	2.74	2.02
CEFS-sl Soil				
KCl extraction added	4.24	3.26	10.31	5.17
$CaCl_2$ extraction added	3.47	2.85	11.23	5.70
Water extraction added	1.57	1.37	3.29	2.33
DUKE-sl Soil				
KCl extraction added	11.43	8.96	17.72	
$CaCl_2$ extraction added	10.66	8.28	15.99	
Water extraction added	5.54	0.48	12.01	

Table 3.11. Predicted concentrations of NH_4^+ using Venterea's equation from the entire range of isotherms and at the low end of the isotherms for the un-fumigated and fumigated soils.

Soil/Treatment	Un-Fumigated Soil		Fumigated Soil	
	All range of isotherms	Low end of the isotherms	All range of isotherms	Low end of the isotherms
BASF-ls Soil	……..……..……. mgNH_4^+ L^{-1}……..……..			
KCl extraction added	2.17	1.72	4.84	3.04
$CaCl_2$ extraction added	0.96	0.83	3.22	2.49
Water extraction added	0.60	0.54	2.62	2.03
CEFS-sl Soil				
KCl extraction added		3.57	9.44	5.02
$CaCl_2$ extraction added		3.02	10.32	5.32
Water extraction added		1.41	2.98	2.33
DUKE-sl Soil				
KCl extraction added	10.64		15.86	
$CaCl_2$ extraction added	9.88		14.25	
Water extraction added	4.93		10.32	

Soil Γ_g was then calculated from measurements of extractable NH_4^+ and H^+ (Table 3.1, 3.2 and 3.3) Eq. (3.9), and from NH_4^+ concentrations in solution calculated from the Langmuir adsorption isotherm and Venterea equations (Table 3.10 and 3.11).

For the same soil conditions, the results from soil bulk extractions used to estimate the compensation point have higher X_g values compared to the X_g predicted by the adsorption isotherms (Table 3.12 and 3.13). We hypothesized that the standard KCl extraction is not the most appropriate method for deriving Γ_g, because the KCl extractant yields more NH_4^+ than is naturally available in the pore water, possibly overestimating what is available for loss to the atmosphere as NH_3. To explore this hypothesis further, extractions with $CaCl_2$ and deionized water were compared to KCl and the sorption curve predictions. The concentration of NH_4^+ and NO_3^-obtained by KCl extraction were greater than those obtained by $CaCl_2$ salt and water solution in all three soils. For example, the concentration of NH_4^+ in unfumigated BASF-ls soil was lower by approximately 3-fold and 4-fold when extracted with 0.01 $CaCl_2$ and water, respectively, and by 1.3-fold and 3-fold with $CaCl_2$ and water extractant for CEFS-sl soil, respectively. However, $CaCl_2$ and water extractions still yielded estimates of NH_4^+ soil solution concentrations and corresponding X_g that are much higher than predicted by the sorption curves.

Table 3.12. Predicted soil compensation point using soil bulk extraction method, Langmuir adsorption isotherm, and Venterea's approach for un-fumigated soils as a function of different chemical extractants of 2M KCl, 0.01 M $CaCl_2$, and water. The entire range and the low end of the isotherms are used to calculate NH_4^+ concentration**.**

Extractant	Soil bulk extraction method	Langmuir isotherm		Venterea's equation	
		All range of isotherms	Low end of the isotherms	All range of isotherms	Low end of the isotherms
	……. μg NH_3 m^{-3}…….				
	BASF-ls un-Fumigated Soil				
2M KCl	636	2.24	1.82	2.24	1.77
0.01 M $CaCl_2$	263	0.99	0.84	0.99	0.85
Water	163	0.62	0.56	0.62	0.56
	CEFS-sl un-Fumigated Soil				
2M KCl	43	0.30	0.23		0.25
0.01 M $CaCl_2$	34	0.25	0.20		0.21
Water	14	0.11	0.10		0.10
	DUKE-sl un-Fumigated Soil				
2M KCl	27	1.87	1.46	1.74	
0.01 M $CaCl_2$	24	1.74	1.35	1.61	
Water	7	0.90	0.08	0.80	

Table 3.13. Predicted soil compensation point using soil bulk extraction method, Langmuir adsorption isotherm, and Venterea's approach for fumigated soils as a function of different chemical extractants of 2M KCl, 0.01 M $CaCl_2$, and water. The entire range and the low end of the isotherms are used to calculate NH_4^+ concentration.

Extractant	Soil bulk extraction method	Langmuir isotherm		Venterea's equation	
		All range of isotherms	Low end of the isotherms	All range of isotherms	Low end of the isotherms
	……. μg NH_3 m^{-3}…….				
	BASF-ls Fumigated Soil				
2M KCl	127	1.87	0.35	4.98	3.13
0.01 M $CaCl_2$	82	3.46	0.24	3.32	2.56
Water	66	2.82	2.08	2.70	2.09
	CEFS-sl Fumigated Soil				
2M KCl	8	0.73	0.37	0.67	0.36
0.01 M $CaCl_2$	9	0.80	0.41	0.74	0.38
Water	2	0.23	0.17	0.21	0.17
	DUKE-sl Fumigated Soil				
2M KCl	26	2.89		2.59	
0.01 M $CaCl_2$	22	2.61		2.33	
Water	12	1.96		1.68	

To better understand whether compensation points derived from the sorption curves are more realistic, a quantitative analysis is required to prove that the sorption curve estimates a small fraction of the total extractable NH_4^+ in solution and therefore a lower compensation point. The NH_4^+ sorption isotherms described by Venterea et al. (2015) allowed calculation of the fraction of sorbed NH_4^+ and the fraction of NH_4^+ in solution ($NH_4^+{}_{(aq)}$), which can be used to correct total extractable NH_4^+ values for compensation point modeling. An example calculation is presented in Table 3.14 where the fraction of NH_4^+ in solution for BASF-ls soil was calculated using the Venterea approach (2.17 mg L^{-1}). The fraction of sorbed NH_4^+ was calculated from the fraction of NH_4^+ in solution accounting for moisture content (0.005 mg Kg^{-1} (2.17 mg L^{-1}*0.002 LH_2O Kg^{-1})). Then the correction factor was calculated as the fraction of sorbed NH_4^+ (0.005 mg Kg^{-1}) to the 2M KCl total extractable NH_4^+ (2.54 mg Kg^{-1}) to give 0.18%.

Table 3.14. Percentage of total NH_4^+ in solution calculated using Venterea's approach for unfumigated soils as a function of different chemical extractants of 2M KCl, 0.01 M $CaCl_2$, and water.

un-Fumigated	Extractant	Soil bulk extraction $mgNH_4^+ kg^{-1}$ soil	Water content $L_{H2O} kg^{-1}$ soil	$mgNH_4^+L^{-1}$ calc from Venterea	Amount of NH_4^+ in solution $mgNH_4^+ kg^{-1}$ soil	% of total NH_4^+ in solution
BASF-ls un-Fumigated Soil						
Full isotherm	2M KCl	2.54	0.002	2.17	0.005	0.18
	0.01 M $CaCl_2$	1.05	0.002	0.96	0.002	0.19
	Water	0.65	0.002	0.60	0.001	0.20
BASF-ls un-Fumigated Soil						
LE of isotherm	2M KCl	2.54	0.002	1.72	0.004	0.14
	0.01 M $CaCl_2$	1.05	0.002	0.83	0.002	0.17
	Water	0.65	0.002	0.54	0.001	0.18
CEFS-sl un-Fumigated Soil						
LE of isotherm	2M KCl	7.71	0.013	3.57	0.045	0.59
	0.01 M $CaCl_2$	6.01	0.013	3.02	0.038	0.64
	Water	2.46	0.013	1.41	0.018	0.73
DUKE-sl un-Fumigated Soil						
Full isotherm	2M KCl	35.8	0.214	10.64	2.274	6.35
	0.01 M $CaCl_2$	31.1	0.214	9.88	2.112	6.79
	Water	9.74	0.214	4.93	1.054	10.82

3.2.2. Relationships Between Patterns of NH_3 Loss and Emission Potentials Estimated from Soil NH_4^+ Extractions and Adsorption Curves

The amount of NH_3 emitted from soil for given soil conditions/characteristics (NH_4^+ concentration, pH, and moisture content) measured using a dynamic flow-through chamber technique was used to evaluate compensation points derived from soil bulk extractions and adsorption curves and to assess whether the compensation points derived from the sorption curve approach are indeed more realistic than those derived from bulk extractions. The soil compensation point is assumed to be in equilibrium with NH_4^+ in the soil solution, governed by temperature and pH. The extractable NH_4^+ for BASF-ls soil was 2.54 $\mu gNH_4^+ g^{-1}$ fresh soil with a soil water content was of 0.004 L H_2O g^{-1} soil. Both values were assumed to represent a depth of 0.5 cm. The $[NH_4^+]$ = 2.69 $x10^{-7}$ M supposed to be present in the soil solution. Together with the soil pH of 6.6 and temperature of 22°C, this equates to X_g = 636 μNH_3 m^{-3}. However, using the adsorption corresponding isotherms, a much smaller value of X_g = 2.24 or 1.82 μNH_3 m^{-3} when calculated from full range and lower end of Langmuir adsorption isotherm, respectively. Table 3.12 and 3.13 present the calculated soil compensation point for unfumigated and fumigated soil using the soil bulk extraction method and the sorption curve at the entire range and the low end of the Langmuir isotherm and Venterea's approach as a function of different chemical extractants of 2M KCl, 0.01 M $CaCl_2$, and water.

Our results agree with other studies. Neftel et al. (1998) used a buried semi-permeable membrane to test reliably small (< 0.1 μg m^{-3}) NH_3 gas-phase concentrations in the soil of a triticale field, which suggested the soil must be a sink of NH_3. Despite large NH_4^+ measurements in soil KCl extracts, which, with soil pH of 6.5, would have produced a concentration of NH_3 pore space of two orders greater than that found in soil and the atmosphere. They inferred from this difference that the measured NH_4^+ in the soil content was not in the soil solution but

adsorbed into soil particles and therefore not accessible for exchange of gases with the atmosphere. Moreover, Nemitz et al. (2000a) also reported significantly lower concentrations of NH_3 within the soil at a depth of 10 cm than just above the litter of oilseed rape.

The chamber NH_3 mass loss was used to quantify a reduction factor that can be applied to bulk soil extractions of NH_4^+ /sorption curve for the purpose of estimating the soil compensation point. We first compare the fraction of extractable NH_4^+ lost as NH_3 for different extraction solutions and for different amounts of NH_4^+ in the soil. For example, 2M KCl extracts the entire NH_4^+ pool, giving us a total mass of NH_4^+ per mass of soil, then we express the mass of NH_3 as a fraction of the 2M KCl extractable NH_4^+ in the soil at time equal zero, this represents a correction factor that could be applied to the 2M KCl extracted NH_4^+ for calculating soil Γ_g. The results of NH_3 loss (μgNH_3) and 2M KCl, 0.01M $CaCl_2$, and water extractable NH_4^+ were used to calculate the ratio of the mass of N lost from the soil as gaseous NH_3 to the mass of NH_4^+ extracted from the soil with different extractants is shown in Table 3.16. Hence, the correction factor is defined as the ratio of the mass of N lost from the soil as gaseous NH_3 to the mass of NH_4^+ extracted from the soil. This number represents the assumed fraction of total NH_4^+ in the soil that is available for loss to the atmosphere under the test conditions. Table 3.16 shows a correction factor derived from Langmuir adsorption isotherms and Venterea's equations over the full range and low end of the isotherms, where the maximum sorption capacity (Q_{max}) presented in Tables (3.4-3.9) was used to calculate the ratio of NH_3 gas loss to the Q_{max}. The soil bulk extraction yields a correction factor an order of magnitude larger than derived from sorption curve (Tables 3.15 and 3.16). The two correction factors are different because Q_{max} is much larger than the extractable NH_4^+ concentrations. Expressed as a percentage, the ratio of NH_3 emission to extractable NH_4^+ is larger but in fact the magnitude of the "correction" would be

smaller than the Q_{max} derived correction. The difference between Q_{max} and NH_3 emission is much larger (expressed as a smaller percentage) and thus the correction would need to be larger. In general, the adsorption isotherm approach appears to be a more viable way to correct the extractable NH_4^+ for determining a more realistic compensation point.

Table 3.15. Estimation of % correction factor (%CF) for un-fumigated soils calculated with different chemical extractants of 2M KCl, 0.01M $CaCl_2$, and Type 1 deionized water. Assumed depth of soil over the calculating NH_3 loss is 0.5 cm.

Extractant	Total mass of NH_3 emitted ($\mu gNH_3\ g^{-1}$ soil)	Extractable NH_4^+ ($\mu g\ NH_4^+\ g^{-1}$ soil)	% CF (%Ratio NH_3-N gas loss/ NH_4^+ extractable)
BASF-ls Soil			
2M KCl	0.34	2.54	13
0.01 M $CaCl_2$		1.05	32
Deionized Water		0.65	52
CEFS-sl Soil			
2M KCl	0.25	7.71	3
0.01 M $CaCl_2$		6.01	4
Deionized Water		2.46	10
DUKE-sl Soil			
2M KCl	0.83	35.8	2
0.01 M $CaCl_2$		31.1	3
Deionized Water		9.74	8

Table 3.16. Estimation of the % correction factor (%CF) for un-fumigated soils using the maximum sorption capacity derived from the Langmuir adsorption isotherms and Venterea's equations over the full range and low end of isotherm as a function of different chemical extractants of 2M KCl, 0.01 M $CaCl_2$, and water. Assumed depth of soil over the calculating NH_3 loss is 0.5 cm.

Extractant	%CF Calculated using Langmuir isotherm		%CF Calculated using Venterea isotherm	
	All range of isotherms	Low end of the isotherms	All range of isotherms	Low end of the isotherms
BASF-ls Soil				
2M KCl	0.25	0.30	0.25	0.31
0.01 M $CaCl_2$	0.24	0.29	0.24	0.29
Water	0.24	0.28	0.24	0.28
CEFS-sl Soil				
2M KCl	0.14	0.18		0.17
0.01 M $CaCl_2$	0.14	0.17		0.16
Water	0.13	0.16		0.16
DUKE-sl Soil				
2M KCl	0.20	0.28	0.68	
0.01 M $CaCl_2$	0.19	0.28	0.61	
Water	0.14	0.20	0.26	

From the extended wetting/drying experiment in Chapter Two (Fig. 2.17) we found that the amount of NH_3 lost does not represent the entire pool of NH_3 in the soil because the emission never went to zero. This is an upper limit on the correction factor. If we performed our calculations assuming that the NH_3 loss we are measuring is actually representative of a smaller mass of soil, we could express this as an equivalent depth of soil within the column. For example, if we assume that the total NH_3 loss we are measuring from BASF-ls originates from only the top 0.5 cm of soil, then the cumulative loss from the soil represents about 13% or 0.3% of the available NH_4^+ in the corresponding mass of soil when calculated using soil bulk extraction and the low end of Langmuir sorption isotherm, respectively. This assumes that the

extractable NH_4^+ number represents a well-mixed column and there is no vertical gradient in extractable NH_4-N (Table 3.16). These numbers seem low and would correspond to very low compensation points.

In addition to the difference in magnitude of the compensation points determined from the bulk extraction versus adsorption isotherm approaches, the two approaches imply different relationships between soil moisture and Γ_g that have implications for the bidirectional flux model. Basically, it is suggested that all NH_4^+ will be in solution when extracted with salt solution. As the soil dries, the volume of the solution becomes smaller, and the concentration in solution must increase. As the soil becomes progressively drier, the compensation point continues to increase infinitely, which is unrealistic.

3.2.3. Impact of Soil Drying and Remobilization of NH_4^+ on Potential NH_3 Emission and Critical Compensation Point

From characterization of the dynamic chamber in Chapter Two, we see that NH_4^+ levels in soil are not static, even over short time periods, and that emissions of NH_3 are driven by drying process in non-amended soil that can extend several days after a rain event. These actions are different but may also amplify reactions association with mineralization of soil organic matter after rain events and release of NH_4^+. The impact of water movement on solute transport within the columns during evaporation was evaluated using non-amended un-fumigated soil (BASF-ls) columns where the soil was placed in the column in 2-cm increments and water (20 mL) was added to each depth increment. Using this approach, the finished columns (N = 3) were set at ~ 80% FC and then allowed to dry down over 120 hours at a air flow rate of 5 LPM. The nitrogen mass balance for the columns used in this experiment is summarized in Table 3.17. At time zero, the mean $NH_4^+ + NO_3^-$ mass in the columns was 3546 µg N. At time-120 hours, the

mean mass of NH_4^+ + NO_3^- had increased to 6632 µg N, or nearly doubled due to mineralization of N. Expressed as a percentage, the net increase in the mass of N in the columns (~ 3086 µg N) was 65.6% for NO_3-N and 34.4% for NH_4-N. Within the soil columns, ~ 6% of N present had shifted from both the lower two depth increments to the surface 0 – 2cm layer (Table 3.16). The source of the new nitrogen in the columns was the result of mineralization of N and then subsequent nitrification to form NO_3^-. As suggested in Fig. 2.9 (Chapter Two), the bulk of mineralization of N may have been completed within the first 24 hours of the experiment. If it is assumed that mineralization was uniform throughout the entire depth of the columns, then ~ 1029 µg N was generated in each depth interval. By time =120 hours, a portion of this new N accounts for the observed increase in NH_4^+, in each depth interval. The remainder was converted to NO_3^-, a portion of which then was redistributed within the columns as they continued to dry down. Continuation of this scenario results in a net gain of ~ 800 µg N in the surface 0 – 2 cm depth increment. This increase came equally from the lower portions of the packed columns. It is likely that this net gain in N involved some movement of NH_4^+, but probably a substantial percentage was in the form of NO_3^-.

The fraction of NH_4^+ available for movement through the soil during drying is the fraction that is actually in solution. If only a small fraction is in solution (0.005 mgNH_4^+ kg^{-1} soil), then it makes sense that only 6% of the increase in NH_4^+ in the 0-2 cm layer during the mass balance experiment could be attributed to vertical movement as shown in BASF-ls soil (Table 3.17).

Table 3.17. Mean Extractable (2M KCL) $NH_4^+$and $NO_3^-$from individual unfumigated non-amended soil (BASF-ls) packed columns (N=3) subjected to one drying cycle ~120 hours in length. Initial water content set at ~ 80% FC. This Table was taken from Chapter Two, Table 2.8.

Depth Increment	NH_4^+	NO_3^-	Sum	Percent Distribution
- cm -	- µg -N -	- µg -N -	- µg -N -	- % -
Time = 0 hours				
0 – 2	446	736	1182	33.3
2 – 4	446	736	1182	33.3
4 – 6	446	736	1182	33.3
Totals=	**1338**	**2208**	**3546**	**100.0**
Time = 120 hours				
0 – 2	1073	1949	3022	45.5
2 – 4	680	1054	1734	26.2
4 – 6	645	1231	1876	28.3
Totals=	**2398**	**4234**	**6632**	**100.0**

The calculated average NH_3 concentrations for the emitted NH_3 during the experiment as a function of time are shown in Fig. 3.13 along with the mean cumulative percent water loss. There was an apparent increase in the integrated average NH_3 concentration up to ~ time = 30 hours, or when ~ 55% of the water present had been lost due to evaporation. During this period the rate in water loss was ~ linear, suggesting a direct impact of water loss on the release of NH_3. At the 40 hour mark, the integrated average NH_3 concentrations decreased and became essentially constant while loss of water continued but slowed (Fig. 3.13).

The cumulative loss of NH_3 for each of the three columns is plotted in Fig. 3.14. As suggested by the preliminary data in Fig. 2.17 (Chapter Two), the loss of NH_3 as the columns dried appeared to segregate into two distinct periods. The first lasted up to approximately the ~ 47 hour mark and appeared to be consistent between the three columns. This corresponds to a cumulative water loss of ~ 60% (Fig. 3.13). Beyond this point, the apparent rate of loss slows and the individual variations between the columns becomes more distinct. In this experiment, the

apparent rate of loss of NH_3 was roughly 0.25 µg N hr^{-1} up to time=47 hours. Beyond 47 hours, the rate of loss varied with a particular column ranging from roughly 0.07 – 0.2 µg N hr^{-1}.

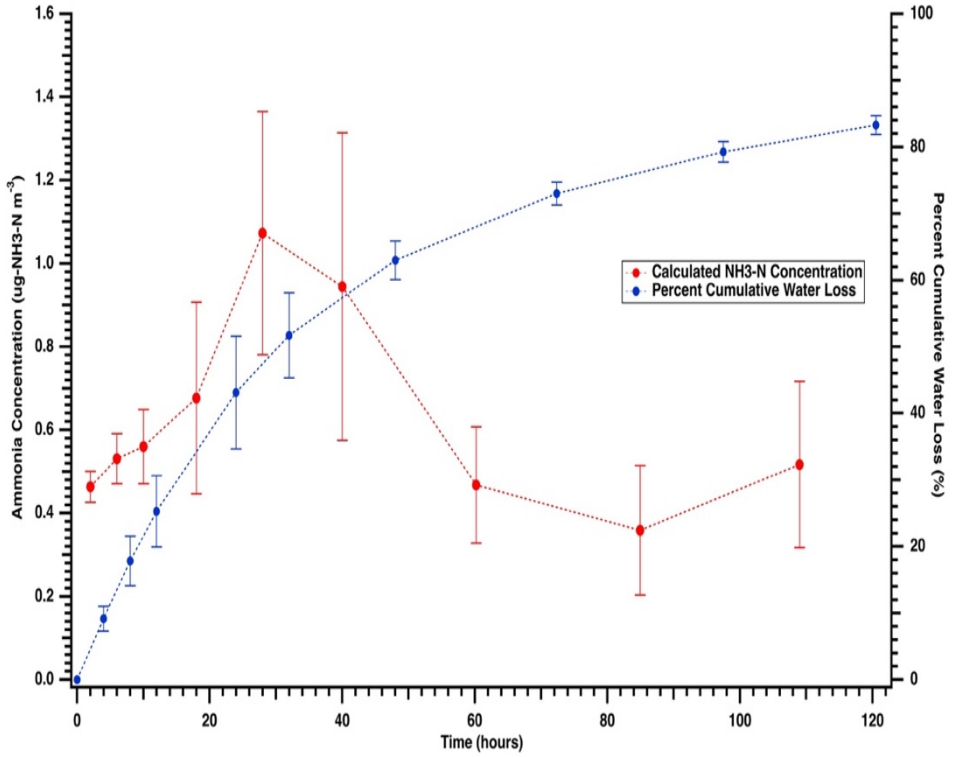

Figure 3.13. Calculated average NH_3 concentration (N=3) per each measurement period and cumulative percent water loss as a function of time. Error bars represent standard deviation. Average NH_3 concentrations are plotted at mid-point of each measurement period. Cumulative water loss is plotted at the end of each measurement period. The dashed lines are added to help visualize overall trends in the data. This figure was taken from Chapter Two, Fig. 2.20.

It appeared NH_3 loss was more a function of water loss in the first ~ 50 hours of the experiment. This further analysis of the dataset indicates that at up to ~ 40% cumulative water loss, NH_3 loss from each column basically fell along the same linear line. This suggests variations introduced through packing of the individual columns were minimal during this period and ability to emit was NH_3 was directly dependent on the conditions driving the rate of water loss within the chambers. To some degree this corresponds to Stage 1 drying of the soil as described by Hillel (2004). It is also apparent that the actual total cumulative loss of NH_3 during this period accounts for a smaller % of total loss than suggested by Fig. 3.14. Less than 5 µg N

was lost before reaching ~ 40% of the cumulative water loss from the columns, or from Fig. 3.13, within the first ~ 24 hours of the experiment.

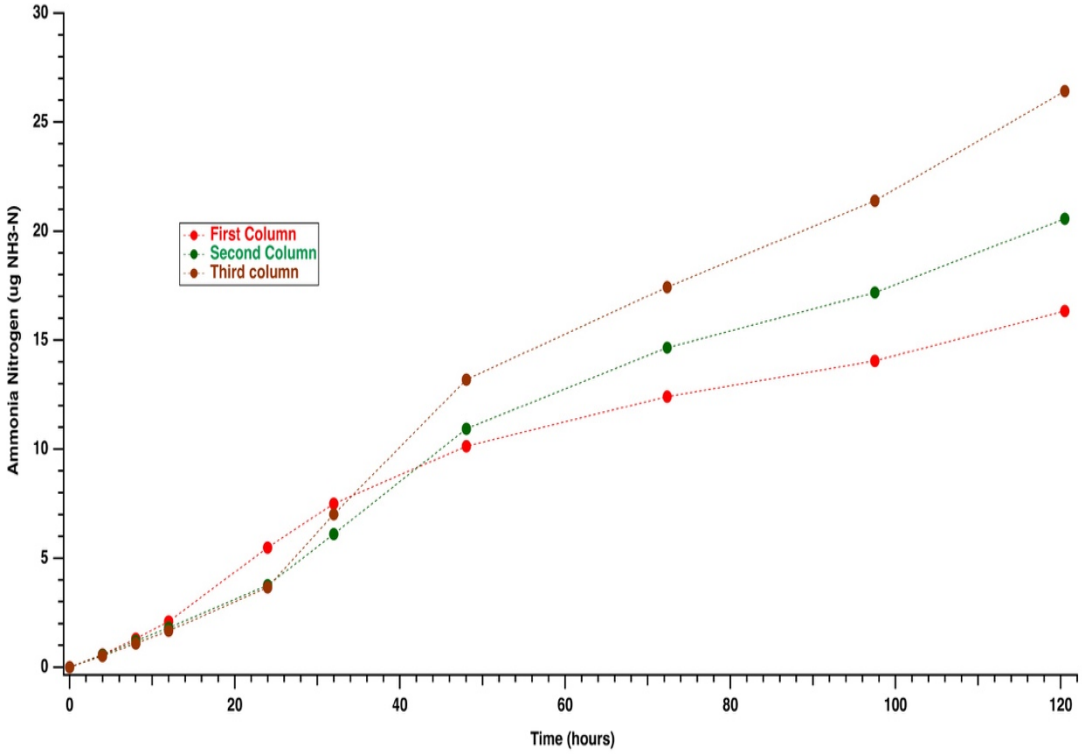

Figure 3.14. Cumulative NH_3 loss from individual soil (BASF-ls) columns as a function of time. The dashed lines are added to help visualize overall trends in the data. This Figure was taken from Chapter Two, Fig. 2.21.

The chamber experiments help to understand the relationships between soil NH_4^+ concentration, water loss, and actual emissions and to understand if the compensation point derived from the adsorption curve approach are indeed more realistic than those derived from bulk extractions. Measured NH_3 loss from the soil, which is an index of emission processes, can be combined with information on drying induced movement of NH_4^+ through the soil profile to elucidate soil NH_3 dynamics. At time zero, NH_4^+ content for non-amended BASF-ls soil was 446 µg, increasing to 1073 µg in the 0-2 cm surface layer at 120 hours.

The extractable NH_4^+ at 120 hours of incubation was 4.96, 3.14, and 2.98 µg/g at depths 0-2, 2-4, and 4-6 cm, respectively. The estimated concentration of NH_4^+ soil solution calculated using Langmuir adsorption isotherm and Venterea's equation at full range was 4.32 mg/L and at the low end isotherms was 3.53 and 3.43 mg L^{-1}, respectively (Table 3.18).

Our results show that changes in NH_4^+ internally within the soil are having an impact on actual and potential NH_3 emissions, most likely through changes in NH_4^+ concentration. Most of the change in NH_4^+ at the surface was due to mineralization, so the pool was changing and there was more NH_4^+ in solution at the surface. Only about 6% of increase in 0-2% layer was associated with vertical movement. The increase NH_4^+ concentration at the surface soil results in an increase in the soil emission potential and soil compensation point assuming the pH and temperature are constant during the time period of the study. Table 3.18 presents results of the soil compensation point that was computed based on the change in extractable NH_4^+ as a function of soil depth using Langmuir adsorption isotherm, Venterea's equations, and soil bulk extraction method. Again, compensation points derived from bulk extractions appear unrealistically high compared to the low NH_3 emission measured from non-amended soil presented in Fig. 3.13. The compensation points derived from the adsorption curve at the low end of the Langmuir and Venterea's isotherms are indeed more realistic than those derived from bulk extractions assuming NH_3 emission occurs in the top 2 cm of soil, and only NH_4^+ in soil the solution is available for emission.

Table 3.18. Predicted NH_4^+ concentration in solution, soil emission potential (Γ_g), and critical compensation point (X_g) using Langmuir adsorption isotherm, Venterea's equations, and soil bulk extraction method for non-amended BASF-ls soil as a function of soil depths at 120 hours of incubation.

Depth Increment	2M KCl Extraction	Langmuir Isotherm			Venterea Isotherm			Soil Bulk Extraction Method	
		Full Range of Isotherm							
-cm-	$\mu NH4^+g^{-1}$	$[NH_4^+]$ mg L^{-1}	Γ_g	X_g μgNH_3 m^{-3}	$[NH_4^+]$ mg L^{-1}	Γ_g	X_g μgNH_3 m^{-3}	Γ_g	X_g μgNH_3 m^{-3}
0 – 2	4.96	4.32	893	4.45	4.32	891	4.44	392826	1960
2 – 4	3.14	2.70	558	2.78	2.70	557	2.78	163373	815
4 – 6	2.98	2.56	529	2.64	2.56	528	2.63	162035	808
		Low End of the Isotherm							
0 – 2	4.96	3.53	728	3.63	3.43	709	3.54		
2 – 4	3.14	2.20	454	2.26	2.14	442	2.20		
4 – 6	2.98	2.08	430	2.14	2.03	418	2.09		

4.0. Discussion

4.1. Factors Controlling the Soil Compensation Point (X_g)

As presented in Chapter Two, Table 2.5, the amount of NH_4^+in the upper layer of soil (0–2 cm) increased significantly within 24 hours, and then declined the next day and immediately the following days. We also saw an increase in the amount of NO_3^-. The decreased in NH_4^+ content is due to the nitrification process and thus may likely reduce the potential for NH_3 emission (Genermont and Cellier, 1997; Sommer et al, 2003; Flechard et al., 2013). The most important mechanisms for the regulating of the new pool of TAN on the surface are: (ii) vertical NH_4^+ soil convection and diffusion; and (ii) NH_4^+ soil cation exchange (CEC) interaction (Sommer et al., 2003; Genmont and Cellier, 1997).

In principle, TAN in soil is distributed between the phases of solid, liquid, and gas. The NH_4^+ on the solid phase exchange site is interacted with NH_4^+ in soil solution (Fleisher et al., 1987). More than 95% of the TAN will be NH_4^+ in the pH < 8 and can be replaced with exchangeable cations. Therefore, the NH_4^+ exchange at the exchange sites can be determined by the activity ratio law (Russels, 1977), the rise in soil water content as a result of rain will change the equilibrium and contribute to the exchange of divalent cations with NH_4^+ (Chung and Zasoski, 1994). In comparison, because the soil solution is concentrated during drying, NH_4^+ will exchange cations on the CEC. Thereby, the NH_4^+ concentration in drying conditions may not linearly increase with water evaporation. Therefore, the exchange process decreases the NH_3 emissions reflected the initial content of TAN per unit time and increases the duration of time with noticeable emission rates, as shown by Fleisher et al. (1987) this effect is most apparent in the soil of high CEC. The retention to CEC over-drying conditions can, in addition to the solid phase theory, help explain why NH_3 emissions can be low from dry soil (Fenn and Kissel, 1976).

The amount of NH_4^+ retained in soil increases due to NH_4^+ adsorption, and the fixation rate decreases with increasing concentrations of NH_4^+ in solution. In addition, the increase in NH_4^+ fixed by the increase in NH_4^+ concentration is higher in soils of high capacity than in low capacity soil. Retention of NH_4^+ increases when soil has been dried after NH_4^+ is added. It probably comes because water is removed and the concentration of NH_4^+ in solution is increased and the lattice is partly contracted, allowing NH_4^+ to be trapped in the interlayers (Black and Waring, 1972). Allison et al. (1953) suggested that soil water may decrease the attached NH_4^+ as clay minerals are enlarged in wet conditions. For dry soils, however, the space of the interlayer is decreased and the NH_4^+ fixation is increased. Osborne (1976) estimates that NH_4^+ fixation in a clay soil moisturized was reduced by 25 percent to 60 percent of its maximum water capacity compared to dry soil.

The existence of NH_3 in equilibrium with NH_4^+ dissolved in soil moisture is essential for the exchange of NH_3 with soil surface. Equation 3.9 may be used to predict the concentration of gaseous NH_3 (X_g) in equilibrium with the concentration of NH_4^+ and pH in soil water (Sutton et al., 1994). In addition to the strong dependence of the NH_4^+ and H^+ concentrations on soil moisture, the rate and quantity of adsorption or desorption at the soil surface is highly dependent on the soil surface temperature and on the soil moisture at the surface. NH_3 loss from the soil to the atmosphere is driven by the difference between the soil compensation point (X_g) and the atmospheric concentration (X_a). As Sakaguchi and Zeng (2009) explained, processes of emission of NH_3 are limited to (i) soil diffusion resistance (R_{soil}) (s m^{-1}), depending on the length ratio of the dry soil layer through which gas has to be diffused to the atmosphere and the coefficient for gas diffusion, and (ii) the resistance to diffusive transportation through the air-side laminar boundary layer in the soil surface (R_{bg}) (s m^{-1}) (Walker et al., 2013). When soil dries, the length

of the diffusion path increases and so Rsoil increases (Walker et al. 2013). Following the parameterizations for Rbg, and R_{soil} described by Pleim (2006) and Cooter et al. (2010), it is concluded that R_{soil} is the limiting resistance. While the dynamics of the TAN and soil water evaporation will drive of the soil NH_3 loss, we find that the loss of NH_3 measured in the soil was strongly linked to soil moisture (Chapter Two, Fig. 2.20). Equation 3.1 ($F_g = \frac{X_g - X_z}{R_{bg} + R_{soil}}$) is directly used to test the potential effect of soil moisture during drying on emission of NH_3. Assuming Rbg, temperature, and flow rate through the chamber are constants, though Rs will be changing. From the previous experiments, we observed that drying increases emissions, which means that the effect of NH_4^+ becoming more concentrated in solution during drying is a stronger effect than the increase in resistance associated with drying, which would reduce emissions. So, the impact on resistance may not be of lesser importance. Figure 2.20 (Chapter Two) shows a time series of a calculated average NH_3 concentration along with percent of cumulative water loss over 120-hour period.

4.2. Relating Measured Emissions to Potential Critical Compensation Point

The question needs to be addressed of why we try to make such a connection between measured NH_3 emissions versus the adsorption isotherm data. First, the apparent response of NH_3 emissions to increased presence of NH_4^+ was suggested in Fig. 2.17 (Chapter Two) and was tested further using packed columns composed unfumigated soil (BASF-ls).

The calculated integrated average NH_3 concentrations as a function of time and rate of NH_4^+ addition are shown in Fig. 3.15. There is definite response in NH_3 emitted as a function of NH_4^+ added, which in general remained relatively constant throughout the course of the experiment. These results are similar to those in Fig. 2.17 (Chapter Two) for the wetting cycles,

indicating that conditions resulting in NH_3 emissions were fairly reproducible for the individual 24-hour measurements followed by addition of water to restore the columns to initial water content at time zero. Overall, the largest changes in NH_3 emissions appeared to be between the first and second set of observations, perhaps due to continued NH_4^+ redistribution in the packed columns after the first wetting cycle.

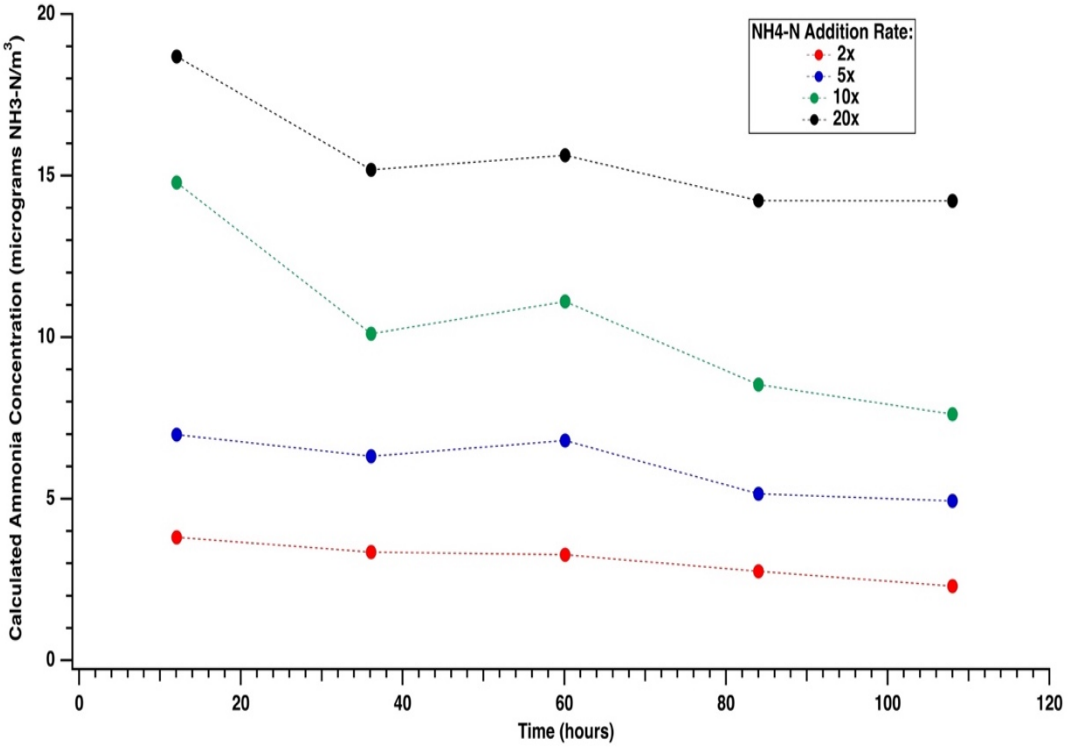

Figure 3.15. Calculated average NH_3 concentration per each 24-hour period as a function of time and rate of NH4-N addition to unfumigated packed soil (BASF-ls) columns. Rate of NH_4^+ addition based on initial NH4-N concentration of ~ 2.2 µg N g^{-1}. Individual data points are plotted at mid-point of each 24-hour measurement period and represent single observations. The dashed lines are added to help visualize overall trends in the data. This Figure was taken from Chapter Two, Fig. 2.18.

The dose-response curve is used to illustrate the link between the concentration of the extractable N and the change in the proportion of NH_3 emission that responds to the N concentration (Fig. 3.16). The fundamental hypothesis is that there are no NH_3 emissions if there

is no extractable NH_4^+ present that can be identified using a batch extraction method. The linearity/shape of the dose-response curve is important because we want to determine the best way to assess whether or not non-modified soil emits NH_3 as an important index of the critical compensation point. When plotting the response of NH_3 emission at various N concentration, the dose-response curve takes the nonlinear form (data is not shown here). Values of extracted NH_4^+ are converted to log values to reduce the dispersion of data, which helps to linearize the curve. Therefore, a better understanding and interpretation can be drawn from this linear equation. By this way we can measure the optimized amount of mineralized N in the soil that contributes to NH_3 emissions. Consequently, the amount of extractable N is plotted on the X axis as the natural logarithm of extractable N concentration in a unit of $\mu g\ g^{-1}$ and response as amount of NH_3 emitted in unit $\mu g\ NH_3$ is plotted on the Y axis using a linear scale (Fig. 3.16). When we take the natural log of the extractable N concentration and plot that (x) versus NH_3 loss (y), a linear response is obtained for 2M KCl: $y = 284.1x - 429.84$; $R^2 = 0.981$ and for 0.01M $CaCl_2$ $y = 380.94x - 546.31$; $R^2 = 0.995$. The slope of the curve indicates the change in the NH_3 loss responding as the N concentrations increases. An increase in the slope of a dose-response curve indicates that as the N-concentration increases, there are increasingly higher emission of NH_3 responses.

The intercepts of the regression lines indicate that there is zero flux at extractable concentrations of 4.2-4.5 $\mu gNH_4^+\ g^{-1}$. In other words, there must be at least 4.2-4.5$\mu g\ NH_4^+\ g^{-1}$ in soil to yield a measurable NH_3 loss under the chamber conditions. However, at these extractable N concentrations, corresponding pH of 5.9 and water content of 0.05, the soil bulk extraction method predicts a compensation point of 23-24 $\mu g\ m^{-3}$ which would certainly yield a measurable emission, which we do not observe.

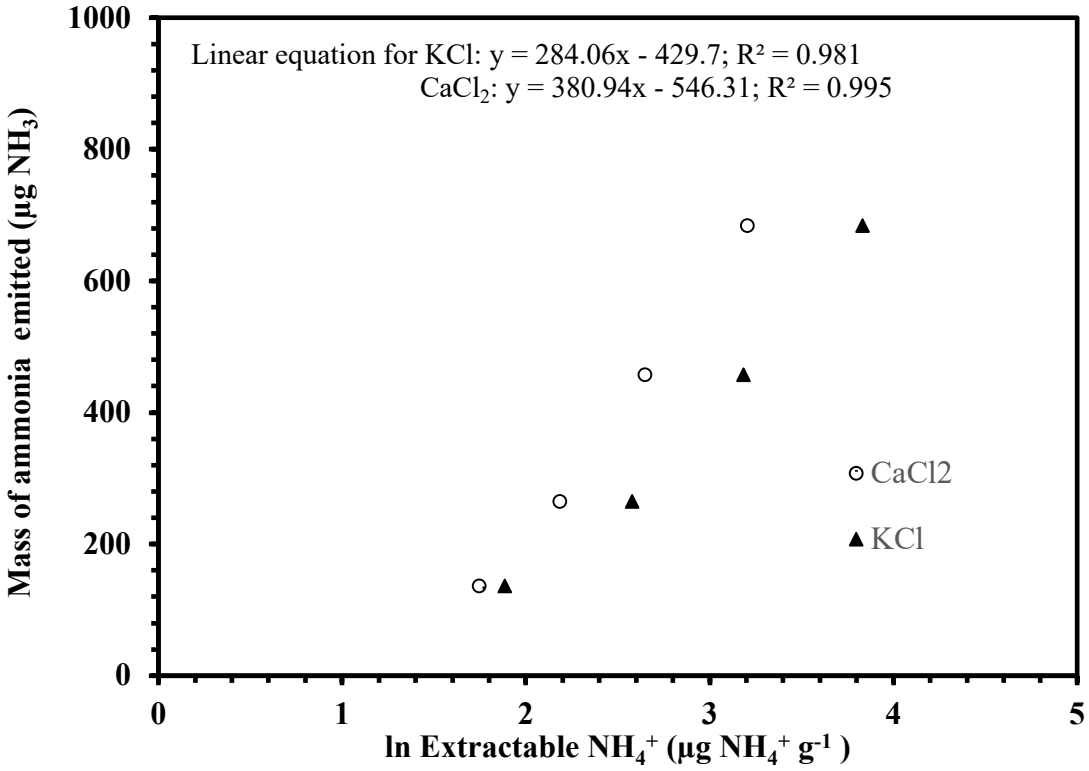

Figure 3.16. The amount of NH_3 emitted as function of natural log extractable NH_4^+ at time = zero. Experimental conditions are exchange rate of air (5.4 vol/min), BASF-ls soil mass (650 g), Soil water content was maintained at 80% of field capacity. NH_4^+ added at rate of 2x, 5x, 10x, and 20x of initial 2M KCl extractable NH_4^+.

Regarding soil compensation point, we compared the calculated NH_3 compensation points for BASF-ls soil by two different approaches: (i) calculation from the pH and NH_4^+ concentration of soil extracts (Table 3.19) and (ii) using Langmuir adsorption isotherm in a way to calculate the fraction of NH_4^+ in the liquid phase that contributed to NH_3 emission (Table 3.20).

The extractable $\mu gNH_4^+ g^{-1}$ from soil per N addition treatment per chamber was given for different extractants KCl, $CaCl_2$, and water at rate of 2x, 5x, 10x, and 20x, respectively (Table 3.19). The estimated soil compensation based on a measure of extractable NH_4 using traditional methods of extractions is also given in Table 3.19. The three extractants for estimating the NH_4^+

concentration produced widely varying estimates and therefore unrealistic values for soil compensation point (Table 3.18).

The critical soil compensation point calculation from the pH and NH_4^+ concentration of soil extracts with 2M KCl were 19, 18, 24, and 17 times higher than the values obtained from Langmuir adsorption isotherm data at NH_4^+ application rate of 2x, 5x, 10x, and 20x, respectively. As discussed earlier, the results presented in Table 3.18 support the hypothesis that common soil extractions (2M KCl) to assess available pools of NH_4^+ present in soils do not yield estimates of Xg consistent with actual measured emissions. Compared to the time zero values of extractable NH_4-N in Table 3.18, the NH_3 loss from the entire soil column accounts for only about 3.2, 3.1, 2.9, and 2.3% of the 2M KCl extractable NH_4^+, 3.7, 4.6, 5 and 4.3%. of the 0.01M $CaCl_2$, and 10.7, 10.4, 9.8, and 7.7% of the water extraction, at application rate of 2x, 5x, 10x, and 20x, respectively. Overall loss of NH_3 during the first 120 hours are 136, 265, 457, and 684 μg.

To relate the sorption isotherms to the concept of compensation point, the fraction of NH_4^+ in solution for a given concentration of total extractable NH_4^+ were examined using Langmuir isotherms over the full range and low end of the isotherm. The low concentration of NH_4^+ calculated at the low end of isotherm is a more realistic method of compensation point determination for unamended soils. This method should theoretically give the most reliable estimates because it provides a more realistic measure of NH_4^+ in the soil solution and therefore Γ_{soil}.

Table 3.19. Soil emission potential and compensation point calculated from the pH and NH_4^+ concentration of soil extracts with different extractants (2M KCl, 0.01M $CaCl_2$, and water) for BASF-ls soil at depth = 0.5 cm under the following conditions: Temperature = 22°C, and pH = 6.57.

Extractant	Application rate of N	Mass NH_3-N loss recovered from soil (μg NH_3)	Extractable N (μg$NH_4^+g^{-1}$)	Γ_g $[NH_4^+]/[H^+]$	X_g (μgNH_3 m^{-3})	Mass NH_3-N loss/mass soil (μg g^{-1})
2M KCl	2x	136	6.59	2.70E+04	135	2.19
	5x	265	13.18	5.40E+04	270	4.27
	10x	457	24.17	1.45E+05	724	7.50
	20x	684	46.14	2.34E+05	1166	11.11
0.01 M $CaCl_2$	2x	136	5.74	2.35E+04	117	2.19
	5x	265	8.89	3.64E+04	182	4.27
	10x	457	14.14	8.49E+04	424	7.50
	20x	684	24.64	1.25E+05	623	11.11
Water	2x	136	1.95	7.98E+03	40	2.19
	5x	265	3.9	1.60E+04	80	4.27
	10x	457	7.15	4.29E+04	214	7.50
	20x	684	13.65	6.91E+04	345	11.11

Table 3.20. Concentration of NH_4^+ in soil solution, soil emission potential, and compensation point calculated from the Langmuir sorption isotherm at full range and end low of the isotherm with different extractants: 2M KCl, 0.01M $CaCl_2$, and water for BASF-ls soil under the following conditions: Temperature = 22°C, and pH = 6.57

Application Rate of N	Extractable NH_4^+	Full Range of Langmuir Isotherm			Low End of the Langmuir Isotherm		
	$\mu gNH_4^+ g^{-1}$	$[NH_4^+]$ mg L^{-1}	Γ_g	X_g $\mu gNH_3 m^{-3}$	$[NH_4^+]$ mg L^{-1}	Γ_g	X_g $\mu gNH_3 m^{-3}$
	2M KCl extraction						
2x	6.59	5.82	1202	5.99	4.76	983	4.91
5x	13.18	12.26	2530	12.62	10.16	2096	10.46
10x	24.17	24.64	5085	25.37	20.93	4320	21.55
20x	46.14	58.23	12018	67.29	53.08	10957	54.66
	0.01M $CaCl_2$ extraction						
2x	5.74	5.04	1040	5.19	4.12	850	4.24
5x	8.89	7.99	1650	8.23	6.57	1356	6.76
10x	14.14	13.25	2735	13.64	11.00	2271	11.33
20x	24.64	25.22	5205	29.14	21.45	4428	22.09
	Water extraction						
2x	1.95	1.66	343	1.71	1.35	279	1.39
5x	3.9	3.38	697	3.48	2.75	568	2.83
10x	7.15	6.34	1309	6.53	5.20	1073	5.35
20x	13.65	12.74	2630	14.72	10.57	2181	10.88

5.0. Summary Thoughts and Future Recommended Research

The soil compensation point is a key parameter in the NH_3 bi-directional exchange model. This research allows us to estimate a comparable critical compensation point for NH_3 in non-amended soils by different approaches: (i) soil extraction, (ii) NH_4^+ adsorption isotherm, and (iii) distribution of NH_4^+ and NO_3^- as a function of water evaporation. From the results of these experiments, the following questions might be considered:

- Traditional extraction of NH_4^+ using concentrated salts does not provide information needed to make soil compensation point calculations – When applying this methodology to calculating NH_3 compensation points, the major consideration is whether or not the NH_4^+ extracted is representative of the soil solution and NH_3 emission. Measurements of NH_3 emission from the soil suggest that the amount of extractable NH_4^+ removed from soils using traditional extraction protocols overestimate the fraction of soil NH_4^+ that is available for soil-atmosphere exchange of NH_3. Part of the reason for this obvious overestimate was proposed for the release of NH_4^+ from microbial cells that are killed during concentrated salt extraction and/or for removal of NH_4^+ from a soil complex that would not be involved kinetically with the NH_3 equilibrium. In order to limit potential soil microbial activity that can compound attempts to relate NH_3 emission potential to the presence of extractable soil NH_4^+, we suggest consideration of fumigation, despite the artifact of rupturing of cell membranes and release of cellular NH_4^+.
- Since NH_4^+ is a simple cation, can a correction factor be applied to these routine methods of extracting NH_4^+ to aid in calculating the compensation point from bulk extractions, or does this research suggest the overestimation is so large that the actual amounts needed to match observed NH_3 emissions is always going to be a very small percentage of extracted NH_4^+ values?

- If a correction factor might work, then do we have an idea of the range and thus how many benchmark soils would need to be characterized in order to make existing databases useable?
- Do we know “soil” pH well enough to use it in these calculations? To describe the emission process properly, we still need to improve our understanding of the controls on soil pH, especially following the addition of N-sources. The dynamics of pH in the soil are a major determinant of the magnitude and duration of NH_3 emissions and we still do not have a reliable way to simulate the variation of these dynamics in soils after application of N-sources. For example, a difference in pH of 0.7 units found for the same soil that has two different reading (6.03 vs 6.68) is sufficient to provide for a 5-fold variance between compensation points of NH_3. pH gradients that occur through the soil profile due to solute transport and losses.

REFERENCES

Allison, F.E. and E.M. Roller. 1955. Fixation and release of ammonium ions by clay minerals. Soil Sci. 80:431-442.

Allison, F.E., J.H. Doetsch and E.M. Roller. 1953. Availability of fixed ammonium in soils containing different clay minerals. Soil Sci. 75:361-382.

Angima, S. 2010. Measuring soil pH, Oregon State University Small Farms Program, .

Antisari, L.V. and P. Sequi. 1988. Comparison of total nitrogen by four procedures and sequential determination of exchangeable ammonium, organic nitrogen, and fixed ammonium in soil. Soil Sci. Soc. Am. J. 52:1020-1023.

Avnimelech, Y. and M. Laher. 1977. Ammonium volatilization from soils: Equilibrium considerations. Soil Sci. Soc. Am. J. 41:1080–1084.

Bates, R.G. and G.D. Pinching. 1949. Acidic dissociation constant of ammonium ion at 0 to 50 C, and the base strength of ammonia. Journal of Research of the National Bureau of Standards 42:419-430.

Beauchamp, E.G. 1982. Fixed ammonium and potassium release from two soils. Commun. Soil Sci. Plant Anal. 13:927-943.

Black, A.S. and S.A. Waring. 1972. Ammonium fixation and availability in some cereal producing soils in Queensland. Aust. J. Soil Res. 10:197-207.

Boatman, C.D. and J.W. Murray. 1982. Modeling exchangeable NH_4^+Adsorption in marine sediments: Process and controls of adsorption. Limnol. Oceanogr. 27:99-110.

Brady, N.C. and R.R. Weil. 1999. The nature of soil properties, 12th edn. prentice hall, inc., upper saddle river, NJ.

Bremner, J.M. and D.R. Keeney. 1996. Determination and isotope-ratio analysis of different forms of nitrogen in soils: 3. exchangeable ammonium, nitrate, and nitrite by extraction-distillation Methods. Soil Sci. Soc. Am. J. 30:577-582.

Brodrick, S., P. Cullen, and W. Maher.1987. Determination of exchangeable inorganic nitrogen species in wetland soils. Bull. Environ. Contam. Toxicol. 38:377-380.

Cai, G.X. 1997. Ammonia volatilization. In: Zhu, Z.L., Wen, Q.X., Freney, J.R. (eds.), Nitrogen in soils of china. kluwer academic publishers, dordrecht/boston/london, pp. 193–213.

Castro, J. and M. Korn. 2004. Deleterious effect of ammonium extraction from soil assisted by ultrasound. Microchemical Journal 78:41-45.

Chang, W.J. and R. Donahue. 2007. Cation exchange due to the diffusion of ammonium from livestock effluent through glacial clay soils. Appl. Geochem. 22:53-68.

Chapman, H.D., 1965. Cation exchange capacity. In: Black CA (ed) Methods of soil analysis. Amer Soc Agron Inc., Madison. pp 891-901.

Chen, C., F.T. Turner and J.B. Dixon. 1989. Ammonium fixation by high-charge smectite in selected Texas Gulf Coast Soils. Soil Sci. Soc. Am. J. 53:1035-1040.

Chung, J. and R.J. Zasoski. 1994. Ammonium-potassium and ammonium-calcium exchange equilibria in bulk and rhizosphere soil. Soil Sci. Soc. Am. J. 58:1368-1375.

Cooter, E., J.O. Bash, J.T. Walker, M. Jones and W. Robarge. 2010. Estimation of NH3 bi-directional flux from managed agricultural soils. Atmos. Environ. 44:2067–2166.

Dasgupta, P.K. and S. Dong. 1986. Solubility of ammonia in liquid water and generation of trace levels of standard gaseous ammonia. Atmos. Environ. (1967) 20:565-570.

David, M., B. Loubet, P. Cellier, M. Mattsson, J.K. Schjoerring, E. Nemitz, R. Roche, M. Riedo, M.A. Sutton, (Bio- och miljösystemforskning, Akademin för ekonomi, teknik och naturvetenskap and Högskolan i Halmstad. 2009. Ammonia sources and sinks in an intensively managed grassland canopy. Biogeosciences 6:1903-1915.

Dawson, G.A. 1977. Atmospheric ammonia from undisturbed land. J Geophys. Res. 82:3125-3133.

Demeyer, P., G. Hofman and O. V. Cleemput. 1995. Fitting ammonia volatilization dynamics with a logistic equation. Soil Sci. Soc. Am. J. 59:261-265.

Demir, A., E. Debik and A. Gunay. 1998. Ammonium removal from aqueous solution by ion exchange using packed bed natural zeolite. Water SA Journal 28:329–335.

Elmacı, ÖL., M. Seçer, O. Erdemir and N. Iqbal. 2002. Ammonium fixation properties of some arable soils from the aegean region of turkey. Eur. J. Agron. 17:199-208.

Esala, M.J. 1994. Deep-freezing pretreatment and time of extraction of soil samples for inorganic nitrogen determination. Commun. Soil Sci. Plant Anal. 25:651-662.

Ewing, G.E. 2006. Ambient thin film water on insulator surfaces. Chem. Rev. 106:1511-1526.

Farquhar, G.D., P.M. Firth, R. Wetselaar and B. Weir. 1980. On the gaseous exchange of ammonia between leaves and the environment: Determination of the ammonia compensation point. Plant Physiol. 66:710-714.

Feagley, S.E. and L.R. Hossner. 1978. Ammonia volatilization reaction mechanism between ammonium sulfate and carbonate systems. Soil Sci. Soc. Am. J. 42:364–367.

Feigenbaum, S., A. Hadas, M. Sofer and J.A.E. Molina. 1994. Clay-fixed labeled ammonium as a source of available nitrogen. Soil Sci. Soc. Am. J. 58:980-985.

Felber, R., F. Conen, C.R. Flechard and A. Neftel. 2012. Theoretical and practical limitations of the acetylene inhibition technique to determine total denitrification losses. Biogeosciences 9:4125-4138.

Fenn, L.B. 1975. Ammonia volatilization from surface applications of ammonium compounds on calcareous soils: III. effects of mixing low and high loss ammonium Compounds. Soil Sci. Soc. Am. J. 39:366-368.

Fenn, L.B. and D.E. Kissel. 1973. Ammonia volatilization from surface applications of ammonium compounds on calcareous soils: I. general Theory1. Soil Sci. Soc. Am. J. 37:855-859.

Fenn, L.B. and D.E. Kissel. 1974. Ammonia volatilization from surface applications of ammonium compounds on calcareous soils: II. effects of temperature and rate of ammonium nitrogen Application. Soil Sci. Soc. Am. J. 38:606-610.

Fenn, L.B. and D.E. Kissel. 1975. Ammonia volatilization from surface applications of ammonium compounds on calcareous soils: IV. effect of calcium carbonate Content. Soil Sci. Soc. Am. J. 39:631-633.

Fenn, L.B. and D.E. Kissel. 1976. The influence of cation exchange capacity and depth of incorporation on ammonia volatilization from ammonium compounds applied to calcareous Soils. Soil Sci. Soc. Am. J. 40:394-398.

Fenn, L.B. and R. Escarzaga. 1976. Ammonia volatilization from surface applications of ammonium compounds on calcareous soils: V. soil water content and method of nitrogen Application. Soil Sci. Soc. Am. J. 40:537-541.

Fenn, L.B. and R. Escarzaga. 1977. Ammonia volatilization from surface applications of ammonium compounds to calcareous soils: VI. effects of initial soil water content and quantity of applied Water. Soil Sci. Soc. Am. J. 41:358-363.

Fenn, L.B., J.E. Matocha and E. Wu. 1981a. A comparison of calcium carbonate precipitation and pH depression on calcium-reduced ammonia loss from surface-applied Urea1. Soil Sci. Soc. Am. J. 45:1128-1131.

Fenn, L.B., J.E. Matocha and E. Wu. 1981b. Ammonia losses from surface-applied urea and ammonium fertilizers as influenced by rates of soluble calcium. Soil Sci. Soc. Am. J. 45:883–886.

Fenn, L.B., R.M. Taylor and J.E. Matocha. 1981c. Ammonia losses from surface-applied nitrogen fertilizer as controlled by soluble calcium and magnesium: General Theory. Soil Sci. Soc. Am. J. 45:777-781.

Ferguson, R.B., D.E. Kissel, J.K. Koelliker and W. Basel. 1984. Ammonia volatilization surface-applied urea: Effect of hydrogen ion buffering capacity. Soil Sci. Soc. Am. J. 48:578–582.

Fernando, W. A. R. Nishantha, K. Xia and C.W. Rice. 2005. Sorption and desorption of ammonium from liquid swine waste in soils. Soil Sci. Soc. Am. J. 69:1057-1065.

Flechard, C.R., C. Spirig, A. Neftel and C. Ammann. 2010. The annual ammonia budget of fertilized cut grassland – part 2: Seasonal variations and compensation point modeling. Biogeosciences 7:537-556.

Flechard, C.R., R.-. Massad, B. Loubet, E. Personne, D. Simpson, J.O. Bash, E.J. Cooter, E. Nemitz and M.A. Sutton. 2013. Advances in understanding, models and parameterizations of biosphere-atmosphere ammonia exchange. Biogeosciences 10:5183-5225.

Fleisher, Z., A. Kenig, I. Ravina and J. Hagin. 1987. Model of ammonia volatilization from calcareous soils. Plant Soil 103:205-212.

Gapon, E.N. 1933. On the theory of exchange adsorption in soils. J. Gen. Chem. 3:144-152.

Gaspard, M., A. Neveu and G. Martin. 1983. Clinoptilolite in drinking water treatment for NH_4^+ removal. Water Res 17:279–288.

Gee, G.W., and J.W. Bauder, 1986. Particle -size analysis. In Methods of soil analysis: Part 1. Physical and mineralogical methods, 2nd Edition. Klute, A. (Ed.), ASA-SSSA, Madison, WI, USA. pp. 383-409.

Génermont, S. and P. Cellier. 1997. A mechanistic model for estimating ammonia volatilization from slurry applied to bare soil. Agric. for. Meteorol. 88:145-167.

Genermont, S., P. Cellier, D. Flura, T. Morvan and P. Laville. 1998. Measuring ammonia fluxes after slurry spreading under actual field conditions. Atmos. Environ. 32:279-284.

GlobalSoilMap. 2015. Specifications, tiered 1 GlobalSoilMap products. release 2.4. French National Institute for Agricultural Research (INRA), Orleans.

Gurovich, E. and Y. Avnimelech. 1977. The distribution of ammonium ion from a localized source into the soil. Plant Soil 46:101-111.

Hansen, K., L.L. Sørensen, O. Hertel, C. Geels, C.A. Skjøth, B. Jensen, E. Boegh, Dept of Physical Geography and Ecosystem Science, Lund University, Lunds universitet and Institutionen för naturgeografi och ekosystemvetenskap. 2013. Ammonia emissions from deciduous forest after leaf fall. Biogeosciences 10:4577-4589.

Hanway, J.J., A.D. Scott and G. Stanford. 1957. Replaceability of ammonium fixed in clay minerals as influenced by ammonium or potassium in the extracting Solution. Soil Sci. Soc. Am. J. 21:29-34

Hargrove, W.L. 1988. Evaluation of ammonia volatilization in the field. J. Prod. Agric. 1:104-111.

He, Z.L., A.K. Alva, D.V. Calvert and D.J. Banks. 1999. Ammonia volatilization from different fertilizer sources and effects of temperature and soil pH1. Soil Sci. 164:750-758.

Heil, G.W. and M. Bruggink. 1987. Competition for nutrients between calluna vulgaris (L.) hull and molinia caerulea (L.) moench. Oecologia 73:105-108.

Hillel, D. 2004. Introduction to environmental soil physics. Elsevier Science & Technology, Burlington.

Hinz, C. 2001. Description of sorption data with isotherm equations. Geoderma 99:225-243.

Hrdina, A., H. Schwartz-Narbonne, A. Moravek and J. Murphy. 2019. Summertime soil-atmosphere ammonia exchange in the Colorado Rocky Mountain Front Range Pine Forest. Soil Syst. 3:15 doi:10.3390/soilsystems3010015.

Hu, J., X.-. Xiao, D.F. Ogletree and M. Salmeron. 1995. Imaging the condensation and evaporation of molecularly thin films of water with nanometer resolution. Science 268:267-269.

James, D.W. and M.E. Harward. 1964. Competition of NH_3 and H_2O for adsorption sites on clay Minerals. Soil Sci. Soc. Am. J. 28:636-640.

Jewitt, T.N. 1942. Loss of ammonia from ammonium sulfate applied to alkaline soils. Soil Sci. 54:401-410.

Jury, W. A., and R. Horton. 2004. Soil Physics, 6th ed., 370 pp., John Wiley, Hoboken, N. J.

Keeney, D. 1982. Nitrogen-availability indices. in: Page, A., Keeney, D. (eds.), methods of soil analysis, part 2: Chemical and microbiological properties, Am. Soc. Agron. Madison, WI, pp. 643-698.

Keerthisinghe, G., K. Mengel and S.K. De Datta. 1984. The release of nonexchangeable ammonium (^{15}N labelled) in wetland rice Soils. Soil Sci. Soc. Am. J. 48:291-294.

Keerthisinghe, G., S.K. DeDatta and K. Mengel. 1985. Importance of exchangeable and non-exchangeable soil NH_4^+ in nitrogen nutrition of lowland rice. Soil Sci. 48:194–201.

Kelleners, T.J. and A.K. Verma. 2010. Measured and modeled dielectric properties of soils at 50 megahertz. Soil Sci. Soc. Am. J. 74:744-752.

Khan, S.A., R.L. Mulvaney and R.G. Hoeft. 2000. Direct-diffusion methods for inorganic-nitrogen analysis of soil. Soil Sci. Soc. Am. J. 64:1083-1089.

Kissel, D.E., L. Sonon, P.F. Vendrell and R.A. Isaac. 2009. Salt concentration and measurement of soil pH. Commun. Soil Sci. Plant Anal. 40:179-187.

Kissel, D.E., M.L. Cabrera and S.E. Paramasivam. 2008. Ammonium, ammonia and urea reactions in soils. p. 101-156. in nitrogen in agricultural systems. Agronomy Monograph No. 49. J.S. Schepers and W.R. Raun, eds. ASA-CSSA-SSSA, madision, WI.

Kithome, M., A.A. Bomke, J.W. Paul and L.M. Lavkulich. 1998. Kinetics of ammonium adsorption and desorption by the natural zeolite clinoptilolite. Soil Sci. Soc. Am. J. 62:622-629.

Klute, A. 1986. Water retention: Laboratory methods. In Methods of soil analysis: Part 1. Physical and mineralogical methods, 2nd Edition. Klute, A. (Ed.), ASA-SSSA, Madison, WI, USA. pp. 635-660.

Koelliker, J.K., and D.E. Kissel. 1988. Chemical equilibria affecting ammonia volatilization. p. 93–109. In B.R. Bock and D.E. Kissel (ed.). Ammonia volatilization from urea fertilizers. Tennessee Valley Authority, Muscle Shoals, AL.

Krupa, S.V. 2003. Effects of atmospheric ammonia (NH 3) on terrestrial vegetation: A review. Environmental Pollution 124:179-221.

Lamm, C.G. and M.H. Nadafy. 1973. Plant nutrient availability in soils. III. studies on potassium in Danish soils. 6. the rate of release and availability of fixed potassium. Agrochimica 17:435–444.

Langford, A.O., F.C. Fehsenfeld, J. Zachariassen and D.S. Schimel. 1992. Gaseous ammonia fluxes and background concentrations in terrestrial ecosystems of the united states. Global Biogeochem. Cycles 6:459-483.

Langmuir, I. 1918. The adsorption of gases on plane surfaces of glass, mica and platinum. J. Am. Chem. Soc. 40:1361-1403.

Li, K., Y. Zhao, X. Yuan, H. Zhao, Z. Wang, S. Li and S.S. Malhi. 2012. Comparison of factors affecting soil nitrate nitrogen and ammonium nitrogen extraction. Commun. Soil Sci. Plant Anal. 43:571-588.

Libohova, Z., S. Wills and N.P. Odgers. 2013. Legacy data quality and uncertainty estimation for united states GlobalSoilMap products. in: GlobalSoilMap: Basis of the global spatial soil information system (eds D. Arrouays, N. McKenzie, J. Hempel, A.C. Richer de Forges & A. McBratney), pp. 63– 68. Taylor &Francis, London.

Lightner, J.W., D.B. Mengel and C.L. Rhykerd. 1990. Ammonia volatilization from nitrogen fertilizer surface applied to orchardgrass sod. Soil Sci. Soc. Am. J. 54:1478-1482.

Lin, S.H. and C.L. Wu. 1996. Removal of nitrogenous compounds from aqueous solution by ozonation and ion exchange. Water Res. 30:1851-1857.

Lumbanraja, J. and V.P. Evangelou. 1994. Adsorption-desorption of potassium and ammonium at low cation concentrations in three Kentucky subsoils. Soil Sci. 157:269-278.

Martin, J.P. and H.D. Chapman. 1951. Volatilization of ammonia from surface-fertilized soils. Soil Sci. 71:25-34.

Massad, R.S., E. Nemitz and M.A. Sutton. 2010. Review and parameterization of bi-directional ammonia exchange between vegetation and the atmosphere. Atmos. Chem. Phys. 10:10359–10386.

Mengel, K. and H.W. Scherer. 1981. Release of nonexchangeable (fixed) soil ammonium under field conditions during the growing season. Soil Sci. 131:226-232.

Meyers, T.P., W.T. Luke and J.J. Meisinger. 2006. Fluxes of ammonia and sulfate over maize using relaxed eddy accumulation. Agric. for. Meteorol. 136:203-213.

Mills, H.A., A.V. Barker and D.N. Maynard. 1974. Ammonia volatilization from soils. Agron J 66:355–358

Mortland, M.M. 1968. Protonation of compounds at clay minerals surfaces. in: Trans. 9th Internat. Congr. Soil Sci.691-699.

Murdock, L. and D. Call. 2006. Managing seasonal fluctuations of soil tests, University of Kentucky cooperative extension.

Murray, J.W., V. Grundmanis and W.M. Smethie JR. 1978. Interstitial water chemistry in the sediment of saanich inlet. Gcochim. Cosmochim. Acta 42:1011-1026.

Nathan, M.V. and G.L. Malzer. 1994. Dynamics of ammonia volatilization from turkey manure and urea applied to soil. Soil Sci. Soc. Am. J. 58:985-990.

Neftel, A. 2013. Interactive comment on “Advances in understanding, models and parameterizations of biosphere-atmosphere ammonia exchange” by C. R. Flechard et al. Biogeosciences Discuss. 10:C1521–C1525.

Neftel, A., A. Blatter, A. Gut, D. Högger, F. Meixner, C. Ammann and F.J. Nathaus. 1998. NH3 soil and soil surface gas measurements in a triticale wheat field. Atmos. Environ. 32:499-505.

Nelson, D.W. 1982. Gaseous losses of nitrogen other than though denitrification. P.327-364. in F.J. Stevenson (ed.) nitrogen in agricultural soils. Agron. Monogr.22.ASA, CSSA, and SSSA, madison, WI.

Nemitz, E., M.A. Sutton, A. Gut, R. San José, S. Husted and J.K. Schjoerring. 2000a. Sources and sinks of ammonia within an oilseed rape canopy. Agric. for. Meteorol. 105:385-404.

Nemitz, E., M.A. Sutton, J.K. Schjoerring, S. Husted and G. Paul Wyers. 2000b. Resistance modelling of ammonia exchange over oilseed rape. Agric. for. Meteorol. 105:405-425.

Nemitz, E., Milford, C. and Sutton, M. A. 2001. A two-layer canopy compensation point model for describing bi-directional biosphere-atmosphere exchange of ammonia. Quarterly Journal of the Royal Meteorological Society 127:815-833.

Nommik, H. and K. Vahtras. 1982. Retention and fixation of ammonium and ammonia in soils. in F. Stevenson (ed.) nitrogen in agricultural systems. Agron. Monogr. 22. ASA, Madison, WI.p. 123–171.

Osborne, G.J. 1976. The significance of intercalary ammonium in representative surface and subsoils from southern new south wales. Aust. J. Soil Res. 14:381-388.

Paliwal, V., and G. L. Maliwal, 1966. Cation Exchange Equilibria in Na-Ca-Mg System of Soils and Clay Minerals. J. Soil Wat. Conserv. India, 14, 44-50.

Paliwal.V., and G. L. Maliwal, 1970. Cation Exchange Equilibria I Na-Ca System of Clay Minerals and Soils. Proceedings of Indian National Science Academy, A 36, 146-153.

Peech, M. 1965. Hydrogen Ion Activity. In: Black, C.A., et al., Eds., Methods of Soil Analysis, Part 2, American Society of Agronomy, Madison, 914-926.

Phillips, S.B., S.P. Arya and V.P. Aneja. 2004. Ammonia flux and dry deposition velocity from near-surface concentration gradient measurements over a grass surface in North Carolina. Atmos. Environ. 38:3469-3480.

Pleim, J. E. 2006. A simple, efficient solution of flux–profile relationships in the atmospheric surface layer, J. Appl. Meteorol. Clim. 45: 341–347.

Prasad, M. 1976. Gaseous loss of ammonia from sulfur-coated urea, ammonium sulfate, and urea applied to calcareous soil (pH 7.3). Soil Sci. Soc. Am. J. 40:130-134.

Raaphorst, W.V. and J.F.P. Malschaert. 1996. Ammonium adsorption in superficial North Sea sediments. Cont. Shelf Res. 16:1415-1435.

Ranjbar, F. and M. Jalali. 2014. Empirical and mechanistic evaluation of $NH_4(+)$ release kinetic in calcareous soils. Arch. Environ. Contam. Toxicol. 66:606-615.

Raven, J.A., B. Wollenweber and L.L. Handley. 1993. The quantitative role of ammonia/ammonium transport and metabolism by plants in the global nitrogen cycle. Physiol. Plantarum 89:512-518.

Rosenfeld, J.K. 1979. Ammonium adsorption in nearshore anoxic sediments. Limnol. Oceanogr. 24:356-364.

Russel, E.W. 1977. Soil conditions and plant growth, 10th edn. Longman, London, New York.

Ryan, J., D. Curtin and I. Safi. 1981. Ammonia volatilization as influenced by calcium carbonate particle size and iron Oxides1. Soil Sci. Soc. Am. J. 45:338-341.

Sakaguchi, K. and X. Zeng. 2009. Effects of soil wetness, plant litter, and under-canopy atmospheric stability on ground evaporation in the community land model (CLM3.5): New Schemes For Clm3.5 Soil Evaporation. J Geophys. Res. Atmos. 114: D01107, doi:10.1029/2008JD010834

Schilt, S., L. Thévenaz, M. Niklès, L. Emmenegger and C. Hüglin. 2004. Ammonia monitoring at trace level using photoacoustic spectroscopy in industrial and environmental applications. Spectrochimica Acta Part A: Molecular and Biomolecular Spectroscopy 60:3259-3268.

Schjoerring, J.K., A. Kyllingsbaek, J.V. Mortensen and S. Byskov-Nielsen. 1993. Field investigations of ammonia exchange between barley plants and the atmosphere. I. concentration profiles and flux densities of ammonia. Plant, Cell Environ. 16:161-167.

Scott, A.D., J.J. Hanway and A.P. Edwards. 1958. Replaceability of ammonium in vermiculite with acid Solutions. Soil Sci. Soc. Am. J. 22:388-392.

Sharpe, R.R. and L.A. Harper. 1995. Soil, plant and atmospheric conditions as they relate to ammonia volatilization. Fertil. Res. 42:149-158.

Sieczka, A. and E. Koda. 2016. Kinetic and equilibrium studies of sorption of ammonium in the soil-water environment in agricultural areas of central Poland. Appl. Sci. 6: 269; doi:10.3390/app6100269.

Singh, G. and B. Prasad. 1997. Removal of ammonia from coke-plant wastewater by using synthetic zeolite. Water Environ. Res. 69:157-161.

Sintermann, J., A. Neftel, C. Ammann, C. Häni, A. Hensen, B. Loubet and C.R. Flechard. 2012. Are ammonia emissions from field-applied slurry substantially over-estimated in european emission inventories? Biogeosciences 9:1611-1632.

Slattery, W. and G. Ronnfeldt. 1992. Seasonal variation of pH, aluminum, and manganese in acid soils from North-Eastern Victoria. Aust. J. Exp. Agric. 32:1105-1112.

Søgaard, H.T., S.G. Sommer, N.J. Hutchings, J.F.M. Huijsmans, D.W. Bussink and F. Nicholson. 2002. Ammonia volatilization from field-applied animal slurry—the ALFAM model. Atmos. Environ. 36:3309-3319.

Soil Survey Staff. 2009. Soil and water chemical extractions and analysis. in: Soil survey field and laboratory methods manual (ed. R. Burt). pp. 179–190. soil survey investigations report no 51, version 1.0. U.S. department of agriculture, natural resources conservation service, washington, DC.

Sommer, S.G., S. Génermont, P. Cellier, N.J. Hutchings, J.E. Olesen and T. Morvan. 2003. Processes controlling ammonia emission from livestock slurry in the field. European Journal of Agronomy 19:465-486.

Sparks, D.L. (ed.) 1996. Kinetics of sorption/release processes on natural particles. in 'structure and surface reactions of soil particles. vol. 4.' (eds PM Huang, N Senesi and J Buffle). John Willey and Sons, New York.

Sterckeman, T. and H. Ciesielski. 1991. Principaux facteurs influant sur la détermination de l'azote minéral des sols, in: L'azote et le soufre dans le sol, edited by P. duc, groupe d'études méthodologiques pour l'analyse des sols. Editions Frontières, Gif-Sur-Yvette, France, ISBN 2-86332-095- 5 (in French).101.

Stratton, J.J., J. Ham and T. Borch. 2018. Ammonia emissions from subalpine forest and mountain grassland soils in rocky mountain national park. J. Environ. Qual. 47:778-785.

Stumpe, J.M., P.L.G. Velk and W.L. Lindsay. 1984. Ammonia volatilization from urea and urea phosphates in calcareous soils. Soil Sci. Soc. Am. J. 48:921-927.

Sutton, M.A., C.E.R. Pitcairn and D. Fowler. 1993. The exchange of ammonia between the atmosphere and plant communities. p. 301-393. *In* Elsevier Science & Technology.

Sutton, M.A., W.A.H Asman, and J.K Schjoerring. 1994. Dry deposition of reduced nitrogen. Tellus. 46B: pp. 255-273

Sutton, M.A., J.K. Burkhardt, D. Guerin and D. Fowler. 1995. Measurement and modelling of ammonia exchange over arable croplands. Studies in Environmental Science 64:71-80.

Thomas, G.W. 1996. Soil pH and soil acidity. In: Methods of Soil Analysis: Part 3 – Chemical Methods, Soil Science Society of America Book Series No 5(ed. J.M. Bigham), pp. 475–490. Soil Science Society of America and American Society of Agronomy, Madison, WI.

Twigg, M.M., E. House, R. Thomas, J. Whitehead, G.J. Phillips, D. Famulari, D. Fowler, M.W. Gallagher, J.N. Cape, M.A. Sutton and E. Nemitz. 2011. Surface/atmosphere exchange and chemical interactions of reactive nitrogen compounds above a manured grassland. Agric. for. Meteorol. 151:1488-1503.

Venterea, R.T., T.J. Clough, J.A. Coulter, F. Breuillin-Sessoms, P. Wang and M.J. Sadowsky. 2015. Ammonium sorption and ammonia inhibition of nitrite-oxidizing bacteria explain contrasting soil N2O production. Scientific Reports 5:121-153.

Verdaguer, A., G.M. Sacha, H. Bluhm and M. Salmeron. 2006. Molecular structure of water at interfaces: Wetting at the nanometer scale. Chem. Rev. 106:1478-1510.

Volkov, A.G., S. Paula and D.W. Deamer. 1997. Two mechanisms of permeation of small neutral molecules and hydrated ions across phospholipid bilayers. Bioelectrochem. Bioenerget. 42:153-160.

Wagner, G.H. and G.E. Smith. 1958. Nitrogen losses from soils fertilized with different nitrogen carriers. Soil Sci. 85:125-129.

Wahhab, A., M.S. Randhawa and S.Q. Alam. 1957. Loss of ammonia from ammonium sulphate under different conditions when applied to soils. Soil Sci. 84:249-256.

Walker, J., P. Spence, S. Kimbrough and W. Robarge. 2008. Inferential model estimates of ammonia dry deposition in the vicinity of a swine production facility. Atmos. Environ. 42:3407-3418.

Walker, J.T., M.R. Jones, J.O. Bash, L. Myles, T. Meyers, D. Schwede, J. Herrick, E. Nemitz and W. Robarge. 2013. Processes of ammonia air-surface exchange in a fertilized Zea mays canopy. Biogeosciences 10:981-998.

Walker, J.T., W.P. Robarge and R. Austin. 2014. Modeling of ammonia dry deposition to a pocosin landscape downwind of a large poultry facility. Agriculture, Ecosystems and Environment 185:161-175.

Walker, J.T., W.P. Robarge, Y. Wu and T.P. Meyers. 2006. Measurement of bi-directional ammonia fluxes over soybean using the modified Bowen-ratio technique. Agric. for. Meteorol. 138:54-68.

Watkins, S.H., R.F. Strand, D.S. DeBell and J. Esch. 1972. Factors influencing ammonia losses from urea applied to northwestern forest Soils1. Soil Sci. Soc. Am. J. 36:354-357.

Wichink Kruit, R. J. (Roy), van Pul, W. A. J., R.P. Otjes, P. Hofschreuder, A.F.G. Jacobs and A.A.M. Holtslag. 2007. Ammonia fluxes and derived canopy compensation points over non-fertilized agricultural grassland in the Netherlands using the new gradient ammonia—high accuracy—monitor (GRAHAM). Atmos. Environ. 41:1275-1287.

Yamulki, S., R.M. Harrison and K.W.T. Goulding. 1996. Ammonia surface-exchange above an agricultural field in southeast England. Atmos. Environ. 30:109-118.

Yang, J.E., E.O. Skogley, B.E. Schaff and J.J. Kim. 1998. A simple spectrophotometric determination of nitrate in water, resin, and soil extracts. Soil Sci. Soc. Am. J. 62:1108-1115.

Yu, X.F., Y.X. Zhang, Y.C. Zou, H.M. Zhao, X.G. Lu and G.P. Wang. 2011. Adsorption and desorption of ammonium in wetland soils subject to freeze-thaw cycles. Pedosphere 21:251-258.

Zarabi, M. and M. Jalali. 2018. Competitive removal of ammonium-nitrogen from aqueous solutions by mineral and organic adsorbents. Commun. Soil Sci. Plant Anal. 49:1129-1143.

Zhang, L., L.P. Wright and W.A.H. Asman. 2010. Bi-directional air-surface exchange of atmospheric ammonia: A review of measurements and a development of a big-leaf model

for applications in regional-scale air-quality models. J Geophys. Res. Atmos.115: D20310, doi:10.1029/2009JD013589

Zhang, Y.Z., S.H. Huang, D.J. Wan, Y.X. Huang, W.J. Zhou and Y.B. Zou. 2007. Fixed ammonium content and maximum capacity of ammonium fixation in major types of tillage soils in Hunan province, china. China. Agric Sci China 6:466-474.

APPENDICES

Appendix A

Annular Denuder Technology

Preparation of denuder coating solution: The annular denuder tubes were coated with a 50:50 mixture of methanol (CH_3OH) and DI water containing 0.5% w/v phosphorous acid (H_3PO_3). A coating solution was prepared by mixing thoroughly of 4 L of methanol, 40 g of phosphorous acid, and 4 L of DI water and were stored in a clean 10 L polyethylene container at room temperature.

Coating Procedure: Approximately 30 mL of a coating solution was added to each denuder tube. The capped denuder was then rotated to distribute the coating solution and uniformly wet all internal surfaces.

Drying Procedure: The coating solution was removed from the denuder tube and placed into the appropriate waste container. Ammonia-free air was then used to dry the denuder tubes. The drying manifold shown in Fig. A2 was used for this purpose. Briefly, the flow-straightener end of the denuder tube was attached to the drying manifold port (Fig. A2) and ammonia-free air allowed to flow through the denuder tube for 15 minutes. The tubes were then reversed, and the process repeated. The acid-coated denuder was then removed from the manifold, capped at both ends with clean Teflon caps and keep them in chemical-free refrigerator until use.

A

3-channel annular denuder

B

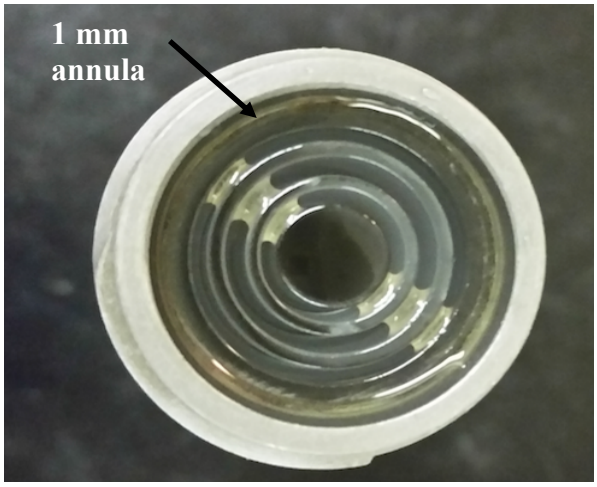

cross-sectional view

Figure A1. A) 3-channel annular denuder (URG-30 x 242mm length). B) Internal view of annular denuder

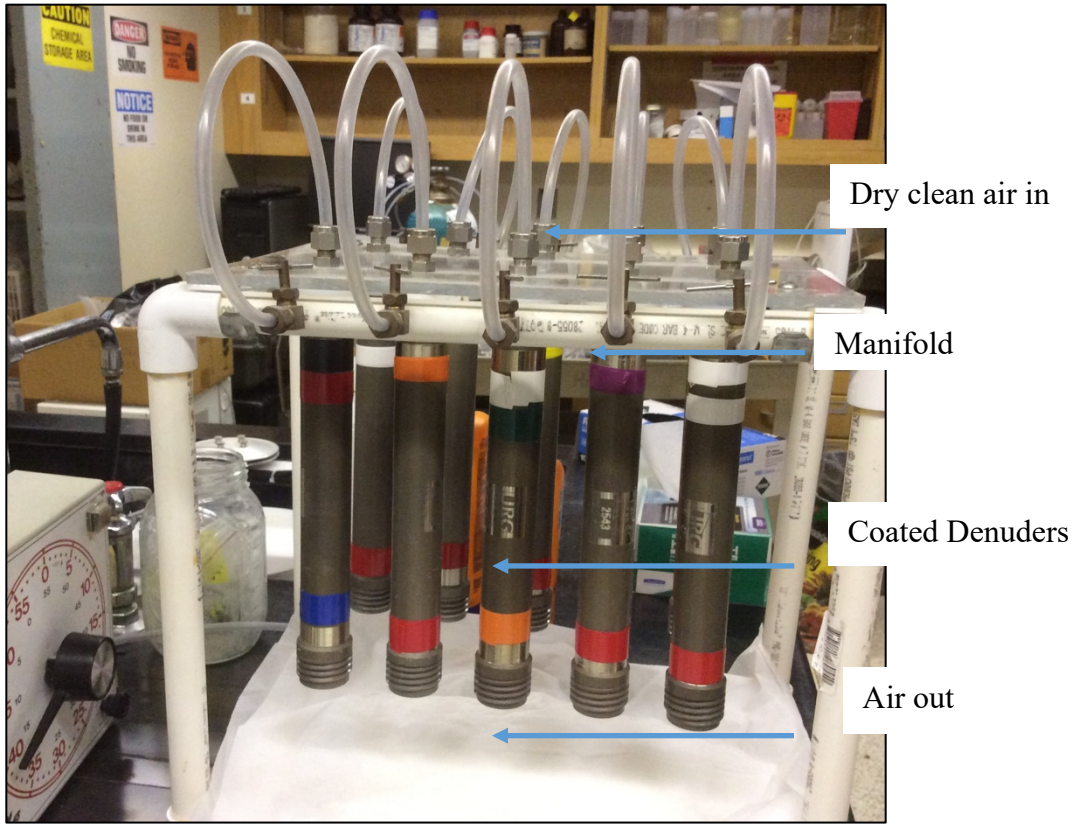

Figure A2. Drying manifold for denuder tube technology

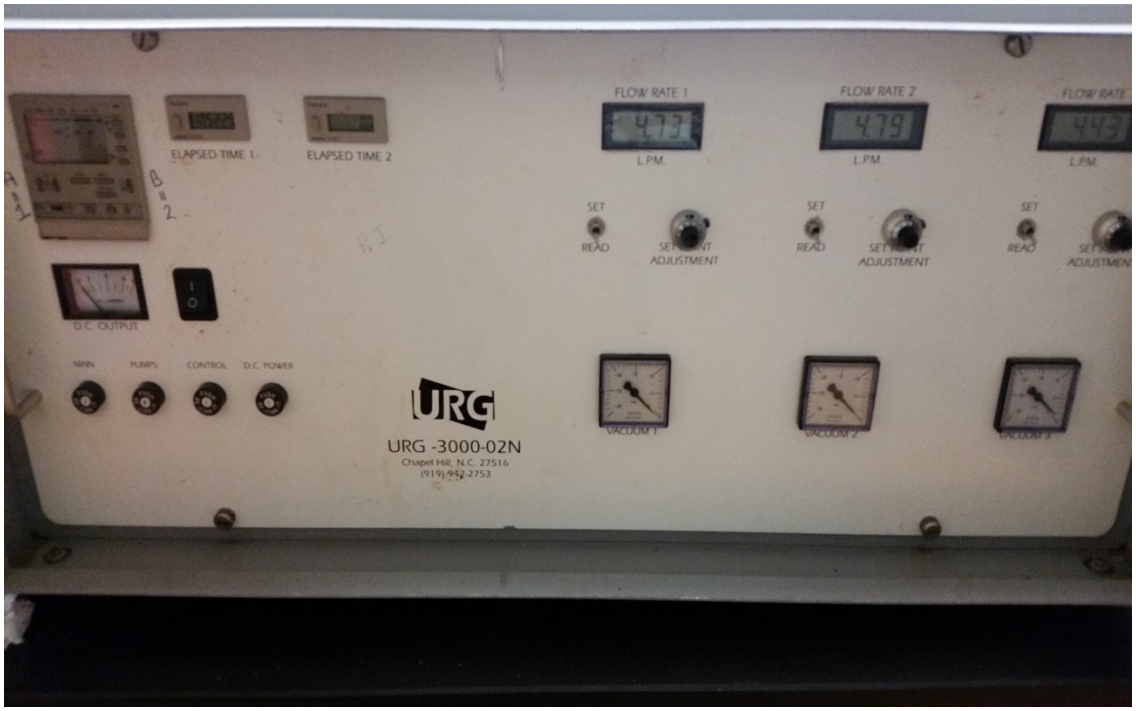

Figure A3. URG-3000 annular denuder system computerized sampling pump

Appendix B

Soil Water Retention Curve

The soil water retention curve (SWRC) shows the relationship between volumetric water content (θ) and matric potential. A pressure plate apparatus (Soilmoisture Equipment Corp, Model 1500F1, Serial No. PV200301625) has been used to determine the retention curve of soil water at pressures of 1, 30 and 150 m-H_2O. Disturbed samples of 5-cm diameter and 1-cm height were collected, wetted from below with water and allowed to saturate overnight. We presumed that the equilibrium was achieved after at least 2 days no outflow was measured. The samples were taken down from the pressurized plate apparatus after equilibrium was attained and the water content was gravimetrically determined (Table B1). For each measurement, duplicates were carried out (Kassel and Nielsen, 1986). Field capacity (FC) is usually determined as the water content of a soil 2 or 3 days after having been thoroughly wetted and drainage has become negligible. The matric pressure head (-1/3 bar or -1/10 bar) were used to determine the amount of water in a soil at FC. For purposes of this study soil water content was initiated at 80% of FC.

Table B1. Soil water retention data for BASF-ls, CEFS-sl, DUKE-sl, and BASF-cl soils

Soil	Pressure (bar)	Moisture content (g/g)	Volumetric water content (cm^3/cm^3)
BASF-ls	0.10	0.096	0.140
	0.33	0.067	0.098
	15	0.026	0.037
CEFS-sl	0.10	0.264	0.302
	0.33	0.171	0.196
	15	0.064	0.074
DUKE-sl	0.10	0.348	0.363
	0.33	0.258	0.269
	15	0.100	0.105
BASF-cl	0.10	0.312	0.357
	0.33	0.251	0.287
	15	0.125	0.143

Appendix C

NH4-N and NO3-N Standard Curves

Data for the standard curves were fitted using a second-order polynomial via IGORPro software (WaveMetric, Inc.) to calculate the concentrations of NH4-N in sample extracts.

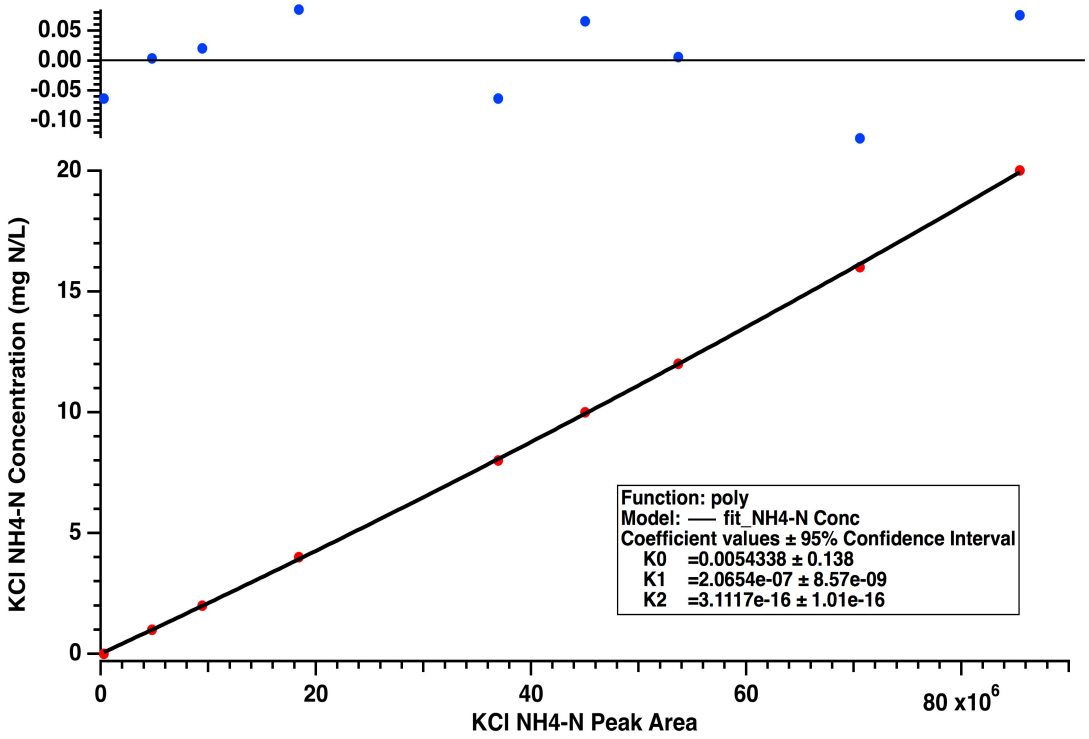

Figure C1. Standard curve for NH4-N made in distilled water used to calculate NH4-N concentration extracted from denuder tubes. At the top of the Figure is the residual plot showing the agreement between the observed values and the predicted values.

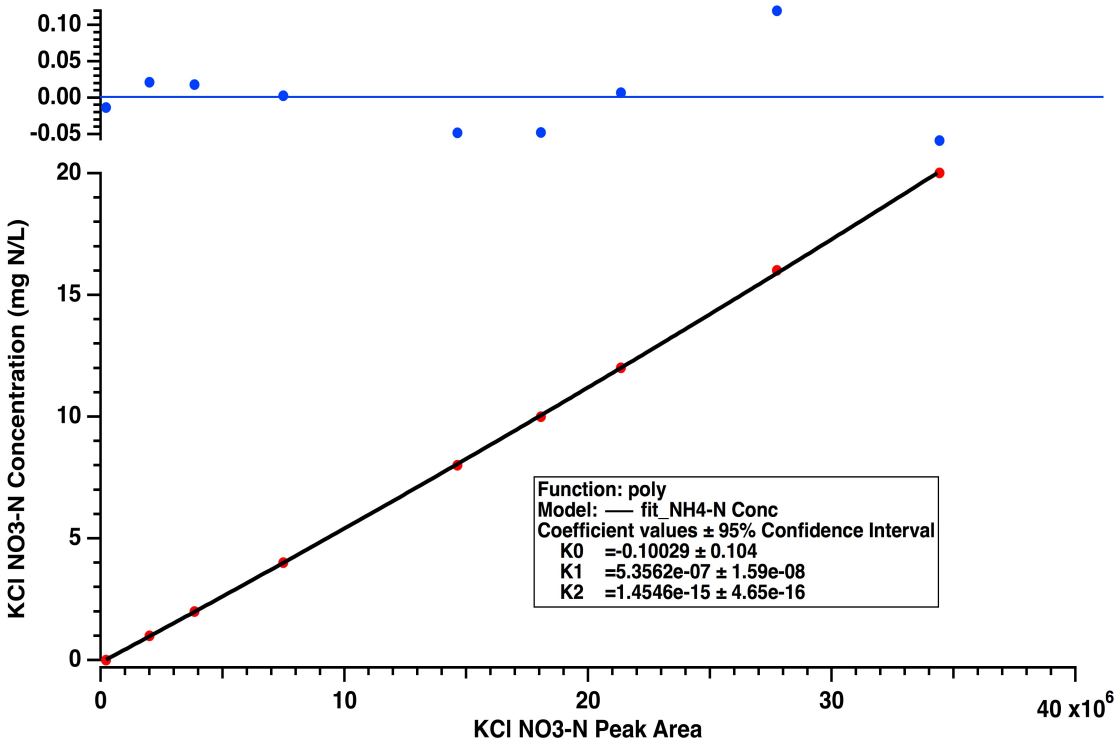

Figure C2. Standard curve for NO3-N made in 2M KCl used with to calculate NO3-N concentration extracted from soil. At the top of the Figure is the residual plot showing the agreement between the observed values and the predicted values.

Appendix D

Calculation of sl-NH_4^+, sl-NH_3, and sr-NH_4^+ using Venterea's et al. (2015) equations for fumigated BASF-ls soil

Measured		pH	Water content	Mu	K venterea	Acid dissociation constant	Calculate coefficients for Eq. 4*			Solve for sl-NH4 using quadratic equation	Calculate sl-NH3 using Eq. 3	Calculate sr-NH4+ using Eq. 1
BASF_ls_FS_Ce (mg/L)	BASF_ls_FS_KCl_Qe (mg/kg)		L H2O/kg soil	mg N/kg soil	mg N/L	K_A	sigma	nu	delta	mg N/L	mg N/L	mg N/kg
0.00	0.00											
0.00	0.00											
3.64	7.89	6.7	0.043	307.15	283.88	5.69E-10	0.043	311.591	-2241.172	7.185	0.02	7.58
3.84	7.79	6.7	0.043	307.13	283.88	5.69E-10	0.043	311.678	-2210.681	7.086	0.02	7.48
9.63	16.44	6.7	0.043	307.13	283.88	5.69E-10	0.043	303.024	-4667.531	15.369	0.05	15.77
10.71	15.68	6.7	0.043	307.13	283.88	5.69E-10	0.043	303.787	-4450.993	14.621	0.05	15.04
14.69	21.43	6.7	0.043	307.13	283.88	5.69E-10	0.043	298.037	-6083.199	20.350	0.06	20.54
15.20	20.60	6.7	0.043	307.13	283.88	5.69E-10	0.043	298.869	-5847.141	19.509	0.06	19.75
23.85	32.24	6.7	0.043	307.13	283.88	5.69E-10	0.043	287.222	-9153.456	31.717	0.10	30.87
24.49	32.30	6.7	0.043	307.13	283.88	5.69E-10	0.043	287.163	-9170.144	31.781	0.10	30.92
53.24	57.11	6.7	0.043	307.13	283.88	5.69E-10	0.043	262.359	-16211.514	61.172	0.19	54.45
56.91	54.17	6.7	0.043	307.13	283.88	5.69E-10	0.043	265.294	-15378.421	57.427	0.18	51.68
122.27	90.10	6.7	0.043	307.13	283.88	5.69E-10	0.043	229.369	-25576.760	109.248	0.34	85.35
125.42	87.71	6.7	0.043	307.13	283.88	5.69E-10	0.043	231.757	-24898.666	105.353	0.33	83.13
186.57	133.82	6.7	0.043	307.13	283.88	5.69E-10	0.043	185.644	-37989.256	195.672	0.61	125.32
191.91	125.57	6.7	0.043	307.13	283.88	5.69E-10	0.043	193.892	-35647.804	176.845	0.55	117.89
274.56	148.02	6.7	0.043	307.13	283.88	5.69E-10	0.043	171.442	-42020.952	231.517	0.72	137.96
288.52	138.90	6.7	0.043	307.13	283.88	5.69E-10	0.043	180.563	-39431.858	207.974	0.65	129.87
363.03	161.87	6.7	0.043	307.13	283.88	5.69E-10	0.043	157.596	-45951.727	271.287	0.85	150.08
366.03	158.33	6.7	0.043	307.13	283.88	5.69E-10	0.043	161.133	-44947.451	260.627	0.81	147.01
440.33	195.61	6.7	0.043	307.13	283.88	5.69E-10	0.043	123.856	-55529.746	393.904	1.23	178.49
440.68	193.37	6.7	0.043	307.13	283.88	5.69E-10	0.043	126.098	-54893.174	384.400	1.20	176.66
629.01	216.76	6.7	0.043	307.13	283.88	5.69E-10	0.043	102.703	-61534.682	495.338	1.55	195.24
797.64	231.67	6.7	0.043	307.13	283.88	5.69E-10	0.043	87.793	-65767.412	581.661	1.82	206.40

Appendix E

Calculation of soil compensation point using adsorption isotherms at full and lower end (LE) of isotherm for unfumigated soils

	Calculation of concentration NH_4^+ from Langmuir isotherm						Soil emission potential and compensation point from adsorption isotherm						
un-Fumigated	Extractant	Soil	soil bulk extraction ($\mu gNH_4^+/g$)	Sorption max (Qmax) mg/kg	K_L	Predicted conc of NH_4^+ Ce mg/L	pH_{H2O}(1:1)	$mgNH_4^+$/L calc from Langmuir	$[NH_4^+]$ M (soil solution)	$[H^+]$ M (soil solution)	Γsoil $=NH_4^+/H^+$	Soil Temperature degrees °C	Xsoil $\mu gNH_3/m^3$
Full isotherm	2M KCl	BASF	2.54	138	0.009	2.18	6.6	2.2	1.21E-04	2.69E-07	449	22	2.24
	0.01 M $CaCl_2$		1.05	140	0.008	0.96	6.6	1.0	5.35E-05	2.69E-07	199	22	0.99
	Water		0.65	140	0.008	0.61	6.6	0.6	3.36E-05	2.69E-07	125	22	0.62
LE of isotherm	2M KCl	BASF	2.54	113	0.013	1.77	6.6	1.8	9.83E-05	2.69E-07	365	22	1.82
	0.01 M $CaCl_2$		1.05	118	0.011	0.82	6.6	0.8	4.54E-05	2.69E-07	169	22	0.84
	Water		0.65	123	0.010	0.54	6.6	0.5	3.02E-05	2.69E-07	112	22	0.56
Full isotherm	2M KCl	CEFS	7.71	201	0.009	4.24	5.4	4.2	2.36E-04	3.89E-06	61	22	0.30
	0.01 M $CaCl_2$		6.01	202	0.009	3.47	5.4	3.5	1.93E-04	3.89E-06	50	22	0.25
	Water		2.46	206	0.008	1.57	5.4	1.6	8.71E-05	3.89E-06	22	22	0.11
LE of isotherm	2M KCl	CEFS	7.71	155	0.016	3.26	5.4	3.3	1.81E-04	3.89E-06	47	22	0.23
	0.01 M $CaCl_2$		6.01	162	0.014	2.85	5.4	2.8	1.58E-04	3.89E-06	41	22	0.20
	Water		2.46	173	0.011	1.37	5.4	1.4	7.62E-05	3.89E-06	20	22	0.10
Full isotherm	2M KCl	Duke	35.8	426	0.008	11.43	5.8	11.4	6.35E-04	1.70E-06	374	22	1.87
	0.01 M $CaCl_2$		31.1	436	0.007	10.66	5.8	10.7	5.92E-04	1.70E-06	349	22	1.74
	Water		9.74	585	0.003	5.54	5.8	5.5	3.08E-04	1.70E-06	181	22	0.90
LE of isotherm	2M KCl	Duke	35.8	302	0.015	8.96	5.8	9.0	4.98E-04	1.70E-06	293	22	1.46
	0.01 M $CaCl_2$		31.1	302	0.014	8.28	5.8	8.3	4.60E-04	1.70E-06	271	22	1.35
	Water		9.74	420	0.049	0.48	5.8	0.5	2.69E-05	1.70E-06	16	22	0.08